THE UNIVERSITY OF HULL

Colloidal Structures with Novel Functions

being a Thesis submitted for the Degree of Doctor of Philosophy
in the University of Hull

by

Nae-Gyu Kang, M.Sc.
(POSTECH, South Korea)

March 2009

To the memory of my father, but not forgotten-
who inspired my curiosity for science

This thesis is dedicated with affection to my sunshine Kyoung-Hee whose courage, lovely smile, and patience have been an inspiration to me.

Where the worm ceases to be the scene of our personal hopes and wishes, where we face it as free beings admiring, asking, and observing, there we enter the realm of Art and Science.

Albert Einstein 1921

Acknowledgements

I would like to express my sincere gratitude to my advisors, Professor Paul D.I. Fletcher and Dr. Paunov, for their patience, understanding, and constant encouragement in their guidance through out this work. They were patiently teaching me the craft and art of scientific research in my PhD periods.

My thanks belong also to the members of our Surfactant & Colloid Group, especially to Mr. Tim Dunstan, Dr. Tim Lees, Dr. Jake Hicks, Dr. Zhenggang Cui and Dr. Mika M. Kohonen for teaching and advising me the laboratory techniques used in surfactant research. Their discussions and comments of experimental results were also very appreciated and admired. I also appreciate Professor Stephen M. Kelly and Professor Paul F. Luckham for their enthusiasm and patience in reading this thesis and giving comments as a committee member. During this work, I received kind help from my colleague graduate students, Mr. Andrew Campbell and Mr. Will Small.

Special thanks to Mr. Tony Sinclair in the University of Hull for his great scanning electron microscope images and his kind comments and support for a preparation of Janus particles.

I also appreciate Professor Wan-Goo Cho, Dr. Myoung-Suk Yoon, Professor Moon-Jeong Rang and Dr. Se-Hoon Kang as my mentors in my company live. Without their encouragement and challenge I would not decide this PhD study and could not be complete and successful.

The financial support and scholarship from University of Hull and LG Household & Health Care Ltd is gratefully acknowledged. I am also grateful to Dr. Cheon-Koo Lee, Dr. Sug-Youn Chang, and Dr. Sang-Jin Kang at LG for their advice and support.

Finally, for encouragement in my Ph.D. study, I specially thank my wife, Kyoung-Hee, and my son, Kyoung-Suk. Despite of long distance between us, my parents and wife's parents have always supported me in whatever and wherever I decided to do and go, therefore, I feel very obligated to them.

Nae-Gyu

Publication and Presentations

The work presented in this thesis has given rise to the following articles and presentations in the journals and conferences mentioned below:

"UV Polymerisation of Surfactants Adsorbed at the Nematic Liquid Crystal-Water Interface Produces an Optical Response", P.D.I. Fletcher, N. G. Kang, V. N. Paunov, *submitted in Soft. Mater. 2008.*

Oral Presentation **"Development of UV sensors based on surfactant adsorption at the liquid crystal-water interface"**, Surfactant & Colloid Workshop, Hull, UK, 20th September 2007.

Oral Presentation **"Development of sensors based on surfactant adsorption at the nematic liquid crystal-water interface"**, at the University of Hull, Department of Chemistry, 10th June 2008.

Oral Presentation **"Development of Sensors Based on Optical Response of 5CB by Adsorption of Surfactants at the Liquid Crystal-Water Interface produces"**, N. G. Kang, P.D.I. Fletcher, V. N. Paunov, *accepted in 3rd Asian Conference on Colloid and Interface Science,* at Jeju Island, South Korea, 11th -14th October 2009.

Abstract

Over the last two decades, many kinds of environmentally responsive materials based on the chemical nature of gels and adsorption of surfactants at various interfaces are proposed. For the development of colloidal systems showing novel functionality we have designed various experimental systems for imaging the adsorption of surfactant at the interface between a nematic liquid crystal (LC) and water, self-propelling stimuli-responsive hydrogels and Janus particles.

Optical textures changes produced by adsorption of a range of surfactants at the LC-water interface have been investigated using polarised and fluorescence microscopy to develop a novel sensor to detect various interfacial phenomena without requiring labelling of the analyte and the use of electroanalytical apparatus.

In chapter 3, we have studied the adsorption of DNA species at the LC-water interface. The adsorption of DNA-surfactant to the interface did not induce homeotropic anchoring of LC due to its highly charged bulky head groups and its bolaform structure at the interface. Whereas single stranded DNA (ssDNA)/cationic surfactant interfacial complex induced homeotropic anchoring of 5CB. Subsequent adsorption of ssDNA to the DNA oligomers/cationic surfactant complex-laden interface resulted in a reorientation of the LC from homeotropic to planar anchoring. With fluorescence microscopy we observed that the change of anchoring of LC is caused by desorption of cationic surfactant from the interfacial complex leaving only DNA at the interface by a salt solution not by a specific hybridisation event. This system has a potential for understanding of the interfacial behaviour of DNA-cationic surfactant complex at the LC-water interface depending on various conditions (e.g., the structure of DNA).

Similar to the non-polymerisable surfactants, the adsorption of polymerisable surfactants with sufficiently long hydrophobic tail groups induced homeotropic anchoring of LC. UV polymerisation of surfactants with a polymerisable group located in the hydrophobic tail region (e.g., sodium oleate) changed the anchoring from homeotropic back to planar. Polymerisation in the hydrophilic head group region did not induce an optical transition. In chapter 4, we demonstrate that these systems can be used to “write with light” on the LC-water interface and that they form the basis of a

UV sensor device in which the optical response is visible to the naked eye under ambient lighting.

In chapter 5, we designed a self-propelling actuator in a liquid that is capable of converting chemical energy produced by the oscillatory Belousov-Zhabotinsky (BZ) reaction and electric fields into mechanical work through the swelling-deswelling oscillation of a gel. A series of modulated bigels composed of *N*-isopropylacrylamide and 2-acrylamido-2-methylpropane sulfonic acid (AMPS) and polymerisable ruthenium catalyst of the BZ reaction were prepared by UV polymerisation. In an aqueous solution containing the BZ substrates, the volume phase transition of the gels on the millimetre scale was not sufficient to move the gels in a liquid due to a low frequency and velocity of chemical wave. However, from these studies, we develop a novel method to synthesise anisotropic bigels composed of two different compositions using UV polymerisation like "bimetal". Cylindrical poly(AMPS) gels (1 mm diameter) showed different reversible electro-actuations in electrolyte solutions: a vibration (at high frequency) and bending (at low frequency) in *ac* electric fields whereas the bending (2 cm length) and propulsion (2 mm length) in *dc* electric fields. Because this electro-actuation is influenced strongly by the size and shape of the gels, it is expected that micro-sized asymmetrical shaped gel will undergo fast actuation and concomitant water exudation in a liquid to move under an electric field.

In chapter 6, we employed the self-propulsion of metal coated Janus particles in liquids driven by osmotic pressure gradient generated through the catalytic enzyme activity and the diffusion of a chemical as an autonomous propelling motor. Spherical platinum (Pt)-coated Janus particles showed a directional movement in aqueous hydrogen peroxide solutions by catalysing the formation of oxygen bubbles at the Pt-end. Meanwhile, invertase and catalase immobilised Janus particles did not show a unidirectional self-propulsion but just a random self-rotation in aqueous solutions containing substrates. These observations suggest that the osmotic pressure gradient at the surface of the particles was not largely enough due to the low coverage of enzymes on the particles and an intrinsic low catalytic activity of enzymes compared to Pt. Through these studies we developed a novel method called the glass sliding technique (GST) to produce metal-coated Janus particles. The method is simple and inexpensive to prepare various functionalised Janus particles (e.g., drug delivery) compared to other reported methods.

List of symbols

Some of the symbols and abbreviations used in this thesis are given here; others are defined locally in the text.

Glossary

A	Absorbance
μg	Microgram
μL	Microlitre
μm	Micrometre
μM	Micromolar
$^{\circ}$C	Centigrade degree
cm	Centimetre
g	Acceleration due to gravity
h	Hour
γ	Surface tension
Hz	Hertz
min	Minute
mL	Millilitre
mM	Millimolar
mm	millimetre
sec	Second
nm	Nanometre
T_m	Melting temperature
V	Volt
vol%	Volume percentage
wt%	Weight percentage
w/v%	Weight per volume percentage
ε_{260}	Molar extinction coefficient at 260 nm
λ	Wavelength

Abbreviations

5CB	4´-pentyl-4-cyanobiphenyl
AAm	Acrylamide
AAc	Acrylic acid
ac	Alternating current
AIBN	2,2'-Azobis(2-methyl-propionitrile)
AMPS	2-acrylamido-2-methyl-1-propanesulfonic acid
APS	Ammonium persulfate
bp	Base pair
cmc	Critical micelle concentration
CML	Carboxylate modified polystyrene latex
cp	Centipoises
CPC	Cetylpyridinium chloride
CTAB	Cetyltrimethylammonium bromide
C_nTAB	Alkyltrimethylammonium bromide of alkyl chain length *n*
dc	Direct current
DCDMS	Dichlorodimethylsilane
DMSO	Dimethylsulfoxide
DNA	Deoxyribonucleic acid
DTAB	Dodecyltrimethylammonium bromide
ds DNA	Double strand DNA
DBTAB	Dodecyl-1,12-bis(trimethylammonium bromide)
DTAB	Dodecyl trimethylammonium bromide
DVB	Divinyl benzene
EDAC	1-Ethyl-2-[3-dimethylaminopropyl]carbodiimide hydrochloride
FITC	Fluorescein isothiocyanate
FTMA	11-(ferrocenylundecyl)trimethylammonium bromide
HTAB	(11-hydroxyundecyl)trimethylammonium bromide

Hz	Hertz
IPA	Isopropanol
GTT	Gel trapping technique
GST	Glass sliding technique
LC	Liquid crystal
MBAAm	*N,N′*-methylene bisacrylamide
MEDDAB	(2-methacryloyloxy) ethyl) dodecyldimethylammonium bromide
MUBDMAB	11-(methacryloyloxy) undecylbutyl dimethylammonium bromide
NIPAAm	*N*-isopropylacrylamide
OTAB	Octyltrimethylammonium bromide
OTS	Octadecyltrichlorosilane
PBS	Phosphate buffered saline
PDMS	Polydimethylsiloxane
PMMA	Polymethyl methacrylate
rpm	Rotation per minute
$Ru(bpy)_3$	Ruthenium-tris(2,2′-bipyridyl)
$Ru(bpy)_2$-$(mvbpy)(PF_6)_2$	Ruthenium(4-vinyl-4′-methyl-2,2′-bipyridine)bis(2,2′ bipyridine)-bis(hexafluorophosphate)
SDS	Sodium dodecyl sulfate
SEM	Scanning electron microscopy
SSC	Saline sodium citrate
ssDNA	Single strand DNA
TAMRA	*N,N,N′,N′*,-tetramethyl-6-carboxyrhodamine
TEMED	*N,N,N′,N′*-tetramethyl-ethylenediamine
TTAB	Tetradecyltrimethylammonium bromide
T_{NI}	Nematic-isotropic transition temperature
UV	Ultraviolet

Table of Contents

ABSTRACT

Chapter 1 **1**

Introduction

1.1 General introduction and project aims **1**

1.2 DNA structure and hybridisation **3**

1.2.1 Structure of DNA 3

1.2.1.1 DNA nucleotides 4

1.2.1.2 DNA double helix 4

1.2.2 Melting and hybridisation of DNA 6

1.3 Surfactants **7**

1.3.1 Introduction 7

1.3.2 Types of surfactants 8

1.3.3 Surfactant adsorption at interfaces 9

1.3.4 Surfactant self-aggregation in water 11

1.3.5 DNA-surfactants 13

1.3.5.1 Surface properties of DNA-surfactants 14

1.3.5.2 Self-recognition between DNA-surfactant monolayers 15

1.3.6 Polymerisable surfactants 15

1.3.6.1 Monomer structures of polymerisable surfactants 16

1.3.6.2 Initiators of polymerisation 16

1.3.6.3 Mechanism of polymerisation 18

1.4 Nematic liquid crystals (LCs) **19**

1.4.1 Introduction 20

1.4.2 Liquid crystal 4-cyano-4´-pentylbiphenyl (5CB) 22

1.4.3 Strategy for inducing of the alignment change of LCs by adsorption of 24

surfactants at the 5CB-water interface 24

1.4.4 Influence of the molecular structure of surfactants on the orientation of 5CB 26

1.5 Anisotropic colloid particles **28**

1.5.1 Preparation of anisotropic Janus particles 29

1.6 Gels and their properties **31**

1.6.1 Classification of gels 31

1.6.2. Hydrogels: Thermodynamics and swelling kinetics 33
1.6.2.1 Thermodynamics 33
1.6.2.2 Swelling kinetics 35
1.6.3. Stimuli-responsive gels 36
1.6.3.1 Introduction 37
1.6.3.2 Temperature sensitive polymer: poly(N-isopropylacrylamide) (PNIPAAm) gels 38
1.6.3.3 pH and electro-responsive poly(2-acrylamido-2-methylpropane-sulfonic acid) (PAMPS) gels 39
39
1.7 Self-oscillating chemical reactions **40**
1.7.1 Introduction 41
1.7.2 Belousov-Zhabotinsky (BZ) reaction 41
1.7.3 Briggs-Raucher (BR) reaction 43
1.8 Presentation of this thesis **43**
1.9 References **45**

Chapter 2 **55**
Experimentals
2.1 Materials **55**
2.1.1 Water 55
2.1.2 DNA oligonucleotides 55
2.1.2.1 Dissolution of the oligonucleotides 57
2.1.2.2 Measurement of oligonucleotides concentrations 57
2.1.2.3 Melting temperature of oligonucleotides 58
2.1.3 Thermotropic liquid crystal 5CB 58
2.1.4 Surfactants and fatty acids 59
2.1.5 Colloid particles and a gelling agent for Janus particles 60
2.1.6 Enzymes 62
2.1.7 Monomers, cross-linker and initiators for hydrogel synthesis 64
2.1.8 Buffers 65
2.1.9 Organic solvents 66
2.2 Methods **68**
2.2.1 Microscopy 68
2.2.1.1 Optical microscopy equipped with crossed polarisers 68

2.2.1.2 Scanning electron microscopy (SEM) 69
2.2.2 Treatment of microscope glass slides with silanizing agents 69
2.2.2.1 Octadecyltrichlorosilane (OTS) treatment on glass slides 69
2.2.2.2 Dichlorodimethylsilane (DCDMS) treatment on glass slides 71
2.2.3 Optical examination of 5CB textures at the LC-water interface 72
2.2.3.1 Preparation of LC optical cells for imaging of 5CB textures 72
2.2.3.2 Observation of the orientational response of 5CB to adsorption of surfactants 74
2.2.4 Polymerisation reactions 75
2.2.4.1 Thermal polymerisation 75
2.2.4.2 UV polymerisation 76
2.2.5 Preparation of Janus particles 79
2.2.5.1 Gel trapping technique (GTT) 80
2.2.5.2 Glass sliding technique (GST) 81
2.2.6 Optical absorbance measurements 83
2.2.7 Drop shape analysis 83
2.2.8 pH measurements 83
2.2.9 Application of electric fields 84
2.2.10 Dispersion of colloid particles in liquids 84
2.2 References 85

Chapter 3 89
Response of the Alignment of LC at the 5CB-Water Interface to Adsorption of DNA Species
3.1 Optical examination of LC textures in a perfusion chamber 90
3.2 Adsorption of DNA-surfactants at the 5CB-water interface 92
3.2.1 Anchoring of 5CB by DNA-surfactants 92
3.2.1 Effect of ionic strength on the anchoring of 5CB in the presence of DNA-surfactants 95
3.2.3 Hybridisation of DNA-surfactant at the 5CB-water interfaces 97
3.2.3 Summary 99
3.3 Adsorption of DNA-cationic surfactant complex at the 5CB-water interface 100
3.3.1 Introduction 100

3.3.2 Anchoring of 5CB by cationic surfactants 103
3.3.3 Anchoring of 5CB by DNA-cationic surfactant complex 106
3.3.3.1 The order of addition of DNA and cationic surfactant 106
3.3.3.2 Hybridisation of DNA-cationic surfactant complex at the 5CB-wtaer interface with complementary DNA 112
3.4 Adsorption of DNA-polymerisable cationic surfactant complex at the 5CB-water interface 116
3.4.1 Anchoring of 5CB by polymerisable cationic surfactants 116
3.4.2 Adsorption of MUBDMAB and MEDDAB at the 5CB-water interface after UV polymerisation 119
3.4.3 Anchoring of 5CB by DNA-polymerisable cationic surfactant complex 122
3.4.4 Effect of UV polymerisation of mixed DNA-MEDDAB adsorbed layer at the LC-water interface 125
3.5 Conclusions 127
3.4 References 129

Chapter 4 132
UV Sensors Based on the Polymerisable Surfactants Adsorption at the 5CB-Water Interface
4.1 Introduction 132
4.1.1 Ultraviolet (UV) radiation 132
4.1.1.1 UV spectrum 132
4.1.1.2 Safety aspects of UV light 134
4.1.1.3 UV Index 134
4.2 Influence of the molecular structure of polymerisable surfactants on the orientation of 5CB at the LC-water interface 136
4.3 Effect of UV polymerisation of adsorbed polymerisable surfactants layer on the LC alignment 141
4.3.1 Effect of the position of the polymerisable group in the surfactant 141
4.3.2 Patterned polymerisation of adsorbed polymerisable surfactant layer at the LC-water interface 146
4.4 Polymerisation of oleic acid monolayer at the 5CB-water interface 151
4.4.1 Effect of oleic acid on the orientation and the nematic-isotropic transition temperature (T_{NI}) of 5CB 151

4.4.2 Anchoring of 5CB by oleic acid 153
4.4.3 Effect of pH and ionic strength on the adsorption of oleic acid at the 5CB-water interface 155
4.4.3.1 Effect of pH 156
4.4.3.2 Effect of ionic strength 161
4.4.3.2 Summary 169
4.5 Preparation of prototype UV sensor 170
4.5.1 Anchoring of 5CB by cross-linked oleic acid/oleate species 170
4.5.2 Effect of temperature on the UV polymerisation of an adsorbed oleic acid/ oleate and DVB mixtures at the LC-water interface 173
4.5.3 Possible UV sensor visible to the naked eye 178
4.6 Conclusions 181
4.7 References 182

Chapter 5 184
Designing Self-propelling Particles Using Stimuli-responsive Gels
5.1 Strategies to develop self-propelling hydrogel particles 184
5.1.1 Self-oscillating hydrogels in the BZ and BR reaction solutions 184
5.1.1.1 Self-oscillation of poly(NIPAAm-co-Ru(bpy)$_3$) gels in the BZ reaction 185
5.1.1.2 Self-oscillation of polyacrylamide (PAA) gels in the BR reaction 187
5.1.2 Electro-responsive polyelectrolyte gels 188
5.1.2.1 Electrical contraction of polyelectrolyte gels 188
5.1.2.2 Electro-response of polyelectrolyte gels in an oppositely charged surfactamt solution 189
5.2 Self-oscillation of hydrogels in the BZ and BR reactions 190
5.2.1 Swelling behaviour of hydrogel in the BZ and the BR reactions 190
5.2.1.1 Self-oscillation of ruthenium catalyst Ru(bpy)$_3^{2+}$ in the BZ reaction 190
5.2.1.2 Swelling behaviour of poly(N-isopropylacrylamide)(PNIPAAm) gel containing Ru(bpy)$_3^{2+}$in the BZ and BR reactions 192
5.2.2 Preparation of anisotrpoic poly(NIPAAm-*co*-Ru(bpy)$_3$-*co*-AMPS) gels 195
5.2.3 UV polymerisation of poly(NIPAAm-*co*-Ru(bpy)$_3$-*co*-AMPS) gels 201
5.2.3.1 Effect of photoinitiator Darocur 1173 on the polymerisation of poly(NIPAAm-co-AMPS) gels 202

5.2.3.2 Synthesis of anisotropic PNIPAAm/poly(NIPAAm-co-AMPS) bigels with a double UV polymerisation 203
5.2.3.3 Preparation of asymmetrical elbow-shaped PNIPAAm/ poly(NIPAAm-co-Ru(bpy)$_3$-co-AMPS) bigels 210
5.2.3.4 Effect of the concentration of cross-linker on the formation of a bigel 212
5.2.3.5 Effect of pH and solvent on the swelling behaviour of anisotropic bigels comprising of poly(NIPAAm-co-AMPS) and PNIPAAm 216
5.3 Preparation of electro-responsive anisotropic polyelectrolyte gels 219
5.3.1 Preparation of electroactuated polyelectrolyte gels 221
5.3.1.1 Bending motion of PAMPS gels in an electrolyte solution 221
5.3.1.2 The motility of PAMPS gels in dc electric field 226
5.4 Conclusions 227
5.5 References 228

Chapter 6 231
Designing Self-propelling Janus Particles
6.1 Strategies to develop self-propelling Janus particles based on osmotic pressure gradient 231
6.2 Enzymatic reaction driven Janus particles 234
6.2.1 Preparation of invertase reaction driven Janus particles 234
6.2.1.1 Immobilisation of invertase on gold (Au)-coated Janus particles 235
6.2.1.2 Fluorescent detection of the immobilised invertase on particles 237
6.2.1.3 Measurement of catalytic activity of the immobilised invertase 240
6.2.1.4 The motility of invertase immobilised Janus particles 242
6.2.2 Preparation of catalase reaction driven Janus particles 243
6.2.2.1 Immobilisation of catalase on Au-coated Janus particles 243
6.2.2.2 Motility of catalase immobilised and platium (Pt)-coated Janus particles in hydrogen peroxide solutions 246
6.3 Diffusion driven porous Janus particles 249
6.3.1 Preparation of Au-coated porous silica Janus particles 249
6.3.2 Preparation of the Au-coated porous Janus particles carrying glucose 254
6.3.3 Motility of glucose absorbed Au-coated porous Janus particles 255
6.4 Conclusions 258

6.5 References **259**

Chapter 7 **262**

Summary of the Main Conclusions and Future Work

7.1 Summary of the main conclusions **262**

7.2 Future work **264**

Chapter 1

Introduction

Chapter 1

Introduction

1.1 General introduction and project aims

This project concerns the development of colloidal systems, which show novel functionality. The overall aim of this work is to explore how some different types of novel functionalities can be built into colloidal systems. These systems include adsorbed monolayers that trigger an optical response in a nematic liquid crystal (LC) film, self-actuating gel particles and self-propelling Janus particles. This section briefly describes some recent studies and background information for developing these colloidal systems and their applications.

The ordering of liquid crystals (LCs) near surfaces of solids has received widespread attention over the past few decades due to the abundance of the associated physical phenomena, as well as its technological importance in electro-optical devices based on LCs.[1,2,3] The self-assembly of surfactants, polymers and proteins at the nematic LC-water interface and the resulting LC orientational and optical changes has been studied extensively over the past decades or so,[4,5,6] mainly by the group of Abbott, who have also published a recent review of the topics.[7] The adsorption-triggered changes in the anchoring of the LC molecules close to the LC-water interface causes molecular orientational changes to propagate to a depth of microns, which then changes the optical appearance of the LC film when viewed through crossed polarisers. In this way, the localised (molecular length scale) surface response of the LC is amplified to the multi-micron length scale to produce an easily visualisable optical change. In chapter 3 and 4, we describe how the effect can be used to image the adsorption of DNA species (e.g., DNA-surfactant), their hybridisation with complementary DNA, and the UV-triggered polymerisation of polymerisable surface-active species at the interface.

Deposition of DNA arrays on solid substrates has become one of the essential tools for high-throughput genetic analysis.[8] Therefore, over the past few years, many research groups have studied DNA-mediated assembly of solid nano- and microparticles functionalised with DNA strands very intensively.[9] Recently, the preparation of DNA oligonucleotide-modified vesicles by chemical attachment of thiol-DNA to a reactive lipid incorporated into the vesicle membrane has been reported.[10] Our group developed novel DNA-surfactants composed of hydrophilic DNA and

hydrophobic alkyl chain groups[11] and prepared DNA functionalised unilamellar vesicles by adsorption of DNA-surfactants in the lipid bilayer.[12] The main advantage of the use of DNA-surfactants is that they facilitate the deposition of DNA chains by adhesion to a hydrophobic surface and adsorption to various liquid interfaces.

Many examples of matter-transporting actuators or devices based on electrolyte polymers have recently been developed. However, the actuation is controlled by on/off switching of external inputs. In contrast, there are several autonomous phenomena that exhibit rhythms and spatial patterns under non-switched conditions. Yoshida and his collaborators have studied a self-oscillating reaction of a synthetic polymer at the macroscopic scale that is produced by dissipating the chemical energy of the Belousov-Zhabotinsky (BZ) reaction that takes place inside a polymer gel.[13,14] Recently, they have succeeded in the development of anisotropic gel particles showing directional locomotion and peristaltic motion in an aqueous solution containing the substrates of the BZ reaction.[15,16] These actuators are based on the reversible volume change of the polymer upon periodic redox changes of ruthenium catalyst moiety: $[Ru(bpy)_2(4\text{-vinyl-}4'\text{-methylbpy})]^{2+} \leftrightarrow [Ru(bpy)_2(4\text{-vinyl-}4'\text{-methylbpy})]^{3+}$, bpy = 2,2′-bipyridine). From these ideas, we attempted to develop self-oscillating gels in liquids by synthesising anisotropic shapes showing an enhanced oscillation frequency to generate enough mechanical oscillating motion for self-propulsion. We discuss some results concerning about this topic in chapter 5.

There has been an increased interest in the preparation of anisotropic colloids, including Janus particles[17,18] and non-spherical “acorn”-shaped particles. A major limitation in nanoparticle-based materials chemistry is the lack of suitable assembly methods for preparing extended two- and three-dimensional architectures with synthetically programmable building blocks. Recently, Mirkin *et al.*[19,20] have reported versatile noncovalent methods for assembling DNA-functionalised nanoparticles building blocks into network materials. These methods could enhance the selectivity of combinatorial oligonucleotide array (or “gene chip”) technology. Paunov and his group developed a novel technique for the preparation of anisotropic particles and microporous surfaces, which are addressed and coated only on a specified portion of the particle surfaces using the gel trapping technique (GTT).[21]

The creation of miniature “engines” that can convert stored chemical energy to mechanical motion is one of the great remaining challenges of nanotechnology.

Whitesides and co-workers have used the catalytic decomposition of hydrogen peroxide to propel cm/mm-scale objects on a water surface.[22] Mallouk and his colleagues have developed anisotropic platinum/gold (Pt/Au) nanorods showing a directional movement in hydrogen peroxide solution, which is comparable to that of flagella bacteria.[23] The driving force that propels these rods arises from an osmotic gradient that is continuously re-established as the rod moves. There are a very large number of enzymes that can catalyse reactions, which can in principle be used to generate gradient-based forces. Therefore, by appropriate design using Janus particles that are asymmetrically immobilised with enzymes, the enzyme catalytic activity might be translated into anisotropic surface force and directionally propel the particles. In chapter 6, we describe some attempts to develop self-propelling particles based on Janus particles using either immobilised enzymes or chemical release to generate an osmotic pressure gradient to produce self-propulsion.

This chapter introduces some of the basic knowledge required for the understanding of the research work presented in chapter 3–6. First, general comments on the nature of DNA, surfactant and LC are presented before our interest is centred on adsorption of surfactant at the LC-water interface. Then, the optical responses of LC at the LC-water interface are considered with the structure of adsorbed surfactant molecules. We briefly mention recent studies for the preparation of Janus particles. In the next section, previous works on the preparation of stimuli-responsive gels are briefly reviewed according to different structures of polymers and chemomechanical energies that have been introduced in those systems. Furthermore, a brief overview of the following chapters introduces the reader to the general development of the thesis.

1.2 DNA structure and hybridisation

Deoxyribonucleic acid (DNA) is the hereditary material present in each living cell that carries the genetic information and is programmable according to the principle of Watson-Crick complementary pairing between DNA oligonucleotide sequences.

1.2.1 Structure of DNA

DNA is a polymer which has a backbone with an alternating sugar-phosphate sequence. The monomer units of DNA are nucleotides, and the polymer is known as a polynucleotide. Each nucleotide consists of a 5-carbon sugar (deoxyribose), a nitrogen-containing base attached to the sugar, and a phosphate group.[24] The deoxyribose sugars

are joined at both the 3´-hydroxyl and 5´-hydroxyl groups to phosphate groups in ester links, also known as phosphodiester bonds.

1.2.1.1 DNA nucleotides

A nucleotide is a nucleoside with one or more phosphate groups covalently attached to the 3´- or 5´-hydroxyl group(s). There are four different types of nucleotides found in DNA, differing only in the nitrogenous base as shown in Figure 1.1. The four nucleotides are given one letter abbreviations as shorthand for the four bases: A is for adenine, G is for guanine, C is for cytosine, and T is for thymine.

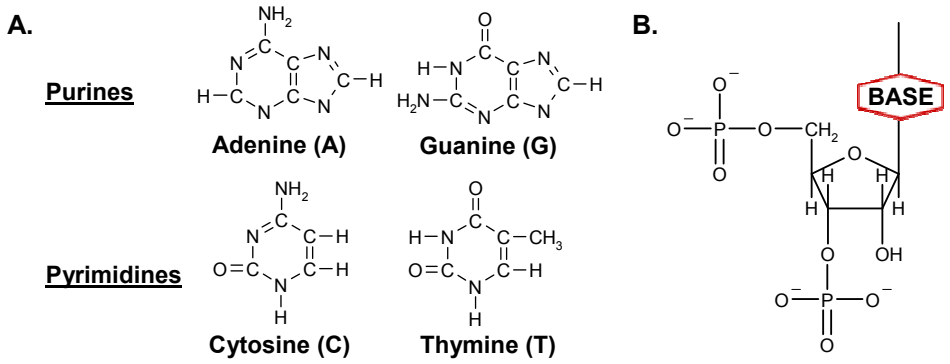

Figure 1.1: Structure of (A) DNA bases and (B) nucleotide.

Adenine and guanine are purines which are the larger of the two types of bases found in DNA. The nine atoms that make up the fused rings (five carbons, four nitrogens) are numbered 1–9. All ring atoms lie in the same plane. Cytosine and thymine are pyrimidines. The six atoms (four carbons, two nitrogens) are numbered 1–6. Like purines, all pyrimidine ring atoms lie in the same plane. The four DNA bases are covalently attached to the C1´ position of a sugar. The deoxyribose sugar of the DNA backbone has 5 carbons and 3 oxygens. The carbon atoms are numbered 1´, 2´, 3´, 4´, and 5´ to distinguish from the numbering of the atoms of the purine and pyrimidine rings. The hydroxyl groups on the 5´- and 3´-carbons link to the phosphate groups to form the DNA backbone.

1.2.1.2 DNA double helix

DNA is a normally double-stranded macromolecule as shown in Figure 1.2. Two polynucleotide chains, held together by weak inter-molecular forces, hydrogen bonding, form a DNA molecule. Within the DNA double helix, Adenosine forms two hydrogen bonds with thymine on the opposite strand, and guanine forms three hydrogen bonds with cytosine on the opposite strand (Figure 1.2A).

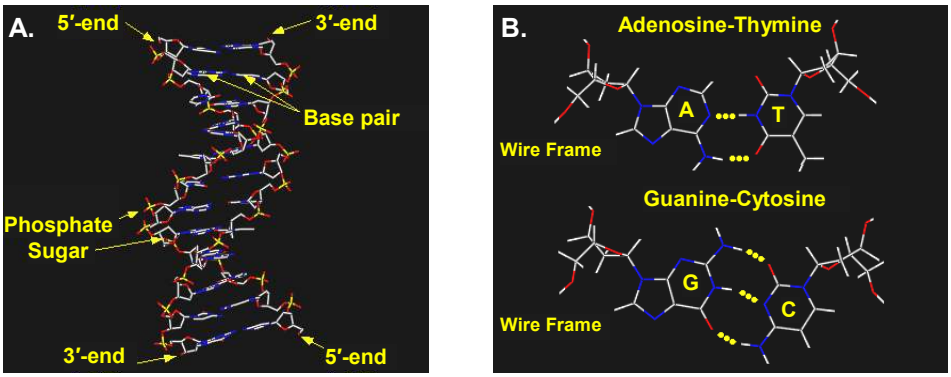

Figure 1.2: (A) Structure of DNA double helix and (B) DNA base pairing between Adenosine-Thymine and Guanine-Cytosine bases.[25]

A-T and G-C base pairs are the same length and occupy the same space within a DNA double helix. Therefore, the DNA molecule has the constant diameter (20 Å). A-T and G-C base pairs can occur in any order within DNA molecules (Figure 1.2B).

Features of the DNA double helix:

- Two DNA strands form a helical spiral, winding around a helix axis in a right handed spiral.
- The two polynucleotide chains run in opposite directions.
- The sugar-phosphate backbones of the two DNA strands wind around the helix axis like the railings of a spiral staircase.
- The bases of the individual nucleotides are on the inside of the helix, stacked on top of each other like the steps of a spiral staircase.

The helix axis is most apparent from a view directly down the axis. The sugar-phosphate backbone is on the outside of the helix where the polar phosphate groups (red and yellow atoms) can interact with the polar environment (Figure 1.3). The nitrogen (blue atoms) containing bases are inside, stacking perpendicular to the helix axis.

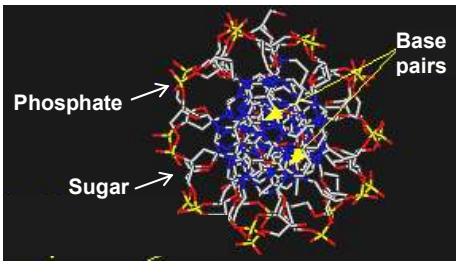

Figure 1.3: View down the helix axis.[25]

In 1953, James Watson and Francis Crick deduced the three-dimensional structure of DNA and immediately inferred its mechanism of replication. The important features of their model of DNA are [24, 26]:

- Two helical polynucleotide chains are coiled around a common axis.
- The purine and pyrimidine bases are on the inside of the helix, whereas the phosphate and deoxyribose units are on the outside.
- The diameter of the helix is 20 Å. Adjacent bases are separated by 3.4 Å along the helix axis and related by a rotation of 36 °. Hence, the helical structure repeats after ten residues on each chains; that is, at an interval of 34 Å.
- The two chains are held together by hydrogen bonds between pairs of bases. Adenine is always paired with thymine. Guanine is always paired with cytosine.
- The sequence of bases along a polynucleotide chain is not restricted in any way. The precise sequence of bases carries the genetic information.

The most important aspect of the DNA double helix is the specificity of the pairing of bases. Watson and Crick deduced that adenine must pair with thymine, and guanine with cytosine, because of steric and hydrogen-bonding factors.

1.2.2 Melting and hybridisation of DNA

The two strands of a DNA helix readily come apart when the hydrogen bonds between its paired bases are disrupted. This can be accomplished by heating a solution of DNA or adding acid or alkali to ionise its bases. The unwinding of the double helix is called "melting" because it occurs abruptly at a certain temperature. The melting temperature (T_m) is defined as the temperature at which half of the helical structure is lost. The melting of DNA is readily monitored by measuring its absorbance of light at a wavelength of 260 nm as shown Figure 1.4. The unstacking of the base pairs results in increased absorbance, an effect called hyperchromism.

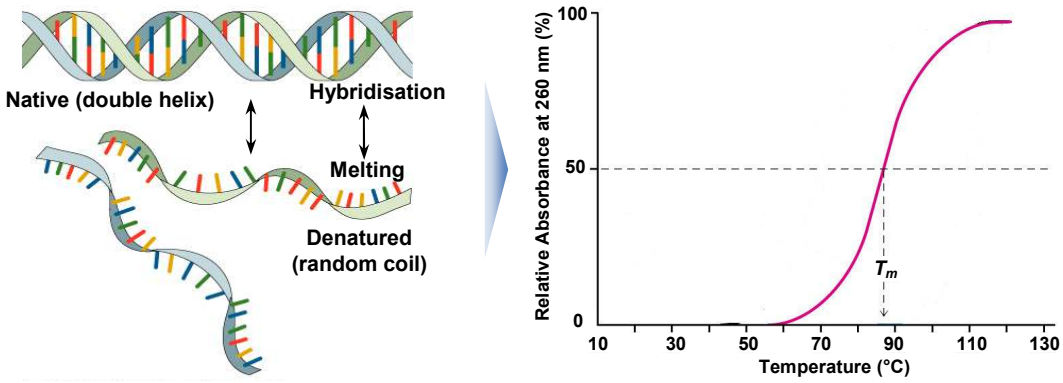

Figure 1.4: An example of a DNA melting curve.[27]

The melting temperature of a DNA molecule depends markedly on its base composition. DNA molecules rich in GC pairs have a higher T_m than those having an abundance of

AT base pairs. GC base pairs are more stable than AT pairs because their bases are held together by three hydrogen bonds rather than by two. Separated complementary strands of DNA spontaneously reassociate to form a double helix when the temperature is lowered below T_m. This renaturation process is sometimes called "annealing" or "hybridisation". The facility with which double helices can be melted and then reassociated is crucial for the biological function of DNA. The main factors affecting T_m are salt concentration, DNA concentration, the presence of denaturants (formamide or dimethylsulfoxide), DNA sequence, and length. Counter-ion identity, modifications (biotin, fluorescent dyes, etc.), solvation effects, and impurities may also affect the T_m. Oligo-modifications tend to decrease the T_m. The magnitude of the decrease depends on the location of the modification (internal being more destabilizing than terminal), and on the overall T_m of the unmodified sequence.

In this thesis we have calculated the values of T_m using the IDT Oligo Analyzer of Integrated DNA Technologies (IDT).[28] This calculator uses the following equation for salt correction for DNA, which was introduced by Owczary *et al.*[29]

$$\frac{1}{T_m(Na^+)} = \frac{1}{T_m(1M)} + (4.29 \cdot f(GC) - 3.95) \times 10^{-5} \cdot \ln[Na^+] + 9.40 \times 10^{-6} \cdot (\ln[Na^+])^2 \quad [1]$$

where T_m (1M) is the melting temperature (°C) in 1 M sodium ion (Na^+), $f(GC)$ is the fraction of GC pairs in the DNA and [Na^+] is the molar concentration of Na^+ in the DNA solution. The program provides the most accurate estimate of T_m with the average error of ± 2 °C.[29]

1.3 Surfactants

1.3.1 Introduction

The word surfactant is a diminutive form of the phrase SURFace ACTive AgeNT. Surfactants are materials that tend to accumulate at surfaces and aggregate in solution. The surfactant molecules consist of a hydrophobic moiety, usually called the tail-group, attached to a hydrophilic moiety, called the headgroup as shown in Figure 1.5.

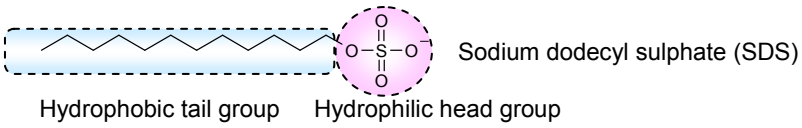

Figure 1.5: Schematic illustration of a typical surfactant molecule.

1.3.2 Types of surfactants

An enormous variety of surfactant structures are available but the following represents some of the major classes of commercial importance. The headgroup is either strongly polar or charged. Surfactants are classified into four groups corresponding to the head group charge.

- Anionics.
- Cationics.
- Zwitterionics.
- Non-ionics.

Differences in the nature of the hydrophobic groups are usually less pronounced than in the nature of hydrophilic groups. Generally, they are long-chain hydrocarbon residues. However, they include such different structures as:

- Straight alkyl chain containing around C_6 to C_{20} groups
- Branched alkyl chain containing around C_6 to C_{20} groups
- Long chain (C_8 to C_{15}) alkyl phenyl groups
- Alkylnaphthalenes and fluoroalkyl groups

Surfactants are also differentiated based on their molecular architectures (Figure 1.6). Beside conventional surfactants with one polar headgroup and one nonpolar tail group, dimeric and oligomeric surfactants have attracted considerable interest in academia and industry. For example, Gemini surfactants are made up of two amphiphilic moieties connected closely to the headgroup by a spacer group whereas, in bolaform surfactants, the connection is close to the end, so that they can be considered as two polar head groups connected by a long hydrophobic chain. In a polymeric surfactant each monomer unit is amphiphilic.

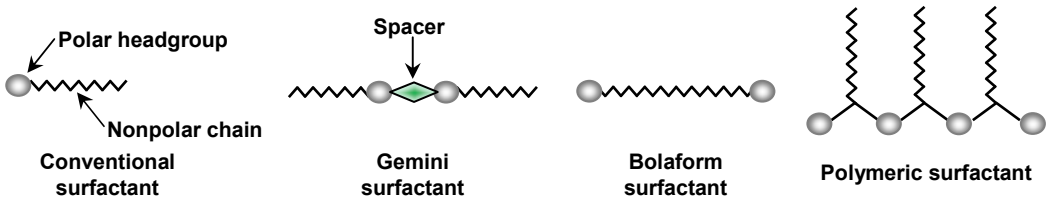

Figure 1.6: Typical examples of the architectures of surfactant molecules.

For example, a type of polymeric surfactant, called a block copolymer, consists of at least two parts. If one part is made of a polar monomer type A, the other part is made of a nonpolar monomer B, the block copolymer will be strongly surface active and show many properties similar to that of a conventional surfactant. If there are two different

blocks it will be called a diblock copolymer. In this thesis we concentrate on conventional and polymeric surfactants.

1.3.3 Surfactant adsorption at interfaces

The amphiphilic nature of a surfactant molecule results in unique phenomena when it is placed in solution, for instance in water. The hydrophilic part of the surfactant molecule has a strong preference for remaining in an aqueous environment and the hydrophobic part favours leaving the aqueous phase. This leads to adsorption at the water-air (or water-oil) interface where the surfactant molecules can orient itself in an energetically favourable configuration, where the hydrophilic head group is in the aqueous phase and the hydrophobic tail group is in the air (oil) phase. This adsorption at an interface is a dynamic equilibrium. The rate at which surfactant molecules arrive at the interface from either adjoining phase is equal to the rate at which molecules leave.

Surface tension is defined as the reversible work required forming a unit area of surface at constant temperature, pressure and composition and it is related to the excess energy of molecules located at the interface. The thermodynamic relationship between quantity adsorbed per unit area and the change in surface tension was first derived in 1878 by J. Willard Gibbs.[30] At constant temperature and pressure we can write for a surface phase:

$$-\,d\gamma = \sum \Gamma_i \, d\mu_i \qquad [2]$$

which relates the change in surface tension γ ($d\gamma$) brought about by changes in chemical potential, μ_i, for all species i, where Γ_i is the number of moles of i per unit area in excess over the same layer thickness in bulk (surface excess concentration). For a solution with only two components, a solvent (1) and an uncharged surface active solute (2)

$$-\,d\gamma = \Gamma_1 d\mu_1 + \Gamma_2 d\mu_2 \qquad [3]$$

The convention chosen by Gibbs was to define the position of the interface such that the surface excess concentration of the solvent Γ_1 is equal to zero. Equation [3] then becomes:

$$-\,d\gamma = \Gamma_2 d\mu_2 \qquad [4]$$

Therefore, the surface tension at the interface is lowered with the presence of a surfactant which absorbs. However for changes in surfactant concentration,

$$d\mu_2 = RT \cdot d\ln a_2 \qquad [5]$$

where R is the gas constant, T is the absolute temperature and a_2 is the activity of component 2 (i.e. surfactant) in solution. So combining equation [4] and [5] gives

$$\Gamma_2 = -(1/RT)\cdot(d\gamma/d\ln a_2) \quad [6]$$

If a dilute surfactant solution is considered, such that the activity of the solute, a_2 can be approximated to the concentration c_2

$$\Gamma_2 \approx -(1/RT)\cdot(d\gamma/d\ln c_2) \quad [7]$$

This is the most commonly used form of the Gibbs adsorption equation. In order to derive equation [7] from equation [2], it has been assumed that the surfactant is a single component, that a dividing surface can be defined for which the surface excess of solvent is zero and the activity of surfactant molecules is equal to the concentration. Figure 1.7 shows how equation [7] is used to determine adsorption of surfactant at an interface.

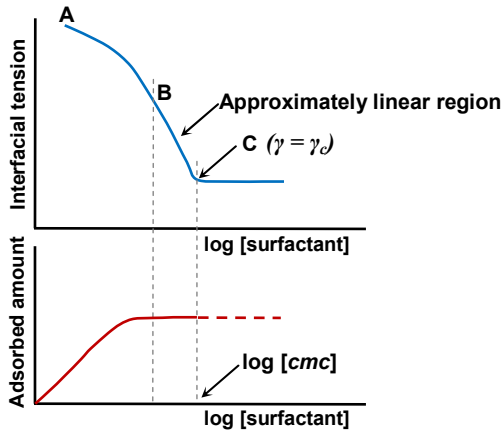

Figure 1.7: Use of the Gibbs equation to determine interfacial adsorption from the variation of interfacial tension with concentration.[31]

In the region from A to B, the surface tension curve falls in a regular manner with a gradually increasing negative slope. This corresponds to a gradual increase in the surface excess of surfactant. For most surfactants a region exists where the graph of γ against $\ln c_2$ is approximately linear. Therefore, according to the equation [7], in this region, the surface excess concentration remains approximately constant. Because the surface excess concentration Γ is expressed in units of moles per unit area, the area per adsorbed surfactant molecule at the interface can be calculated by taking the reciprocal of Γ. Table 1.1 shows some typical values of the minimum area per adsorbed surfactant molecule at the air-water interface for various surfactants derived using the Gibbs equation and surface tension data.[31]

Table 1.1: Some approximate values for the area per molecule of surfactants at the air-water interface at 25 °C determined from tension data using the Gibbs equation[31]

Surfactant	Minimum area per molecule (nm^2)
$C_{12}H_{25}SO_4Na$	0.41
$C_{12}H_{25}N(CH_3)_3Br$	0.56
$C_{12}H_{25}N(CH_3)_2CH_2CO_2$	0.57
$C_{10}H_{21}(OCH_2CH_2)_4OH$	0.41
$C_{12}H_{25}(OCH_2CH_2)_4OH$	0.49
$C_{12}H_{25}(OCH_2CH_2)_6OH$	0.58
$C_{12}H_{25}(OCH_2CH_2)_9OH$	0.62
$C_{16}H_{33}(OCH_2CH_2)_{12}OH$	0.58

1.3.4 Surfactant self-aggregation in water

Surfactants spontaneously aggregate in water and form well-defined structures such as spherical micelles, cylinders, bilayers etc. This spontaneous aggregation of surfactant molecules occurs at a defined concentration, the critical micelle concentration (cmc). Above the cmc, the hydrophobic chains of the surfactants gather inside the aggregate and the polar head groups orient towards the aqueous phase. The result is a spherical object of typically 30–100 surfactant molecules with an oily environment inside as shown in Figure 1.8.

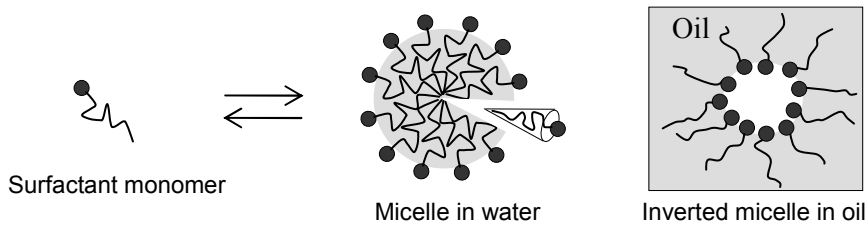

Figure 1.8: Schematic cross-section through a spherical micelle in water. A shell of polar head groups surrounds the hydrophobic core formed by the hydrocarbon chains. The micellar structure is in equilibrium with monomers in solution.

A micelle contains a certain number of surfactant molecules, the mean micellar aggregation number (N_{agg}). Not all micelles are constituted by precisely the same number of surfactants. With increasing concentration of surfactant, the mean aggregation number generally increases with increasing total concentration. Surfactants not only aggregate in spherical micelles but also form cylindrical micelles, bilayers, inverted micelles, etc. The type of aggregate structure formed depends on different factors. An important factor is the so-called surfactant parameter, also referred to as the packing ratio.[32]

$$N_s = \frac{V_C}{L_C \sigma_A} \qquad [8]$$

where V_C is the volume of the hydrophobic part of the surfactant, L_C is the length of the hydrocarbon chains, and σ_A is the effective area per head group. For ionic surfactants σ_A depends on both the electrolyte and the surfactant concentration. The surfactant parameter relates the geometry of the molecule to the preferred curvature of the aggregates formed. Small values of N_s imply highly curved aggregates. Figure 1.9 shows the surfactant parameters of simple geometric objects. For a cone of height L_C and a surface area σ_A the surfactant parameter, N_s is 1/3. For a wedge of height L_C and a surface area σ_A it is 0.5 and for a cylinder it is 1.[33]

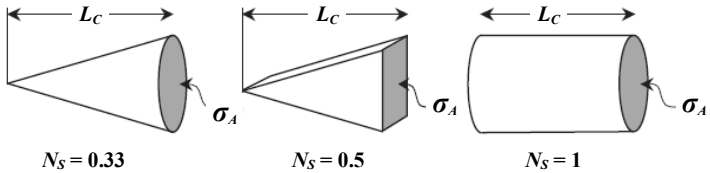

Figure 1.9: Surfactant parameters for a cone, a wedge and a cylinder.[33]

Spherical micelles are formed for $N_S \leq 0.33$. For SDS ($N_S = 0.36$), which tends to form spherical micelles in water, the aggregation number is 56 and the radius of the hydrophobic interior, which is roughly equal to L_C, is 1.7 nm. The effective head group area is 0.62 nm^2. This is significantly larger than the actual cross-sectional area of a sulfate group of 0.27 nm^2 because the effective head group area σ_A is determined by two opposing effects: hydrophobic attraction and later repulsion between head groups. Most ionic surfactants form micelles at low salt concentrations because the electrostatic repulsion leads to large head group areas. With increasing salt concentration the surfactant parameter increases and other structures are formed as shown Figure 1.10.

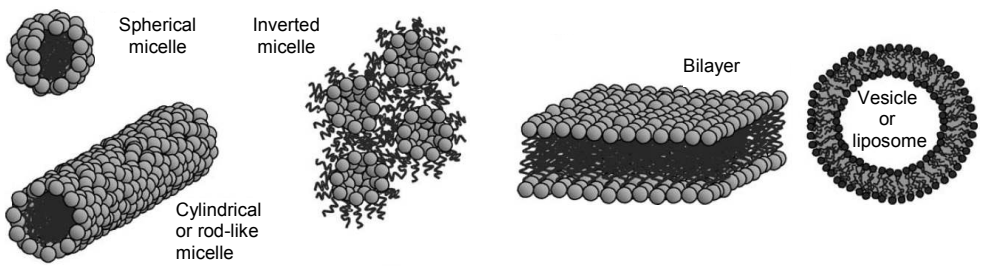

Figure 1.10: Aggregates formed by surfactants.[33]

Rod-like cylindrical micelles are formed when $N_S \approx 0.5$ and the cylinders often form into a hexagonal liquid crystal phase at high surfactant concentrations. Single-chained surfactants with charged head groups, such as SDS, at high salt concentration are in this

category. Bilayers are preferentially formed for N_S = 0.5–1.0. Biological lipids that form bilayers cannot pack into micellar or cylindrical structures because of their small head group area and their too bulky alkyl chains. Lipids with surfactant parameters slightly below 1 tend to form flexible bilayers or vesicles. Lipids with N_S = 1 form planar bilayers and lamellar structures at high concentration. A lamellar phase consists of stacks of roughly parallel planar bilayers.

1.3.5 DNA-surfactants

DNA is not only an important biological material, but also an interesting anionic polyelectrolyte with a double helical rod-like structure. Recent research on DNA reveals that DNA can act as a good template or as a component in future nanodevices[34] and also serve as a good component to fabricate higher-order or hierarchical DNA-based molecular assemblies.[35, 36] By using self-assembled monolayers and DNA surface immobilisation, some groups have investigated DNA hybridisation,[37] DNA microarrays[38] or orientation control of DNA[39]. It is also possible to synthesise DNA-surfactants consisting of a hydrophobic tail and DNA head, which are capable of surfactant-like adsorption and aggregation in addition to DNA-DNA recognition.[11,12,40,41]

The DNA-surfactant is an amphiphilic molecule composed of a large hydrophobic group (e.g., cholesteryl- and saturated dodecyl ($C_{12}H_{24}$-O) tail groups) covalently attached to one end (3´- or 5´-) of a short, synthetic oligonucleotide that is a negatively charged hydrophilic group as shown Figure 1.11A.

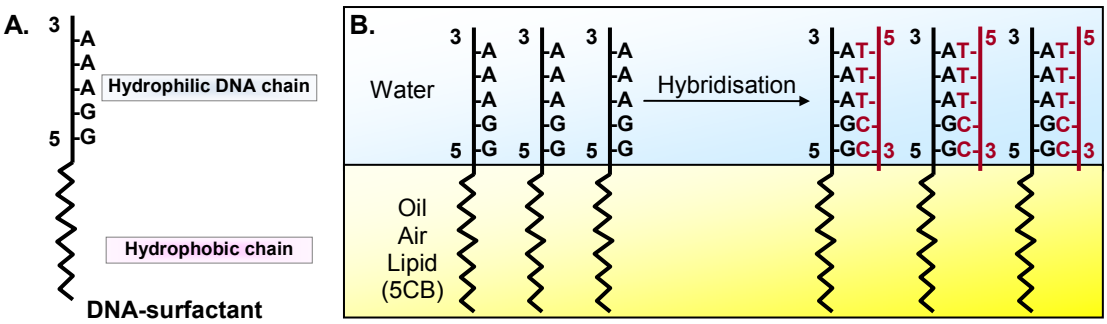

Figure 1.11: Schematic representation of the concept of the DNA-surfactants and their properties. (A) The DNA-surfactants can adsorb at various liquid surfaces, including the air-water and oil-water interfaces as well as lipid bilayers. (B) The Watson-Crick interaction between DNA-surfactant monolayers adsorbed at liquid surfaces or lipid bilayers can lead to specific programmable interactions between fluid surfaces.

1.3.5.1 Surface properties of DNA-surfactant

DNA-surfactant is surface active and reduces the interfacial tension of the dodecane-water interface using Krüss drop shape analysis tensiometry (Figure 1.12A). Figure 1.12B shows the decane-water interfacial tension isotherm for the palindromic DNA-surfactant cholesteryl -5'-AAAAAATTTTTT-3'. The cmc of the same cholesteryl DNA-surfactant was determined by tensiometric measurement to be about 6 μM in pure water without the presence of added background electrolyte by tensiometric measurement.[41]

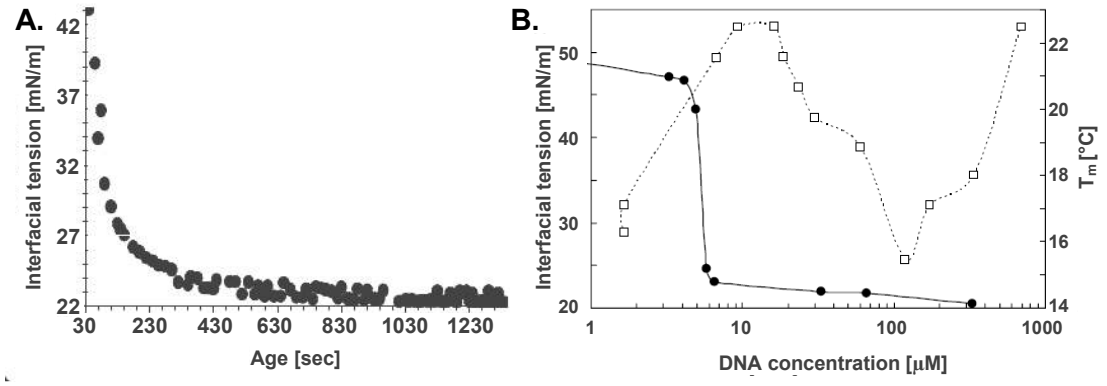

Figure 1.12: (A) Dodecane-water interfacial tension versus time for an aqueous solution containing 68.5 μM of cholesteryl-5'-AAAAAATTTTTT-3' at 20 °C. (B) Interfacial tension isotherm of cholesteryl-5'-AAAAAATTTTTT-3' at the decane-water interface at 20 °C. The right handed side axis gives the melting temperature of the palindromic DNA-surfactant in bulk of the solution (open square symbol). The lines are guides to the eye. Data are from Ref.41.

For palindromic DNA-surfactants, there is an interesting interplay between DNA-DNA hybridisation and micellisation as the DNA melting temperature (T_m) at which the double strand forms, overlaps with the cmc (Figure 1.12B). However, it is not determined yet that the sharp drop in the interfacial tension at the cmc (6 μM) is caused due to the micelle formation of a surfactant with nominally 12 negative charges per molecule or hybridisation of palindromic DNA-surfactants in bulk of the solution which produces dimers of higher surface activity than monomers.

Saturated dodecyl modified DNA-surfactants were also surface active similar to cholesteryl DNA-surfactants. All DNA-surfactants do not lead to large reductions of the surface free energy of the system and this might be due to strong electrostatic effects at high surface concentrations.

1.3.5.2 Self-recognition between DNA-surfactant monolayers

Hybridisation of single strands of DNA to their complementary sequences is the essence of the DNA chip and the DNA microarray. The DNA-surfactant remains adsorbed at the oil-water interface upon hybridisation with complementary DNA chain. Similarly, complementary DNA-surfactants can be used to functionalise fluid surfaces and program the interactions between them based on Watson-Crick pairing. For the short base sequences used, internal hairpin formation is not expected to occur. By selecting the appropriate DNA base sequences, the interaction between the fluid surfaces functionalised with DNA-surfactants can be programmed with the level of specificity of the enzyme-substrate interaction (Figure 1.13).[11,12,40]

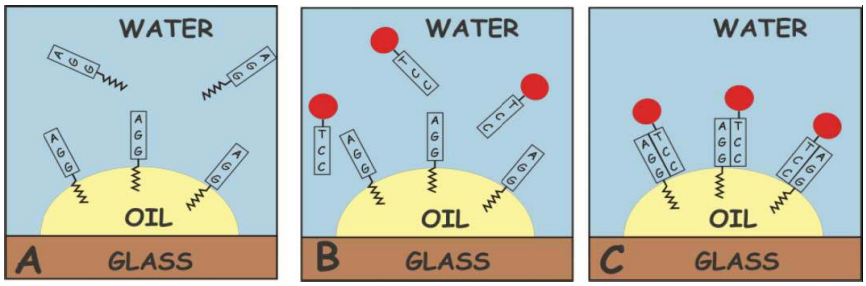

Figure 1.13: Schematic of the hybridisation achieved with DNA-surfactants. (A) An oil drop deposited on a glass slide under water is exposed to a solution of DNA-surfactant. (B) The solution is replaced with a solution of complementary fluorescently tagged DNA which can hybridise with the DNA-surfactant monolayer (C) adsorbed at the oil-water interface.[12]

1.3.6 Polymerisable surfactants

At the forefront of nanotechnology, organized self-assembled surfactant phases have received a lot of attention as possible reaction and templating media. Surfactant molecules can self-assemble into a variety of objects such as micelles, rod like structures, vesicles, or a lamellar phase[42], depending on the surfactant structures.[43] However, due to their dynamic nature, conventional surfactant structures have limited integrity, therefore limited application of individual particles.[44]

Polymerisable surfactants, on the other hand, offer potential for developing hybrid nanosized reaction and templating media with constrained geometries. Among other parameters, polymerisable surfactant composition and molecular structure play an extremely important role in the polymerisation process, and essentially govern the final properties of the polymer.

The polymerisable surfactants used in this study contain a polymerisable group such as a methacrylate group in the surfactant molecules and, once polymerised, are very difficult to be desorbed from the interface because the cross-linked network can be formed between surfactant molecules by polymerisation. [45] Additionally, the polymerisable surfactant can be polymerised with an added cross-linker to form an integrated polymeric material, which can be used to further modify the polymeric properties.

This section describes some common features of polymerisable surfactants and the separate steps involved in their polymerisation via free radicals.

1.3.6.1 Monomer structures of polymerisable surfactants

To design a polymerisable surfactant, a simple and versatile way is to use an ionic surfactant with a polymerisable counterion. In the literature, there are many examples of cationic surfactants with anionic polymerisable counterions [46] such as acrylate, methacrylate, and vinyl or divinylbenzoate and fewer concerning anionic surfactants with cationic polymerisable counterions.[47] The molecular architecture can be varied in many respects with respect to the polymer geometry, the nature of polymer backbone and the incorporation of spacer groups controlling the distance of the surfactant fragments from the polymer backbone. The reactive polymerisable group can be placed at the end of hydrophobic tail (T-type), in the middle of hydrophobic tail, or neat the hydrophilic head group (H-type), as illustrted in Figure 1.14.

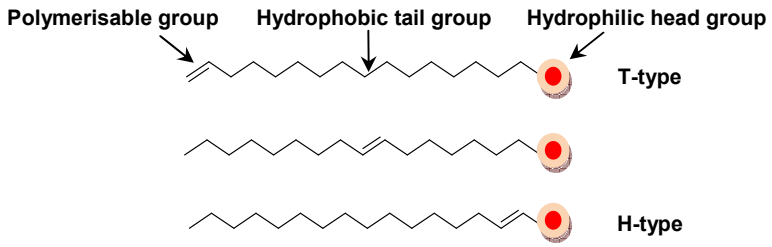

Figure 1.14: Examples of positions of reactive polymerisable group within polymerisable surfactants.

1.3.6.2 Initiators for polymerisation

A variety of chain initiators can be used to start the polymerisation. Several methods of producing free radical initiators are possible and include thermal decomposition, redox reactions, ionising radiation and photolysis.

The choice of initiator types depends on the polymerisable species and desired polymer structures.

(i) thermal decomposition (e.g., benzoyl peroxide)

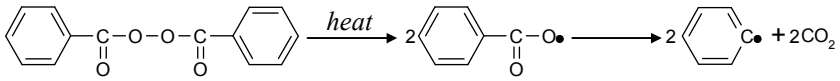

(ii) redox reaction

A radical is produced by the reduction of one species in its reaction with a reducing agnet to yield a free radical. For example, the addition of a ferrous ion (Fe^{2+}) salt to hydrogen peroxide results in oxidization of the ferrous ion (Fe^{2+}) to ferric ion (Fe^{3+}) and reduction of the peroxide to an OH^- ion and a free radical $OH^\bullet$.

$$H_2O_2 + Fe^{2+} \rightarrow Fe^{3+} + OH^- + OH^\bullet$$

(iii) ionising radiation

High energy particles (e.g., α or β) or electromagnetic (e.g., γ or X-rays) radiation can be used to produce radicals in a three stage process involving ejection of an electron from an initiator molecule followed by dissociation of the initiator and electron capture of the polymerisable material to produce a propagating radical molecule.

- Ejection: $C \sim\!\!\rightarrow C^\bullet + e^-$
- Dissocitation: $C^+ \rightarrow A^\bullet + Q^\bullet$
- e^--capture: $Q^+ + e^- \rightarrow Q^\bullet$

(iv) photolysis

This method involves the irradiation of an initiator molecule, which decomposes to form two radical containing molecules using UV, which then initiates the polymerisation reaction (e.g., photolysis of azobisisobutyronitrile (AIBN)).[50]

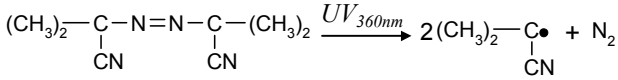

Photo-polymerisation is an efficient process in which liquid monomer is converted to polymer via a photoinitiated process. To date, photo-polymerisation has been used primarily to induce curing of thin coatings and adhesives.[48] Photo-polymerisation have been mainly used in this thesis because the other methods require either inconvenient reaction conditions or the presence of highly reactive species that would disturb the liquid crystal (LC)-water interface to a significant extent and may prevent the microstructure of the LC-water interface from being retained during the

polymerisation process. For example, a UV photoinitiator, 2-hydroxy-2-methyl-1-phenyl-1-propanone (Darocur 1173, Ciba Fine Chemicals) has been mainly used for the polymerisation of polymerisable surfactants and for hydrogel synthesis because water-soluble chemical initiators (e.g., potassium persulfate) usually require heating above 70 °C for thermal polymerisation otherwise 5CB transits from nematic to isotropic phase at ~36 °C. Darocur 1173 is a highly efficient liquid photoinitiator that is used to initiate the photo-induced radical polymerisation of chemically unsaturated hydrocarbon or surfactants with polymerisable groups (Figure 1.15). It belongs to the class of type *I* photoinitiators which undergo a unimolecular bond cleavage upon irradiation to yield free radicals (i.e. intramolecular cleavage).[49]

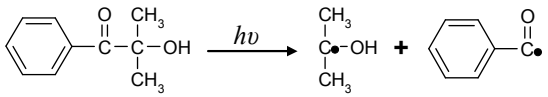

Figure 1.15: Photolysis of Darocur 1173.

On the other hand, type *II* photoinitiators undergo a bimolecular reaction where the excited state of the photo-initiator interacts with a second molecule (e.g., a co-initiator) to generate free radicals (i.e. intermolecular cleavage).

1.3.6.3 Mechanism of polymerisation

There are some important factors to consider in a free-radical polymerisation. First, the monomer(s) does not ainticipate in any reaction at ambient temperature. Second, it needs an initial energy input, either heat or light, to produce radicals that initiate polymerisation and propagate to produce a high level of polymerisation before termination. The conversion of monomer to polymer is highly exothermic, inducing a self-propagating thermal wave or reaction. Polymerisation by free radical addition can be seperarted into three distinct stages as follows.[50]

(i) Initiation

As described above, the polymerisation reaction is initiated by a source of radicals produced according to necessary reaction conditions. Usually, the initiator molecules (I) should be chosen that they do not to interfere with any equilibrium which is described to be maintained during the polymerisation reactions. The initiator radical ($I^{\bullet}$) reacts with a polymerisable monomer (M) to form a monomer radical ($IM^{\bullet}$). Once this initial source of free radicals has been produced, the

polymerisation chain reaction should sustain itself. Photo-initiation is used as an example below:

$$I \xrightarrow{h\upsilon} I^{\bullet} \quad ; \quad I^{\bullet} + M \rightarrow IM^{\bullet}$$

(ii) Propagation

The monomer radical then reacts with a second polymerisable monomer to form a dimer radical ($IM_2^{\bullet}$). This chain propagation proceeds by addition, forming a polymer chain. This chain reaction can lead to polymers containing over 1,000 units, so the presence of the initiator molecule at the chain end has little or no consequence to the overall polymer structure.

$$(IM^{\bullet} + M_1 \rightarrow IM_2^{\bullet})_n \rightarrow IM_n^{\bullet}$$

This continues until a termination reaction occurs.

(iii) Termination

The chain propagation reactions of a single growing polymer chain in radical addition polymerisation is terminated long before all the reactive monomer in solution is used up by the growing polymer chain. This is a result of the high reactivity of radical species which quickly react to form inactive covalent bonds. Several termination reactions are possible: (a) the combination of two growing chain ends, (b) the combination of a growing polymer chain end and an active initiator radical, (c) transfer of the active centre to the solvent, or (d) interaction of the radicals with inhibitors (e.g., oxygen). The length of the final polymer chain is inversely proportional to the concentration of active radical species present in a particular system[50] due to the increased rate of termination reactions. Hence low concentrations of initiator are necessary to produce long polymer chains.

Typically the polymer formed has the same chemical composition as the monomer, *i.e.* each unit in the chain is a complete monomer and not a residue as in most step growth reactions.

1.4 Nematic liquid crystals (LCs)

The experimental system that is the focus of the chapter 3 and 4 is a simple and broadly useful system for the study of adsorption and association of surfactants based on the orientational behaviour of a thermotropic liquid crystal (LC).

1.4.1 Introduction

LCs represent a class of materials which are characterised by a level of order and mobility that is intermediate between that of crystalline solids and isotropic liquids (Figure 1.16). Small organic molecules (e.g., cyanobiphenyls) that exhibit liquid crystallinity in the absence of solvent phases are described as thermotropic LCs in acknowledgement of their temperature-dependent phase properties (Figure 1.16A). In the simple LC phase, one molecular axis tends to point along a preferred direction as the molecules undergo diffusion. This preferred direction is called the director and is denoted by the unit vector ***n*** **(**Figure 1.16B).

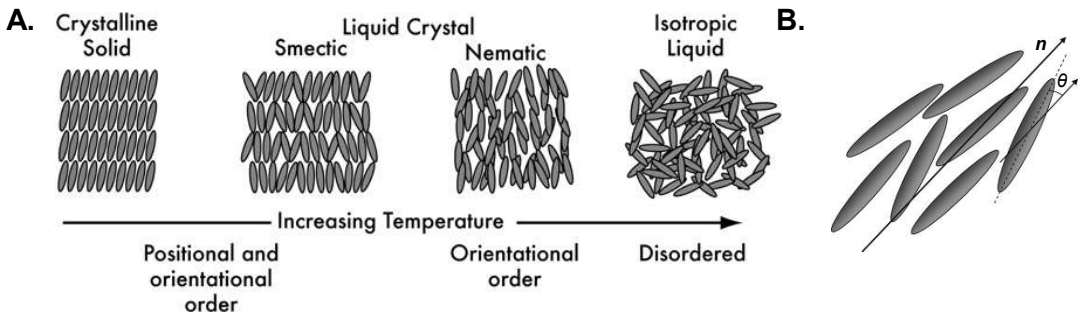

Figure 1.16: Schematic illustration of (A) the molecular-level organisation of solid, liquid crystalline and isotropic liquid phases and (B) the director of a nematic liquid crystal.[7]

Anchoring orients the LC director at the boundary of interest and is defined by two angles: zenithal (θ) and azimuthal (ϕ) (Figure 1.17). The zenithal angle may be planar (director aligned parallel to the interface), homeotropic (director aligned perpendicular to the interface), or tilted (director aligned at an intermediate angle). The angle is commonly defined as 0 ° for homeotropic and 90 ° for planar alignment.

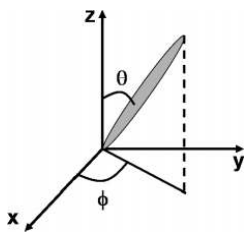

Figure 1.17: Zenithal angle, θ, is the angle between the LC director and the *z*-axis. Azimuthal angle, ϕ, is the angle between the director projection on the *x*-*y* plane and the *x*-axis.[7]

The optical anisotropy of a nematic LC molecule creates a difference in the refractive indices of light polarised parallel and perpendicular to the molecular director called birefringence. When viewed between a set of crossed polarisers, birefringence in the

plane of polarisation results in the transmission of light which is determined by thickness of the LC layer and the average zenithal angle of the LC director. In this thesis we focus on thermotropic nematic LCs that are immiscible with aqueous phases and possess long-range orientational order but no long-range positional order at ambient temperature (i.e. nematic phase) (Figure 1.17). A range of molecules (e.g., surfactants, lipids, polymers) dissolved in an aqueous phase can assemble at an interface defined by the immiscible LC and the aqueous phase.

We describe four important properties of thermotropic LCs that are required to understand their orientational behaviour at the interfaces, as described in this thesis.

- Molecules in LCs (mesogen), when placed into contact with a confining medium (e.g., solid, vapour, immiscible liquid), will tend to order in ways that reflect interactions defined by the chemistry and geometry of the interfacial region called the anchoring of LC by interfaces. The surface induced ordering of LCs typically extends over a distance of ~100 μm from interfaces and is direct consequences of the long-range orientational ordering of molecules within the liquid crystalline state.
- The degree of alignment is quantified by an orientational order parameter, S, that is defined as the average of the second Legendre polynomial[52]:

$$S = \langle P_2(\cos\theta) \rangle = \left\langle \frac{3\cos^2\theta - 1}{2} \right\rangle \qquad [9]$$

  where θ is the angle between the axis of a particular moelcule and director $\boldsymbol{n}$: S = 0 corresponds to a completely disordered (isotropic) material, and S = 1 describes a perfectly orientationally ordered material. Typical values of S for LCs are 0.3 to 0.8.
- The orientational ordering of LCs near interfaces is remarkably sensitive to the details of the interactions between the mesogens and the confining medium.[1] This surface energy associated with the phenomenon is typically on the order of 10^{-2}–10^{-3} J/m^2 and is referred to as the anchoring energy of LC by interfaces.[51] Thus, subtle changes in the topography and chemical functionality of interfaces will lead to orientational transitions in LCs because mesogens possess liquid-like mobilities.
- Optical anisotropy caused by the preferred orientations of mesogenes within LCs provides a straightforward way to transduce changes in the orientations of bulk LCs into optical signals that are easily read using ambient light and the naked eye.

Many important applications of LCs are governed by their properties in thin films.[52] The thickness of films may exceed hundreds of nanometres or even microns, since the orientational and positional order induced in a LC by a substrate can propagate through many molecular layers. The insertion of LCs into narrow capillaries or the progressive confinement of LC layers between two flat solid substrates further increases the range of film thickness in which surface effects should be appreciated. Extensive studies of anchoring and alignment of LCs by various substrates have been carried out, leading to the acquisition of comprehensive body of empirical knowledge to date.[53,54].

1.4.2 Liquid crystal 4-cyano-4´-pentylbiphenyl (5CB)

The experiments in the chapter 3 and 4 are based on films of 5CB contacted with an aqueous phase. With increasing temperature, 5CB undergoes a phase transition at 24.0 °C from crystalline to nematic phase (Figure 1.18). At 35.1 °C there is a first-order phase transition to an isotropic liquid.[57] The 5CB molecules are partially paired into dimers of 5CB with anti-parallel dipole moments whose length is 25 Å, while the length of the individual molecule is 18.7 Å. [55] The alignment of 5CB at the 5CB-air interface is known to be homeotropic.[56]

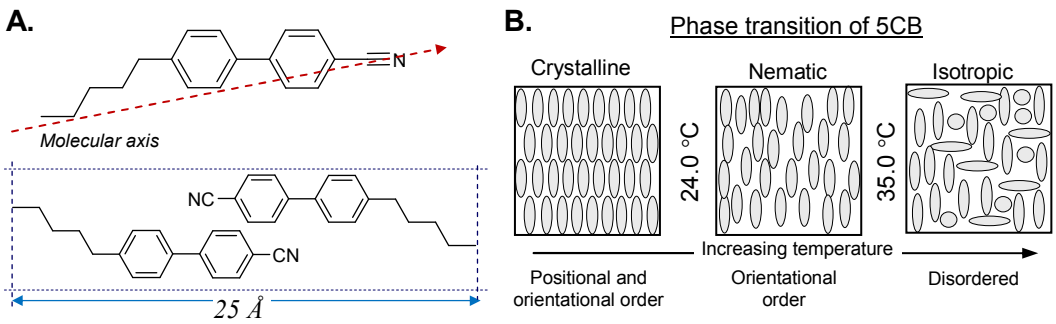

Figure 1.18: (A) Chemical structure of 4-cyano-4'-pentylbiphenyl (5CB) and the alignment of dimers is shown schematically. (B) Schematic illustration of the organisation of 5CB at molecular-level.

The detailed properties of the 5CB are given in Table 1.2.[57]

Table 1.2: Properties of 5CB

T = 21.4°C, λ = 632.8nm		Viscosity η [Pa s] T = 26 °C
n_o	n_c	
1.5287	1.7162	0.03

n_o = the index of refraction parallel to the optical axis of 5CB

n_c = the index of refraction perpendicular to the optical axis of 5CB

While a droplet of 5CB spreads spontaneously at the air-water surface into a ~2 μm thick film with an easily interpreted optical appearance characteristic of planar anchoring at the 5CB-water interface (Figure 1.19A), the presence of SDS in the aqueous phase resulted in the partial dewetting of the LC from the aqueous interface (Figure 1.19B).[58]

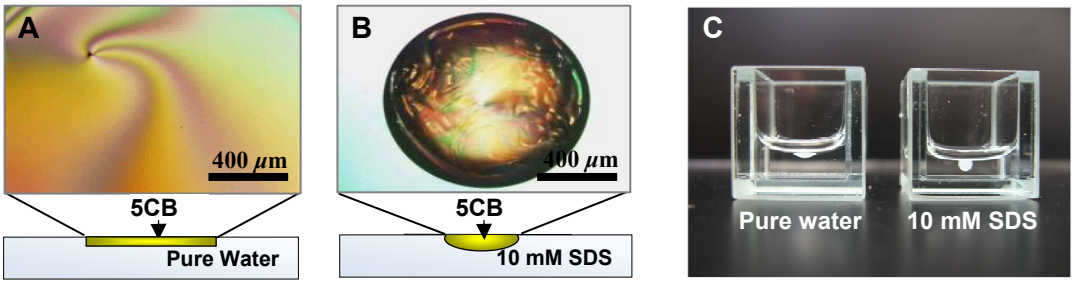

Figure 1.19: Optical images of 5CB between crossed polarisers after depositing it onto the surface of (A) water and (B) water containing 10 mM SDS at room temperature. Optical image C was captured with a digital camera (Cannon IXUS 750) using the same samples for images A and B.

In a previous study,[58] the 5CB confined by an electron microscope (EM) grid (115–292 μm) shows either planar anchoring alignment between alkanethiol ($CH_3(CH_2)_{15}SH$)-treated gold films or homeotropic alignment between octadecyltrichlorosilane (OTS)- treated glass (Figure 1.20).

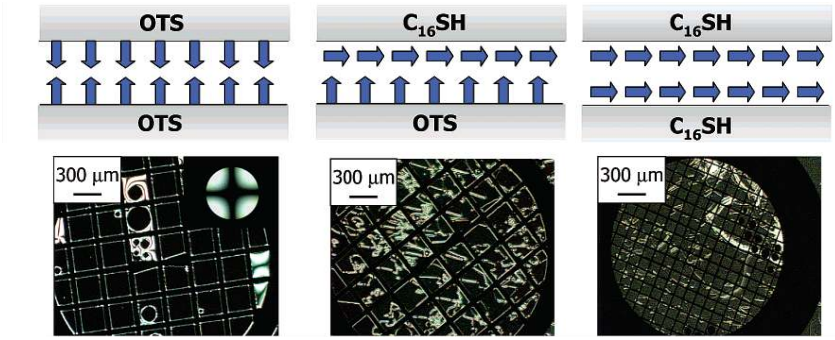

Figure 1.20: Optical images of 5CB confined between glass substrates that were treated to align 5CB in either a planar or homeotropic orientation. The cartoons above the optical images represent the surface treatment and the alignment of 5CB. The bottom row of images corresponds to 5CB confined to copper grids placed between the substrates. In both cases, the thickness of the LC film was held constant at ~20 μm. Optical examination was performed using crossed polarisers.[58]

Moreover, the presence of EM grids on OTS coated glass slides could produce even stable LC film after in contact with an aqueous solution containing SDS. In the next section we describe how this geometry provides an experimental system to observe the adsorption of surfactants at the LC-water interface.

1.4.3 Strategy for inducing of the alignment of LCs by adsorption of surfactants at the 5CB-water interface

The interfacial thermodynamics involving LCs is an active area of research because electrical and mechanical properties are strongly influenced by surface conditions. Because the optical response is a function of orientations, which in turn is a function of surface conditions, nematic LCs have been shown to have unique capabilities to detect surface adsorption events as well as surface topography. Biological, medical, and material applications of LC surface sensor systems have been widely investigated. For example, thin nematic LC crystal films can be an efficient biosensor, able to detect ligand-receptor events on treated solid surfaces.[5] It is widely known that surfaces can preferentially align LCs. The planar interface permits straightforward interpretation of the anchoring of the LCs at the interfaces that result from reversible adsorption phenomena. The approach permits the formation of stable and approximately planar interfaces between a water-immiscible LC and aqueous phase that can be readily exchanged. The change in composition of the aqueous phase makes possible studies of surfactant adsorption as well as desorption. Furthermore, a past study using freely suspended nematic films of 5CB hosted within copper EM grids with spacing of 450 μm reported that nucleation of the nematic phase from the grid surface upon cooling can lead to orientations of the LCs that are strongly influenced by contact with the grids.[59] A number of other authors have reported on the influences of surfactants including SDS and alkyltrimethylammonium bromide (C_nTAB) on the orientations of LCs that possess interfaces with aqueous systems by using emulsions of aqueous solutions and nematic LCs. The stability of the emulsions also depends strongly on the anchoring of the LCs as well as the presence and type of surfactants present. Abbott *et al.*[4,58] reported a simple and elegant experimental system in which nematic LC films of 5CB are confined within copper or gold EM grids and contacted with a supporting silanized glass surface as shown in Figure 1.21. The use of copper grids builds on the report of Nazarenko and Nych who reported observation of nematic phases of 5CB confined to copper grids and in contact with air (not aqueous solutions).[59]

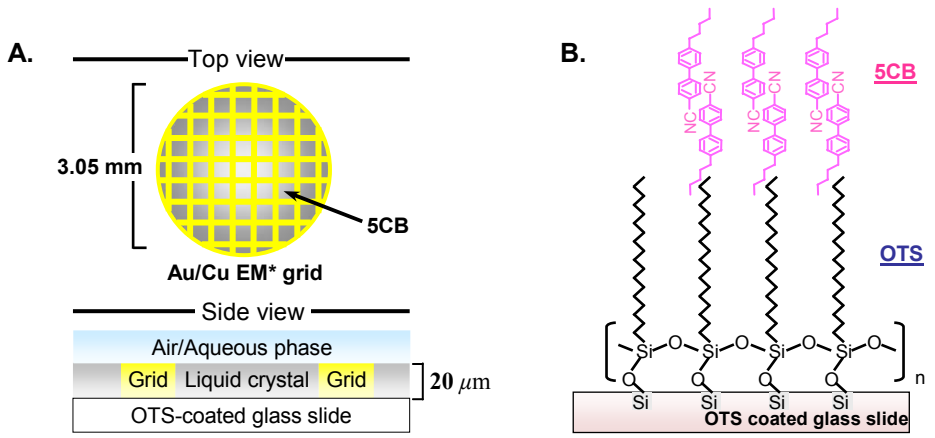

Figure 1.21: Schematic illustration of (A) the experimental geometry used to study the adsorption of surfactants at stable interfaces between aqueous phase and 5CB which is hosted in the pores of an electron microscopy (EM) grid and (B) the alignment of 5CB at a glass slide treated with a self-assembled monolayer of octadecyltrichlorosilane (OTS).

They have also shown that LCs are able to optically detect ionic surfactant adsorption at the LC-water interface through changes in orientation. For example, they studied nematic LC films of 5CB in contact with aqueous solutions of SDS. For a SDS free interface the director 5CB orientation is parallel to the LC-water interface, while for a SDS-laden interface the orientation is perpendicular to the LC-water interface as shown in Figure 1.22.

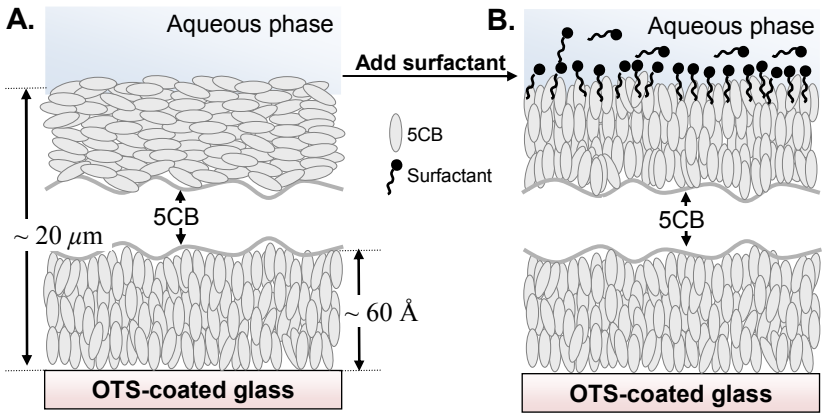

Figure 1.22: Schematic illustration of the alignment of 5CB induced by adsorption of SDS at the LC-aqueous interface: (A) SDS-free interface; (B) SDS-laden interfaces.

As LC films are supported on a grid structure placed over a surface-treated solid substrate, their presence adds additional contributions to the adsorption-driven orientational transition, but the main issue is that SDS adsorption, thus, results in the planar-homeotropic transition. The transition of the alignment of 5CB from planar to

homeotropic can be easily detected under a microscope equipped with crossed polarisers. In Figure 1.23A, the bright optical appearance is the result of the in-plane birefringence of the LC. The colours of the LC which are faint yellow, pink, or green in grids depend on the retardance of the LC, which in turn is a function of thickness of the film of LC as well as its orientation.

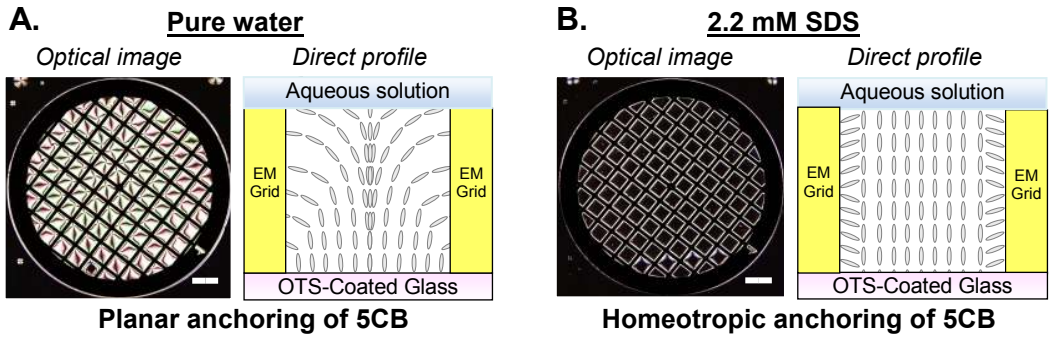

Figure 1.23: Anchoring of 5CB by aqueous solutions of SDS. Optical images between crossed polarisers and schematic side views of the LC optical cells showing the molecular alignment of 5CB immersed under (A) pure water (planar anchoring) or (B) 2.2 mM aqueous solution of SDS (homeotropic anchoring). For the optical images, the scale bars are 400 μm.

1.4.4 Influence of molecular structure of surfactants on orientation of 5CB

Abbott *et al.*[4,7] established criteria for the surfactants that give rise to particular orientations of 5CB by comparing the influence of a series of surfactants (Figure 1.24).

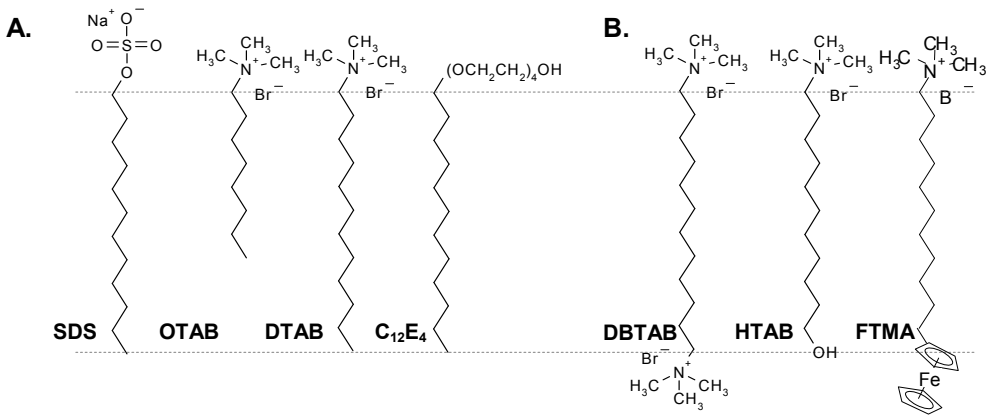

Figure 1.24: Chemical structures of surfactants that adopt tilted configurations (A) and looped configurations (B) at the air-water or oil-water interfaces.

Typical linear surfactants [alkyltrimethylammonium bromides (C_nTABs, n > 8), SDS, and N,N-dimethylferrocenylalkyl ammonium bromides (FC_nABs, n > 12)] that assume tilted orientations at air-water or oil-water interfaces can give rise to a

homeotropic orientation of 5CB at concentrations greater than those associated with the onset of adsorption to the air-water interface. In contrast, Figure 1.25 shows that surfactants that have a bolaform structure [(11-hydroxyundecyl)trimethylammonium bromide (HTAB), dodecyl-1, 12-bis(trimethylammonium bromide) (DBTAB), 11 (ferrocenyl-undecyl)trimethylammonium bromide (FTMA)] and which adopt looped configurations at air-water or oil-water interfaces cause planar anchoring of 5CB.

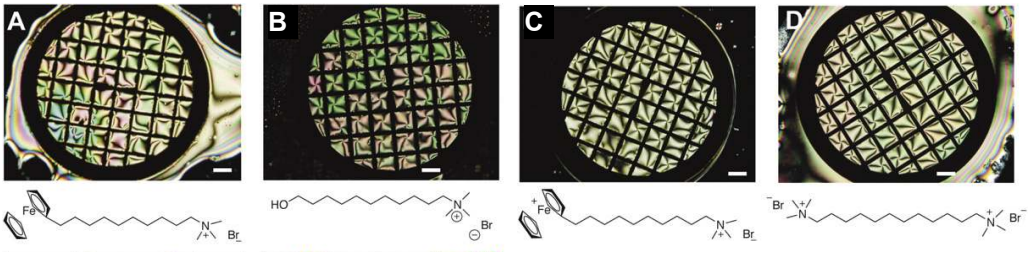

Figure 1.25: Anchoring of 5CB by surfactants that looped configurations at interfaces. Optical images of 5CB between crossed polarisers contacted with aqueous solutions of (A) 0.01 mM FTMA, (B) 10 mM HTAB, (C) 0.01 mM oxidized FTMA, (D) 10 mM DBTAB. All scale bars represent 300 μm. Data are from Ref.7.

By comparing SDS (anionic), dodecyltrimethylammonium bromide (DTAB, cationic), and tetra (ethylene glycol) monododecyl ether ($C_{12}E_4$, non-ionic), the orientations of the 5CB is found not to be strongly dependent on the head group charge (Figure 1.26).

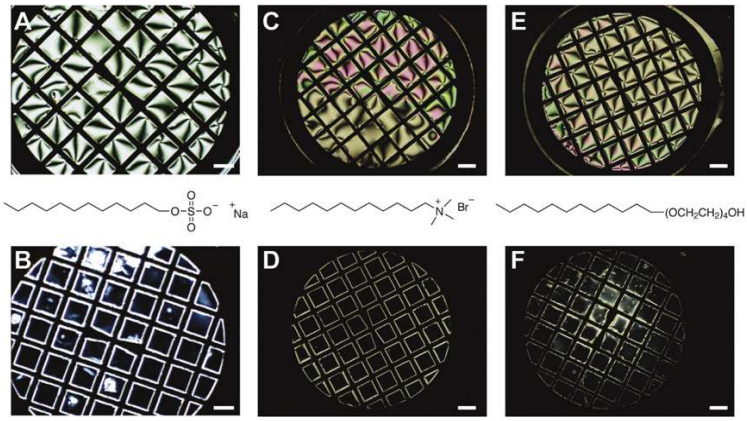

Figure 1.26: Influence of surfactant head group on the anchoring of 5CB. Optical images of 5CB between crossed polarisers hosted in a copper grid and contacted with aqueous solutions of (A) 0.1 mM SDS, (B) 10 mM SDS, (C) 0.1 mM DTAB (C_{12}TAB), (D) 10 mM DTAB, (E) 1 μM $C_{12}E_4$, (F) 100 μM $C_{12}E_4$. All scale bars represent 300 μm. Data are from Ref.7.

The results above suggest that the molecular-level interactions between 5CB and the aliphatic chains of the adsorbed surfactant are more important to the anchoring of

5CB. Figure 1.27 shows the optical textures of 5CB in contact with different concentrations of octyltrimethylammonium bromide (OTAB) and DTAB. The orientation of the 5CB remained planar when contacted with aqueous solutions of OTAB (Figure 1.27A) up to limit of solubilisation of 5CB by OTAB (~300 mM). In contrast to the results with OTAB, the adsorption of DTAB (Figure 1.27B) at the LC-water interface causes the orientation of 5CB to change from planar to homeotropic anchoring, consistent with the observation obtained using SDS and $C_{12}E_4$ (Figure 1.26).

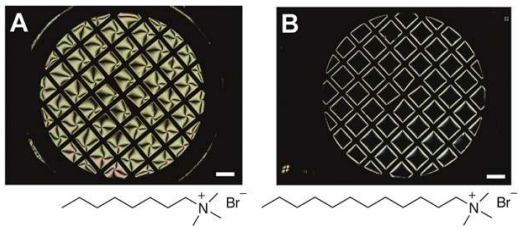

Figure 1.27: Anchoring of 5CB as function of tail length of C_nTAB surfactants. Optical images between crossed polarisers contacted with aqueous solutions (0.1 M Li_2SO_4, pH 2) of (A) 100 mM OTAB (C_8TAB) and (B) 10 mM DTAB (C_{12}TAB). All scale bars represent 300 μm. Data are from Ref.7

Surfactants with short alkyl chains (n = 8 for C_nTAB and n = 12 for FC_nAB), cause the orientation of 5CB to remain planar to the interface up to concentrations at which the 5CB begins to be solubilised by the surfactant. These results support the proposal that interactions between the aliphatic chains of the surfactant and 5CB, which are influenced by the conformations of the tails of the surfactants, largely dictate the orientation of the 5CB.

1.5 Anisotropic colloid particles

Studies on monodisperse colloidal spheres have played a vast role in the development of colloid science in the past century. Some of their more recent functional application such as colloidal crystals for materials of photonic band-gap properties can be found in numerous review papers.[60,61,62] The most studied and best established examples of such colloidal materials have been inorganic silica colloids and polymer latexes.

The first anisotropy which has been observed for colloidal particles is that their shape as commonly found in nature in the form of biological cells, viruses and inorganic mineral particles such as clays, bentonite, aragonite, calcite, etc. Only a few colloidal systems present perfect spherical shapes. Numerous methods for the preparation of colloid particles of non-symmetrical shape have been developed, although the use of

such types of colloid suspensions for the fabrication of new materials presenting novel symmetric or aggregation behaviour is still at an early stage.

1.5.1 Preparation of anisotropic Janus particles

This section describes some of the main techniques which have been reported for the fabrication of solid colloid particles presenting an anisotropic character. As this thesis is concerned with the preparation of anisotropic microparticles with a metal coating layer on a hemisphere of particles, attention is mainly focused on methods capable of fabricating such particles in the micro metre size range.

A traditional goal in colloid and nanoparticle science was to obtain particles that are homogeneous in their chemical composition, and applications of this kind continue to have value in applications such as painting, ceramics, and photonic materials.

Alternatively, one can produce particles whose surface chemical composition differs on two sides of the particle.[63] Anisotropic surface chemical composition, superposed on a homogeneous shape, could introduce asymmetric interactions that induce particles to self-assemble. A vast range of "Janus" materials have been reported in the literature such as dendrimers, LCs,[64] micelles,[65] and solid particles.

The concept of "Janus" colloidal particle was introduced by de Gennes *et al.*[63] on the basis of dissymmetric surface treatment of colloids because Janus is referred to the Roman god Janus who possesses two faces opposite to each other.[63,67] The term "Janus" has now been used as a broader definition of the particle anisotropy which defines any particle presenting two hemispheres of different properties (hydrophilicity, surface coating, materials, etc.) although this term was originally used to define the particles where two hemispheres have different hydrophilicity. Janus-type spherical particles can be used as microrheological probes. With magnetic fields being used to exert force on one side of the particle, Janus type spherical particles can be manipulated by controlled magnetic fields. Janus particles can also be used as potential building blocks for new three-dimensional (3D) self-assembled structures,[66] however this purpose requires a method to produce large quantities of material. In 1988, Casagrande *et al.* first reported the modification of part of the originally hydrophilic surface of glass beads.[67] They prepared microparticles with two different hemispheres of opposite wetting behaviour in which the unprotected part of the particles were treated with octadecyltrichlorosilane. Thus they observed the different contact angles of water depending on the hydrophilic-hydrophobic properties of the particle. Recently, Fujimoto *et al.* developed an

alternative technique to modify part of the surface of particles adsorbed at an interface.[68,69] This method was used to fabricate particles of hydrophilicity gradient using a Langmuir-Blodgett trough to first prepare the particle monolayer and collect it on a glass surface. The trough was also used to compress a polymer monolayer which was then transferred onto the exposed surface of the particles. Modification of particle surfaces at a liquid-liquid interface was also used by Ikeda *et al.*[70] to prepare Janus particles of surface hydrophilicity gradient. Duguet *et al.*[71] prepared Janus particles in which one hemisphere of silica particles were decorated with gold colloids when spread as a monolayer at gas-liquid and gas-solid interfaces. The particles were also partially coated with sputtered gold when spread at the gas-liquid interface. An alternating method of producing colloidal particles of asymmetric coating in micron size range has been reported by Hugonnot *et al.*[72] A strongly focused laser beam was used to generate a different coating on the surface of silica microparticles by micro-photochemical deposition of different metals in a reactive solution. This method appears to be very precise with respect to the control of the degree of anisotropy created. However, it can only produce a restricted number of particles because they have to be individually modified.

Recently, Paunov *et al.* developed a new technique called the "gel trapping technique" (GTT) for the fabrication of anisotropic microparticles with a diameter ranging from several hundred nanometers to several hundred micrometers.[21,73] This technique is based on spreading of the particles (e.g., polystyrene latex or silica microparticles) suspended in alcohol solution as a monolayer on the air-water or oil-water interface and subsequently gelling of the water phase with a nonadsorbing polysaccharide (e.g., gellan). The particle monolayer partially embedded in the surface of the gel is then replicated and lifted up with poly(dimethylsiloxane) (PDMS) elastomer, which allows the particles embedded within the PDMS surface. The specified portion of the particles' surface are sputtered with a thin layer of metal (e.g., gold, chromium) and subsequently the particles were isolated mechanically from the PDMS surface to prepare Janus particles. This method was also extended to print one colloidal monolayer onto another colloidal monolayer, which produces "raspberry"-like supraparticles when the two particle monolayers are of very different size and stable particle doublets when the particles are of comparable size.[74]

1.6 Gels and their properties

Polymers such as proteins, polysaccharides and nucleic acids are present as basic components in living organic systems. Synthetic polymers, which are designed to mimic these biopolymers, have been developed into a very active field due to their industrial and scientific value. They have been progressively developed from the description of the unique properties of biopolymers. In this section, we describe the key properties about the hydrogel and their applications.

1.6.1 Classification of gels

Polymers-solvent mixtures with three-dimensional (3D) network structures, slightly cross-linked to each other, form gels.[75] Because of the cross-linked structure they are insoluble in any solvent, but can swell in a solvent and adsorb a significant fraction (~2000 times the polymer weight) of the solvent within their structure. This property is in contrast to most industrial materials such as metal, ceramics, and plastics, which are dry and hard. A deformed gel, in turn, changes its chemical potential, behaving as an energy transducer. Thus, a polymer gel shows a variety of stimuli-responsive actions, responding to external environmental changes including electrical, thermal, and chemical responses. Gels can also be defined as a "infinitive structure" indicating that all polymer chains of the network are connected to each other and form one, big molecule. They can also be described as two component materials, which consist of a small fraction of polymer network and a large amount of fluid filling the interstitial spaces of the network. When the network is thermodynamically compatible with the solvent it starts to swell and prevents it from escaping, holding large amount of solvent inside. For example, only one gram of gelatin powder is necessary to gel 100 g of water.[76] This fact has strong influence on properties of the gel, because swollen gels are in state between solids and liquids, and, as a matter of fact, they show the properties of both. In fully swollen state, the gel acts as a soft material with properties close to liquids. The network is solvated by large amount of trapped solvent, and polymer chains exhibit great mobility. However, even in these conditions they keep the shape like a solid.

A special place between the varieties of gels belongs to hydrogels where water is the swelling agent gels because of the prefix 'hydro'. Because of the similarity of hydrogels to the human body, there are wide applications in the biomedical field. The

unique properties of hydrogels have been also used in agriculture, cosmetics industry or in separation processes.[77,78,79,80,81,82] Hydrogels are also crossed-linked network of hydrophilic polymers which possess the ability to absorb large amount of water and swell, while maintaining their 3D structure. This definition differentiates hydrogels from gels, which are polymeric networks already swollen to equilibrium, and further addition of fluids results only in dilution of the polymeric network as shown in Figure 1.28.

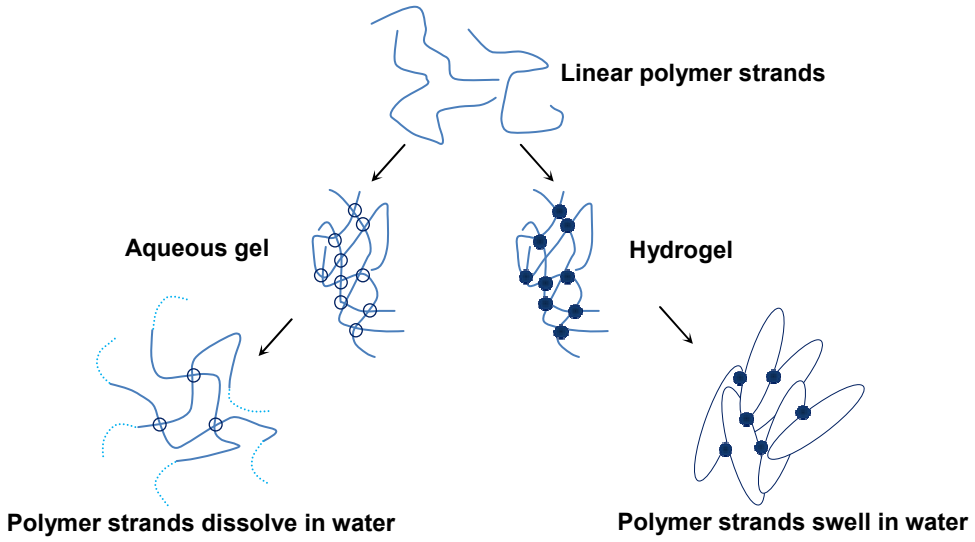

Figure 1.28: Polymer strands forming a gel and a hydrogel, showing different behaviour in an aqueous environment. Solid circles represent covalent cross-links and hollow circles represent virtual cross-links formed by entanglements.[83]

The formation of a polymer network can be achieved mainly in two ways. The most common one is covalent cross-linking, generally obtained by addition of cross-linking agents to the mixture of monomer and initiator. The other possible route is the step addition polymerisation of oligomeric multifunctional precursors. Hence, cross-linking points are permanent and fixed. On the other hand, gels can also be formed via secondary forces like hydrogen bonding or electrostatic interactions. When secondary forces are applied, so-called physical networks are formed.

Gels can be classified according to other criteria. For example, four classes of gels can be distinguished depending on the type of cross-linking by Flory[84] as follows:

- Well ordered lamella structures (e.g., soap gels or clays)
- Covalent polymer networks completely disordered
- Polymer networks formed by physical association, predominantly disordered but including some local ordered regions

• Amorphous globular structures (e.g., aggregated globular proteins)

With respect to size, gels can be classified into two groups: macrogels (bulk gels with size larger than 100 μm) and microgels which have average diameter (smaller than 100 μm). Specially, additional subgroup of nanogels (smaller than 200 nm) can be defined to emphasize nano-dimension sizes.

For macrogel formation, high monomer or initial polymer concentration is required. However, under these conditions, a tendency to create undesirable higher cross-linking density on the outside part of the gel (skin-layer formation phenomenon) exists. For *in situ* gel formation an important parameter is also the reactivity ratio between monomer and cross-linker. If the reactivity of cross-linker is too high or too small in comparison to monomer, cross-linking reaction intensifies at the beginning or at the end of the reaction, respectively, resulting in undesired microgelation. As the result, structure of formed macrogels is inhomogeneous, containing a lot of different defects as shown in Figure 1.29.

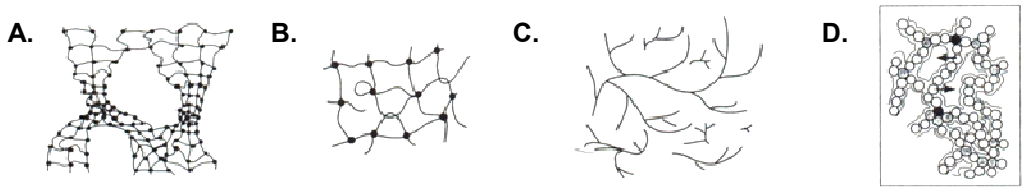

Figure 1.29: Different types of inhomogeneities in polymer gels. A) spatial, B) topological, C) connectivity, D) mobility defects. [85]

In comparison to macrogels, microgels are synthesised in dilute solution, where the distance between molecules is larger. Under such conditions intermolecular cross-linking is more difficult therefore intramolecular cross-linking is favorable. As the result the polymer network consists of only several cross-linked polymer chains.

1.6.2 Hydrogels: Thermodynamics and swelling kinetics

1.6.2.1 Thermodynamics

Stimuli-responsive polymers are plastic materials with 3D network and cross-linked polymers are insoluble in certain solvents such as water but swell by solvent adsorption due to the interconnections between the polymer chains. Stimuli-responsive hydrogels show a phase transition behaviour shown in Figure 1.30.

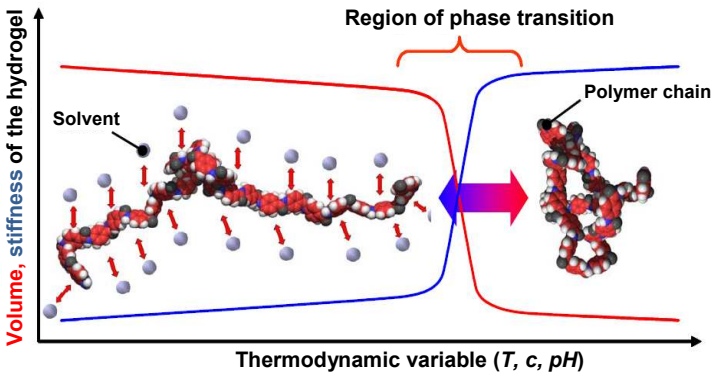

Figure 1.30: Phase transition behaviour of stimuli-responsive hydrogels.[86] The swollen phase of the gel (left) is dominated by polymer-water interactions obtaining the best mixing of the polymer chains and the aqueous solution. The shrunken phase of the hydrogel (right) is determined by polymer-polymer-interactions, which remove water out of the gel. Near the phase interface, within the range of phase transition, small alterations of a thermodynamic value result in a change of the phase of the hydrogel.

In a separated phase, the hydrogel reaches its maximal value of hydrophobicity and shrinks mainly due to the interactions between polymers. However, in the second phase, the gel gains it maximum of hydrophilicity and swells by polymer-water interactions. In a system, at the boundary between these two phases, a small alternation of thermodynamic variable (i.e. temperature, solvent composition) results in an abrupt change in physical properties of hydrogel (i.e. volume, mass, stiffness).

The interactions between polymer and water in the second phase generate osmotic pressure $\Delta\pi_{mix}$ acting expansively. Due to the interaction between polymers the polymer network counteracts this expansion by elastic force respected by $\Delta\pi_{elast}$. The hydrogel obtains its swelling equilibrium at the balance of the pressures, which can be described by

$$\Delta\pi = \Delta\pi_{elast} + \Delta\pi_{mix} = 0 \qquad [10]$$

Temperature sensitive hydrogels such as poly(*N*-isopropylacrylamide) (PNIPAAm) gel have a slightly hydrophobic nature and contain side groups interacting with water molecules by hydrogen bonds causing the swelling of hydrogels. These hydrogen bonds depend on the temperature and break apart at a critical temperature called lower critical solution temperature (LCST). Above LCST the hydrophobic nature of the gel dominates resulting in a shrinking of the gel.

1.6.2.2 Swelling kinetics

The swelling and shrinking of hydrogels requires a transport of solvent and two transport mechanisms have to be considered for an initiation of a volume phase transition. First, the initiating stimulus has to be transferred into the hydrogel, such as the difference of temperature, solvents or ions which is associated with a change of a balance of the osmotic pressure. The transport occurs either energetically by heat transfer which is described by the thermal transfer coefficient, D_T or by continuous mass diffusion of a solvent into the hydrogel described by the spontaneous mass transfer coefficient, D_S shown in Figure 1.31.

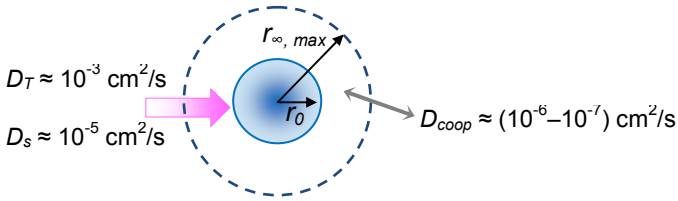

Figure 1.31: Transport processes at swelling and shrinking of hydrogels. r_0 and $r_{\infty,\max}$ are the initial and the maximal radius in the swelling equilibrium.[86]

Secondly, the hydrogel swells or shrinks absorbing or releasing swelling agents to obtain a swelling equilibrium of the changed osmotic pressure balance. Hence, the polymer chains of the network have to be moved to obtain their new positions. Tanaka and co-workers developed the model of "collective" or "cooperative" diffusion characterized by the cooperative diffusion coefficient D_{Coop}.[87,88]

For a spherical gel as shown in Figure 1.31, this theory predicts a characteristic time constant of swelling process (τ) as following:

$$\tau = \left(\frac{r^2}{D_{Coop}} \right) \qquad [11]$$

where r is the final radius and the characteristic dimension, respectively.

The radius of the hydrogel during the swelling process is expressed as

$$r(t) = r_0 + (r_{\infty,\max} - r_0)\left(1 - e^{\frac{-t}{\tau}}\right) \qquad [12]$$

whereas the shrinking processes follows

$$r(t) = r_0 + (r_{\infty,\max} - r_0)e^{\frac{-t}{\tau}} \qquad [13]$$

This theory describes the unloaded and free swelling behaviour without influence of the surrounding area. The measured swelling times correlate excellently with the calculated data using this theory. However the uninfluenced free swelling of gels without an externally applied force can hardly be used for functional sensor and actuator elements. The characteristic of the swelling kinetics of polyelectrolyte gel in presence of buffer ions was investigated by Lesho and co-workers.[89] In this case the characteristic time constant (τ_{bdr}) describing a "buffer-mediated diffusion reaction" is given by:

$$\tau_{bdr} = \frac{\delta^2}{\pi^2 D_{HB}} \left[1 + \frac{\beta_{gel}}{(1+H_0)\beta_{HB}} \right] \qquad [14]$$

where δ is gel thickness, D_{HB} is the diffusivity of the buffer molecules into the gel, H_0 is the hydration, which is defined as the ratio of liquid to solid volume, β_{gel} is buffer capacity of the hydrogel, and β_{HB} is buffer capacity of the buffer solution.

According to the equations above the characteristic hydrogel dimension should be as small as possible to obtain small characteristic time constants due to the square dependency. For swelling in an aqueous solution containing salt, the time constant decreases with increasing the capacity of the buffer solution, otherwise it increases with increasing the buffer capacity of the hydrogel.

1.6.3 Stimuli-responsive gels

Hydrogels are formed with a three-dimensional network of polymer chains, where some parts are solvated by water molecules but the other parts are chemically or physically linked with each other. Based on these cross-linked networks of hydrogels, the dimensions of stimuli-responsive hydrogels could be dramatically changed by an alternative change of hydrophobicity and hydrophilicity in the molecular structure of the swollen polymer chains.[83, 90, 91] This type of hydrogel has a cross-linked network structure containing the stimuli-responsive component in the polymer chains, which causes dramatic swelling/deswelling according to the change in stimuli. Other forms of stimuli-responsive hydrogels could be reversibly transformed to solutions due to environmental stimuli changes, showing solution-gelation transition by altering the hydrophobic interactions of cross-linked areas in an aqueous system.[92] Therefore, this type of stimuli responsive polymer has been developed for a phase change rather than a dimension change, to be used for example, as injectable hydrogels.[93]

In chapter 5, the behaviour of stimuli-responsive hydrogels with either ionic strength, or electric field sensitivity is described. Therefore, in this section, we briefly describe stimuli-responsive properties of hydrogels and the influence of structure and additives on these properties.

1.6.3.1 Introduction

One approach involves the response of a polymer system to stimuli, which is a common process for biopolymers in living organisms. These properties of biopolymers are based on highly cooperative interactions, which can provide significant driving forces for the responses caused by small environmental changes. For the past several decades, the concept of cooperative interactions between the functional segments of biopolymer has led to the creative idea to invent novel synthetic polymer systems that are environmentally responsive to stimuli in some controlled ways.[83,94]

Stimuli-responsive polymers are defined as polymers that undergo relatively large and abrupt, physical or chemical changes in response to small external changes in the environmental conditions. Names coined for 'stimuli-responsive' polymers have been given as stimuli-sensitive,[95] intelligent,[96] smart,[97] or environmentally sensitive polymers.[98] These polymer systems might recognize a stimulus as a signal, judge the magnitude of this signal, and then change their chain conformation in direct response.[99] Figure 1.32 shows many different stimuli to modulate the response of polymer systems.

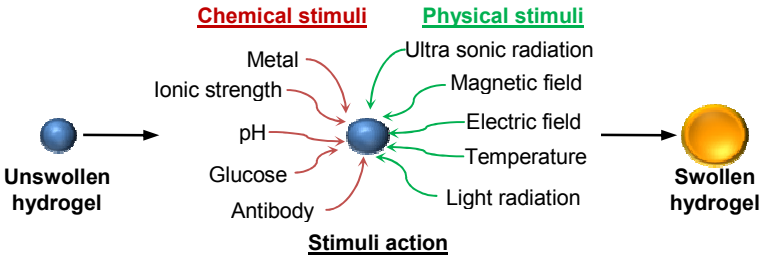

Figure 1.32: Stimuli responsive swelling-deswelling behaviour of hydrogels.[86]

These stimuli could be classified as either physical or chemical stimuli. Chemical stimuli, such as pH, ionic factors, and chemical agents, will change the interactions between polymer chains or between polymer chains and solvents at the molecular level. The physical stimuli, such as temperature, electric or magnetic fields, and mechanical stress, will affect the level of various energy sources and alter molecular interactions at critical onset points. These responses of polymer systems are very useful in bio-related applications such as drug delivery,[83,95,98] biotechnology[95,97] and chromatography.[100,101] Some systems have been developed to combine two or more stimuli-responsive

mechanisms into one polymer system. For instance, temperature-sensitive polymers may also respond to pH changes.[102] On the other hand, some research groups have reported that two or more signals could be simultaneously applied in order to induce response in so-called dual-responsive polymer systems.[103] Recently, biochemical stimuli have been considered as another category, which involves the responses to antigen, enzyme, ligand, and biochemical agents.

1.6.3.2 Temperature sensitive polymers: poly(N-isopropylacrylamide) (PNIPAAm) gels

Important recent advances in PNIPAAm-based systems have been focused on mechanistic understanding of phase transition, fine control of the structure-property relationship, and novel biomedical applications. The PNIPAAm copolymers have been studied for many applications that take advantage of their thermosensitive properties in water such as varying their shape and volume in response to changes in temperature. PNIPAAm gels undergo a volume phase transition around 32 ^{o}C, the "lower critical solution temperature" (LCST) of PNIPAAm homopolymer in water (Figure 1.33).[104]

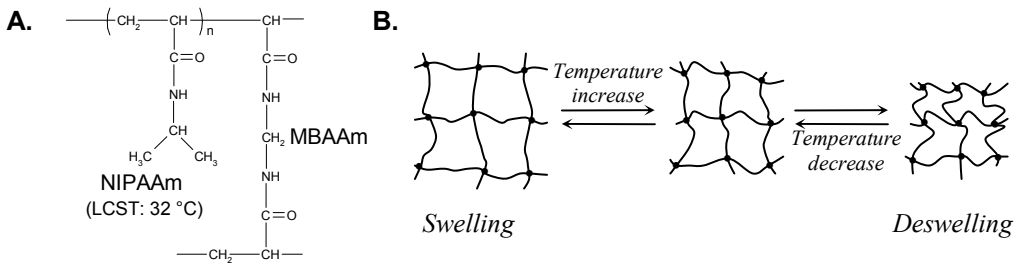

Figure 1.33: (A) Structure of PNIPAAm gel cross-linked by a cross-linker *N,N′*-methylene bisacrylamide (MBAAm). (B) Shrinking mechanism for conventional PNIPAAm gel undergoing temperature induced collapse in aqueous media.

Kinetics and thermodynamics of the phase transition might be controlled by well-designed molecular parameters. Much attention has been focused on the nature of this transition because of its potential application in the thermoresponsive drug delivery system,[105] artificial muscle,[106] membrane separation,[107] and surfaces in biomaterials.[108] However, the kinetics of the volume transition is slow and this has limited the application of these systems. One approach to design a faster gel response has been to graft hydrophilic (e.g., acrylic acid or methacrylic acid) or thermoresponsive oligomers (e.g., poly(ethylene oxide)) to the gel network.[109] This method has been successfully applied but is limited to low molecular weights and low concentrations of the grafted

chains. The incorporation of free polymer chains into thermoresponsive PNIPAAm gels alters the kinetics of the LCST volume phase transition. Faster kinetics is associated with higher concentrations of free polymer chains and more hydrophobic polymers.

1.6.3.3 pH and electro-responsive poly(2-acrylamido-2-methylpropane-sulfonic acid) (PAMPS) gels

Amphiphilic water soluble polymers and their hydrophobically driven self-association have been studied extensively because of their potentials in industrial and biological applications.[110,111] In this section, we concentrate on the properties of a polyelectrolyte gel which is a charged polymer network with ions fixed on the backbone of the polymer chains and counter-ions that are distributed in the voids of the polymer network. A polyelectrolyte gel has the ability to swell in water and can absorb a significant amount of water within its structure, but dissolve in water. For instance, polyelectrolyte PAMPS gels have sulfonate groups which are deprotonated and protonated depending on the surrounding conditions (Figure 1.34) as following:

- In a basic condition: $[RSOOOH]_{gel} + [OH^-]_{aq} \rightarrow [RSOOO^-]_{gel} + H_2O$ (Deprotonation)
- In an acidic condition: $[RSOOO^-]_{gel} + [H^+] \rightarrow [RSOOOH]_{gel}$ (Protonation)

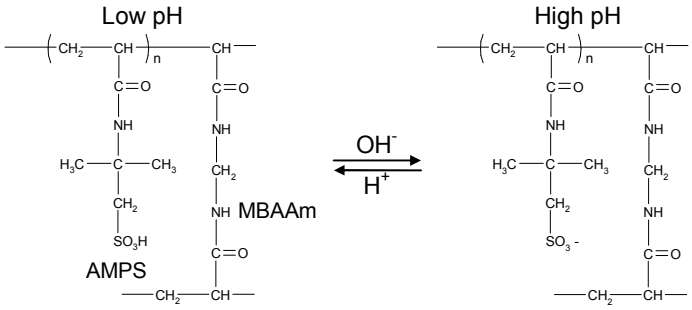

Figure 1.34: Structure of PAMPS gel which is cross-linked by a cross-linker MBAAm and its pH-dependent ionisation.

Therefore, in a basic solution, the density of likewise charged groups within the network strongly increases accompanied by an adequate generation of mobile counterions inside the gel, which induces the phase transition due to electrostatic repulsion. Otherwise in acidic condition, the gel protonates and results in a decrease of both the charge density and the content of mobile counterions within the gel network leading to gel shrinking.

The phase transition of the gels occurs at the apparent acid dissociation constant pK_a of the hydrogel which is approximately close to the pK_a of the ionisable group. Therefore, the hydrogel shows a drastic swelling behaviour at the apparent pK_a of the

gel and stops swelling behaviour after completing the ionisation of the ionisable groups. Figure 1.35 shows the general behaviour of the three types of polyelectrolyte gels.

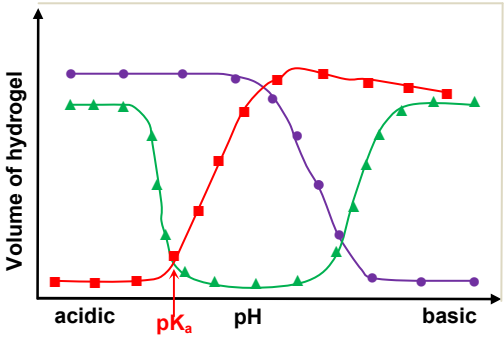

Figure 1.35: Phase transition behaviour of polyelectrolyte hydrogels.[86] Acidic hydrogels (■) are ionized by deprotonation in basic solutions, which have an excess of hydroxyl groups. Basic hydrogels (●) swell in acidic solutions due to the ionization of their basic groups by protonation. Amphiphilic hydrogels (▲) contain both acidic and basic groups. Therefore, they show two phase transitions.

The contribution of the electrostatic interaction of polyelectrolyte hydrogels to the balance of the osmotic pressure has to be considered as an expansive pressure $\Delta\pi_{ion}$, so that the equation [10] in section 1.6.2.1 must be rewritten to

$$\Delta\pi = \Delta\pi_{elast} + \Delta\pi_{ion} + \Delta\pi_{mix} = 0 \qquad [15]$$

The mobility of counterions of the gel should be high enough to make their release into the surrounding solution. However, the hydrogel exchanges its counterions with an appropriate ion from the surrounding to keep the charge balance inside the gel. Finally the solvent in the surroundings leads to a change of the swelling equilibrium of the gel by the changed osmotic pressure of the gel. At high ionic strength a polyelectrolyte shielding reduces the osmotic pressure thus leading to shrinking of the gel.[112] The contribution of the ionic strength $\Delta\pi_{surr}$ to the balance of osmotic pressure has to be considered additive:

$$\Delta\pi = \Delta\pi_{elast} + \Delta\pi_{ion} + \Delta\pi_{mix} + \Delta\pi_{surr} = 0 \qquad [16]$$

1.7 Self-oscillating chemical reactions

In chapter 5, we discuss the novel gel system, which autonomously repeats its swelling-deswelling behaviour periodically in a closed solution without on-off switching of external stimuli. In this section, we describe the Belousov-Zhabotinsky (BZ) and Brigs-Rauscher (BR) reactions, which are considered as the energy source of the mechanical oscillation of the gel.

1.7.1 Introduction

Many kinds of stimuli-responsive gels exhibit abrupt volume phase transitions in response to external stimuli and many applications for these gels have been explored. One of the aims in these applications is to develop a system with the biomimetic function where materials sense environmental changes by themselves and go into action. In the human body there are many physiological phenomena that continue cyclic changes in a nonequilibrium state as their own native state such as glycolysis, heartbeats, or human biorhythm. If such self-oscillation is achieved for colloid particles, new possibilities will be created, such as novel biomimetic intelligent materials exhibiting rhythmic action like a pacemaker. Applications such as a self-walking microacutator or a micropump with peristaltic motion like worms, and oscillatory drug release synchronized with cell cycles also may be possible.

In recent years, marked attention has been paid to oscillatory processes typically in biological objects at organ, cellular, subcellular, and molecular levels. Artificial oscillating systems consisting of chemical reactions are the simple artificial model for these oscillatory systems observed in biological systems. The BZ and BR reactions are the typical reactions in this context, and many people are involved in investigating them both experimentally and theoretically.[113] They represent a nonlinear and oscillating reaction in which there is cyclic reaction similar to that of a metabolic reaction network. They are facile oxidations of organic or inorganic substrates (malonic, citric, oxalic acids, acetone, phenols, NADH, Br^-, I^-, SO_3^{2-}, $S_2O_3^{2-}$, Sn(II), and HS^-) by strong oxidants ($KBrO_3$, KIO_3, H_2O_2, and O_2) catalyzed by metal ions (Ce^{4+}/Ce^{3+}, Mn^{3+}/Mn^{2+}, Fe^{3+}/Fe^{2+}, Co^{3+}/Co^{2+}).[114] In these reactions, metal ions play the role of one-electron oxidants.

1.7.2 Belousov-Zhabotinsky (BZ) reaction

For most chemical reactions, a state of homogeneity and equilibrium is quickly reached. The BZ reaction is a remarkable chemical reaction that maintains a prolonged state of non-equilibrium leading to macroscopic temporal oscillations and spatial pattern formation that is very life-like. This rhythmical process is controlled by feedback mechanism in which intermediate molecules or ions decisively influence initial, or intermediate reactions. The oscillating reaction of potassium bromate with cerium sulphate (Ce^{4+}) was discovered, by accident, by Belousov in 1958 and was

systematically investigated and developed by Zhabotinsky in the following years.[115] He characterised its chemistry and showed that, in an unstirred system, the reaction spontaneously gave rise to a "target pattern" or spirals of oxidised blue ferrin in an initially homogenous dish of reduced, red ferroin-dominated solution as shown in Figure 1.36.

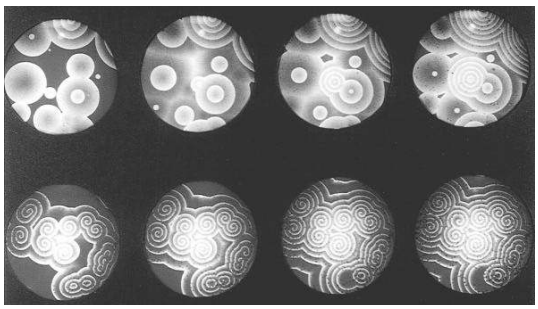

Figure 1.36: Chemical waves in the BZ reaction. Top: target patterns in a thin film of reagent (1.5 mm). Bottom: spiral waves in reagent similar to above except for less acidic. Both sequences from left to right are at 60 sec intervals.[116]

Under appropriate conditions, the BZ reaction shows autonomous oscillations in its redox potential. The overall process is the oxidation of an organic substrate such as malonic acid with the coexistence of an oxidizing agent e.g., sodium bromate and metal ions such as Ce^{3+}, Mn^{2+}, Ru^{2+}, or Fe^{2+}. In the course of the reaction, the catalyst ion periodically oscillates between the oxidized and reduced states as long as the substrate exists. Spatial chemical waves and patterns associated with this reaction are traditionally detected by optical methods that take advantage of the colour changes associated with the ionic state of the transition metal ions. The most popular reaction of the BZ reactions for study of chemical waves is the Fe^{2+}-catalyzed reaction.[117] In this case a dramatic colour change from red to blue accompanies the change from Fe^{2+} [ferroin] to Fe^{3+} [ferrin]. Recently, the BZ reaction catalyzed by Ru^{2+} has been also reported in pattern formation experiments.[118] The photochemical properties of the ruthenium complex have led to new and exciting results in the area of pattern control and manipulation by light.[119,120,121] This system also exhibits remarkable colour contrast.

The overall reaction may be divided into the following three main processes:[122,123] 1) consumption of bromide ion (I), 2) autocatalytic reaction of bromous acid with oxidation of the catalyst (II), and 3) organic reaction with reduction of the catalyst (III).

I. $BrO_3^- + 2Br^- + 3H^+ \rightarrow 3HOBr$

II. $BrO_3^- + HBrO_2 + 2M_{red} + 3H^+ \rightarrow 2HBrO_2 + 2M_{ox} + H_2O$ (catalyst oxidisation)

III. $2M_{ox} + MA + BrMA \rightarrow fBr^- + 2M_{red}$ + other products (catalyst reduction)

Total: $2BrO_3^- + 3CH_2(COOH)_2 + 2H^+ \rightarrow 2BrCH(COOH)_2 + 3CO_2 + 4H_2O$

where M is metal catalyst, MA is malonic acid ($CH_2(COOH)_2$) and *f* is the stoichiometric factor to step III.

The BZ reaction has many similarities to a metabolic reaction network, and it has been used as a chemical model for understanding many biological phenomena, such as biorhythms, pattern formations, self-organisation, etc.[124]

1.7.3 Briggs-Rauscher (BR) reaction

The BR reaction, which was discovered in 1973,[125] is among the most popular oscillating reactions, and it is very convenient for the demonstration of nonlinear chemical dynamics.[126] The classical BR reaction system includes malonic acid, Mn^{2+} ions which are components of the BZ oscillating reaction, hydrogen peroxide, and iodate ions which are components of the Bray-Liebhafsky (BL) oscillating reaction in acidic solution. If starch is used as an indicator for enhancing the colour due to iodine, the oscillations usually persist for only around 10 min in a closed system and follow the colour sequence from colourless to yellow to deep blue before repeating with a frequency of several cycles per minute.

The overall stoichiometric change is suggested to be.[127,128]

$$IO_3^- + 2H_2O_2 + CH_2(COOH)_2 + H^+ \rightarrow CHI(COOH)_2 + 2O_2 + 3H_2O \qquad (S1)$$

This change can be generated by two stoichiometric processes designated S2 and S3

$$IO_3^- + 2H_2O_2 + H^+ \rightarrow HOI + 2O_2 + 2H_2O \qquad (S2)$$

$$HOI + CH_2(COOH)_2 \rightarrow CHI(COOH)_2 + H_2O \qquad (S3)$$

If Mn^{2+} is also present, the same process (S2) can also take place much more quickly. Cooke[129] found that various substitutions could be made in the classical BR reaction and still maintain oscillations. For instance, the malonic acid can be replaced by acetone. The behaviour of these two substrates is different as a result of greater oxidation of organic material in the malonic acid system, but the underlying mechanism seems to be closely related.

1.8 Presentation of this thesis

This thesis is organised as follows:

In chapter 2, we present details of all the different materials as well as the main techniques, which have been used in this work. This section contains the description of

methods common to most of the work reported in this thesis. Our modified method to detect the adsorption of surfactants at the LC-water interface was described in detail with comparison to previous published studies. However, each separate result chapter presents some more details about the specific experiments it describes.

In Chapter 3, the alignment of the nematic LC 5CB was examined to detect the adsorption of DNA-surfactants, DNA-cationic surfactant complexes and DNA-cationic polymerisable surfactant complexes at the LC-water interface in order to determine whether adsorption of these molecules could induce a transition of the anchoring of the LC to detect the hybridisation of DNA. Fluorescence microscopy was used to assess whether the adsorbed DNA species are hybridised with a complementary sequence at the LC-water interface.

In chapter 4, UV polymerisation of an adsorbed polymerisable surfactant layer at the LC-water interface was examined together with its effect on the anchoring of 5CB depending on the molecular structures of the surfactants. The possibility that the experimental system is able to detect UV radiation and act as the basis of a UV sensor is examined.

In chapter 5, we designed a different type of self-propelling hydrogel particles. First, we investigated the swelling-deswelling behaviour of anisotropic hydrogels driven by self-oscillating chemical reactions. To fabricate the required anisotropic structures, a modulated bigel structure was prepared with a newly developed double UV polymerisation method. Secondly, we used a polyelectrolyte hydrogel that shows an electroactuation under an electric field. The electro-responses of synthesised gels were investigated in various salt solutions under direct current (*dc*) and alternating current (*ac*) electric field conditions.

Finally, in chapter 6, some different strategies to prepare Janus particles having self-propulsion properties are discussed. In these strategies the driving force for the propulsion of a particle is an osmotic pressure gradient generated by the catalytic activity of an immobilised enzyme on the surface of the particle or the diffusion of organic chemical species stored in the particle. We also present a modified novel method for preparation of the metal coated Janus particles where the metal layer provides not only a surface for immobilisation of enzymes, but also a barrier preventing a diffusion of organic chemical species from the particles.

1.9. References

1. P. G. de Gennes and J. Prost, *The physics of liquid crystals*, 2nd ed.; Clarendon Press, Oxford, 1993.
2. J. Cognard, "Alignment of nematic liquid crystals and their mixtures", *Mol. Cryst. Liq. Cryst.* **1982**, *Suppl. Ser 1*, 1-77.
3. B. Jérôme, "Surface effects and anchoring in liquid crystals", *Rep. Prog. Phys.* **1991**, *54*, 391-451.
4. N. A. Lockwood and N. L. Abbott, "Self-assembly of surfactants and phospholipids at interfaces between aqueous phases and thermotropic liquid crystals", *Current Opinion in Colloid & Science* **2005**, *10*, 111-120.
5. V. K. Gupta, J. J. Skaife, T. B. Dubrovsky and N. L. Abbott, "Optical amplification of ligand-receptor binding using liquid crystals", *Science* **1998**, *279*, 2077-2080.
6. B-W. Lee and N. A. Clark, "Alignment of liquid crystals with patterned isotropic surfaces", *Science* **2001**, *291*, 2576-2580.
7. N. L. Lockwood, J. K. Gupta and N. L. Abbott, "Self-assembly of amphiphiles, polymers and proteins at interfaces between thermotropic liquid crystals and aqueous phases", *Surf. Sci. Rep.* **2008**, *63*, 255-293.
8. A. Kumar, O. Larsson, D. Parodi and Z. Liang, "Silanized nucleic acids: a general platform for DNA immobilisation", *Nucleic. Acids Res.* **2000**, *28*, e71
9. R. L. Letsinger, R. A. Alul, F. Farooqui, S. M. Gryaznov and O. Kinster, "Synthesis and properties of modified oligonucleotides", *Nucleic Acid Symp.Ser* 1991, *24*, 75-78.
10. C. Yoshina-Ishii and S. G. Boxer, "Arrays of mobile tethered vesicles on supported lipid bilayers", *J. Am. Chem. Soc.* **2003**, *125*, 3696–3697.
11. C. Xu, P. Taylor, M. Ersoz, P. D. I. Fletcher and V. N. Paunov, "Microcontact printing of DNA-surfactant arrays on solid substrates", *J. Mater. Chem.* **2003**, *13*, 3044-3048.
12. C. Xu, P. Taylor, P. D. I. Fletcher and V. N. Paunov, "Adsorption and hybridisation of DNA-surfactants at fluid surfaces and liquid bilayers", *J. Mater. Chem.* **2005**, *15*, 394-402.
13. R. Yoshida, T. Takahashi, T. Yamaguchi and H. Ichijo, "*Self*-oscillating gel", *J. Am. Chem. Soc.* **1996**, *118*, 5134-5135.
14. R. Yoshida, E. Kokufuta and T. Yamaguchi, "Beating polymer gels coupled with a nonlinear chemical reaction", *Chaos* **1999**, *9*, 260-266.

15. S. Maeda, Y. Hara, T. Sakai, R. Yoshida and S. Hashimoto, “Self-walking gel”, *Adv. Matter.* **2007**, ***0000***.*00*. 1-5.
16. S. Maeda, Y. Hara, R. Yoshida and S. Hashimoto, “Peristaltic motion of polymer gels”, *Angew. Chem. Int. Ed.* **2008**, *47*, 6690-6693.
17. C. Casagrande, P. Fabre, E. Rhaphaël and M. Veyssié, “"Janus Beads": Realization and behaviour at water/oil Interfaces”, *Europhys. Lett.* **1989**, *9*, 251-255.
18. O. J. Cayre, V. N. Paunov and O. D. Velev, “Fabrication of dipolar colloid particles by microcontact printing”, *Chem. Commun.* **2003**, 2296 - 2297.
19. R. C. Mucic, J. J. Storhoff, C. A. Mirkin and R. L. Leysinger, “DNA-directed synthesis of binary nanoparticle network materials”, *J. Am. Chem. Soc.* **1998**, *120*, 12674-12675.
20. T. A. Taton, G. Lu and C. A. Mirkin, “Two-colour labelling of oligonucleotide array via size-selective scattering of nanoparticle probes”, *J. Am. Chem. Soc.* **2001**, *123*, 5164-5165.
21. V. N. Paunov and O. J. Cayre, “Supraparticles and "Janus" particles fabricated by replication of particle monolayer at liquid surfaces using a gel trapping technique”, *Adv. Mater.* **2004**, *16*, 788-791.
22. R. F. Ismagilov, A. Schwartz, N. Bowden and G. M. Whitesides, “Autonomous movement and self-assembly”, *Angew. Chem., Int. Ed.* **2002**, *41*, 652-654.
23. W. F. Paxton, K. C. Kistler, C. C. Olmeda, A. Sen, S. K. St. Angelo, Y. Cao, T. E. Mallouk, P. E. Lammert and V. H. Cresp, “Catalytic nanomotors: Autonomous movement of striped nanorods”, *J. Am. Chem. Soc.* **2004**, *126*, 13424-13431.
24. L. Stryer, *Biochemistry,* 3rd ed., W.H Freeman and Co., New York, 1988.
25. DNA figures and Discussion: *http://www.chemistry.oregonstate.edu/courses/ch130/latestnews/ch130ln.htm.* [Accessed on 26 November 2008].
26. D. Voet, J. Voet and C. W. Pratt, *Fundamentals of Biochemistry*, John Wiley & Sons Inc., 1999.
27. R. Horton, L. A. Moran, R. S. Oschs and J. D. R. K. G. Scrimgeour, *Principles of Biochemistry*, in *http://cwx.prenhall.com/horton/*, Pearson Education, Prentice-Hall Inc., 2002.
28. Integrated DNA Technologies Oligo Analyzer*: http://eu.idtdna.com/analyzer/Applications/OligoAnalyzer/*, [Accessed on 4 December 2008].

29. R. Owczarzy, Y. You, B. G. Moreira, J. A. Manthey, L. Huang, M. A. Behlke and J. A. Walder, "Effects of sodium ions on DNA duplex oligomers: Improved predictions of melting temperatures", *Biochemistry* **2004**, *43*, 3537-3554.
30. J. W. Gibbs, On the equilibrium of heterogeneous substances, in *Collected Works*, Yale University Press, *1*, 219, 1948.
31. J. H. Clint, *Surfactant aggregation*, Blackie & Son Ltd., London, 1992.
32. J. N. Israelachvili, D. J. Mitchell and B. W. Ninham, "Theory of self-assembly of hydrocarbon amphiphiles into micelles and bilayers", *J. Chem. Soc. Faraday Trans II* **1976**, *72*, 1525-1548.
33. H-J. Butt, K. Graf and M. Kappl, *Physics and Chemistry of Interfaces*, Wiley-VCH GmbH & Co. KGaA, Weinheim, 2003.
34. E. Winfree, F. Liu, L. A. Wenzier and N. C. Seeman, "Design and self-assembly of two-dimensional DNA crystals", *Nature* **1998**, *394*, 539-544.
35. M. L. M. Anderson, *Nucleic Acid Hybridisation*, 1st ed., Springer-Verlag, New York, 1998.
36. S. M. Melnikov and B. Lindman, "Solubilisation of DNA-cationic lipid complexes in hydrophobic solvents: A single-molecule visualization by fluorescence microscopy", *Langmuir* **1999**, *15*, 1923-1928.
37. M. Sajapipat, R. Sanedrin and F. Zhou, "Selective Desorption of alkanethiols in mixed self-assembled monolayers for subsequent oligonucleotide attachment and DNA hybridisation", *Langmuir* **2001**, *17*, 7637-7644.
38. E. A. Smith, M. J. Wanat, Y. Cheng, S. V. P. Barreita, A. G. Frutos and R. M. Cron, "Formation, spectroscopic characterization, and application of sulfhydryl-terminated alkanethiol monolayers for the chemical attachment of DNA onto gold surfaces", *Langmuir* **2001**, *17*, 2502-2507.
39. E. Huang, F. Zhou and L. Deng, "Studies of surface coverage and orientation of DNA molecules immobilised onto preformed alkanethiol self-assembled monolayers", *Langmuir* **2000**, *16*, 3272- 3280.
40. P. Taylor, **2005** *Self-recognizing surfaces using DNA surfactant* (PhD thesis) University of Hull.
41. V. N. Paunov, C. Xu, P. Taylor, M. Ersoz and P.D.I. Fletcher, "Properties and applications of novel DNA-based surfactants", *Mater. Res. Soc. Symp. Proc.* **2004**, *845*, AA6.4.1-AA6.4.6.

42. K. Holmberg, B. Jönsson, B. Kronberg and B. Lindman, *Surfactants and Polymers in Aqueous Solution*, 2nd ed., Wiley, New York, 2003.
43. K. Esumi and M. Ueno, *Structure-Performance Relationship in Surfactants*, 2nd ed., Marcel Dekker, New York, 2003.
44. M. Summers and J. Eastoe, "Applications of polymerisable surfactants", *Adv. Colloid. Interface. Sci.* **2003**, *100-102*, 137-152.
45. A. Guyot, "Advances in reactive surfactants", *Adv. Colloid. Interface. Sci.* **2004**, *108-109*, 3-22.
46. M. J. Gerber, S. R. Kline and L. M. Walker, "Characterisation of rodlike aggregates generated from a cationic surfactant and a polymerisable counterion", *Langmuir* **2004**, *20*, 8510-8516.
47. K. Hirano and H. Fukuda, "Polymerisable ion-paired amphiphiles", *Langmuir* **1991**, *7*, 1045-1047.
48. C. Nason, T. Roper, C. Hoyle and J. A. Pojman, "UV-induced frontal polymerisation of multifunctional (meth)acrylates", *Macromolecules* **2005**, *38*, 5506-5512.
49. L. Lecamp, F. Houllier, B. Youssef and C. Bunel, "Photoinitiated cross-linking of a thiol-methacrylate system", *Polymer* **2001**, *42*, 2727-2736.
50. J. M. G. Cowie and V. Arrighi, *Polymer: Chemistry and Physics of Modern Materials*, 2nd ed.: CRC Press Inc., Glasgow, 1991.
51. O. D. Lavrentovich, "Topological defects in dispersed liquid crystals, or words and worlds around liquid crystal drops", *Liquid crystals* **1998**, *24*, 117-125
52. P. J. Collins and J. S. Patel, *Handbook of Liquid Crystal Research*, Oxford University Press, New York, 1997.
53. D. K. Scwartz, "Instant patterns in thin films", *Nature* **1986**, *362*, 593-594.
54. J. S. Foster and J. E. Frommer, "Imaging of liquid crystals using a tunnelling microscope", *Nature* **1998**, *333*, 542-545.
55. F. Vandenbrouck, S. Bardon, M. P. Valignat and A. M. Cazabat, "Wetting Transition and divergence of the extrapolation length near the nematic-isotropic transition, *Phys. Rev. Lett.* **1998**, *81*, 610-613.
56. V. K. Gupta, W. J. Miller, C. L. Pike and N. L. Abbott, "Using isotropic, nematic, and smectic fluids for the study of self-assembled monolayer formed from alkanthiols on gold", *Chem. Mater.* **1996**, *8*, 1366-1369.

57. V. Kitaev and E. Kumacheva, “Thin films of liquid crystals confined between crystalline surfaces”, *J. Phys. Chem. B* **2000**, *104*, 8822-8829.
58. J. M. Brake and N. L. Abbott, “An experimental system for imaging the reversible adsorption of amphiphiles at aqueous-liquid crystal interfaces”, *Langmuir* **2002**, *18*, 6101-6109.
59. V. Nazarenko and A. Nych, “Multistable alignment in free suspended nematic liquid crystal film”, *Phys. Rev. E* **1999**, *60*, R3495-3497.
60. E. Matijevic, “Preparation and properties of uniform size colloids”, *Chem. Mater.* **1993**, *5*, 412-426.
61. E. Matijevic, “Uniform inorganic colloid dispersions. Achievements and challenges”, *Langmuir* **1994**, *10*, 8-16.
62. Y. Xia, B. Gates, Y. Yin and Yu Lu, “Monodispersed colloidal spheres: old materials with new applications”, *Adv. Mater.* **2000**, *12*, 693-713.
63. P. G. de Gennes, ”Soft matter”, *Rev. Mod. Phys.* **1992**, *64*, 645-648.
64. I. M. Saez and J. W. Goodby, “Design and properties of "Janus-like" supermolecular liquid crystals”, *Chem. Commun.* **2003**, *14*, 1726–1727.
65. R. Erhardt, A. Bker, H. Zettl, H. Kaya, W. Pyckhout-Hintzen, G. Krausch, V. Abetz and A. H. E. Müller, “Janus Micelles”, *Macromolecules* **2001**, *34*, 1069-1075.
66. H. Xu, R. Erhardt, V. Abetz, A. H. E. Müller and W. A. Goedel, “Janus micelles at the air/water interface”, *Langmuir* **2001**, *17*, 6787-6793.
67. C. Casagrande and M. Veyssié, “Janus beads-realization and 1st observation of interfacial properties”, *C. R. Acad. Sci. Paris* **1988**, *306*, 1423-1425.
68. K. Fujimoto, K. Nakahama, M. Shidara and H. Kawaguchi, “Preparation of unsymmetrical microspheres at the interfaces”, *Langmuir*, **1999**, *15*, 4630-4635.
69. K. Nakahama, H. Kawaguchi and K. Fujimoto, “A Novel Preparation of non-symmetrical Microspheres using the Langmuir-Blodgett technique”, *Langmuir*, **2000**, *16*, 7882-7886.
70. S. Ikeda, H. Nur, T. Sawadaishi, K. Ijiro, M. Shimomura and B. Ohtani, “Direct observation of bimodal amphiphilic surface structures of zeolite particles for a novel liquid-liquid phase boundary catalysis”, *Langmuir*, **2001**, *17*, 7976-7979.
71. L. Petit, J-P. Manaud, C. Mingotaud, S. Ravaine and E. Duguet, “Sub-micrometer silica spheres dissymmetrically decorated with gold nanoclusters”, *Mater. Lett.* **2001**, *51*, 478-484.

72. E. Hugonnot, A. Carles, M-H. Delville, P. Panizza and J-P. Delville, “"Smart" surface dissymmetrization of microparticles driven by laser photochemical deposition”, *Langmuir* **2003**, *19*, 226-229.
73. V. N. Paunov, “Novel method for determining the three-phase contact angle of colloid particles adsorbed at air-water and oil-water interfaces”, *Langmuir* **2003**, *19*, 7970-7976.
74. O. Cayre, V. N. Paunov and O. D. Velev, “Fabrication of asymmetrically coated colloid particles by microcontact printing techniques”, *J. Mater. Chem.* **2003**, *13*, 2445-2450.
75. Y. Osada, *Gels Handbook*, Academic Press, San Diego, 2001.
76. M. Shibayama and T. Tanaka, “Volume phase transition and related phenomena of polymer gels”, *Adv. Polym. Sci.* **1993**, *109*, 1-62.
77. A. S. Hoffman, “Applications of thermally reversible polymers and hydrogels in therapeutics and diagnosis”, *J. Control. Release* **1987**, *6*, 297-305.
78. A. S. Hoffman, “"Intelligent" polymers in medicine and biotechnology”, *Artif. Organs* **1995**, *19*, 458-467.
79. K-F. Arndt, D. Kuckling and A. Richter, “Application of sensitive hydrogels in flow control”, *Polym. Adv. Tech.* **2000**, *11*, 496-505.
80. C. Ramkinsson-Ganorkar, F. Liu, M. Baudyš and S. W. Kim, “Modulating insulin-release profile from pH/thermosensitive polymeric beads through polymer molecular weight”, *J. Control. Release* **1999**, *59*, 287-298.
81. G. V. Rama-Rao, M. E. Kruk, S. Balamurugan, H. Xu, Q. Xu and G. P. Lopez, “Synthesis and characterisation of silica-poly(*N*-isopropylacrylamide) hybrid membranes: Switchable molecular filters”, *Chem. Mater*. **2002**, *14*, 5075-5080.
82. Y. S. Park, Y. Ito and Y. Imanishi, “Permeation control through porous membranes immobilised with thermosensitive polymer”, *Langmuir* **1998**, *14*, 910-914.
83. P. Gupta, K. Vermani and S. Garg, “Hydrogels: from controlled release to pH-responsive drug delivery”, *Drug discovery today* **2002**, *7*, 569-579.
84. P. J. Flory, “Introductory lecture”, *Disc.Faraday Soc.* **1974**, *57*, 7-18.
85. M. Shibayama and T. Norisuye, “Gel formation analyses by dynamic light scattering, *Bull. Chem. Soc. Jpn.* **2002**, *75*, 641-659.
86. A. Richter, G. Paschew, S. Klatt, J. Lieng, K-F. Arndt and H-J. P. Adler, “Review on hydrogel-based on pH sensors and microsensors”, *Sensors* **2008**, *8*, 561-581.

87. T. Tanaka and D. J. Fillmore, "Kinetics of swelling of gels", *J. Chem. Phys.* **1979**, *70*, 1214-1218.

88. Y. Li and T. Tanaka, "Kinetics of swelling and shrinking gels", *J. Chem. Phys.* **1990**, *92*, 1365-1371.

89. M. J. Lesho and N. F. Sheppard, "A method for studying swelling kinetics based on measurement of electrical conductivity", *Polym. Gels Networks* **1997**, *5*, 503-523.

90. I. Varga, T. Gilnyi, R. Mszros, G. Filipcsei, and M. Zrnyi, "Effect of cross-link density on the internal structure of poly(N-isopropylacrylamide) microgels", *J. Phys. Chem. B.* **2001**, *105*, 9071-9076.

91. R. Yoshida, K. Uchida, Y. Kaneko, K. Sakai, A. Kikuchi, Y. Sakurai and T. Okano, "Combtype grafted hydrogels with rapid de-swelling response to temperature changes", *Nature* **1995**, *374*, 240-242.

92. H. Lin and Y. Cheng, "In-situ thermoreversible gelation of block and star copolymers of poly(ethylene glycol) and poly(*N*-isopropylacrylamide) of varying architectures", *Macromolecules* **2001**, *34,* 3710-3715.

93. A. Hatefia and B. Amsdena, "Biodegradable injectable in situ forming drug delivery systems", *J. Control. Release* **2002**, *80*, 9-28.

94. T. Okano, editor, *Biorelated polymers and gels*. San Diago, CA: Academic press, 1998.

95. B. Jeong and A. Gutowska, "Lessons from nature: stimuli responsive polymers and their biomedical applications", *Trends in Biotechnology* **2002**, *20*, 305-311.

96. A. Kikuchi and T. Okano, "Intelligent thermoresponsive polymeric stationary phases for aqueous chromatography of biological compounds", *Prog. Polym. Sci.* **2002**, *27*, 1165-1193.

97. I. Y. Galaev and B. Mattiasson, "'Smart' polymers and what they could do in biotechnology and medicine", *Trends in Biotechnology* **2000**, *17*, 335-340.

98. Y. Qui and K. Park, "Environment-sensitive hydrogels for drug delivery", *Adv. Drug Delivery. Rev.* **2001**, *53,* 321-339.

99. T. Okano, *Biorelated polymers and gels*, Academic Press, San Diago, 1998.

100. J. Kobayashi, A. Kikuchi, K. Sakai and T. Okano, "Aqueous chromatography utilizing hydrophobicity-modified anionic temperature-responsive hydrogel for stationary phases", *J. Chromatography. A* **2002**, *958*, 109-119.

101. S. Anastase-Ravion, Z. Ding, A. Pellé, A. S. Hoffman and D. Letourneur, "New antibody purification procedure using a thermally responsive poly(*N*-isopropyl-

acrylamide)-dextran derivative conjugate", *J. Chromatography. B* **2001**, *761*, 247-254.

102. V. T. Pinkrah, M. J. Snowden, J. C. Mitchell, J. Seidel, B. Z. Chowdhry and G. R. Fern, "Physicochemical properties of poly(*N*-isopropylacrylamide-co-4-vinyl-pyridine) cationic polyelectrolyte colloidal microgels", *Langmuir* **2003**, *19*, 585-590.

103. M. Kurisawa and N. Yui, "Dual-stimuli-responsive drug release from inter-penetrating polymer network-structured hydrogels of gelatin and dextran", *J. Control. Release* **1998**, *54*, 191-200.

104. J. Hoffmann, M. Plötner, D. Kuckling and W. -J. Fischer, "Photopatterning of thermally sensitive hydrogels useful for microactuators", *Sensor. Actuat. A* **1999**, *77*, 139-144.

105. L-C. Dong and A. S. Hoffman, "Synthesis and application of thermally reversible heterogels for drug delivery", *J. Control. Release* **1990**, *13*, 21-31.

106. N. Kato, S. Yamanobe and F. Takahashi, "Property of magneto-driven poly(*N*-isopropylacrylamide) gel containing γ-Fe_2O_3 in NaCl solution as a chemo-mechanical device", *Mater. Sci. Eng. C* **1997**, *5*, 141-147.

107. N. Reber, R. Spohr, A. Wolf, H. Omichi, M. Tamada and M. Yoshida, "Closure characteristics of a thermally responsive single ion-track pore determined by size exclusion method", *J. Membr. Sci.* **1998**, *140*, 275-281.

108. T. Okano, N. Yamada, M. Okuhara, H. Sakai and Y. Sakurai, "Mechanism of cell detachment from temperature-modulated, hydrophilic-hydrophobic polymer surfaces", *Biomaterials* **1995**, *16*, 297-303.

109. Y. Kaneko, S. Nakamura, K. Sakai, A. Kikuchi, T. Aoyagai, Y. Sakurai and T. Okano, "Deswelling mechanism for comb-type grafted poly(*N*-isopropylacrylamide) hydrogels with rapid temperature responses", *Polym. Gels Networks* **1998**, *6*, 333-345.

110. S. E. Webber, "Polymer Micelles: An Example of Self-Assembling Polymers", *J. Phys. Chem. B* **1998**, *102*, 2618-2626.

111. P. Linse and M. Malmsten, "Temperature-dependent micellisation in aqueous block copolymer solutions", *Macromolecules* **1992**, *25*, 5434-5439.

112. A. E. English, T. Tanaka and E. R. Edelman, "Equilibrium and non-equilibrium phase transitions in copolymer polyelectrolyte hydrogels", *J. Chem. Phys.* **1997**, *107*, 1645-1654.

113. P. E. Depoy and D. M. Mason, "Periodicity in chemically reacting systems", *Faraday Symp. Chem. Soc.* **1974**, *9*, 47-54.

114. R. J. Field and M. Burger, Eds. *In Oscillations and Travelling Waves in Chemical Systems*, Wiley-Interscience: New York, 1985.

115. A. M. Zhabotinsky, "Periodic liquid-phase oxidation reactions", *Dokl. Akad. Nauk SSSR* **1964**, *157*, 392-395.

116. I. R. Epstein and K. Showalter, "Nonlinear chemical dynamics: Oscillations, Patterns, and Chaos", *J. Phys. Chem.* **1996**, *100,* 13132-13147.

117. A. T. Winfree, "Scroll-shaped waves of chemical activity in three dimensions", *Science* **1973**, *181*, 937-939.

118. L. Kuhnert and H.-J. Krug, "Kinetics of chemical waves in the acidic borate malonic acid-$Ru(bpy)_3^{2+}$ system in comparison with the ferroin system, *J. Phys. Chem.* **1987**, *91*, 730-733.

119. L. Kuhnert, "A new optical photochemical memory device in a light sensitive chemical active medium", *Nature* **1986**, *319*, 393-394.

120. M. Markus, Zs. Nagy-Ungvarai and B. Hess, "Phototaxis of spiral waves", *Science* **1992**, *257*, 225-227.

121. M. K. R. Reddy, Zs. Nagy-Ungvarai and S. C. Muller, "Effect of visible light on wave propagation in the ruthenium-catalysed Belousov-Zhabotinsky reaction", *J. Phys. Chem.* **1994**, *98*, 12255-12259.

122. M. S. Paoletti and T. H. Solomon, "Front propagation and mode-locking in an advection-reaction-diffusion system", *Phys. Rev. E* **2005**, *72*, 046204:1-046204:10.

123. R. Yoshida, M. Tanaka, S. Onodera, T. Yamaguchi and E. Kokufuta, "In-phase synchronisation of chemical and mechanical oscillations in self-oscillating gels", *J. Phys. Chem. A* **2000**, *104*, 7549-7555.

124. M. A. Marek, S.C. Müller, T. Yamaguchi, and K. Yoshikawa, Eds.: "Dynamism and regulation in nonlinear chemical systems", *Physica D*, *84* (Special volume), Elsevier Science Publishers B. V., Amsterdam, 1995.

125. T. S. Briggs and W. C. Rauscher, "An oscillating iodine clock," *J. Chem. Educ.* **1973**, *50*, 496.

126. I. R. Epstein and J. A. Pojman, *An Introduction to Nonlinear Chemical Dynamics*; *Oscillation, Waves, Patterns, and Chaos*, Oxford University Press: New York, 1998.

127. R. M. Noyes, "Mechanism of some chemical oscillators", *J. Phys. Chem.* **1990**, *94*, 4404-4412.

128. P. Ševčík, K. Kissimonová and L. Adamčíková, "Oxygen production and numerical simulations of the interphase transport in the modified oscillating Briggs-Rauscher reaction", *J. Phys. Chem. A* **2003**, *107*, 1290-1295.

129. D. O. Cooke, "The hydrogen peroxide-iodic acid-manganese (ii)-acetone oscillating system: Further observations", *Int. J. Chem. Kinet.* **1980**, *12*, 683-698.

Chapter 2

Experimentals

Chapter 2

Experimental

2.1 Materials

2.1.1 Water

Water was first purified by a reverse osmosis system Elgastat Prima® (Elga, UK) and then passed through a Milli-Q reagent water system (Millipore, UK). Surface tension was typically measured between 71.5 and 72.5 mN/m at room temperature (20–25 °C), which is in good agreement with literature values for water-air surface.[1] The measured resistivity always exceeded 18 MΩ cm. The purified water was passed through 0.2 μm pore sized syringe filter (Whatman, UK) with a syringe for all experiments with DNA.

2.1.2 DNA oligonucleotides

The DNA oligonucleotides were synthesised to our specifications (usually at the 1000 nmol scale), purified by high performance liquid chromatography (HPLC) and lyophilised by Alpha DNA (Quebec, Canada), which is a company specialising in DNA synthesis. This company uses the phosphoramidite method of oligonucleotide synthesis.[2] The synthesis is performed with the growing DNA chain attached to a solid support so that excess reagents that are in the liquid phase can be removed by filtration. The synthesis proceeds in the 3′→ 5′ direction; this means that the new nucleotide is attached to the 5′-end of the growing chain.

Different modifications can be easily incorporated into an oligonucleotide at the time of synthesis. This is achieved using specialized phosphoramidite reagents for 5'-modifications. The 5′-end modification is also cheaper than the 3′-end one. In the current work, amphiphiles containing 10–12 DNA bases were synthesized by attaching a hydrophobic group at the 5′-end of DNA base. This was usually cholesteryl or multiple saturated dodecyl (C_{12}) hydrocarbon chains joined together by an ether linkage (see Figure 2.1). The DNA-surfactants that have been used are listed in the following Table 2.1.

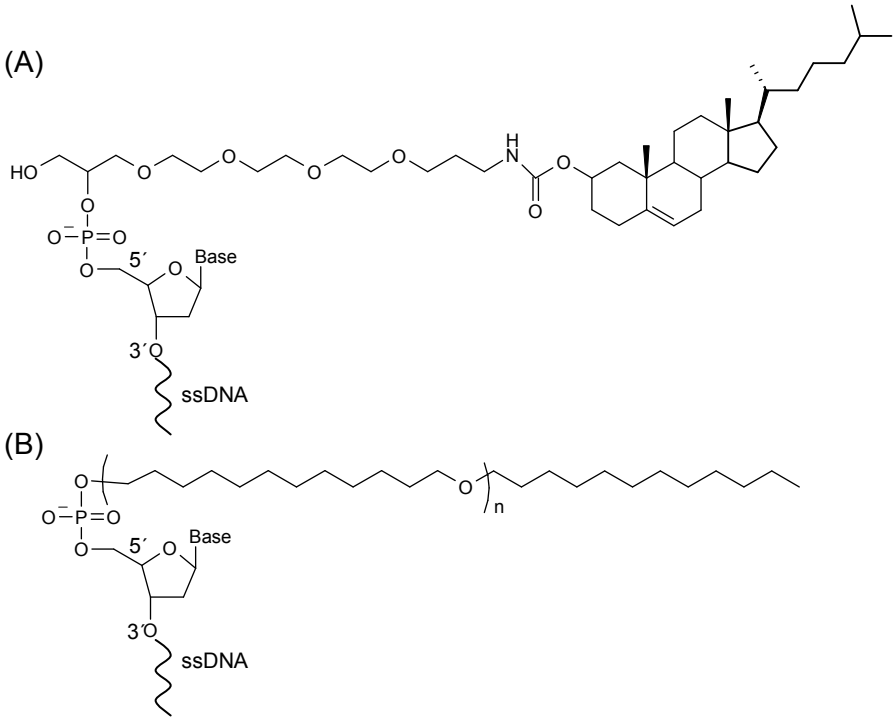

Figure 2.1: A) Cholesteryl modified DNA single strand oligonucleotides. B) Multiple C_{12} chains (n = 2, 3 and 4) modified oligonucleotide. Both of the two modifications are located at the 5′-end of the DNA chain. 'Base' represents the last base at the 5′-end of the single DNA strand.

Table 2.1: Specification of the DNA surfactants

Oligonucleotide structure	Modification of 5′-end of the DNA chain
• C12-O-C12 -5′-TTTTTTCCCCCC-3′ • C12-O-C12-5′-GGGGGGAAAAAA-3′	1 saturated dodecyl hydrocarbon chain (i.e. $(C_{12}O)_2$-5′-end).
• C12-O-C12-O-C12-5′-TTTTTTCCCCCC-3′ • C12-O-C12-O-C12-5′-GGGGGGAAAAAA-3′	3 saturated dodecyl hydrocarbon chains (i.e. $(C_{12}O)_3$-5′-end).
• C12-O-C12-O-C12-O-C12-5′-TTTTTTCCCCCC-3′ • C12-O-C12-O-C12-O-C12-5′-GGGGGGAAAAAA-3′	4 saturated dodecyl hydrocarbon chains (i.e. $(C_{12}O)_4$-5′-end).
• Cholesteryl-5′-TTTTTTCCCCCC-3′ • Cholesteryl-5′-GGGGGGAAAAAA-3′	Cholesteryl group (i.e. Cholesteryl-5′-end).

In our experiments, several kinds of fluorescent dyes labelled to the 5′- or 3′-end oligonucleotide were also used. *N,N,N′,N′*-tetramethyl-6-carboxyrhodamine (TAMRA) and fluorescein isothiocyanate (FITC) were used as fluorescent modification of DNA oligonucleotide, (Table 2.2 and Figure 2.2). The fluorescent DNA oligonucleotides were also purchased from Alpha DNA.

Table 2.2: Specification of the fluorescent oligonucleotides

Fluorescent oligonucleotide	Observations
TAMRA-5´-TTTTTTCCCCCC-3´ 5´-GGCCAGTCACTG-3´-TAMRA	TAMRA is *N,N,N′,N′*-tetramethyl-6-carboxyrhodamine $\lambda_{max.abs}$ = 543 nm, $\lambda_{max.em}$ = 570 nm
FITC-5´-TTTTTTCCCCCC-3´ 5´-GGCCAGTCACTG-3´-FITC	FITC is fluorescein isothiocyanate $\lambda_{max.abs}$ = 490 nm, $\lambda_{max.em}$ = 510 nm

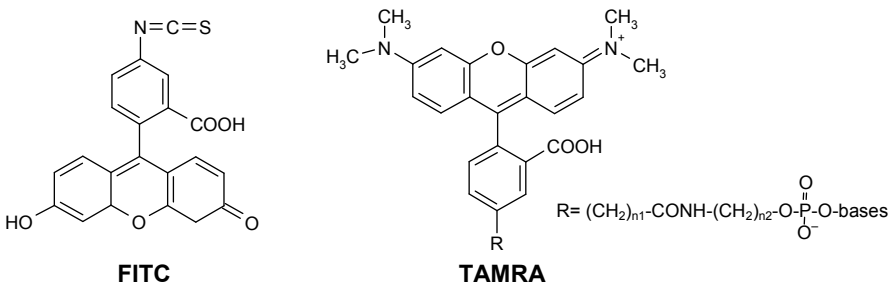

Figure 2.2: Chemical structures of the fluorescent dyes in the present study: FITC was used in both free dye and conjugated form; TAMRA modified to DNA probes.

2.1.2.1 Dissolution of the oligonucleotides

HPLC purified and lyophilised DNA oligomers were dissolved in 400 μL of pure water which was filtered with a 0.2 μm pore sized GD/X syringe filter (Whatman, UK). HPLC purified and lyophilised DNA-surfactants were dissolved in Tris buffer (10 mM, pH 8.0 in pure water) which was also filtered with a syringe filter. All DNA oligomers and DNA-surfactants were stored at – 4 $^{\circ}$C before use.

2.1.2.2 Measurement of oligonucleotides concentrations

The concentration of the oligonucleotides was determined by measuring the absorbance at 260 nm using a UV spectrophotometer. 10 μL of the stock solution was diluted with 1990 μL of buffer or pure water in order to fill a quartz cuvette (light path length = 1 cm) with a solution 1–5 μM of oligonucleotide, and the absorbance measured. The concentration was calculated using the Lambert-Beer equation:

$$A_{260nm} = \varepsilon_{260} \cdot l \cdot c_{DNA} \qquad [1]$$

where A is the absorbance at 260 nm; ε_{260} is the molar extinction coefficient (mL mmoles^{-1} cm^{-1}) of the oligonucleotide; l is the path length of the quartz cuvette (1 cm); c is the concentration of the oligonucleotide in mmole millilitres^{-1}.

The extinction coefficient is a unique physical property for each oligonucleotide. The value of the extinction coefficient (ε_{260}) equals the absorbance at 260 nm that results from 1 mmole of oligonucleotide dissolved in 1 mL volume (a 1 M solution) when measured in a standard 1 cm path-length cuvette.[3] The extinction coefficient for an oligonucleotide can be directly calculated from the base sequence using established constants.[4] It is determined by both base order (sequence) and base composition. Modifications such as fluorescent groups also affect the absorbance of an oligonucleotide. The value of ε_{260} was calculated by using the Integrated DNA Technologies (IDT) Oligo Analyzer available on the IDT web site.[5] Once the molar extinction coefficient was calculated, from equation (1) the concentration of the oligonucleotide in the cuvette was:

$$c_{DNA} = \frac{A_{260nm}}{\varepsilon_{260} \cdot l} \qquad [2]$$

The final concentration of the stock solution was obtained by multiplying c with the dilution factor.

2.1.2.3 Melting temperature of oligonucleotides

The melting temperature was also calculated using the IDT's T_m Calculator (also available from The Oligo Analyzer on the IDT web site). The values of T_m are predicted using an equation that takes in account the oligonucleotide concentration, the concentration of monovalent cations (T_m are often determined in Na^+ buffers) and the effects of neighbouring bases (base stacking)[6], as explained in the Introduction.

2.1.3 Thermotropic liquid crystal (LC) 5CB

The liquid crystal that has been studied in the experimental system in chapter 3 and 4 is 4-pentyl-4'-cyanobiphenyl (5CB). 5CB is the most frequently used thermotropic liquid crystal which forms a nematic phase at ambient temperatuer (e.g., 25 °C). 5CB was purchased from Kingston chemicals Ltd. (Hull, UK) and used as received without any further purification.

Table 2.3: Specification of thermotropic liquid crystal 5CB

Structure	Specifications
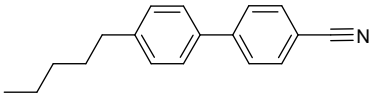	• Purity: ≥ 99.5 % • Transition temperature from crystal to nematic: 24.0 °C Transition temperature from nematic to isotropic: 35.01 °C • Density: 1.008 g/cm^3

The physical properties of 5CB are same as those mentioned in many references.[7,8]

2.1.4 Surfactants and fatty acids

For the examination of the alignment change of 5CB at the LC-water interface, different types of surfactants were used. Their structures and properties with their critical micelle concentrations (cmc) are shown in Figure 2.3 and Table 2.4.

(2-(methacryloyloxy)ethyl) dodecyldimethylammonium bromide (MEDDAB)[9,17] and 11-(methacryloyloxy) undecylbutyl dimethylammonium bromide MUBDMAB were obtained from Avecia Ltd. (Manchester, UK) and were purified and measured (by Epton titration[10]) as described in a previous study.[11] These two polymerisable cationic surfactants bearing functional methacrylate groups in different positions were used as an alternate of cationic alkyltrimethylammonium bromides.

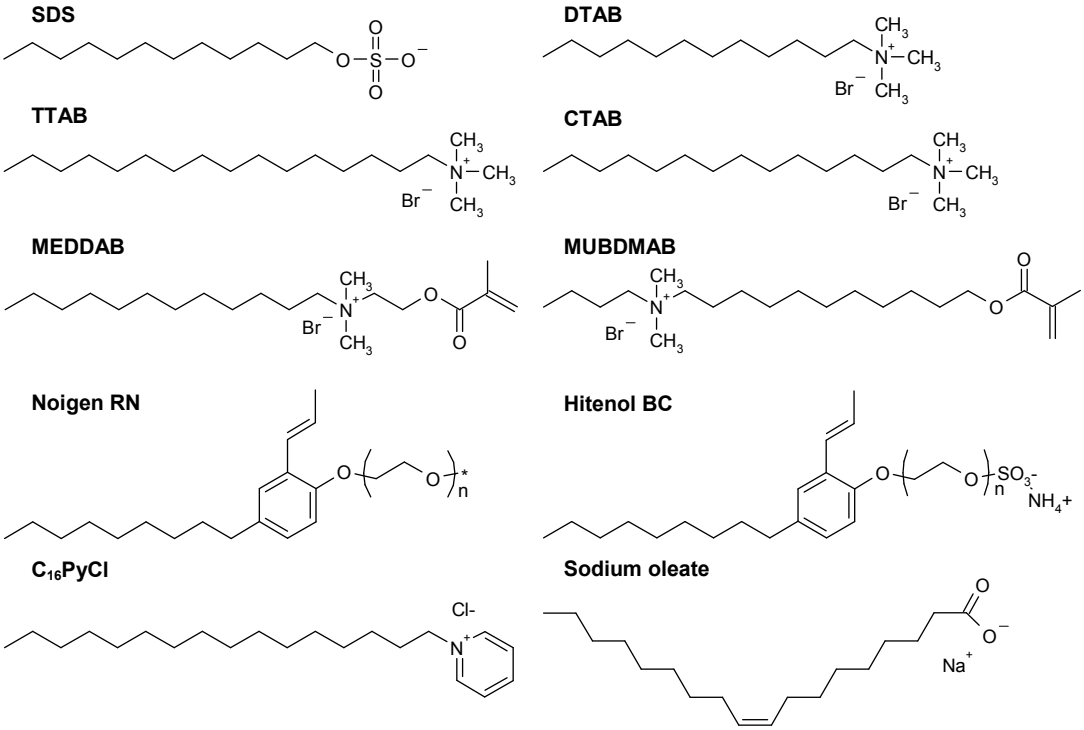

Figure 2.3: Chemical structures of surfactants that adsorb at the 5CB-water interface.

Table 2.4: Characteristics of the surfactants

Product	Purity	Manufacturer	Type/Observations
Sodium dodecyl sulfate (or SDS)	98.5 %	Aldrich	Anionic cmc = 8.36×10^{-3} M[12]
Dodecyltrimethylammonium bromide (or DTAB)	97.6 %	Aldrich	Cationic cmc = 1.41×10^{-2} M[13]
Tetradecyltrimethylammonium bromide (or TTAB)	> 98 %	Fluka Chemicals	Cationic cmc = 4.0×10^{-3} M[14]
Cetyltrimethylammonium bromide (or CTAB)	99 %	Fluka Chemicals	Cationic cmc = 1.0×10^{-3} M[15]
Cetylpyridinium chloride (or C_{16}PyCl, CPC)	> 98 %	Fluka Chemicals	Cationic cmc = 1.0×10^{-3} M[16]
(2-(methacryloyloxy) ethyl) dodecyldimethylammonium bromide (or MEDDAB)	≥ 99 %	Avecia Ltd.	Cationic polymerisable cmc = 4.0×10^{-3} M[17]
11-(methacryloyloxy) undecylbutyl dimethylammonium bromide (or MUBDMAB)	≥ 82 %	Avecia Ltd.	Cationic polymerisable
Polyoxyethylene alkylphenyl ether (Noigen RN-10, -20)	> 99 %	Daich Kogyo Seiyaku	Non-ionic polymerisable
Polyoxyethylene alkylphenyl ether ammonium sulphate (Hitenol BC-10, -20)	> 97 %	Daich Kogyo Seiyaku	Anionic polymerisable Hitenol BC-10: cmc = 8.7×10^{-5} M[18] Hitenol BC-20: cmc = 1.0×10^{-4} M[18]
cis-9-Octadecenic acid (or oleic acid)	99 %	Sigma-Aldrich	$pK_a = 4.8$
cis-9-octadecenic acid sodium salt (or sodium oleate)	> 99 %	Fluka Chemicals	cmc= 6.0×10^{-4} M[19]

2.1.5 Colloid particles and a gelling agent for Janus particles

For the preparation of Janus particles using the gel trapping technique (GTT) and the glass sliding technique (GST), colloid particles and other chemicals were needed. The characteristics of most of these are described in the following paragraphs.

Several different types of colloidal particles were used in our experiments. As this thesis is in part concerned with a new method for the preparation of metal coated Janus particles, commercial samples of monodisperse colloid particles were also used. The main characteristics of the different samples of monodisperse spherical particles used in our studies are summarised in Table 2.5.

Table 2.5: Characteristics of the polystyrene latex/PMMA particles

Particle (surface groups)	Particle diameter/μm	Manufacturer
Divinylbenzene/carboxylate modified polystyrene latex	3.1 ± 0.28	Interfacial Dynamics Corporation (IDC)
Carboxylate modified (CML) polystyrene latex	9.8 ± 0.66	
Carboxylated polystyrene latex	15.5 ± 1.1	Microparticles GmbH
Polymethyl methacrylate (PMMA)	87.5 ± 1.6	

We also used hydrophilic fumed silica particle, Aeroperl® 300/30 (Evonik Degussa, US) and the characteristics of which are given in the following Table 2.6.

Table 2.6: Characteristics of the fumed silica particle used in our studies

Properties	Typical value
Average primary particles size	~30 μm
Tap density of particles	~280 g/dm^3
Moisture content after 2 h at 105 °C	≤ 3.5 wt%
pH in 4 wt% dispersion in water	4.0 ~ 6.0

The silica particles with a diameter larger than 60 μm were separated using a 60 μm sized metal test sieve (Endecotts Ltd., UK).

The following polysaccharides were used as gelling agents. Gellan gum is a linear anionic polysaccharide produced by the microorganism *pseudomonas elodea*. Kelcogel® with low acyl content was supplied by CP Kelco (Liverpool, UK).[20] It was passed through a C_{18}-column to remove any amphiphilic impurities as explained later in section 2.2.1.2. The structure of gellan is shown in Figure 2.4.

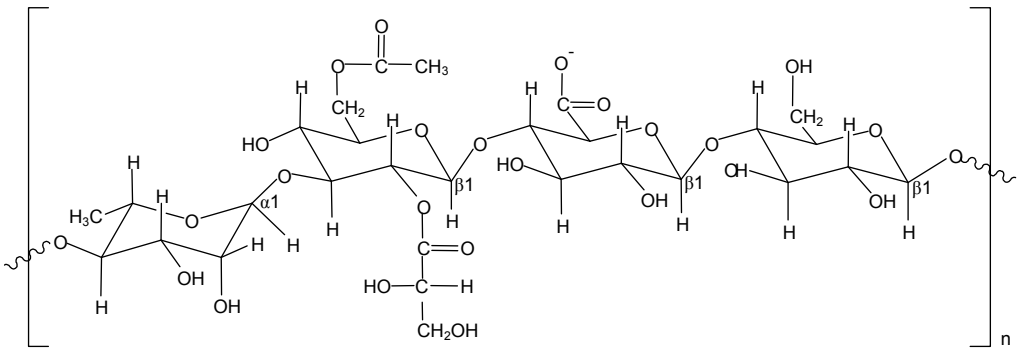

Figure 2.4: Chemical structure of gellan gum Kelcogel® used in our experiments.

Glucose (from Sigma, α-D-Glucose anhydrous, > 99.5 % purity) and sucrose (from BDH, > 99 % purity from sugar cane) were also used in our studies.

2.1.6 Enzymes

Two kinds of enzymes were used for the preparation of enzymatic reaction driven self-propelling particles (section 6.2) as shown in Table 2.7. They were used without any additional purification.

Table 2.7: Characteristics of the enzymes used for self-propelling particles

Enzyme	Manufacturer	Purity/Activity
Invertase from baker's yeast (*Saccharomyces. cerevisiae*)	Sigma-Aldrich	Grade VII, > 300 units /mg of solid [a]
Catalase from bovine liver, aqueous suspension	Sigma-Aldrich	10,000–40,000 units /mg of protein [b]

a. One unit will decompose 1.0 μmole of H_2O_2 per min at pH 7.0 at 25 °C from Sigma-Aldrich.

b. One unit will hydrolyze 1.0 μmole of sucrose per min at pH 4.5 at 55 °C from Sigma-Aldrich.

Invertase is an enzyme mainly used for the production of invert sugar in the food industry.[21] Invertase from baker's yeast is a glycoprotein containing 50 % mannan and 2–3 % glucosamine. Invertase catalyzes the follwing reaction:

$$\text{Sucrose} + H_2O \rightarrow \text{Glucose} + \text{Fructose}$$

Rafiinose and methyl-β-D-fructofuranoside may also be utilized as substrates. Reported Michaelis constant (K_m) are 25 mM for sucrose and 150 mM for rafiinose.[22] In this study, one unit of invertase was defined as the amount of enzyme able to hydrolyze 1.0 μmole of sucrose to invert sugar per min at pH 4.5 at 55 °C.[23]

Catalase consists of four identical subunits each equipped with an Fe^{3+} porphyrin (Por) IX (heme) in the active site. The catalytic cycle of catalase involves a two-step reaction. In the first step (equation 3), the enzyme (Fe^{3+} Por) in the resting state reduces a hydrogen peroxide molecule to water and generates a ferryl porphyrin (Fe^{4+} Por) with a porphyrin π-cation radical (Fe^{4+}=O $Por^{+\bullet}$), so-called compound *I*. In the second step, compound *I* oxidizes a second hydrogen peroxide molecule to molecular oxygen and water (equation 4).[24]

$$\text{Catalase } (Fe^{3+}\ \text{Por}) + H_2O_2 \rightarrow \text{Compound } I\ (Fe^{4+}{=}O\ Por^{+\bullet}) + H_2O \qquad [3]$$

$$\text{Compound } I\ (Fe^{4+}{=}O\ Por^{+\bullet}) + H_2O_2 \rightarrow \text{Catalase } (Fe^{3+}\ \text{Por}) + H_2O + O_2 \qquad [4]$$

The reactive intermediate compound *I* is also observed when organic peroxides are used

as substrates, and the rate of formation of compound *I* decreases with an increase in the molecular size of the leaving group (e.g., H- > CH_3- > $HOCH_2$- > CH_3CH_2- > CH_3CO- > CH_3-$(CH_2)_2$- > CH_3-$(CH_2)_3$-OOH). Moreover, compound *I* has the potential to oxidize short-chain alcohols such as methanol and ethanol. The reaction rate constant of catalase is dependent on the molecular size of the substrate (Tables 2.8 and 2.9).[25, 26]

Table 2.8: Comparison of compound *I* formation rates of bovine liver catalase in the reaction with hydrogen peroxide (H_2O_2), methyl hydroperoxide (CH_3OOH), peracetic acid (CH_3COOOH), and *tert*-butyl hydroperoxide [$(CH_3)_3COOH$][25]

Enzyme	Hydrogen peroxide	Methyl hydrogen peroxide	Peracetic acid	*t*-butyl hydrogen peroxide
Rate (M^{-1} s^{-1})	3.5×10^7	2.54×10^6	5.22×10^5	1.82×10^4

Table 2.9: Catalytic properties of horse liver catalase compound *I* at pH 6.7[26]

Substrates	Hydrogen peroxide	Methyl hydrogen peroxide	Ethyl hydrogen peroxide
Rate (M^{-1} s^{-1})	3×10^7	8.5×10^5	2×10^4

We used some chemicals for the immobilisation of enzymes onto the surfaces of polystyrene latex particles as follows (Table 2.10):

Table 2.10: Characteristics of the chemicals used in the immobilisation of enzymes

Name	Manufacturer	Purity	Observations
N-ethyl-*N*′-(3-dimethylamino-propyl) carbodiimide hydrochloride (or EDAC)	Fluka Chemicals	99.9 %	Coupling agent
2-(*N*-morpholino)ethanesulfonic acid (MES) monohydrate	Sigma-Aldrich	≥ 99.0 %	For 0.025 M buffer solution at pH 6.0
Fluorescein isothiocyanate isomer *I* (or FITC)	Sigma-Aldrich	90 %	Fluorescent marker, λ_{abs} = 492 nm, λ_{em} = 518 nm in 20 mM CAPS ($C_9H_{19}NO_3S$), pH 10

Fluorescein isothiocyanate isomer *I* was used for the detection of invertase adsorbed at the surface of polystyrene latex particles after immobilisation of enzyme.

2.1.7 Monomers, cross-linker and initiators for hydrogel synthesis

For the preparation of stimuli-responsive hydrogels, various kinds of monomers were used and polymerised by UV polymerisation according to the experimental conditions. They are listed in the Table 2.11 and their structures are shown in Figure 2.5.

Table 2.11: Characteristics of the monomers, initiators, and accelerator

Name	Purity	Manufacturer	Observations
N-isopropylacrylamide (or NIPAAm)	97 %	Sigma-Aldrich	Neutral monomer
Acrylamide (AAm)	≥ 99 %	Sigma-Aldrich	Neutral monomer
Acrylic acid (or AAc), anhydrous	≥ 99 %	Fluka Chemicals	Anionic monomer
2-acrylamido-2-methyl-1-propanesulfonic acid (or AMPS)	99 %	Sigma-Aldrich	Anionic monomer
N,N´-methylene bisacrylamide (or MBAAm)	≥ 98 %	Sigma-Aldrich	Cross-linker
Divinyl benzene (or DVB)	80 %	Sigma-Aldrich	Cross-linker Mixture of isomers, inhibited with 4-t-butylcatechol
Ruthenium (II)-tris(2,2´-bipyridyl) dichloride hexahydrate (or $Ru(bpy)_3Cl_2 \cdot 6H_2O$)	-	Sigma-Aldrich	Metal catalyst for the BZ reaction
Ruthenium(4-vinyl-4-methyl-2,2´-bipyridine)bis(2,2´-bipyridine)bis (hexafluorophosphate) (or $Ru(bpy)_2(mvbpy)(PF_6)_2$	≥ 99 %	Cyanagen (Bologna, Italy)	Catalytic metallic monomer for the BZ reaction
2,2'-azobis(2-methyl-propionitrile) (or AIBN)	≥ 98 %	Acros Organics	Thermal initiator
2,2-dimethyl-2-hydroxyacetophenone (or Darocur 1173)	> 95 %	Ciba Fine Chemical	Photoinitiator
2,2-dimethoxy-2-phenylacetophenone	99 %	Aldrich	Photoinitiator
N,N,N′,N′-tetramethyl-ethylenediamine (or TEMED)	> 99%	Fluka Chemicals	Accelerator

NIPAAm was recrystallized from hexane before use and other chemicals were used as received.

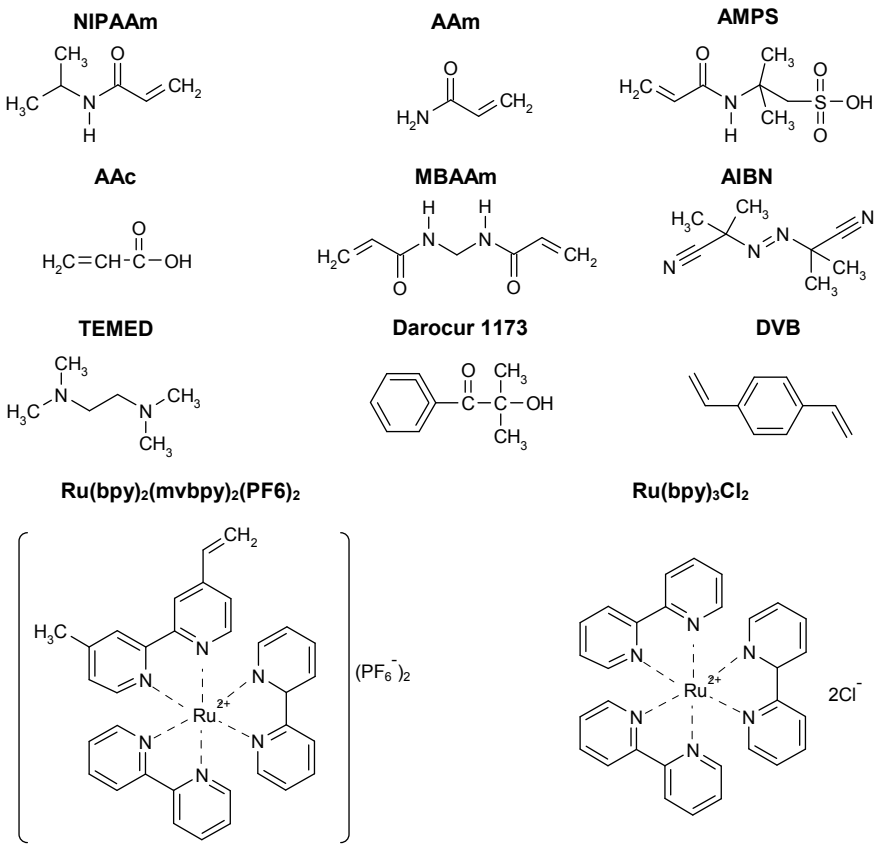

Figure 2.5: Chemical structures of chemicals used for the preparation of hydrogels except for DVB used as a cross-linker in the polymerisation of surfactants.

2.1.8 Buffers

Table 2.12 lists the buffer solutions, with the suppliers and specifications. These buffers were used after filtering with a 0.2 μm pore sized GD/X syringe filter (Whatman, UK) without further treatment. Some buffers were freshly prepared by mixing the components listed in the composition column in Table 2.12 (home prepared buffers). The pH was measured using a pH meter and adjusted by adding a few drops of sodium hydroxide (aqueous solutions of 5 M concentration prepared using NaOH pellets and pure water) or hydrochloric acid (5 M HCl aqueous solutions from Sigma-Aldrich).

Table 2.12: Specification of the buffers

Name	Manufacturer	Observations
20× Saline Sodium Citrate Buffer Concentrate (or 20× SSC)	Fluka Chemicals	Solution of: 0.3 M sodium citrate, 3 M NaCl, pH 7.0 in water (DNase free condition)
Phosphate Buffered Solution (or PBS)	Sigma-Aldrich	0.1 M phosphate, pH 7.5, sterile
Trizma® (pre-set crystal) (Registered trademark for tris(hydroxymethyl)aminomethane)	Sigma-Aldrich	Commonly called Tris, it is a salt used to prepare 0.05 M solution with pH of 7 at 25 °C

Home prepared buffers	
Name	**Composition**
Phosphate Buffer A	0.01 M of NaH_2PO_4, 10^{-4} M of EDTA, 0.1 M NaCl, pH = 7.03
Phosphate buffer B	0.1 M NaH_2PO_4, pH 7.0
SPSC buffer	1 M NaCl, 50 mM NaH_2PO_4, pH 6.5
Hybridisation buffer (HB)	0.09 M sodium citrate, 0.9 M NaCl and 0.01 NaH_2PO_4, 1 mM EDTA, 10 μg/ml salmon sperm DNA, pH 7.0
Hybridisation buffer solution (HBS)	0.09 M sodium citrate, 0.9 M NaCl and 0.01 M NaH_2PO_4, 1 mM EDTA
HEPES buffer	10 mM HEPES sodium salt, 5 mM EDTA, pH 6.7
TE buffer	10mM Tris (hydroxymethyl) aminomethane (called Trizma®), 1 mM Na_2 EDTA, 0.1 M NaCl, pH 7.0
Phthalate buffer	0.1 M potassium hydrogen phthalate, pH 4.0

2.1.9 Organic solvents

Organic solvents were used for different purposes such as the recrystallization of monomers for hydrogel synthesis (hexane) and the OTS treatment of glass slides (heptane). Their characteristics are listed in Table 2.13. Decane and hexadecane were purified by passing twice through a SEP-PAK® column (Millipore, US).

Table 2.13: Characteristics of the organic solvents used

Name	Purity	Manufacturer	Observations
Decane	> 99 %	Sigma	Purification with SEP-PAK® column (see section 2.2.5.1)
Hexadecane	> 99 %	Lancaster	
Toluene	99 %	Fisher Scientific	Purification with alumina column (see section 2.2.2.1)
Heptane	99 %		
Hexane	99 %		
Methanol	99.8 %		
Ethanol	absolute, 99 %		
Dichloromethane	> 99 %		
Isopropanol (or IPA)	99.7 %	BDH	
Dimethylsulfoxide (or DMSO)	≥ 99.5 %	Fluka Chemicals	

Different miscellaneous chemicals also used in the experiments described in this thesis are summarised in the following Table 2.14.

Table 2.14: Characteristics of miscellaneous chemicals used

Name	Purity	Manufacturer	Observations
Octadecyltrichlorosilane (or OTS)	> 90 %	Sigma	Silanising agent
Dichlorodimethylsilane (or DCDMS)	> 99.5 %	Fluka Chemicals	
Hydrogen peroxide	30 wt% solution in water	Fisher Scientific	For 'Piranha' solution
Sulfuric acid	98 %		
Ethylenediaminetetraacetic acid (or EDTA)	99 %	Prolabo	
Ethylenediaminetetraacetic acid disodium salt (or Na_2EDTA)		Sigma Aldrich	
Polydimethylsiloxane (Sylgard®184) (or PDMS)		Dow Corning	Two part curable silicone elastomer
Sodium bromate (or NaBrO)	≥ 99.0 %	Fluka Chemicals	Substrates in the BZ or BR reactions
Nitric acid, fuming 100 %	≥ 99.5 %		
Malonic acid (or MA)	≥ 99.0 %		
Manganese(II) sulfate monohydrate ($MnSO_4 \cdot H_2O$)	≥ 99.0 %		
Silver nitrate (or $AgNO_3$)	≥ 99.0 %		For removing Cl^- ions from $[Ru(bpy)_3Cl_2]$
Sodium bromide (or NaBr)	≥ 99.0 %	Lancaster	

2.2 Methods

2.2.1 Microscopy

2.2.1.1 Optical microscopy equipped with crossed polarisers

Two different microscopes were used in this study to characterise our samples.

Olympus BX51

This is an optical fluorescence microscope fitted with crossed polarisers and an Olympus microscope digital camera system DP70 consisting of a 1.45 million pixel charge coupled device (CCD). Using this DP70 system, the maximum image resolution of 4080×3072 pixels can be obtained. Images were processed using Image Pro® Plus software (MediaCybernetics, MD, US). This microscope was fitted with a series of fluorescence filter sets corresponding to the adsorption and emission wavelengths of specific dyes[27] (Table 2.15).

Table 2.15: Characteristics of the different filter sets fitted on the Olympus BX51 fluorescence microscope and names of the corresponding fluorescent dyes

Filter set name	Description	$\lambda_{excitation}$ (nm)	$\lambda_{emission}$ (nm)	Fluorescent dye
U-MWIBA2	Wide-band with band pass barrier filter	460-490	510-550	FITC, Eosin-isothiocyanate, Neuro-Dio
U-MWIG2	Wide-band with interference barrier filter	520-550	580 IF*	Rhodamine, Tetramethylrhodamine isothiocyanate (TRITC)
U-M51004V2	FITC/TRITC filter set	~490-510 ~560-585	~525-545 ~600-635	FITC, Neuro-DiO, Rhodamine, Nile Red

**High-performance interference type filter having a steep cutting edge, and excellent spitting characteristics.*

It is used with a series of objectives UPlan FI 4×/0.13, UPlan FI 10×/0.30, UPlan FI 20×/0.50, UPlan FI 40×/0.75 and UPlan FI 100×/0.30 magnification and two additional Long Working Distance (LWD) lenses of LM Plan FI 20×/0.40 and LM Plan FI 50×/0.50 magnification.

Nikon LaboPhot microscope

This is an optical transmitted microscope fitted with crossed polarisers and the following objectives: Nikon Plan 4×/0.10, Nikon Plan 10×/0.25, Nikon LWD 40×/0.65,

100×/1.25 Carl Zeiss. The microscope is equipped with QICAM FAST monochrome digital camera (QIMAGING, Canada) with the maximum image resolution of 1392 × 1040 pixels for grey optical images. Images were processed using Image Pro® Plus software.

2.2.1.2 Scanning Electron Microscopy (SEM)

Scanning electron microscopy (SEM) was used for observation of metal coated Janus particles before the immobilisation of enzymes by the EVO® 60 scanning microscope (Carl Zeiss SMT Ltd. Cambridge, UK). The gold (Au)-coated Janus polystyrene latex particles needed to be coated with a carbon layer since the specimens examined by SEM must be able to withstand the strong electric currents produced by the electron beam. Samples that do not conduct electricity can be damaged by the charges that can build up. Non-conductive specimens must first be coated with a thin layer of conductive material. Therefore, before imaging, the samples were coated with a ~10 nm carbon layer (spectrally pure graphite) by using a Polaron gold/palladium sputter coater (Polaron, East Sussex, UK) fitted with a planetary-motion sample rotation device. The SEM images were taken after observation of the whole sample in order to obtain a representative image using secondary electrons and backscattered electrons. The secondary electron image is good for the best resolution of fine surface topological features; otherwise the backscattered electron image gives contrast based on atomic number to resolve microscopic composition variations as well as topological information. The observation angle was also varied from 0 ° (view from the top) to ~85 ° (side view), depending on the aim of the experiments. The Au-coated Janus particles produced by fumed silica particles were not coated with a carbon layer before observation.

2.2.2 Treatment of microscope glass slides with silanizing agents

2.2.2.1 Octadecyltrichlorosilane (OTS) treatment on glass slides

Glass microscope slides were cleaned according to a procedure detailed in an earlier publication.[28] Briefly, the slides were immersed in a piranha solution [70 vol% sulfuric acid and 30 vol% hydrogen peroxide (30 wt% in water)] for 1 h at room temperature (Warning: piranha solution reacts strongly with organic compounds and should be handled with extreme caution; do not store the solution in closed containers.)

The slides were then (a) rinsed with pure water for at least 2 min; (b) drained of water and then rinsed with ethanol several times without permitting the surface of the slide to dry; (c) drained of ethanol and then rinsed three times using methanol and then immediately dried in dry oven at 70 °C for a minimum 2 h and baked on a hot plate at ~100 °C for > 2 h prior to OTS deposition. A 1 mM OTS solution was prepared by adding OTS to heptane that was purified by passage through an aluminium oxide column. Since OTS is easily hydrolysed under the influence of atmospheric humidity and may then form undefined polymerised material (Figure 2.6), the silane containing solutions were always freshly prepared and used within 2 h of their preparation.[29] The slides were immersed in the 1 mM OTS in heptane solution for 1 h at room temperature. They were rinsed with methylene chloride, ethanol, and methanol and dried in a dry oven at 70 °C before use. The quality of the OTS layer was tested by forming a sandwich of treated OTS slides spaced by copper electron microscope (EM) specimen grids. 5CB was confined in the grids between the OTS treated slides and the resulting optical texture was examined using polarised light to confirm homeotropic anchoring of 5CB expected for glass slides properly coated with OTS.[28] Any samples not exhibiting homeotropic anchoring of 5CB were discarded.[30] The quality of the OTS layer was also checked by measuring the alignment of 5CB on an OTS treated glass slide with the upper 5CB surface open to air. Since the 5CB-air surface is known to cause homeotropic anchoring of 5CB, the observed texture should be homeotropic anchoring.[30]

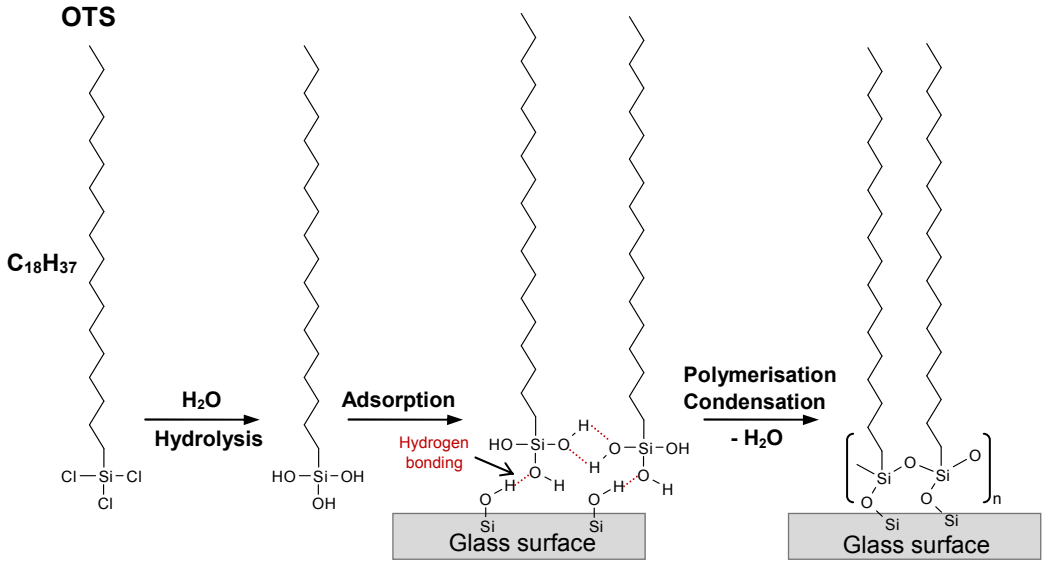

Figure 2.6: Chemisorption of *n*-octadecyltrichlorosilane (OTS) on a glass slide.

2.2.2.2 Dichlorodimethylsilane (DCDMS) treatment of glass slides

For preparation of a patterned hydrophobized glass slide using masking tapes, DCDMS was chosen as a silanizing agent so as not to disrupt the masked areas during the silanisation reaction (Figure 2.7). The DCDMS silanisation reaction is performed by exposing the glass surface to the vapour of DCDMS at room temperature.

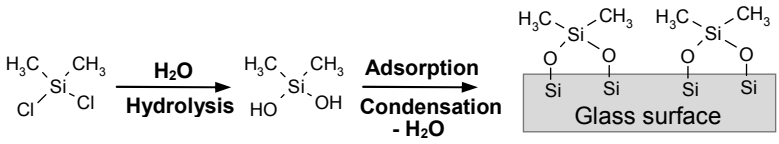

Figure 2.7: Patterned hydrophobic glass slide preparation using dichlorodimethylsilane (DCDMS). DCDMS only reacts with silanol groups on the unmasked surface of a glass surface.

The piranha solution cleaned suitably masked glass slides were placed in a glass bottle (~200 mL volume) containing 200 μL of DCDMS for > 12 h at room temperature. After peeling off the masking tapes they were rinsed with methylene chloride, ethanol, and methanol and dried in a dry oven at 60 °C before use.

Contact angles of water drops on Teflon substrates, OTS- and DCDMS-treated glass slides under air were measured by using a Krüss Drop Shape Analysis System (DSA-10) with a thermostated chamber at 20 °C. In a previous study,[31] the contact angle of water on Teflon® is about 110 degrees. Moreover, with increasing the Teflon surface roughness, an increase in values of the measured contact angles was observed to 129 ± 4 degrees.[31] The OTS- and DCDMS treatment produced a surface with a water contact angle of > 100 degrees and was sufficient to induce homeotropic anchoring of the 5CB (Table 2.16).[32]

Table 2.16: Three-phase contact angles of water drops on polymer substrates under air at 20 °C

Substrate	Contact angle at the air-water interface/deg.
Teflon Thread Seal Tape	130 ± 1
OTS treated glass slide	119 ± 4
DCDMS treated glass slide	103 ± 2
Polycarbonate cover of perfusion chamber	83 ± 4

2.2.3 Optical examination of 5CB textures at the LC-water interface

2.2.3.1 Preparation of LC optical cells for imaging of 5CB textures

A detailed description of the methods used to prepare and examine the LC optical cell is given an early publication.[33] Briefly, the copper (Cu) and gold (Au) electron microscope (EM) grids were cleaned sequentially in methylene chloride, ethanol, and methanol, then dried in a dry oven at 70 °C for 2 h, and then heated at ~100 °C for > 5 h. Several types of EM grids were used in this study. 100 mesh Cu or Au grids (20 μm thickness, 218 μm inner grid square side length and 47 μm bar width) from Agar Scientific (Stansted, Essex) and 50 mesh Au grid (11 μm thickness, 434 μm inner grid square side length and 93 μm bar width) from Fisher Scientific (Pittsburgh, PA). The grids were then placed onto the surface of OTS treated glass. 0.5 μL of 5CB was dispensed onto the grid with a 1 μL using an Eppendorf pipette, and excess 5CB was removed by contacting a 5 μL capillary tube (Drummond Scientific, Broomall, PA) with the 5CB droplet on the grid. This step resulted in consistent filling of the grids prior to exposure of the grid to various solution conditions. The surface of the 5CB in contact with the aqueous phase was approximately flat as determined by concurrent focus of the grid and 5CB under an optical microscope at objective powers ranging from 4× to 50× magnification. The exposure of the LC optical cells to an aqueous solution of surfactant was performed in two different ways:

1) 60 mm glass dish: The LC optical cell was heated to ~40 °C (above the nematic-isotropic transition temperature of 5CB of ~35 °C) and then immediately immersed in piranha-cleaned glass dishes containing 20 mL of a given aqueous solution of surfactants held at room temperature (~20 °C).
2) Perfusion chamber with internal volume 60 μL (Sigma-Aldrich): The LC optical cell was heated to ~40 °C and then incubated at room temperature for ~1 min to be homeotropic anchoring of 5CB under air. After confirming homeotropic anchoring of 5CB in all inner grid squares, the optical cell was mounted within a perfusion chamber which was then filled with ~55 μL of an aqueous solution. The perfusion chamber enabled easily exchange of the aqueous solution using the syringe connection.

A schematic representation of this system is shown in Figure 2.8.

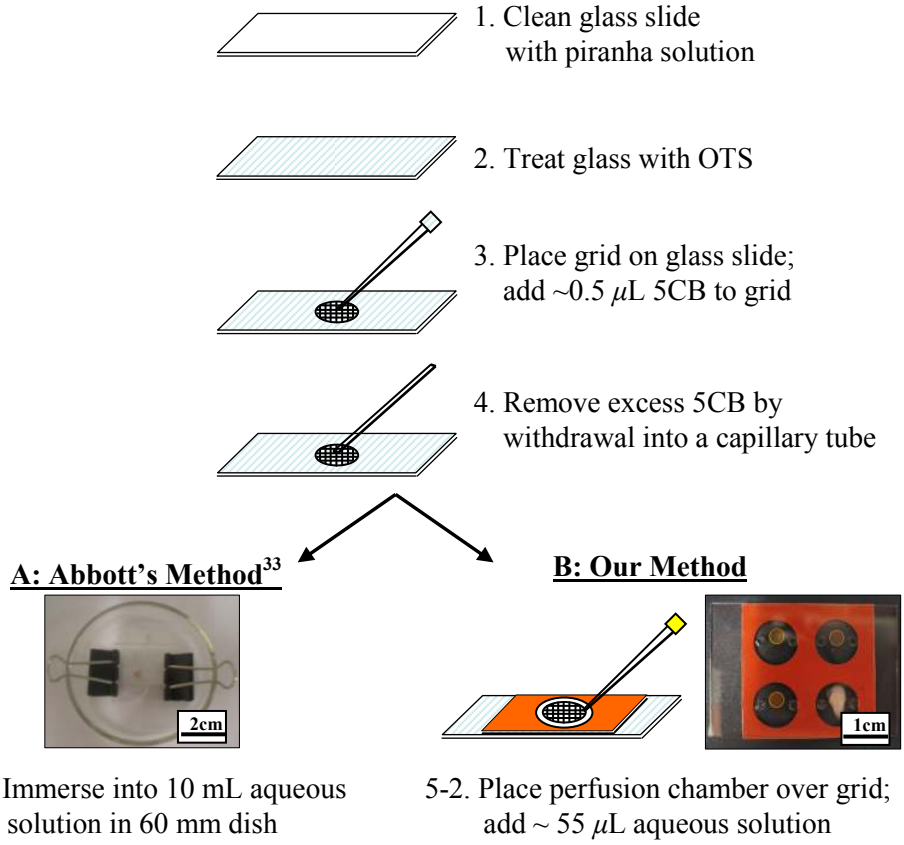

Figure 2.8: Schematic representation of the procedures used to prepare LC imaging experimental systems in either a 60 mm glass dish (A) or a perfusion chamber (B).

The exchangeable volume of a perfusion chamber (original volume minus the EM grid volume) was approximately 55 μL. The orientation of 5CB was examined using plane-polarised light in transmission mode on an Olympus BX51 microscope (colour image) or Nikon LaboPhot microscope (grey image) with crossed polarisers. The LC optical cell with 5CB impregnated grid was placed on a rotating stage located between the polarisers. All images were captured using a digital camera and processed using image analysis software with the light intensity set to ~50 % of full illumination described in section 2.2.1. Homeotropic orientation of 5CB was determined by the absence of transmitted light during a full 360 ° rotation of the sample.

2.2.3.2 Observation of the orientational response of 5CB to adsorption of surfactants

The effect of the various concentrations of DNA surfactants and conventional surfactants on the anchoring of the 5CB was studied for concentrations above and below the critical micelle concentrations (cmc) of the surfactant. Effects of electrolyte concentration on the adsorption of surfactant and response of LC was further examined by adding sodium chloride and lithium sulphate to the above surfactant solutions in concentration ranging from 0 to 0.1 M. All surfactants solutions were prepared immediately before each experiment and kept at room temperature before adsorption of surfactant on the LC optical cells was performed. Each cell was allowed to equilibrate for 20 min before optical observations were initiated. This equilibrium period was largely determined by the time required to prepare each cells for observation, although optical examinations within a few seconds of exposure of the LC to the aqueous phase have been conducted except for DNA surfactants. All experiments were done at room temperature (22 ± 2 °C) except for the polymerisation of oleic acid at various temperatures. In this case, the temperature was controlled using a PE 120 cooling-heating stage (± 0.1 °C, Linkam Scientific Instrument Ltd. UK) controlled by a PE 94 temperature programmer with different heating/cooling rates (Figure 2.9). The temperature mentioned in this thesis is the setting temperature of the surface of PE120 cooling-heating stage. The true cell temperature of a LC optical cell is deviated ± 2 °C compared to the setting temperature when we measured it using infra red (IR) thermometer. The alignment of 5CB at all surfactants remained unchanged for at least 4 h after initial 20 min equilibrium periods.

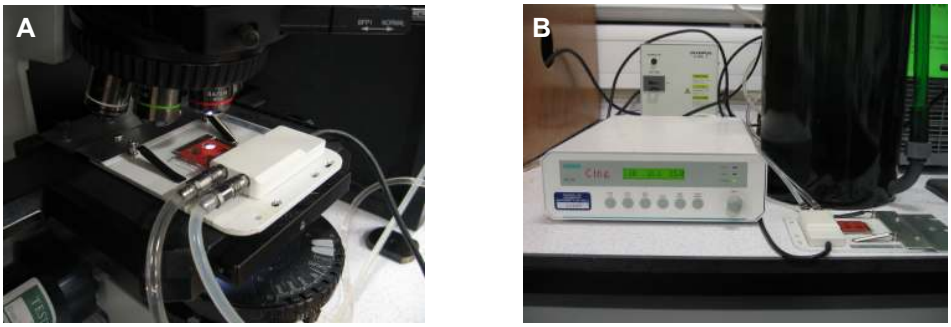

Figure 2.9: (A) PE120 heating and cooling stage set-up on the BX51 microscope. (B) PE94 temperature controller used during UV irradiation.

2.2.4 Polymerisation reactions

2.2.4.1 Thermal polymerisation

In this section, we describe two different thermal polymerisation methods using two different initiators which are activated at different temperatures. We describe two examples using these methods; the amounts of monomers, initiators, and activators in the various experiments were different depending on the purpose and are detailed in the relevant section of the chapter 5.

Polymerisation of poly(NIPAAm-co-AAc) gel with APS at low temperature[34]

Gel samples were prepared by mixing the monomers, *N*-isopropylacrylamide (NIPAAm), acrylic acid (AAc), acrylamide (AAm), and cross-linker *N,N′*- methylene bisacrylamide (MBAAm) in 1 mL of nitrogen-purged pure water. *N,N,N′,N′*-tetramethylethylenediamine (TEMED, accelerator) (9.36 μL) and ammonium persulfate (APS, initiator) (1mg) were then added into the oxygen-free aqueous solution. Then, the reaction was allowed to continue for 1 h at 0 °C using a test tube into which glass capillaries or silicone tubes had been previously inserted. After the gelation was completed, the gels were taken out of the capillaries or silicone tubes and thoroughly washed with pure water. All gel samples were cut into cylinders of 1 mm in length.

Polymerisation of poly(NIPAAm-co-Ru(bpy)$_3$-co-AMPS) gel with AIBN at high temperature[35]

0.156 g of NIPAAm, 16.2 mg of ruthenium(4-vinyl-4′-methyl-2,2′-bipyridine)bis(2,2′-bipyridine)bis(hexafluorophosphate) [Ru(bpy)$_2$(mvbpy)(PF$_6$)$_2$] for the BZ reaction, 2.8 mg of MBAAm as a cross-linker, and 6.6 mg of 2,2′-azobis(isobutyronitrile) (AIBN) as an initiator were dissolved in the mixed solvent of methanol (0.5 mL) and dimethylsulfoxide (DMSO) (0.1 mL). 5.5 mg of 2-acrylamide-2-methylpropane sulfonic acid (AMPS) was dissolved in pure water (0.4 mL). Then the two solutions were mixed together and purged with dry nitrogen gas for 10 min. The monomer solution was injected between DCDMS treated patterned hydrophobic glass plates separated by silicone rubber as a spacer (thickness: 0.5 mm, length: 6.0 mm, width: 3 mm) using a syringe, and then polymerised at 60 °C for 18 h. After gelation, the gel strip was soaked in pure methanol for a day to remove unreacted monomers. The gel was carefully hydrated through dipping it in a graded series of methanol-water mixture, for 1 day each in 75, 50, 25 and 0 vol% of methanol in water.

2.2.4.2 UV polymerisation

UV polymerisation was used for the polymerisation of polymerisable surfactants at the 5CB-water interface and the synthesis of hydrogel. Photoinitiation of the polymerisation of acrylates by UV irradiation has been reported.[36]

UV cell for polymerisation

In order to select a suitable cover for the top of the UV polymerisation cell through which UV light would pass, the UV absorbance spectra of various materials were measured so that a cover could be selected which would not absorb most of the UV emitted by the UV source. The UV emission spectra of the light source were obtained from the manufacturers. UV-visible spectra were obtained using a UV/vis spectrophotometer (ATI Unicam UV3 model, Cambridge, UK). The spectrophotometer was initially zeroed with empty sample holder and an empty reference cuvette holder. To record the spectra, the test sample was mounted vertically against the sample beam cuvette holder with an adhesive tape. Because of its good UV transmittance, it was decided to use a perfusion chamber as a UV polymerisation cell to obtain reproducible polymerised materials and to minimise termination effects of the polymerisation process due to atmospheric oxygen.[10] Aqueous solutions of polymerisable materials to be polymerised were added to a perfusion chamber and the hole of the perfusion chamber was covered with Seal Tabs (Sigma-Aldrich) to prevent its exposure to air.

UV sources

Two different types of UV sources were used to initiate UV polymerisation as shown in Table 2.17.

Table 2.17: Specifications of the UV light sources

Source	Lamp Type	Emission wavelength/ nm
UV SpotCure Lamp [a] (L1 short wave)	400 W (high energy)	UVA and UVB (254–365 nm)
UV Curing Lamp [b]	2 × 6 W (low energy)	UVA (360 nm)

[a] Manual for UVP's SpotCure curing system (UVP, US)

[b] Product specification for UV Chamber (Agar Scientific, UK)

Firstly, a UVP SpotCure lamp (UVP, CA) was used for covering the UVA and UVB wavelength ranges (wavelength: 280–400 nm). This source was fitted with 400 W short wave Hg lamp and UV fibre optic wand and was used to irradiate a UV polymerisation cell from above with the wand tip located 20 mm above the cell (Figure 2.10).

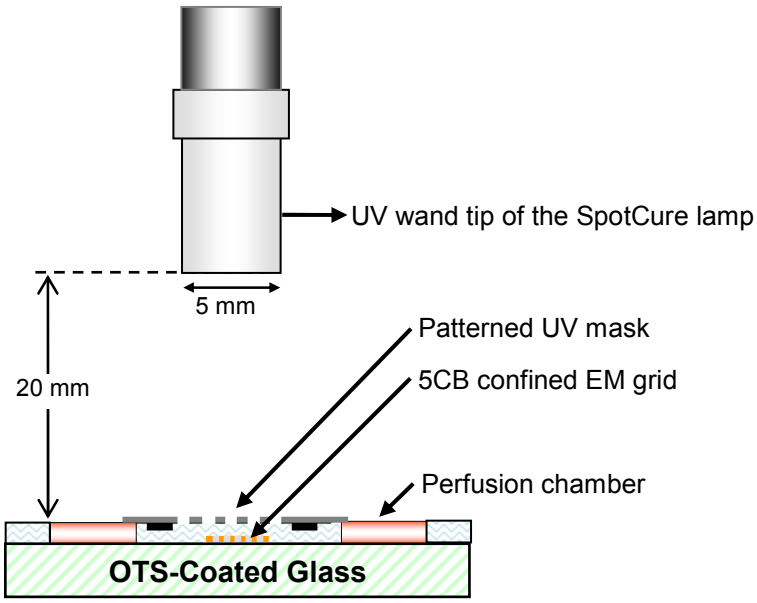

Figure 2.10: Schematic illustration of polymerisation of surfactants using the UV SpotCure lamp (UVP). The UV wand is set up with 20 mm distance from the LC optical cells to minimize heating to the sample.

From the specification of the manufacturer, the light intensity of this lamp is 15 mW/cm^2 at 254, 310, and 365 nm measured at 50 mm from the tip of wand using UVP's UVX radiometer. The light spot diameter at 50 mm from the wand tip is about 50 mm. The diameter of the light spot was measured for different distance and found to be proportional to the distance between the wand tip and the sample (Table 2.18).

Table 2.18: Relation of the distance from UV source and diameter of UV light

Distance	Diameter of exposed light
10 mm	~14 mm
20 mm	~22 mm
30 mm	~32 mm
40 mm	~44 mm
50 mm	~50 mm

For the same light source, the incident light intensity is related with the exposed area as follows:

$$I_b = \left(\frac{r_a^2}{r_b^2}\right) \times I_a \qquad [5]$$

where I_a and I_b are the incident light intensities and r_a and r_b are the radii of the light spot at different distance a and b between a wand and a sample.

Therefore, in our experimental configuration with 20 mm distance between the wand and the sample (Figure 2.10), the incident intensity (mainly at wavelengths 254, 310, and 365 nm) at the cell surface was estimated to be ~77 mW/cm^2[(25/11)^2 × 15 mW/cm^2 ≈ 77 mW/cm^2].

Secondly, a UV curing lamp from Agar scientific (Stansted, Essex) having two 6 W Hg lamps filtered to emit a main wavelength of 360 nm was used for UVA radiation. The lamp was usually located 30 mm above the polymerisation cell for a polymerisation.

We next describe the main procedures used to UV polymerise polymerisable surfactants and monomers for hydrogel synthesis.

Polymerisation of polymerisable surfactants at the 5CB-water interface

Three main procedures were used to polymerise surfactants at the 5CB-water interface. In procedure 1 and 2 the surfactant was added initially in the water phase but they differ in that procedure 1 removes excess non-adsorbed surfactant before UV irradiation whereas samples prepared using procedure 2 contain excess non-adsorbed surfactant in the aqueous phase during UV irradiation. In procedure 3, the polymerisable surfactant oleic acid was added in the 5CB phase instead of the water phase.

Procedure 1

(a) add aqueous surfactant solution into a perfusion chamber and equilibrate for 20 min.
(b) flush chamber with 200 μL (= approximately 4 replacement chamber volumes) of water containing the required concentration of photoinitiator Darocur 1173 and equilibrate for 20 min.
(c) irradiate with UV sources for the desired time and equilibrate for 20 min.

(d) record microscope images between crossed polarisers.

Procedure 2

(a) add aqueous surfactant solution plus Darocur 1173 into a perfusion chamber and equilibrate for 20 min.

(b) irradiate with UV sources for the desired time and equilibrate for 20 min.

(c) record microscope images between crossed polarisers.

Procedure 3

(a) dissolve the oleic acid in 5CB solution.

(b) prepare the Darocur 1173 solution in buffer solution with required pH and ionic strength.

(c) load the 5CB and aqueous phases and incubate for 1.5 h and then record microscope images.

(d) irradiate with UV curing lamp located 30 mm above a polymerisation cell for 30 min.

(e) record microscope images between crossed polarisers versus time.

Polymerisation of monomer solutions for hydrogel synthesis

NIPAAm (0.1722 g), AMPS (5.5 mg), $Ru(bpy)_2(mvbpy)(PF_6)_2$ (5 mg), MBAAm (2.8 mg) as a cross-linker, and 2 vol% Darocur 1173 as a photoinitiator were dissolved in a N_2 gas-purged mixture of ethanol (0.5 mL) and DMSO (0.1 mL). The monomer solution was injected either between a glass slide and a Teflon plate or between a glass slide and a perfusion chamber separated by a silicone spacer with 0.5–1.0 mm thickness. The polymerisation was performed with a UV curing lamp (2 × 6 W, peak wavelength 360 nm, Agar Scientific, UK) which was positioned at 20 mm height with irradiation for 5–30 min at room temperature depending on the reaction condition. After gelation, the gel strip was soaked in pure ethanol for a day to remove unreacted monomers. The gel was carefully hydrated through dipping it in a graded series of ethanol-water mixtures, for 1 day each in 75, 50, 25 and 0 vol% of ethanol in water.

2.2.5 Preparation of Janus particles

A key aspect to preparing a self-propelling particle is the design of the asymmetric particles consisting of one hemisphere coated with a metal (e.g., gold, chromium, platinum etc.) which is for the immobilisation of enzymes (e.g., invertase,

catalase) or for the suppression of diffusion of solutes with the other hemisphere is incompatible with the linkage of enzymes or able to release solutes into the liquid. Therefore, we need to protect a part of the spherical particle surface whilst coating the exposed part with a metal. In this section we briefly describe the gel trapping technique (GTT)[37] and a new simple method, the glass sliding technique (GST) for this purpose.

2.2.5.1 Gel trapping technique (GTT)

Partial metal-coated Janus particles were prepared according to a procedure detailed in an earlier publication as shown in Figure 2.11.[38]

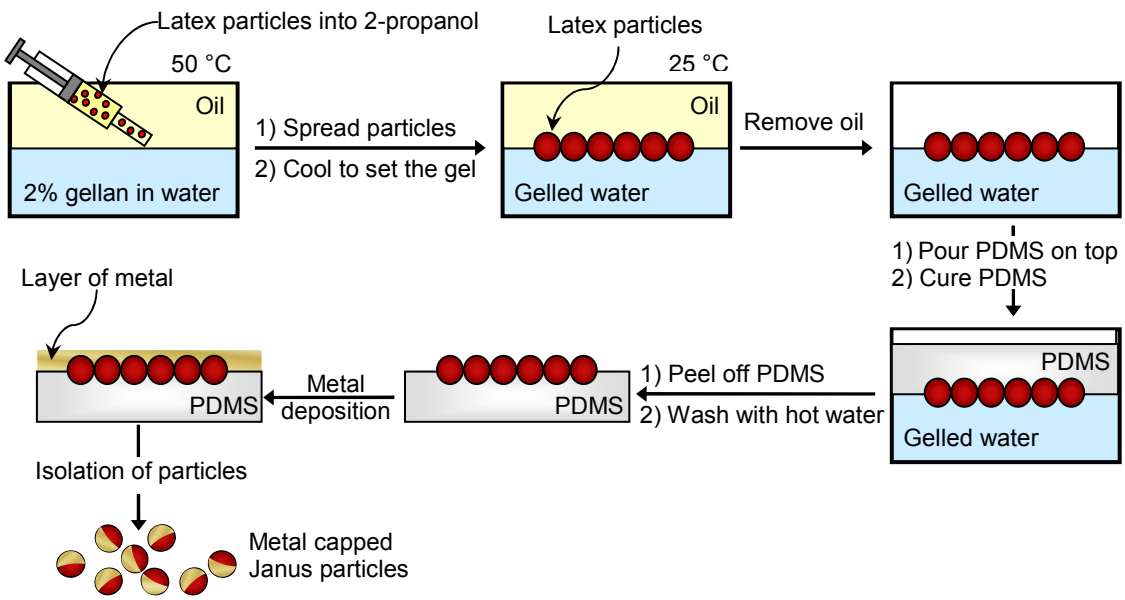

Figure 2.11: Schematic of the preparation of metal coated Janus particles based on the gel trapping technique (GTT).[39]

Gellan gum (Kelcogel®, CP Kelco, UK) was initially dispersed as 0.5 wt% in pure water and heated to 95 °C in a water bath for 15 min to dissolve and hydrate. To purify gellan from surface-active contaminations, the hot solution was passed twice through a C_{18}-silica chromatographic column (Phenomenex) preactivated with an acetonitrile-water [80:20% (v/v)] mixture and flushed several times with hot pure water. The column was heated during the filtration to avoid undesirable retention of gellan due to gelling. The gellan solution eluted from the column was collected, dried, and redissolved. Bubbles were removed from the hot solution by centrifugation. The gelling temperature of 2.0 vol% gellan solution is in the range of 40–45 °C, but the setting of the gel does not happen instantaneously even if the solution is quickly cooled to room temperature. Hexadecane was used as an oil phase after additional purification by

passing through a SEP-PAK® alumina B cartridge column (Waters, Millipore Co. MA) twice. PDMS Sylgard® 184 elastomer (Dow Corning) was used in a ratio of 10:1 with respect to the curing agent. One sample of monodisperse carboxylate latex particles (IDC, US) and one sample of polymethyl methacrylate (PMMA) particle (microParticlesGmbH, Germany) of sizes ranging from 3.1 to 87.5 μm were used without further purification. 2-propanol (BDH, U.K.) was used as a spreading solvent to spread particles at the air-water and the hexadecane-water interface. After curing of the PDMS, the particles were coated with chromium and gold using an Edward High Vacuum Evaporator (Edward High Vacuum International, West Sussex, UK) on the partially embedded particle monolayer on PDMS. The resultant Janus particles were subsequently removed mechanically from the interface for further modifications. A chromium adhesion layer (thickness of 10–15 nm) promotes adhesion between of the surface of particles and Au film (thickness of 10–15 nm). This is similar to the use of a thin layer of titanium to promote adhesion of a 20 nm thick film of Au to the glass slide for formation of monolayer of alkanethiols on a glass slide.[33]

2.2.5.2 Glass sliding technique (GST)

For an alternative method for metal coating of silica particles, we have developed a modified method as shown in Figure 2.13.

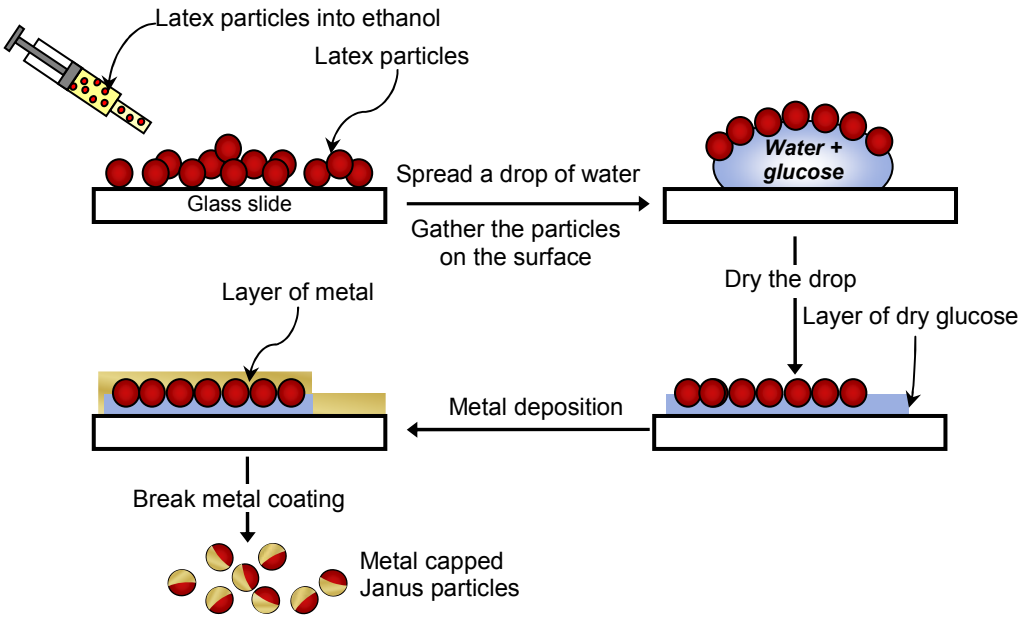

Figure 2.13: Schematic of the glass sliding technique (GST) for preparation of metal coated Janus particles.

The particles were dispersed in 2-propanol using sonication and spread on a cleaned glass slide. Glucose solution was used in order to protect the low hemisphere of the particle because it is expected to be easily dissolved with water and release the metal coated Janus particle after a metal coating.

The concentration of glucose was sufficient to embed approximately half of the particle in the glucose after evaporating the water from the glucose solution, as shown in Figure 2.14.

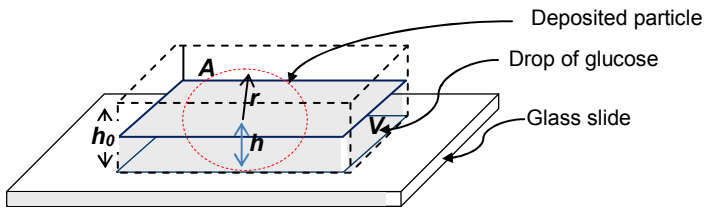

Figure 2.14: Schematic illustration of the protection of particle surface with glucose solution. A: the volume of a drop to peel off the monolayer of the particles from a glass slide (e.g., 0.1 mL), A is the surface area occupied by a monolayer of the particles, h_0 is the thickness of the glucose layer just after deposited, h is the thickness of the glucose layer after dried.

After evaporating water from a glucose solution $h = r$ therefore, the percentage of glucose into a drop is

$$V = A \times h \qquad [6]$$

$$h = h_0 \times c \qquad [7]$$

$$c = \frac{r}{h} = r \times \frac{A}{V} \qquad [8]$$

where c is the volume percentage of glucose into a drop, V is the volume of a drop to peel off the monolayer of the particles from a glass slide (e.g., 0.1 mL), A is the surface area occupied by a monolayer of the particles, h_0 is the thickness of the glucose layer just after deposited, h is the thickness of the glucose layer after dried, r is the radius of particles.

After evaporating 2-propanol, the particles were floated using a glucose solution and packed into a dense monolayer by using a disposable plastic pipette as shown in Figure 2.13. After drying in air metal coated Janus particles were produced by the same procedure described in section 2.2.5.1 by Cr and Au coating. 25 mM SDS solution was

used to isolate Au-coated particles from the glass slide after Au coating step. However, in most cases pure water is sufficient for this purpose and was used as an isolating solvent in most experiments.

2.2.6 Optical absorbance measurements

Optical absorbance measurements were performed using a UV/vis spectrophotometer (ATI Unicam UV3 model, Cambridge, UK) and quartz cuvettes with 1 cm path length. The spectrophotometer was initially zeroed with sample and reference chambers holding the appropriate cells without the absorbing species present. The temperature of the cuvette holder was controlled using a thermostatic bath.

2.2.7 Drop shape analysis

The hydrophobicity of silanised glass substrates was determined measuring three-phase contact angles of water drops on the silanised substrates under air using a drop shape analysis system (DSA 10 Mk2 from Krüss GmbH, Germany). This device consists of three components:

- A Krüss G10 contact angle-measuring instrument (goniometer).
- A video measuring system (video camera combined with set of optical lenses) to record the drop image.
- A video frame grabber board combined with the appropriate software.

This instrument allows the determination of interfacial tensions of liquids surrounded by vapours or liquids in addition to the determination of contact angle in any systems consisting of liquid, vapour, and flat solid.

2.2.8 pH measurements

All pH measurements were performed using a Fisher Hydrus 400 pH meter (Thermo Orion, US) fitted with a combined calomel/glass electrode. The meter was calibrated regularly with ready-made pH 4, pH 7 and pH 10 buffer solutions (BDH, purity 98%).

2.2.9 Application of electric field

A number of our experiments necessitated the use of electric field generators, which were connected to our specially designed electrochemical cells. Typically, a 20 MHz Function/Arbitrary waveform generator model 33220A (Agilent Technologies, CA) and high voltage power amplifier Trek model 610C (Trek Inc., NY) were used. It is capable of supplying direct current (*dc*) and alternating current (*ac*) electric field from 0 to 10 V with respect to *dc* electric field and from 0 to 100 MHz, 0 to 10V (peak to peak) with respect to *ac* electric field. For the motility of hydrogel based particles in polyelectrolyte solutions an *ac* electric field with amplitude in the range of 0.5–10 V (peak to peak) and low frequency (0.1–1 Hz) was used. The *ac* electric field followed a sinusoidal waveform. The applied electric voltage between the electrodes was measured with a digital meter Meterman 27XY (Wavetek, CA).

2.2.10 Dispersion of colloid particles in liquids

To disperse colloidal particles into liquid phases Ultrasonic Processor Model VC 100 (Sonic & Materials Inc., Danbury, US) was used and the specification is in detail as following:

Probe: 3 mm titanium microtip and can process between 250 μL and 10 mL.

Net power output: 100 watts, Frequency: 20 kHz.

Timer: Variable from 1 second to 10 hours.

Pulser: On and off cycle are independently controllable from 1 to 10 sec.

Colloidal particles were usually dispersed into ethanol or 2-propanol at 20–30 of amplitude level for 3–5 min in pulse-off mode.

2.3 References

1. R. C. Weast and M. J. Astle, *CRC Handbook of Chemistry and Physics 62 ed.*, CRC Press: Boca Raton, Florida, 1981.
2. L. J. McBride and M. H. Caruthers, "An investigation of several deoxynucleotide phosphoramidites useful for synthesizing deoxyoligonucleotides", *Tetrahedron. Lett.* **1983**, *24*, 245-248.
3. J. Sambrook, E. F. Fritsch, and T. Maniatis, *Molecular Cloning: a Laboratory Manual*; Cold Spring Harbour Laboratory Press: New York, 1989.
4. C. R. Cantor, M. M. Warshaw, and H. Shapiro, "Oligonucleotide interactions. III. Circular dichroism studies of the conformation of deoxyoligonucleotides", *Biopolymers* **1970**, *9*, 1059-1077.
5. http://eu.idtdna.com/analyzer/Applications/OligoAnalyzer/2008 [Accessed 26 Sept 2008)
6. R. Owczarzy, Y. You, B. G. Moreira, J. A. Manthey, L. Huang, M. A. Behlke, and J. A. Walder, "Effects of sodium ions on DNA duplex oligomers: Improved predictions of melting temperatures", *Biochemistry* **2004**, *43*, 3537-3554.
7. P. J. Collings and M. Hird, *Introduction to Liquid Crystals Chemistry and Physics*, Taylor & Francis, London, 1997.
8. V. Kitaev and E. Kumacheva, "Thin films of liquid crystals confined between crystalline surfaces", *J. Phys. Chem. B* **2000**, *104*, 8822-8829.
9. F. Yan and J. Texter, "Capturing nanoscopic length scales and structures by polymerisation in microemulsions", *Soft Matter.* **2006**, *2*, 109-118.
10. H. De. Bruyn, R. G. Gilbert, and B. S. Hankett, "Retardation by oxygen in emulsion polymerisation", *Polymer* **2003**, *41*, 8633-8639.
11. M. R. Porter, **2004** *Preparation and Characterization of Polymer Films from Polymerisable Microemulsions* (PhD thesis) University of Hull.
12. W. S. Ang, S. Lee, and M. Elimelech, "Chemical and physical aspects of cleaning of organic-fouled reverse osmosis membranes", *J. Memb. Sci.* **2006**, *272*, 198-210.
13. M. F. Ottaviani, P. Andechaga, N. J. Turro, and D. A. Tomalia, "Model for the interactions between anionic dendrimers and cationic surfactants by means of the spin probe method", *J. Phys. Chem. B* **1997,** *101,* 6057-6065.

14. S. Panmai, R. K. Prud'homme, D. G. Peiffer, S. Jockusch, and Nicholas J. Turro, "Interaction between hydrophobically modified polymers and surfactants: A fluorescence study", *Langmuir* **2002,** *18,* 3860-3864.
15. S. S. Berr, "Solvent isotope effects on alkyltrimethylammonium bromide micelles as a function of alkyl chain length", *J. Phys. Chem.* **1987**, *91*, 4760-4765.
16. R. Aubourg, A. Bee, S. Cassaignon, V. Monticone, and C. Treiner, "Adsorption isotherm of cetylpyridinium chloride with iron III salts at air/water and silica/water interfaces", *J. Colloid. Interface. Sci.* **2000**, *230***,** 298-305.
17. M. Dreja, W. Pyckhout-Hintzen, and B. Tieke, "Copolymerisation behavior and structure of styrene and polymerisable surfactants in three-component cationic microemulsion", *Macromolecules* **1998**, *31*, 272-280.
18. *Effects of polymerisation on admicelle formation and adsolubilizatoin using polymerisable surfactants*: http://www.aocs.org/member/division /surface /am08pres/Attaphong.pdf [Accessed 26 Sept 2008].
19. P. Messina, M. A. Morini, and P. C. Schulz, "Aqueous sodium oleate-sodium dehyrocholate mixtures at low concentration", *Colloid Polym. Sci.* **2003**, *281*, 1082-1091.
20. G. R. Sanderson, *Gellan gum.* In P. Harries, *Food Gels*, Elsevier, NY, 1990.
21. A. Tanriseven and S. Dogan, "Immobilisation of invertase within calcium alginate gel capsules", *Proc. Biochem.* **2001**, 36, 1081-1083.
22. A. Goldstein and J. O. Lampen, "β-D-fructoforanoside fructohydrolase from yeat", *Methods Enzymol.* **1975**, *42*, 504-511.
23. *Specification of invertase from baker's yeast (S. cerevisiae) from Sigma-Aldrich*: http://www.sigmaaldrich.com/catalog/search/ProductDetail/SIGMA/I4504, [Accessed 17 October 2008]
24. I. Hara, N. Ichise, K. Kojima, H. Kondo, S. Ohgiya, H. Matsuyama, and I. Yumoto, "Relationship between the size of bottleneck 15 from iron in the main channel and the reactivity of catalase corresponding to the molecular size of substrates", *Biochemistry* **2007**, *46*, 11-22.
25. G. R. Schonbaum and B. Chance, Catalase, in *The enzymes* (Boyer, P. D., Ed.) pp 363-408, Academic Press, New York. 1976.
26. A. Deisseroth and A. L. Dounce, "Catalase: Physical and chemical properties, mechanism of catalysis, and physiological role", *Physiol. Rev.* **1970**, *50*, 319-374.
27. www.olympus.co.uk/micro/products.2004 [Accessed 26 July 2008].

28. J. J. Skaife and N. L. Abbott, "Quantitative characterization of obliquely deposited substrates of gold by atomic force microscopy: Influence of substrate topography on anchoring of liquid crystals", *Chem. Mater.* **1999**, *11*, 612-623.
29. J. Sagiv, "Organized monolayers by adsorption. 1. Formation and structure of oleophobic mixed monolayers on solid surfaces", *J. Am. Chem. Soc.* **1980**, *102*, 92-98.
30. V. Nazarenko and A. Nych, "Multistable alignment in free suspended nematic liquid crystal film", Phys. Rev. E **1999**, *60*, R3495-3497.
31. M. Krasowska, K. Terpilowski, E. Chibowski, and K. Malysai, "Apparent contact angles and time of the three phase contact formation by the bubble colliding with Teflon surfaces of different roughness", *Physicochem. Problems Mineral Process*, **2006,** *40*, 293-306.
32. A. D. Price and D. K. Schwartz, "Fatty-acid monolayers at the nematic/water interface: Phase and liquid crystal alignment", *J. Phys. Chem. B* **2007**, *111*, 1007-1015.
33. J. M. Brake and N. L. Abbott, "An experimental system for imaging the reversible adsorption of amphiphiles at aqueous-liquid crystal interfaces", *Langmuir* **2002**, *18*, 6101-6109.
34. R. Yoshida, G. Otoshi, T. Yamaguchi, and E. Kokufuta, "Travelling chemical waves for measuring solute diffusivity in thermosensitive poly(*N*-isopropylacrylamide) gel", *J. Phys. Chem. A.* **2001**, *105*, 3667-3672.
35. S. Maeda, Y. Hara, T. Sakai, R. Yoshida, and S. Hashimoto, "Self-walking gel", *Adv. Matter.* **2007**, *000.00*. 1-5.
36. W. R. P. Raj, M. Sasthav, and H. M. Cheung, "Formation of porous polymeric structures by the polymerisation of single-phase microemulsions formulated with methyl methacrylate and acrylic acid", *Langmuir* **1991**, *7*, 2586-2591.
37. O. J. Cayre and V. N. Paunov, "Contact angles of colloid silica and gold particles at air-water and oil-water interfaces determined with the gel trapping technique", *Langmuir* **2004**, *20*, 9594-9599.
38. V. N. Paunov, "Novel method for determining the three-phase contact angle of colloid particles adsorbed at air-water and oil-water interfaces", *Langmuir* **2003**, *19* 7970-7976.

39. V. N. Paunov and O. J. Cayre, “Supraparticles and “Janus” particles fabricated by replication of particle monolayers at liquid surfaces using a gel trapping technique”, *Adv. Mater.* **2004**, *16*, 778-791.

Chapter 3

Response of the Alignment of LC at the 5CB-water Interface to Adsorption of DNA species

Chapter 3

Response of the Alignment of 5CB at the LC-Water Interface to Adsorption of DNA Species

The orientation of nematic LC molecules at the 5CB-water interface can be altered by adsorption of surfactants.[1,2,3,4,5,6,7] The transition of alignment of 5CB depends on the molecular structure of surfactants and the ionic strength of the aqueous phase. The work reported here, therefore, aims to investigate this LC amplified response mechanism to detect the adsorption of DNA species at the interface (e.g., homeotropic anchoring) and the hybridisation of DNA bound to the interface (e.g., planar or tilted anchoring) through the alternation of the alignment of LC at the interface as shown in Figure 3.1.

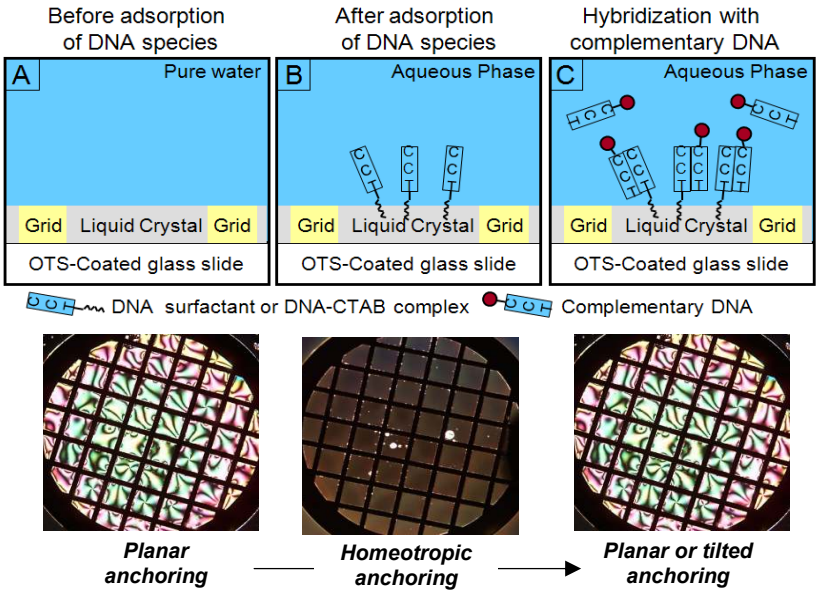

Figure 3.1: Schematic illustration of the expected LC response by adsorption of DNA species at the 5CB-water interface and hybridisation of interface bound DNA species with its complementary DNA.

In this chapter, we seek to characterise the response of the alignment of 5CB at the LC-water interface by adsorption of DNA-surfactant and DNA-cationic surfactant complex using our modified experimental imaging system. If the triggered 5CB alignment at the LC-water interface can also be reverted by hybridisation of the complementary DNA, this experimental system would be useful for detecting nucleic acid hybridisation at fluid interfaces.

This approach to the detection of DNA hybridisation does not require labelling of the probe DNA, does not require the use of electroanalytical apparatus, and is sufficiently simple that it may find use in genetic assays and imaging of spatially resolved DNA chip libraries.

3.1 Optical examination of LC textures in a perfusion chamber

As described in the experimental section (section 2.2.3), our first experimental studies were to investigate the reproducibility of the optical response of 5CB at the LC-water interface using a perfusion chamber (60 μL internal volume) as a reservoir of surfactant solutions instead of a petri-dish (10 mL internal volume) which has been used in Abbott's experimental system to efficiently manipulate a micro scale of DNA hybridisation. Thus, we observed the optical response of 5CB at the LC-water interface by adsorption of SDS (e.g., the transition and reversibility of the alignment of 5CB) using a perfusion chamber and confirmed that two systems have the same optical response. The key results for the adsorption of SDS at the LC-water interface are consistent with Abbott's results[3] and are summarized as follows:

- For the 5CB-water interface above 1 mM of SDS, the optical texture of the LC is homeotropic and increasing the SDS concentration above its cmc does not change the optical texture (Figure 3.2). Homotropic anchoring was indicated by the appearance of dark regions of LC within some of the grid squares.
- The transition in anchoring of 5CB is reversible, indicating reversible adsorption and desorption of SDS from the LC-water interface (Figure 3.3).
- The addition of electrolyte (NaH_2PO_4) to SDS solution promotes a transiton of alignment of LC from planar to homeotropic at fixed SDS concentraton (Figure 3.4A). The exposure of 5CB to electrolyte dissolved in water in the absence of surfactant resulted in no apparent deviation of the LC anchoring from planar orientation (Figure 3.4C).
- The concentration of SDS required to induce the anchoring transtion is independent of the size of the inner grid square side length and the volume of aqueous solution (data not shown in here).

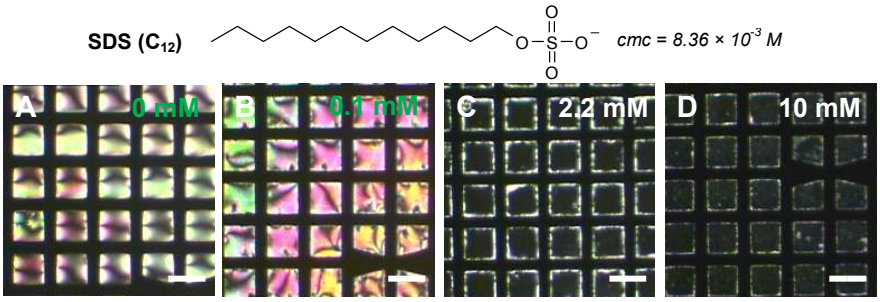

Figure 3.2: Optical images of 5CB between crossed polarisers as a function of SDS concentrations: (A) 0 mM; (B) 0.1 mM; (C) 2.2 mM; (D) 10 mM in a perfusion chamber. All scale bars represent 100 μm.

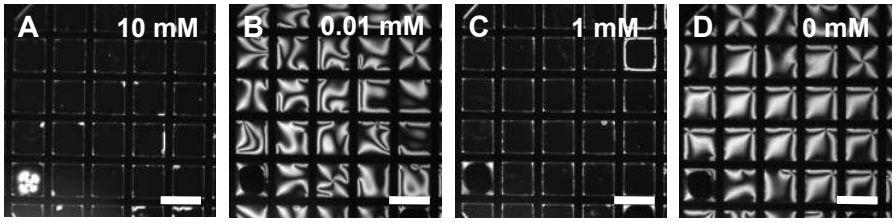

Figure 3.3: Reversibility of adsorption of SDS at the LC-water interface. Optical images of 5CB between crossed polarisers sequentially exposed to aqueous solutions containing SDS concentrations of (A) 10 mM, (B) 0.01 mM, (C) 1 mM, and then (D) 0 mM. All scale bars represent 300 μm

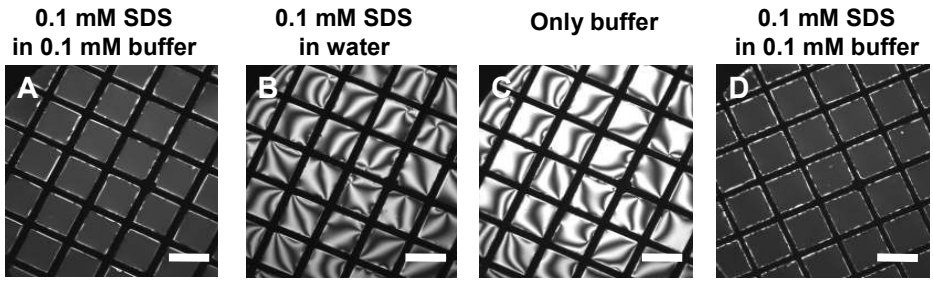

Figure 3.4: Effect of ionic strength on adsorption of SDS at the LC-water interface. Optical images of 5CB between crossed polarisers after sequential incubation with various aqueous solutions: (A) 0.1 mM SDS in 0.1 M phosphate buffer (0.1 M NaH_2PO_4, pH 7.0); (B) 0.1 mM SDS in pure water; (C) 0.1 M phosphate buffer; (D) 0.1 mM SDS in 0.1 M phosphate buffer. All scale bars represent 300 μm.

Thus, we conclude that the imaging system using a perfusion chamber with 60 μL of an aqueous solution containing a surfactant can be used to study interfacial phenomena using a microgram scale of material such as DNA hybridisation at the LC-water interface.

3.2 Adsorption of DNA-surfactants at the 5CB-water interface

Whereas the studies described until now address the adsorption of soluble surfactants at the LC-water interface, this section reports that the same experimental system can be used to characterise fluid interfacial assemblies formed by DNA species and hybridisation with their complementary DNA at the LC-water interface.

3.2.1 Anchoring of 5CB by DNA-surfactants

We used a range of DNA-surfactant samples based on either cholesteryl or multiple saturated dodecyl ($C_{12}H_{24}$) hydrocarbon chain conjugated to DNA chains by an ether linkage. Here we report measurements of the anchoring of 5CB in contact with aqueous solutions of DNA-surfactants $(C_{12}\text{-O})_n$-5'-GGGGGGAAAAAA-3', $(C_{12}\text{-O})_n$-5'-TTTTTTCCCCCC-3' (n = 2, 3 and 4) and cholesteryl-5'-GGGGGGAAAAAA-3' as a function of their bulk concentrations. The optical textures of 5CB following the adsorption of these DNA-surfactants to the LC-water interfaces are shown in Figure 3.5 respectively. Generally, the equilibrium alignment of 5CB was observed to occur within 3 h of exposure of 5CB to each DNA-surfactant aqueous solutions and remained unchanged for at least 9 h.

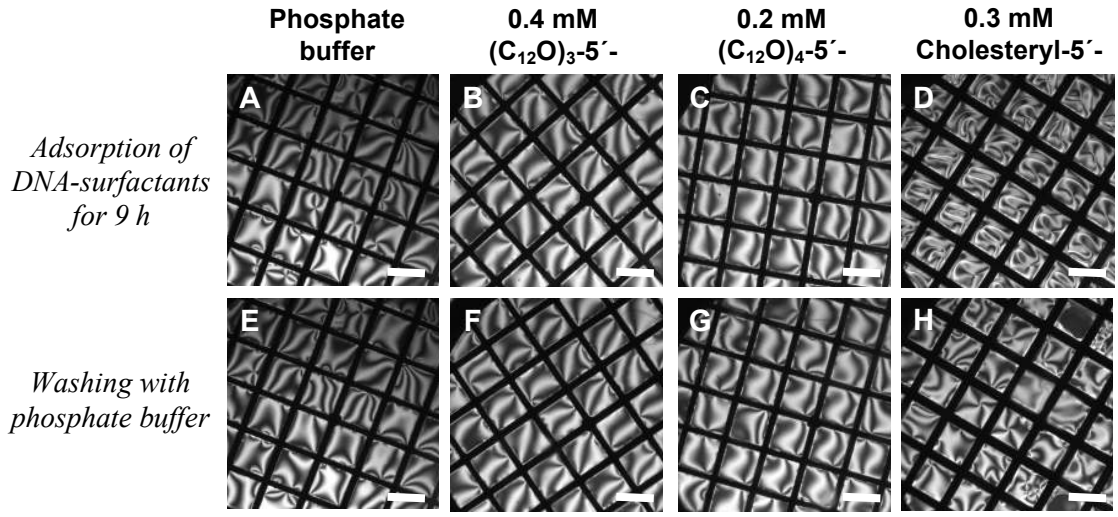

Figure 3.5: Influence of alkyl groups of DNA-surfactants on the anchoring of 5CB at the LC-water interface. Optical images of 5CB between crossed polarisers contacted with phosphate buffer solution (0.1 M NaH_2PO_4, 1 mM $EDTANa_2$, pH 7) of (B) $(C_{12}O)_3$-5´-GGGGGGAAAAAA-3´, (C) $(C_{12}O)_4$-5´-GGGGGGAAAAAA-3´, (D) cholesteryl-5´-GGGGGGAAAAAA-3´ for 9 h and then washed with 4 perfusion chamber volumes of phosphate buffer. All scale bars represent 300 μm.

For $(C_{12}O)_3$-5'-GGGGGGAAAAAA-3' (Figure 3.5B) and $(C_{12}O)_4$-5'-GGGGGGAAAA AA-3' (Figure 3.5C), the optical textures are similar to that seen in that contacted with phosphate buffer (Figure 3.5A). Brushes like textures emanating from a single line defect were observed within most grid squares. However, at 0.3 mM of cholesreryl-5'-GGGGGGAAAAAA-3' (Figure 3.5D), the optical texture of the 5CB appears to be slightly distorted planar anchoring compared to the images which were observed with DNA-surfactant having a same DNA sequence (Figure 3.5C). All observed textures indicate an alignment of 5CB that is not perpendicular to the interface between 5CB and the aqueous solution of all DNA-surfactants (tilted or planar anchoring). Measurements of the orientation of 5CB performed at other bulk concentrations of $(C_{12}O)_n$- and cholesteryl-5'-end modified DNA-surfactant failed to reveal the presence of homeotropic anchoring of 5CB (data not shown here).

We further examined the adsorption of cholesteryl modified DNA-surfactant which shows the distorted planar anchoring of LC (Figure 3.5D) in contrast to a series of dodecyl alkyl chain modified DNA-surfactants (Figure 3.5B and C). Figure 3.6 shows the optical images after contacted with aqueous solutions containing cholesteryl-5´-GGGGGGAAAAAA-3´ DNA-surfactant in phosphate buffer. For DNA-surfactant concentrations up to 0.1 mM (Figure 3.6B) the observed optical texture is similar to that seen in phosphate buffer (Figure 3.6A) indicating a planar or tilted anchoring.

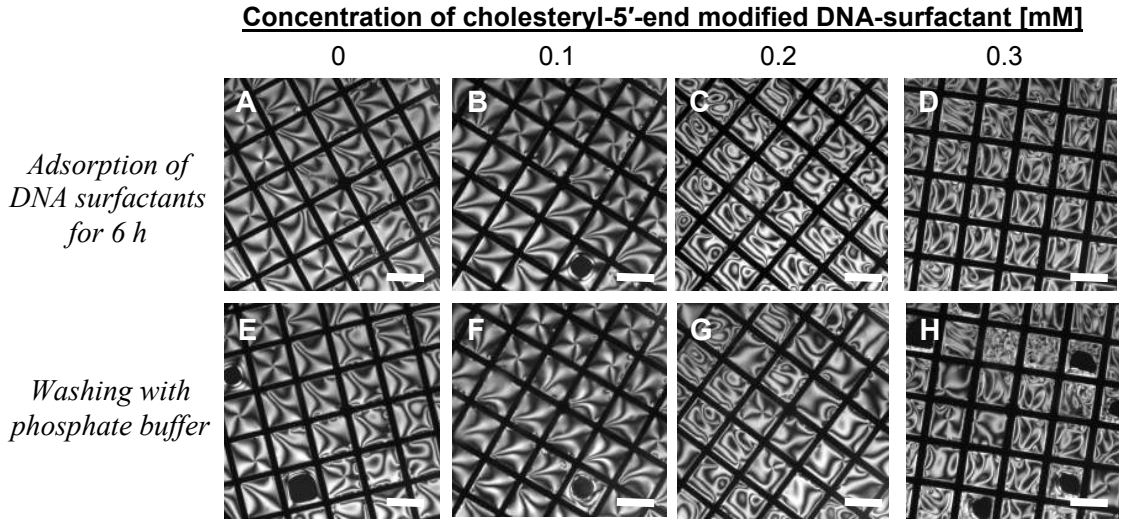

Figure 3.6: Optical images of 5CB between crossed polarisers after contacted with cholesteryl-5´-GGGGGGAAAAAA-3´ DNA-surfactant in phosphate buffer (0.1 M NaH_2PO_4, 1 mM $EDTANa_2$, pH 7) for 6 h and washed with 4 perfusion chamber volumes of phosphate buffer. All scale bars represent 300 μm.

However, at DNA-surfactant concentrations ranging from 0.2 to 0.3 mM (Figure 3.6C and D) the optical texture of the LC appears to be different that observed at lower concentrations of the DNA-surfactant. After washing with phosphate buffer the optical textures in some grid squares have reverted to the planar anchoring. This means that the adsorption of the DNA-surfactant might change the alignment of LC into a distorted alignment, however, the interface bound DNA-surfactant is slightly desorbed from the interface by washing with a salt solution. The observation of planar anchoring of LC upon exposure to a 0.3 mM solution of the DNA-surfactant is consistent with a low level of surface activity and adsorption of DNA-surfactants such that 5CB is contacting a largely surfactant-free interface. In contrast, SDS that leads to high surface coverage of surfactant at the air-water and oil-water interfaces produces a homeotropic anchoring of 5CB at the LC-water interface.[3] In addition, the observation of the optical responses up to 0.4 mM DNA-surfactant, failed to reveal the presence of homeotropic anchoring.

According to a previous study[9], DNA-surfactant shows relatively slow adsorption at the oil-water interface because the equilibrium surface tension at the dodecane-water interface is established after more than 40 min. It suggests that DNA-surfactant is also likely to adsorb slowly at the LC-water interface rather SDS to change the alignment of 5CB from planar to homeotropic. Thus, we increased an incubation time (> 12 h) to establish a full adsorption of DNA-surfactant at the LC-water interface (Figure 3.7).

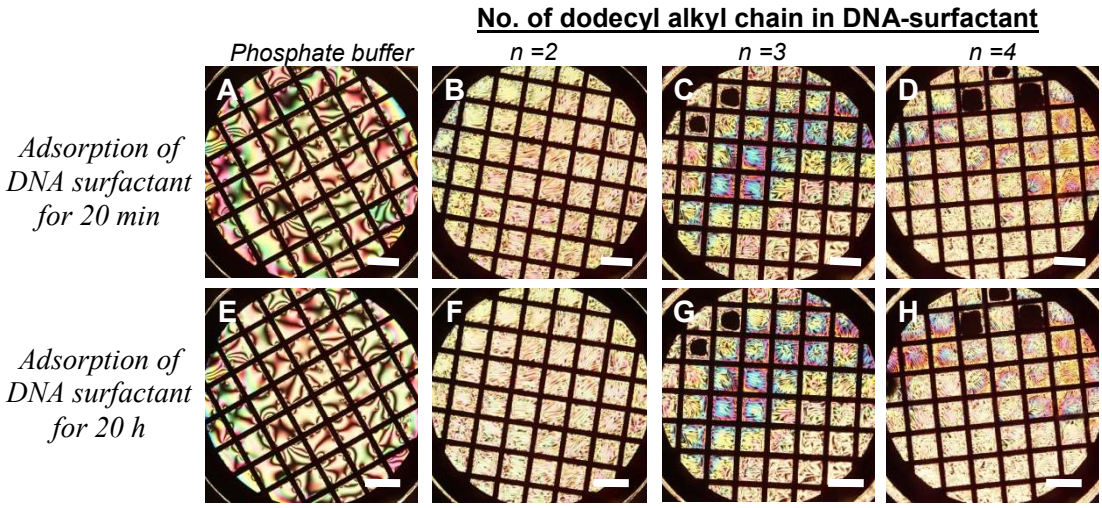

Figure 3.7: Optical images of 5CB between crossed polarisers contacted with aqueous solutions containing 300 μM $(C_{12}O)_n$-5′-TTTTTTCCCCCC-3′ DNA-surfactants in phosphate buffer (0.1 M NaH_2PO_4, 1 M NaCl, 1 mM $EDTANa_2$ at pH 7.0) for 20 min and 20 h. All scale bars represent 300 μm. For image C, D, G, H, the black squares in the grids corresponds to a square which were empty of 5CB.

However, the adsorption of DNA-surfactants does not trigger the transition of texture of 5CB even after a longer incubation time (> 20 h). Therefore, DNA-surfactants are not likely to interact strongly with the LC to change the alignment of 5CB from planar to homeotropic anchoring at the LC-water interface. It might come from their highly charged bulky head groups which are very different from those of common surfactants (e.g., sulphate group of SDS, quaternary ammonium group of cetyltrimethylammonium bromide (CTAB)).

3.2.2 Effect of ionic strength on the anchoring of 5CB in the presence of DNA-surfactants

We note that the addition of electrolyte to a surfactant solution can promote the adsorption of ionic surfactants to the LC-water interface and decrease the critical concentration to change the alignment of 5CB from planar to homeotropic anchoring.[3,6] We hypothesized, therefore, that the electrolyte acts to screen electrostatic repulsion among negatively charged head groups of DNA-surfactant, thus enabling them to adsorb densely at the LC-water interface and to induce a transition of LC alignment at constant concentration. However, addition of 2.0 M NaCl in phosphate buffer did not induce homeotropic anchoring of 5CB after incubation with various DNA-surfactants which have different DNA sequences and alkyl modifications as shown in Figure 3.8. On the other hand, the adsorption of two 5′-cholesteryl modified DNA-surfactants show very different optical textures. One shows a planar anchoring of 5CB (Figure 3.8D) whereas another shows a distorted planar anchoring of 5CB (Figure 3.8G) which is similar to the other experimental results using the same 5′-cholesteryl modified DNA-surfactant (Figure 3.5 and 3.6). It means that the quality of DNA-surfactant (e.g., a yield of a conjugate between DNA and hydrophobic tail group) or the impurity in a storage solution might cause a different optical texture of LC by different adsorption of DNA-surfactant at the LC-water interface even at the same concentration of same structured DNA-surfactants. Additionally, the optical texture of LC was also planar anchoring at low ionic strength, similar to that at high ionic strength and in pure water shown in Figure 3.9.

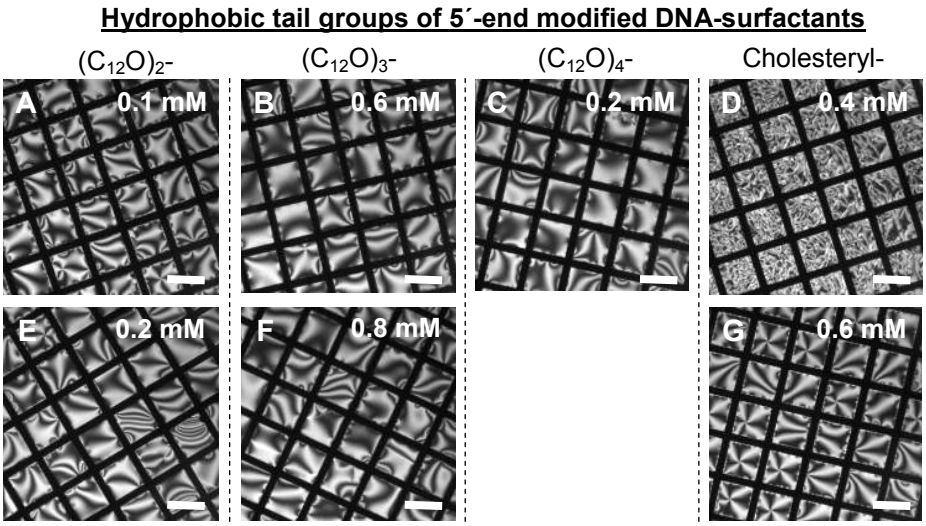

Figure 3.8: Optical images of 5CB between crossed polarisers contacted with aqueous solutions containing various DNA-surfactants in phosphate buffer (0.1 M NaH_2PO_4, 2 M NaCl, 1 mM $EDTANa_2$ at pH 7.0) for 20 h. The DNA sequences of each DNA-surfactant as follows: (A) $(C_{12}O)_2$-5´-TTTTTTCCCCCC-3´; (B) $(C_{12}O)_3$-5´-GGG GGGAAAAAA-3´; (C) $(C_{12}O)_4$-5´-CAGTGACTGGCC-3´; (D) cholesteryl-5´-TTTTT TCCCCCC-3´; (E) $(C_{12}O)_2$-5´-GGGGGGAAAAAA-3´; (F) $(C_{12}O)_3$-5´-TTTTTTCCCC CC-3´; (G) cholesteryl-5´-GGGGGGCCCCCC-3´. All scale bars represent 300 μm.

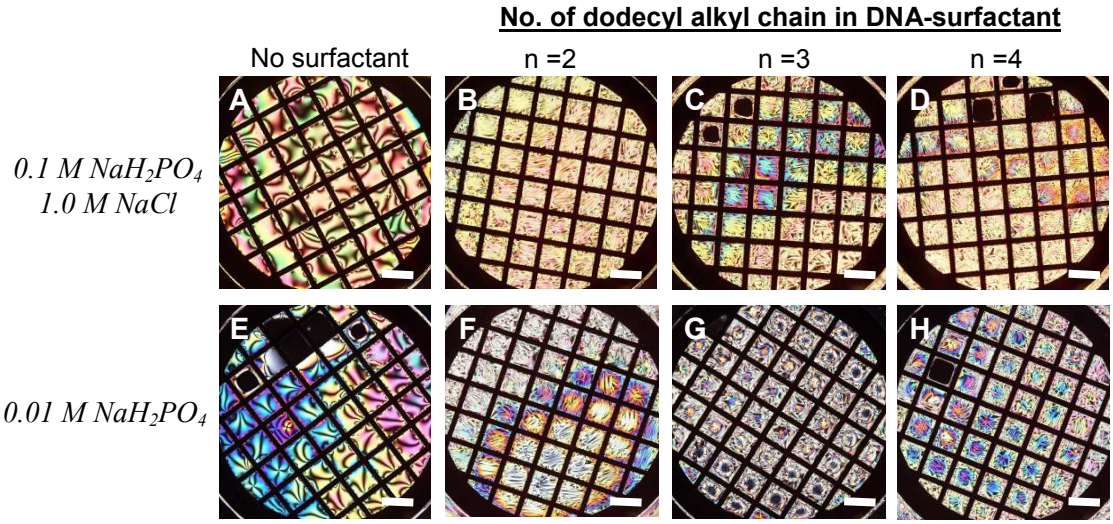

Figure 3.9: Optical images of 5CB between crossed polarisers contacted with aqueous solutions containing $(C_{12}O)_n$-5´-TTTTTTCCCCCC-3´ DNA-surfactants with different ionic strengths. 300 μM DNA-surfactant solutions [B-D] were in an aqueous solution of 0.1 M NaH_2PO_4, 1 M NaCl, 1 mM $EDTANa_2$ at pH 7.0 and [F-H] in 0.01M NaH_2PO_4, 1 mM $EDTANa_2$ at pH 7.0. All scale bars represent 300 μm. For image C, D, E and H, the black squares in the grids correspond to a square which were empty of 5CB.

3.2.3 Hybridisation of DNA-surfactant at the 5CB-water interfaces

As previously discussed, DNA-surfactants could not change the alignment of 5CB from planar to homeotropic anchoring at the LC-water interface. Thus, we determined whether DNA-surfactant molecule can adsorb at the LC-water interface and hybridise with a complementary DNA although it cannot change the alignment of 5CB at the LC-water interface. We conducted the following DNA hybridisation experiment as illustrated in Figure 3.10.

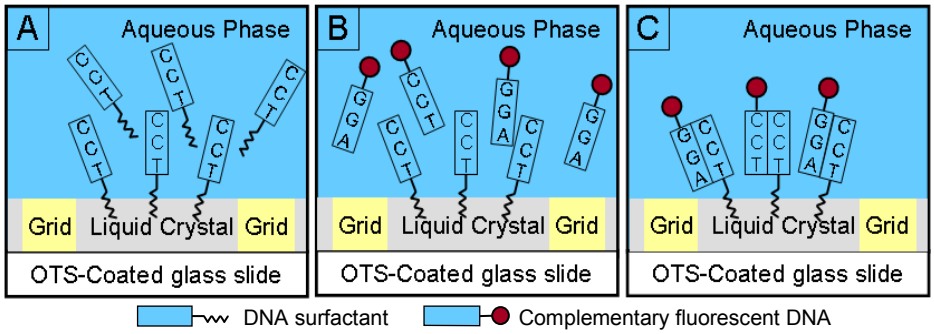

Figure 3.10: Scheme of the hybridisation of interface bound DNA-surfactant at the LC-water interface. (A) Adsorption of DNA-surfactant at the LC-water interface. (B) Replacement of an aqueous phase with a solution containing fluorescence tagged complementary DNA. (C) Remove the excess of DNA and detect the fluorescence signal at the LC-water interface under a fluorescent microscope.

We exposed 5CB and hexadecane which were confined in EM grids to a solution of 5´-cholesteryl modified DNA-surfactant and then to a solution of fluorescence tagged complementary DNA. We also conducted a control experiment where the LC treated with the same DNA-surfactant was exposed to a solution of a non-complementary fluorescent DNA probe. The hybridisation experiment followed a procedure detailed in an earlier publication.[8,9] Two EM grids hosting 5CB were covered with a perfusion chamber with internal volume 60 μL. Both chambers were filled with 60 μL of 100 μM cholesteryl-5´-GGGGGGAAAAAA-3´ DNA-surfactant in prehybridisation buffer (0.09 M Na-citrate, 0.9 M NaCl, 0.01 M Na-phosphate, 1 mM EDTA, 10 μg/ml salmon sperm DNA, pH 7.0) and left for 1.5 h to enable the DNA-surfactant to adsorb and equilibrate at the LC-water interface. Then both chambers were washed with 60 μL of prehybridisation buffer three times. After that one chamber was filled with a solution containing the complementary TAMRA tagged DNA (TAMRA-5´-TTTTTTCCCCCC-3´) and another with a non-complementary TAMRA tagged DNA (TAMRA-5´-

GGCCAGTCACTG-3´). Finally, the two chambers were washed with 60 μL of prehybridisation buffer twice and characterized under a fluorescent microscope. The LC optical cells were imaged to check the presence of a fluorescent signal from the LC-water interface at 568 nm excitation wavelength and tetramethylrhodamine isothiocyanate (TRITC) filter set. A control experiment was conducted with hexadecane film confined in EM grids instead of 5CB using the same procedure above.

The results are presented in Figure 3.11 where LC was imaged under both fluorescent and polarised light. We observed a fluorescent signal for TAMRA-DNA from the hexadecane-water interface which indicates a specific hybridisation of the TAMRA-DNA probe to the bound cholesteryl DNA-surfactant (Figure 3.11E). As seen from the fluorescent image in Figure 3.13F, there is no fluorescence from the interface under the same condition, which is a result of the lack of complementary between the DNA-surfactant and the used TAMRA DNA probe. This result and the past studies[9,10,11] suggest that DNA- surfactants can adsorb at the oil-water interface and can hybridise with the complementary DNA. The two images in Figure 3.11C and G show the case of the complementary DNA probe for the DNA-surfactant adsorbed at the LC-water interface.

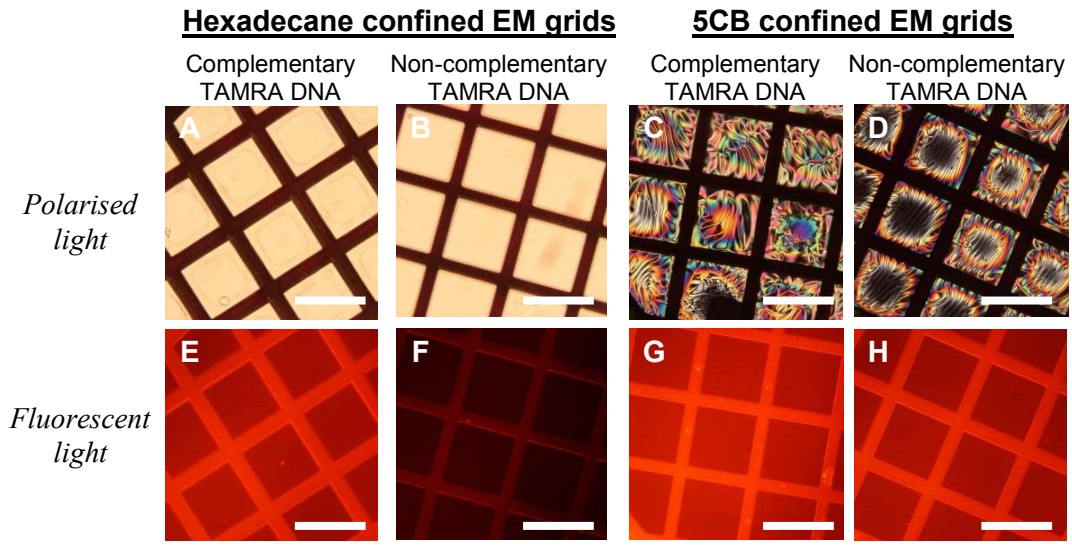

Figure 3.11: Optical images of 5CB between crossed polarisers contacted with cholesteryl-5´-GGGGGGAAAAAA-3´ DNA-surfactants which have been hybridised with a TAMAR labeled complementary (TAMRA-5´-TTTTTTCCCCCC-3´) and non-complementary DNA oligomer (TAMRA-5´-GGCCAGTCACTG-3´). (A-B): Polarised light, (C-D): transmitted light and (F-H): TRITC filter. All scale bars represent 300 μm.

However, there is also non-specific fluorescent signal of the TAMRA-DNA probe at the LC-water interface and the surface of EM grids at the same condition (Figure 3.13G and H), which results from the interaction between TAMRA-DNA and the metal surface of EM grids or TAMRA-DNA and LC. Moreover, these non-specific bindings of DNA were not desorbed from the interface even after excess of washing. Therefore, it is suggested that another fluorescent tagged molecule (e.g., FITC) should be used in the DNA hybridisation experiment to examine the interaction between TAMRA and 5CB or between DNA and 5CB.

3.2.4 Summary

These results when combined, lead us to conclude that DNA-surfactant cannot trigger the transition of texture of 5CB from planar to homeotropic anchoring independent of the kind of their hydrophobic tail groups, their concentrations and ionic strength of an aqueous solution. By comparing the texture difference between SDS and DNA- surfactant, two main reasons may give rise to a planar anchoring of 5CB at the LC-water interface as shown Figure 3.12.

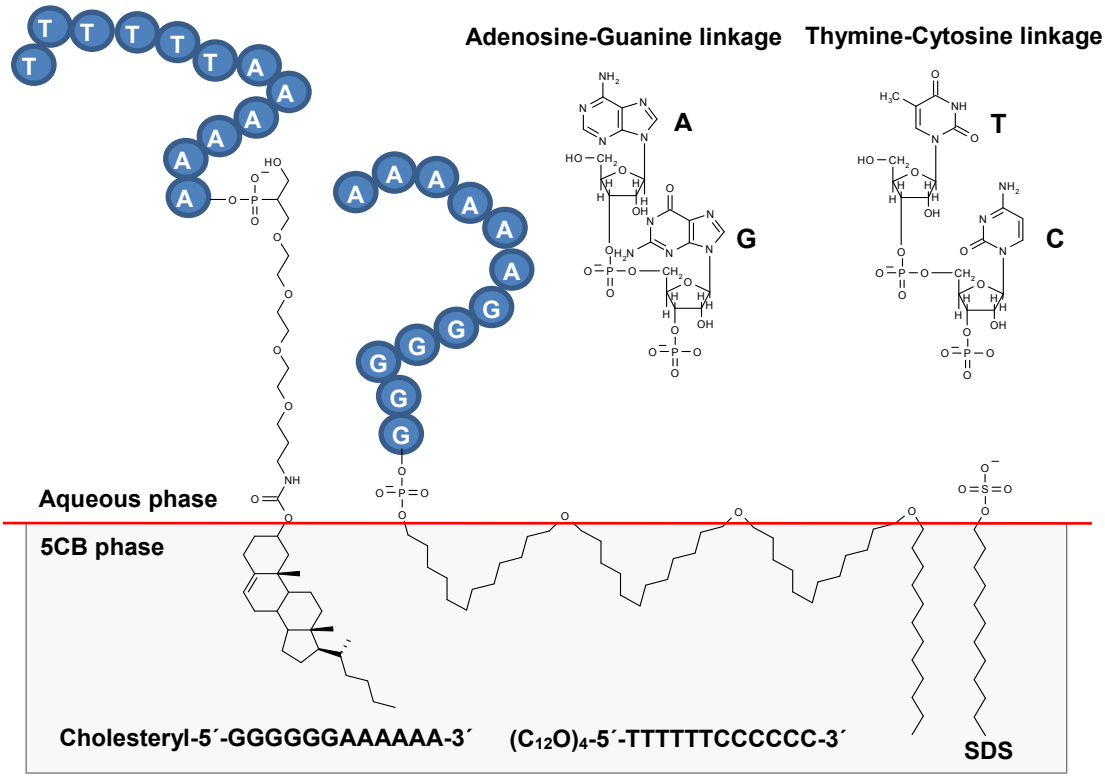

Figure 3.12: Proposed interfacial configuration of cholesteryl and dodecyl alkyl chain modified DNA-surfactants at the 5CB-water interface compared to SDS. The saturated dodecyl alkyl group modified DNA-surfactant is likely to adopt a looped configuration at the LC-water interface by its ether linkage.

First, in contrast to SDS, [12] the dodecyl alkyl chain of modified DNA-surfactants might adopt the looped configuration at the LC-water interface to cause planar anchoring of LC regardless of the number of dodecyl chain group. This is similar to the surfactant having a bolaform structure (e.g., dodecyl-1, 12-bis(trimethylammonium bromide)).[12] Second, although the nature of small sized head groups of surfactants (e.g., SDS, CTAB) does not strongly influence the orientation of the LC[3,4,6] the bulky electronegatively charged DNA head groups of DNA-surfactants could not produce a dense enough monolayer at the LC-water interface to change the orientation of 5CB by their high surface area.

If the looped configuration of DNA-surfactants at the LC-water interface is important in the apparent insensitivity of the anchoring of 5CB, then the complex formed between DNA and cationic surfactant is likely to influence the orientation of 5CB. In the next section, we address the adsorption of a DNA-cationic surfactant complex on the orientation of 5CB.

3.3 Adsorption of DNA-cationic surfactant complex at the 5CB-water interface

3.3.1 Introduction

Cationic surfactants (e.g., CTAB or DTAB) bind electrostatically to the negatively charged phosphate groups of DNA to produce water-insoluble complexes which strongly adsorb at both the hydrophilic and hydrophobic surface.[13] We expect that these complexes may also adsorb at the LC-water interface and the hybridisation of the interface bound DNA will alter the charge balance. This is likely to affect the surface orientation of the LC and hence produce an observable optical effect. This approach does not require any special modification of the DNA (e.g., the preparation of DNA-surfactants). Complex formation between cationic surfactants and DNA has been studied extensively in recent years.[14,15] The DNA-cationic surfactant systems have a number of applications: DNA can be extracted by condensation and precipitation by using cationic surfactant; CTAB has been used for DNA renaturation and ligation. Quaternary ammonium surfactants can be used, in small amounts, for positive charging of neutral liposomes, improving their DNA transfection efficiency. In bulk, the binding of cationic surfactants to DNA appears to be analogous to binding of surfactants to oppositely charged synthetic polymers in general. It was demonstrated through the use

of cationic surfactant-selective electrodes that cationic surfactants bind to the negatively charged DNA macromolecule in a cooperative manner.[13,16]

The binding of cationic surfactants proceeds in two stages. In the first stage, surfactants exchange with counterions condensed on the DNA chain. At a certain critical surfactant concentration, a highly cooperative binding of surfactant occurs which is typically followed by phase separation.[16] For high molecular weight DNA the cooperative binding of surfactants cause a condensation (a discrete transition from coil to globule state) of the DNA chain. For short DNA chains (i.e. low molecular weight DNA) the DNA chain is too short and rigid to loop back to interact with surfactant aggregates on other parts of the polymer chain. Thus, condensation of short chain DNA does not occur before inter-molecular interactions with other complexes leads to phase separation (i.e. precipitation of DNA-surfactant complexes). For a short DNA chain (e.g., 220 base pairs) no surfactant induced condensation of the DNA chain occurs before phase separation. Instead, the surfactant molecules self-organize on the surface of the DNA according to a "beads on necklace" model.[13] High molecular weight DNA molecules, which condense on addition of small amount of cationic surfactants, do not adsorb on hydrophilic silica prior to phase separation. However, DNA-surfactant complexes formed from low molecular weight DNA were found to adsorb. For these complexes surfactants interact with DNA, without condensation of the DNA. Adsorbed DNA-surfactant complexes can be easily removed from the hydrophilic silica surface when replacing the bulk DNA-surfactant solution with pure salt solution. At the hydrophobic surface the DNA adsorbs without addition of cationic surfactant. However, with addition of a very small amount of surfactant, a rapid increase in adsorbed amount and a simultaneous decrease in adsorbed layer thickness are observed. This compaction of the adsorbed layer is to some extent reversible when replacing the bulk DNA-surfactant solution with pure salt solution.

The structure of the adsorbed layer of DNA on the hydrophobic surface (e.g., hydrophobized silica) depends on the conformation of DNA (i.e. single stranded or double stranded) and molecular weight. Low molecular weight DNA, for which the surfactant interact with DNA without condensation of the formed complexes adsorb to a considerable extent. Moreover, the surfactant adsorbs at the hydrophobic surface and acts as an anchor point for the DNA molecules. Therefore, we used a cationic surfactant

molecule as an anchoring molecule for DNA oligomer to the LC-water interface and to change the alignment of 5CB by adsorption of the DNA-cationic surfactant complex.

Different types of DNA adsorb to the hydrophobic silica surface by hydrophobic interaction (Figure 3.13A).[17] Moreover, no detectable desorption of DNA occurred by replacing with high ionic strength solution (e.g., 10 mM NaBr) after adsorption (Figure 3.13B). Although both CTAB and CTAB-free DNA readily adsorb to hydrophobic surface, a large synergistic increase in the adsorbed amount is observed when both CTAB and DNA present (Figure 3.13C).

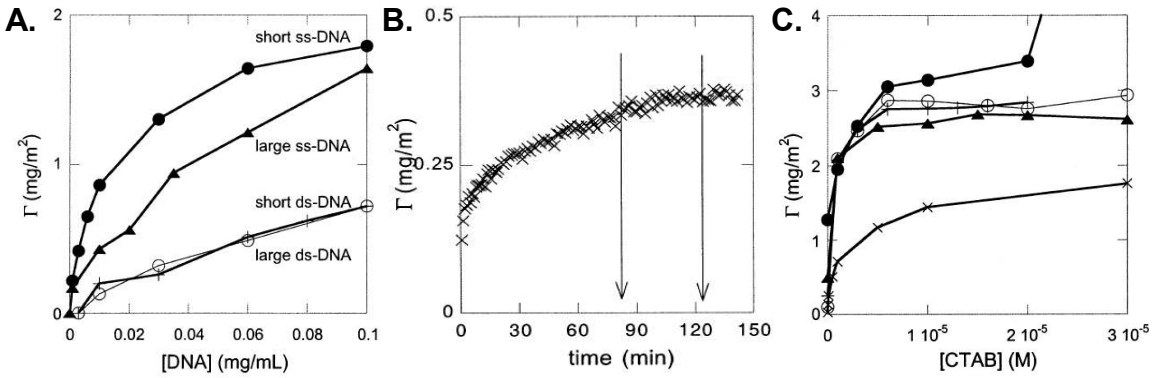

Figure 3.13: (A) Adsorption isotherms of different DNA samples at the hydrophobic silica-water interface in 10 mM NaBr solution. (+): 2000 base pairs (bp) double strand (ds) DNA; (○): 146 bp ds-DNA; (▲): 2000 bp single strand (ss) DNA; (●): 100 bp ss-DNA. (B) Adsorbed DNA amount as a function of time at hydrophobic surfaces for 2000 bp ds-DNA. A 0.03 mg/mL portion of DNA was injected at 0 min, followed by the addition of 1×10^{-6} M SDS at 80 min. Rinsing with 10 mM NaBr solution was performed at 125 min. (C) Adsorption isotherm for different DNA-CTAB complexes at the hydrophobic silica-water interface. For short ss-DNA at 3×10^{-5} M CTAB, the surface excess concentration increases to 8 mg/m^2 from 0.95 mg/m^2. (×): CTAB alone; (+): 2000 bp ds-DNA; (○): 146 bp ds-DNA; (▲): 2000 bp ss-DNA; (●): 100 bp ss-DNA. Data are from reference [17].

Rinsing with 10 mM NaBr solution removes CTAB from the adsorbed layer at the hydrophobic silica-water interface, leaving only DNA (Figure 3.14A).[17] A less dense layer is obtained by simultaneous addition of DNA and CTAB than in the case of sequential addition of CTAB and DNA for short single-stranded DNA (Figure 3.14B). Therefore, the final structure of the adsorbed layer depends on the history of formation of the DNA-cationic surfactant complexes.

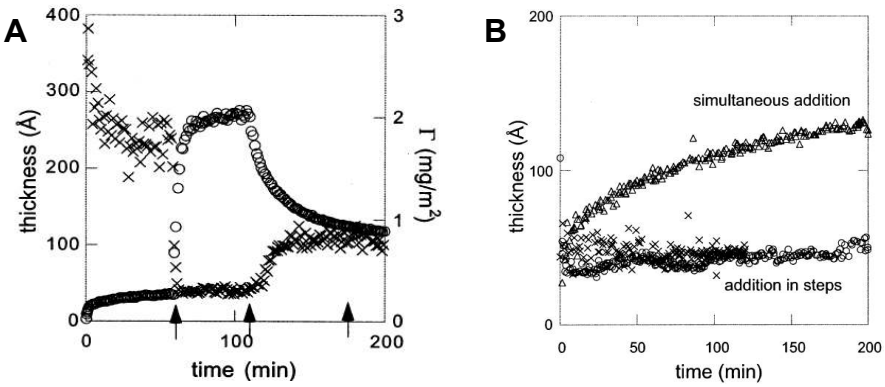

Figure 3.14: Adsorbed amount (○) and layer thickness (×) as a function of time for DNA-CTAB complexes at hydrophobic silica surface. (A) At 0 min, 0.02 mg/mL long ds-DNA was added. 1×10^{-6} M CTAB was added at 60 min followed by rinsing with 10 mM NaBr solution at 110 min. Arrows refer to changes in bulk concentration. (B) Layer thickness of DNA-CTAB complexes as a function of time. A 0.02 mg/mL portion of 146 bp ds-DNA and 1×10^{-6} M CTAB in 10 mM NaBr solution was used. DNA-CTAB complexes were simultaneously added at 0 min (Δ), CTAB was added at 0 min to a surface previously covered with 146 bp DNA (○), and DNA was added at 0 min to a surface previously covered with CTAB (×). Data are from reference [17].

3.3.2 Anchoring of 5CB by cationic surfactants

On the basis of the results of Lindman *et al.*,[17,25,26,27] DNA-cationic surfactant complex is likely to adsorb at the LC-water interface and the adsorbed DNA-cationic surfactant complex can hybridise with its complementary DNA with showing different LC textures according to the interfacial events. To address this proposition we firstly investigated the anchoring of 5CB by cetyltrimethylammonium bromide (CTAB), tetradecyltrimethylammonium bromide (TTAB), and cetylpyridinium chloride (CPC). Figure 3.15, 3.16 and 3.17 show the optical textures of 5CB in contact with aqueous solutions containing of CTAB, TTAB, and CPC. The adsorption of CTAB, TTAB, and CPC at the LC-water interface caused the transition of the orientation of 5CB from planar to homeotropic anchoring similar to SDS. However, the surfactant concentration at which the transition occurs is significantly different for CTAB, TTAB, and CPC.

Bulk concentrations of ~0.05 mM CTAB resulted in homeotropic alignment of 5CB (Figure 3.15) whereas bulk concentrations of ~0.5 mM TTAB (Figure 3.15) and ~0.06 mM CPC (Figure 3.17) gave rise to the same transition of anchoring of 5CB.

These concentrations exceed the concentrations at which the onset of surface activity (e.g., 0.5 μM for CTAB) is measured at an air-aqueous phase.[18]

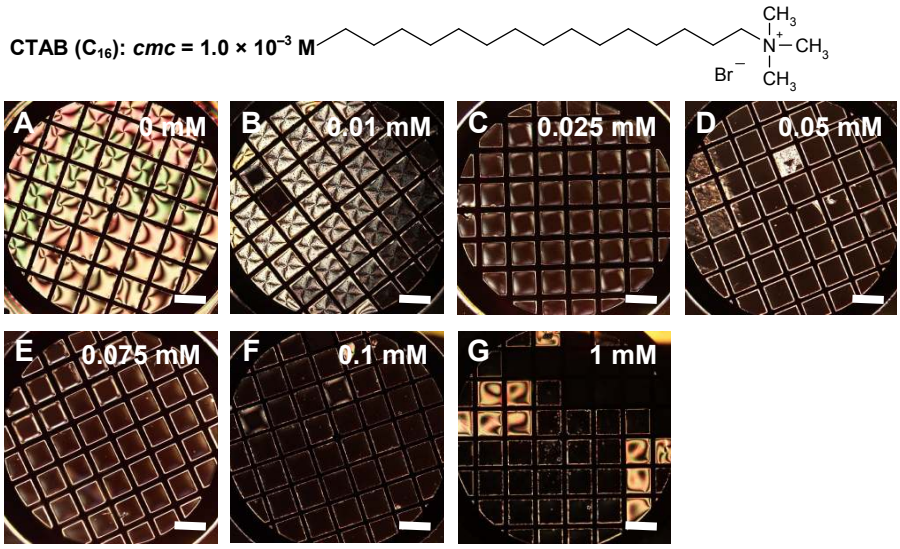

Figure 3.15: Optical images of 5CB between crossed polarisers after incubation with an aqueous solution containing CTAB in pure water as a function of CTAB concentration: (A) 0 mM; (B) 0.01 mM; (C) 0.025 mM; (D) 0.05 mM; (E) 0.075 mM; (F) 0.1 mM; (G) 1.0 mM. All scale bars represent 300 μm.

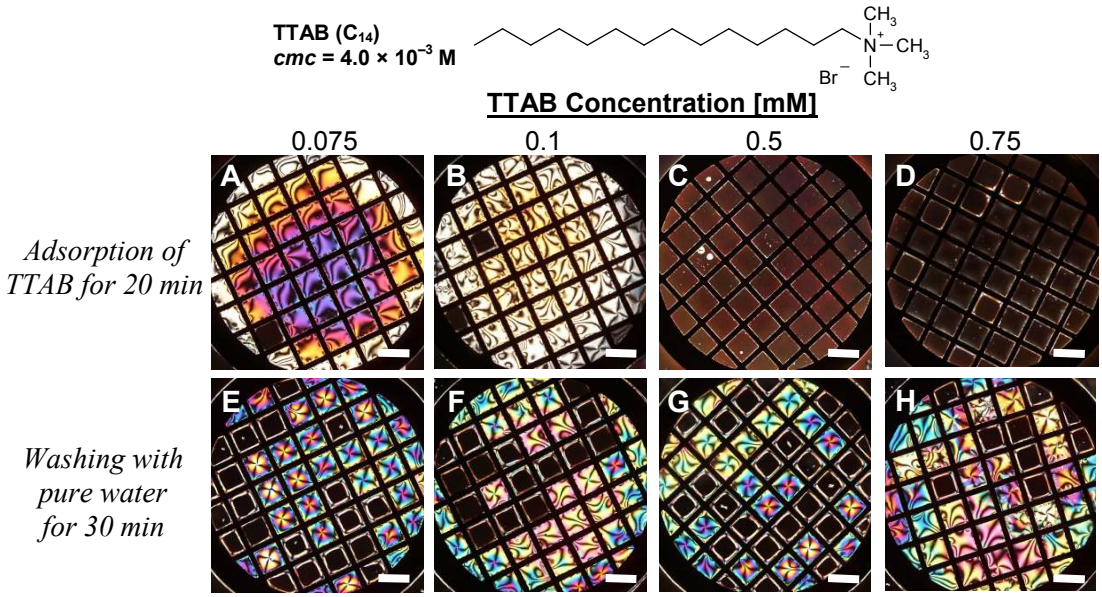

Figure 3.16: Optical images of 5CB between crossed polarisers after incubation with TTAB aqueous solution for 20 min and after washing with 4 perfusion chamber volumes of pure water. All scale bars represent 300 μm. For images A, B, E, F, G and H, the black square in the grid corresponds to a square which was free of 5CB.

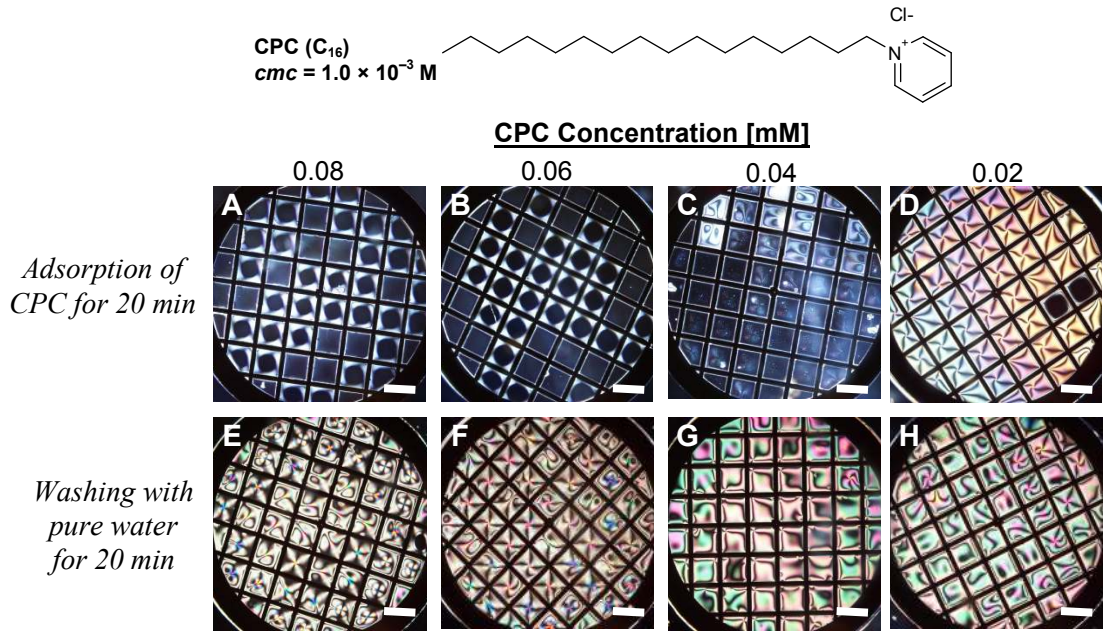

Figure 3.17: Optical images of 5CB between crossed polarisers after incubation with CPC aqueous solutions for 20 min and after washing with 4 perfusion volumes of pure water at room temperature. All scale bars represent 300 μm. For images A, B and D, the black square in the grid corresponds to a square which was free of 5CB.

The concentrations over which all of the anchoring transitions occurred correlate with the concentration regime where these surfactants are known to adsorb strongly at the air-water and oil-water interface like SDS. These results are also consistent with Abbott's suggested anchoring mechanism[4] by which the anchoring of LC might be influenced by the length of surfactants. With decreasing the chain length, the surfactant will possess lower limiting areal densities. Thus, the limiting surface density of TTAB is likely to be less than CTAB and CPC. The penetration of 5CB into the surfactant layer may increase with increasing alkyl chain length[19] and may promote an extension of the alkyl chain of the surfactant as well as an orientation of the 5CB that is closer to the normal of the interface (i.e. homeotropic anchoring).

Our investigations of surfactant behaviour at the 5CB-water interfaces have been usually carried out above the Krafft temperature to ensure adequately solubility and equilibration between the adsorbed and dissolved state of the surfactant. Therefore, CPC is more useful to be further studied in our experimental system because of its lower Krafft temperature than TTAB and CTAB.

An aqueous solution containing 0.01 mM CTAB causes a planar anchoring of the 5CB at the LC-water interface, however, addition of 0.1 M Li_2SO_4 at the same CTAB concentration induces homeotropic anchoring of LC at the interface similar to the addition of 0.1 M NaH_2PO_4 in SDS solution (Figure 3.18).

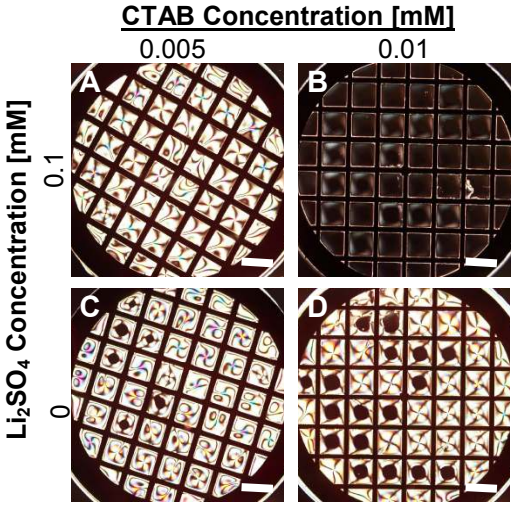

Figure 3.18: Influence of electrolyte on the adsorption of CTAB at the LC-water interface. Optical images of 5CB between crossed polarisers after incubation with aqueous solution containing various concentrations of CTAB in 0.1 M Li_2SO_4 for 20 min. All scale bars represent 300 μm. For images C and D, the black square in the grid corresponds to a square which was free of 5CB.

The fact that the addition of salt decreases the bulk concentration of CTAB like SDS, at which the anchoring of 5CB changes from planar to homeotropic, suggests that the dominant role of the surfactant head group is that of determining the interfacial density of the adsorbed surfactant.

3.3.3 Anchoring of 5CB by DNA-cationic surfactant complex

3.3.3.1 The order of addition of DNA and cationic surfactant

The interaction between DNA and cationic surfactants (CTAB, TTAB, and CPC) were investigated by the alignment change of 5CB according to the variation of the [cationic surfactant]/[DNA] mixing ratios. A special attention was given to the amount of desorption of interface bound DNA-cationic surfactant complex after washing with buffer or pure water.

Figure 3.19 shows the anchoring of 5CB by the co-adsorption of DNA and CTAB mixtures as a function of surfactant concentration. We varied the CTAB concentration

at fixed DNA concentration (50 μM) in phosphate buffer (0.1 M NaH_2PO_4, 1 mM $EDTANa_2$, pH 7.0) to form DNA-cetyltrimethyl ammonium (CTA) complexes and analyzed with respect to optical images change from homeotropic to planar anchoring. By observing the dependence of the homeotropic anchoring of LC on the mixing molar ratio, homeotropic anchoring starts at mixing molar ratio ≈ 2. The result shows that the DNA makes a complex with CTAB and cannot adsorb at the LC-water interface enough to cause a transition from planar to homeotropic anchoring of LC (Figure 3.19A) at mixing molar ratios below 2 although DNA-free CTAB readily causes a homeotropic anchoring at the same concentration (data not shown).

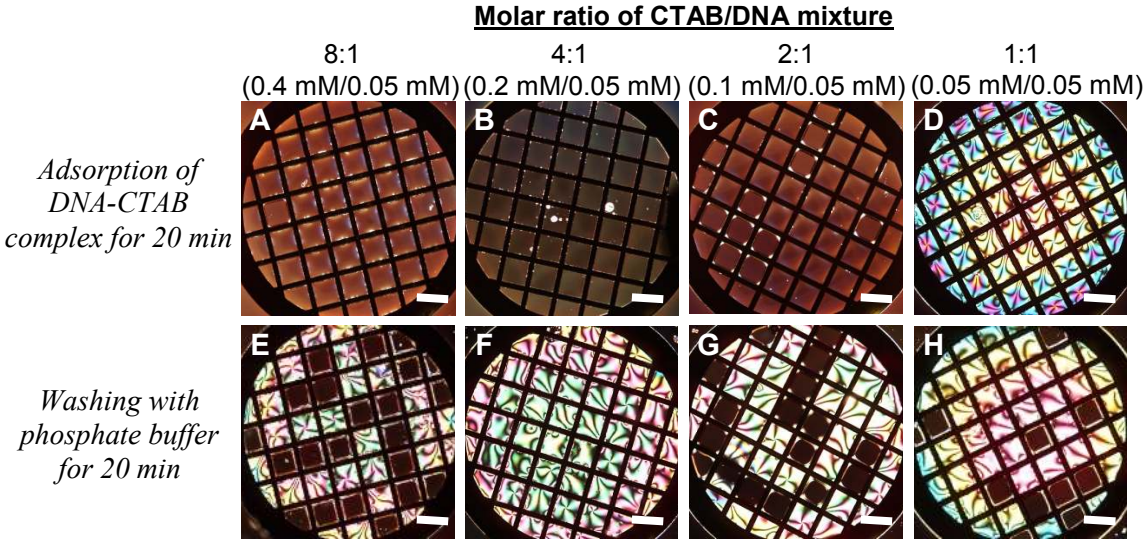

Figure 3.19: Optical images of 5CB between crossed polarisers after incubation with DNA-CTAB mixture in phosphate buffer (0.1 M NaH_2PO_4, 1 mM $EDTANa_2$, pH 7.0) according to the mixing molar ratios and washing with 1 perfusion chamber volume of phosphate buffer. All scale bars represent 300 μm.

The interaction of short DNA fragments in dilute solutions with the cationic surfactant such as DTAB results in the formation of soluble complexes with concentrations below 0.3 mg/cm^3 and binding ratio that is the number of surfactants per DNA phosphate group less than 0.8.[13] Therefore, at low binding ratios, DNA molecules might form a soluble complex with CTAB which does not adsorb at the LC-water interface and does not change the anchoring of LC (Figure 3.19A). In contrast, DNA and CTAB mixtures cause a transition from planar to homeotropic anchoring of 5CB with increasing mixing molar ratio of CTAB and DNA (Figure 3.19B-D). However, the triggered homeotropic anchoring reverted to planar anchoring by washing with only 1 perfusion chamber volume of buffer solution. This result proposes that the formed DNA-

cetyltrimethylammonium ion (CTA^+) complex could not be sustained at the LC-water interface or CTA^+ ion might be released from the complex with leaving DNA alone at the LC-water interface by washing with a buffer solution.

We also explored the anchoring of LC when contacted with an aqueous solution of DNA-CPC mixture by varying the mixing molar ratio of CPC and DNA from 10 to 1 at fixed 0.1 mM CPC concentration. Although homeotropic anchoring induced by adsorption of DNA-CPC mixture were reverted to planar anchoring in many compartments of EM grids after washing with 2 perfusion chamber volumes of pure water, some squares maintained their triggered homeotropic anchoring (Figure 3.20I-K) in contrast to DNA-CTAB mixture (Figure 3.19E-H). The boundaries between these two different anchoring behaviours were generally defined by the EM grid. This result suggests that the grids compartmentalize the LC and its interface.

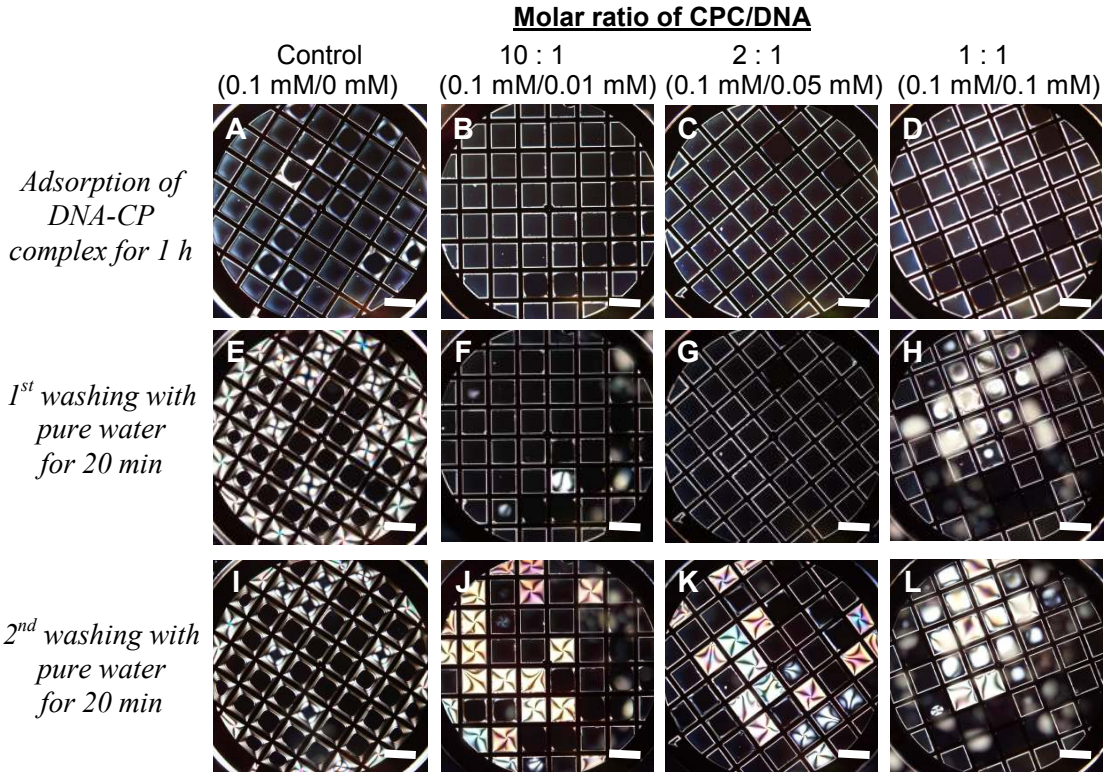

Figure 3.20: Optical images of 5CB between crossed polarisers after incubation with 5´-TTTTTTCCCCCC-3´ DNA and CPC mixtures in pure water according to the mixing molar ratio. The chambers were washed with 1 perfusion chamber volume of pure water at each time and incubated for 20 min. All scale bars represent 300 μm.

We predict that the LC texture difference between the interface bound DNA-CTA and DNA-cetylpyridinium ion (CP^+) complexes after washing might mainly come from the

different dissolution behaviour of cationic surfactants in pure water for DNA-CP complex and in a salt solution for DNA-CTA complex because DNA-free CTAB and CPC show a similar behaviour to the anchoring of 5CB at the LC-aqueous interface. The results correspond qualitatively to DNA adsorption at the hydrophobic silica surface that was previously reported by Cárdenas *et al.*[17]

We also investigated the effect of the ionic strength on the formation of DNA-cationic surfactant complex. In a previous study,[15] the addition of NaBr facilitates formation of precipitate for lower amount of DNA and surfactant aggregates. DNA and CPC mixture in 10 mM NaCl solution is likely to be less desorbed from the LC-water interface (Figure 3.21J, L) than in pure water (Figure 3.21I, K). At the same mixing ratio, the homeotropic anchoring of 5CB triggered by a higher total concentration of DNA and CPC (Figure 3.21L) was less reverted to planar than that of a lower total concentration (Figure 3.21J) in the same salt solution after washing with pure water.

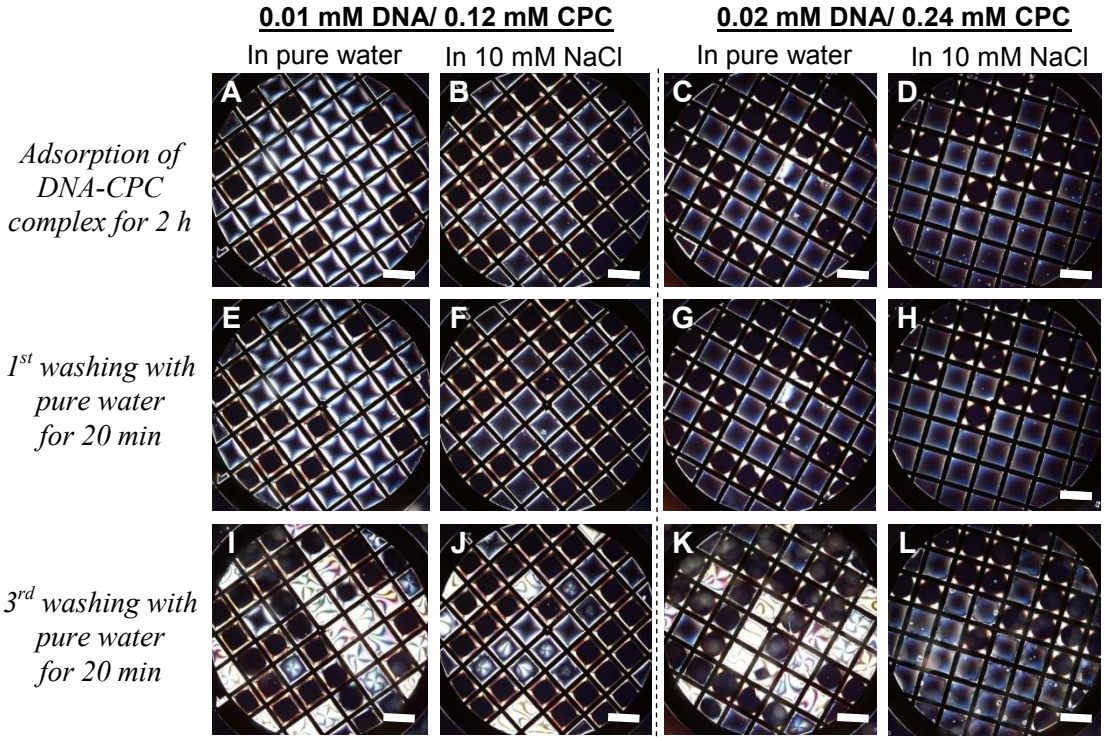

Figure 3.21: Optical images of 5CB between crossed polarisers after incubation with 5′-TTTTTTCCCCCC-3′ DNA and CPC mixture in pure water and 10 mM NaCl at a molar mixing ratio of DNA : CPC = 1 : 12. The chambers were washed with 1 perfusion chamber volume of pure water at each wash. All scale bars represent 300 μm.

To observe the interfacial behaviour of DNA-cationic surfactant complex at the LC-water interface in detail, we used fluorescently-tagged DNA for formation of DNA-

cationic surfactant complex. Fluorescent microscopy has been used for the observation of single DNA molecules in solutions and the effects of cationic surfactants on its conformational behaviour.[20] Using a fluorescent DNA-cationic surfactant complex, the adsorption and desorption of cationic surfactant and DNA at the LC-water interface are detected separately using a cross-polarised and a fluorescent light microscopes.

Figure 3.22 shows the adsorption and desorption of fluorescent DNA-CTA complex at the LC-water interface. Surfactant-free DNA adsorbed at the hydrophobic OTS coated glass slide, the copper grid surface, and the LC-water interface after washing with pure water (Figure 3.22G). Although DNA is a highly negative charged molecule, with a charge density corresponding to one charge per 1.7 Å in the case of B-DNA,[21] it also contains hydrophobic nitrogenous base structures. Therefore, interactions between these hydrophobic surfaces and the hydrophobic parts of the DNA molecule drive its adsorption to the surfaces. Figure 3.22C shows that the co-adsorption of FITC tagged DNA and CTAB mixture causes a transition from planar to homeotropic anchoring of 5CB.

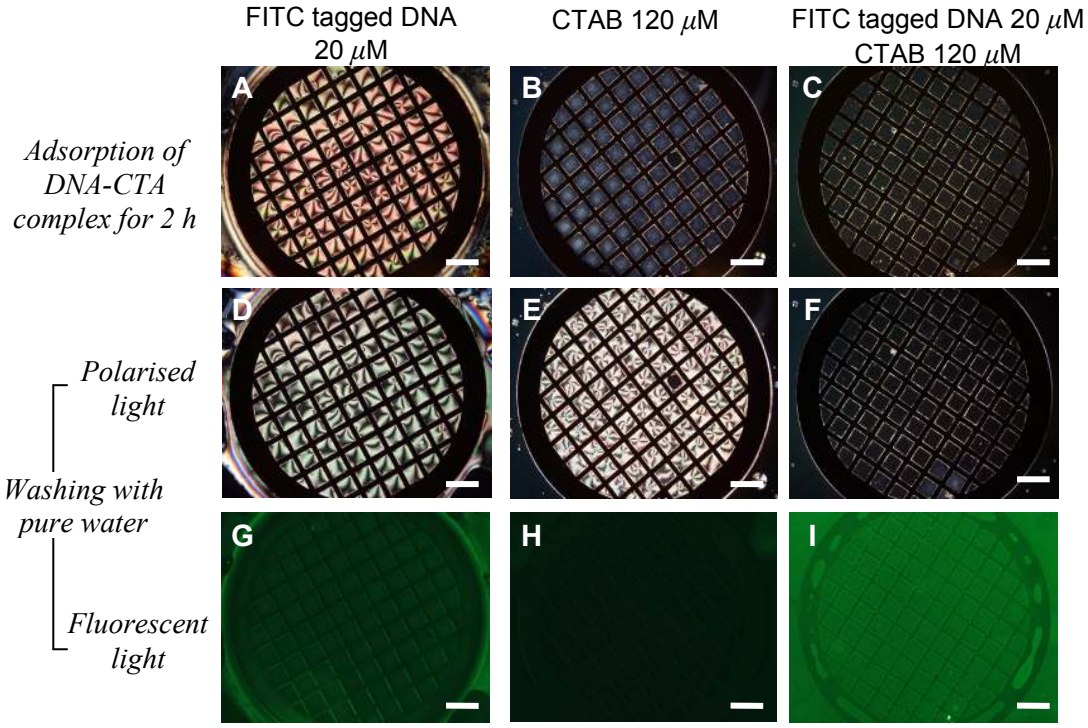

Figure 3.22: Optical images of 5CB between crossed polarisers after incubation with (A) FITC tagged DNA (FITC-5′-TTTTTTCCCCCC-3′); (B) CTAB; (C) FITC tagged DNA-CTAB mixture in 10 mM NaBr solution. The chambers were washed with 6 perfusion chamber volumes of pure water. All scale bars represent 300 μm.

The triggered transition (i.e. homeotropic anchoring) was not reverted to planar anchoring even after washing with 6 perfusion chamber volumes of pure water (3.22F). This behaviour is different from that observed in case of only CTAB (3.22E) which is easily desorbed from the LC-water interface.

Although the surfactant-free DNA readily adsorbs at the LC-water interface (Figure 3.22G), a large synergistic increase in adsorbed amount of DNA is observed when both CTAB and DNA are present simultaneously (Figure 3.22I). Due to electrostatic interactions, CTAB is expected to preferentially interact with DNA rather than the surface. Thus, most surfactant molecules should be complexed to DNA instead of directly adsorbed to the surface. Supporting this idea is the observation that the homeotropic anchoring of 5CB caused by the co-adsorption of DNA and CTAB is more sustained after the same washing process. In a previous study,[17] a similar behaviour was obtained for different types of DNA (e.g., single and double stranded DNA with different molecular weight) indicating a synergistic increase in the adsorbed amount when the both CTAB and DNA are present as compared to the surface excess concentration of either of the individual components on hydrophobic silica surface using ellisopmetry.

To investigate the interfacial behaviour of the mixed DNA-CTA adsorbed layer at the LC-water interface after washing with a salt solution the aqueous phase was replaced with pure water and 10 mM NaBr solution sequentially. As shown in Figure 3.23F, replacing the DNA-CTAB mixture solution with pure water can not cause a transition of anchoring of 5CB. On the other hand, the replacing with 10 mM NaBr solution leads to a transition from homeotropic to planar anchoring of 5CB although it could not fully remove the fluorescent intensity of DNA at the LC-water interface. This result indicates that rinsing with a salt solution removes the cationic surfactant molecules from the mixed DNA-CTA adsorbed layer, leaving only DNA molecules at the LC-water interface.

To summarize, the results are close to the key observations from Cárdenas *et al.* using ellipsometry.[17] First, the structure of the mixed DNA-CTA adsorbed layer is neutral despite the large excess of negative charges in the bulk. Secondly, rinsing with a salt solution (e.g., 10 mM NaBr) induces desorption of the cationic surfactant, leading to a denser DNA layer structure at the hydrophobic silica surface than those formed by surfactant-free DNA.

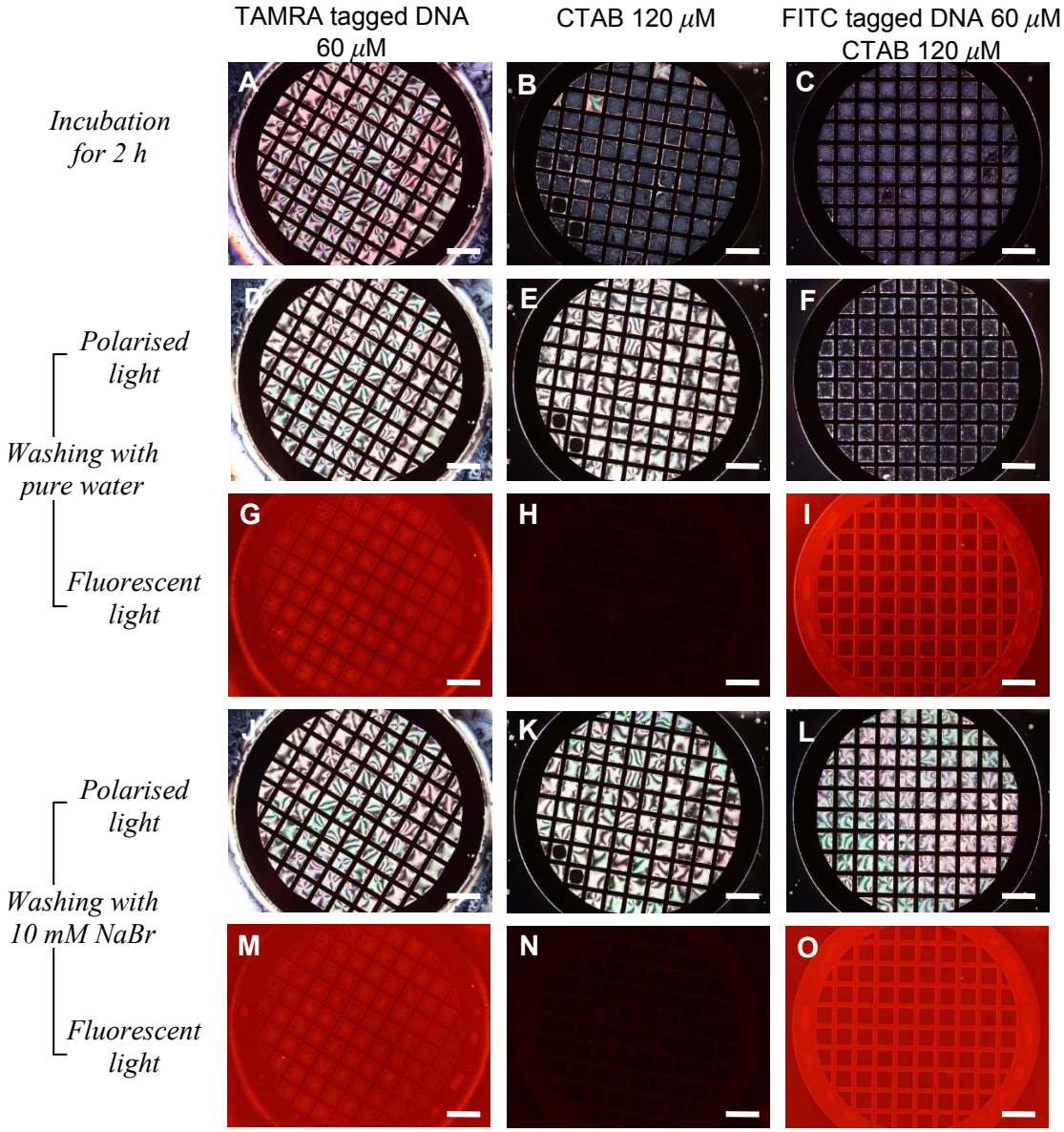

Figure 3.23: Optical images of 5CB between crossed polarisers after incubation with (A) TAMRA tagged DNA (TAMRA-5′-TTTTTTCCCCCC-3′); (B) CTAB; (C) TAMRA tagged DNA-CTAB mixture in 10 mM NaBr solution. The chambers were washed with 6 perfusion chamber volumes of pure water and then 4 perfusion chamber volumes of 10 mM NaBr solution sequentially. All scale bars represent 300 μm.

3.3.3.2 Hybridisation of DNA-cationic surfactant complex at the 5CB- water interface with complementary DNA

In the hybridisation reaction the washing with a salt solution [e.g., SSC solution (0.015 M sodium citrate, 0.15 M NaCl pH 7.0)] is necessary to remove a non-specific binding of DNA occurring during the DNA hybridisation reaction. We investigated the

effect of washing with a salt solution on the mixed DNA-cationic surfactant adsorbed layer at the LC-water interface during the hybridisation reaction as illustrated in Figure 3.24.

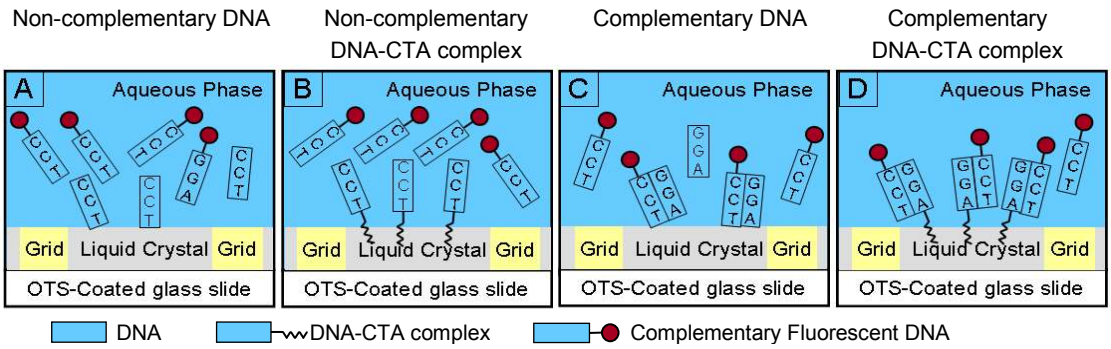

Figure 3.24: Schematic illustration of the hybridisation of the mixed DNA-CTA absorbed layer at the 5CB-water interface with a complementary DNA. (i) Adsorption of DNA and DNA-CTA complex at the 5CB-water interface. (ii) Hybridisation of the DNA and mixed DNA-CTA adsorbed layer with a complementary or non-complementary fluorescent DNA probes. DNA-CTA adsorbed layer (Image D) is expected to show a strong fluorescent intensity rather than the CTAB free DNA adsorbed layer (Image C) at the LC-water interface.

We first observed the anchoring of 5CB when in contact with aqueous solutions containing DNA-CTAB mixtures and confirmed that the alignment of 5CB was homeotropic (images not shown in here) which is consistent with previous results shown in Figure 3.22 and 3.23. The optical textures of 5CB following the hybridisation of the complementary and non-complementary DNA to the mixed DNA-CTAB adsorbed layer at the LC-water interface are shown in panels B and D of Figure 3.25 respectively. The homeotropic anchoring in both panels indicates the DNA-CTAB adsorbed layer is not desorbed during the hybridisation reaction. However, as shown in Figure 3.25J and L, washing with saline sodium citrate buffer (0.015 M sodium citrate, 0.15 M NaCl, pH ~7.0) solution leads to the transition from homeotropic to planar anchoring of 5CB. On the other hands, the strong fluorescent signal from the hydrophobic surfaces (i.e. LC-water interface, copper EM grid surface and OTS coated glass slide) was sustained after the washing. These results suggest that the washing with a salt solution removes CTA^+ ion from the mixed DNA-CTA adsorbed layer, leaving only DNA at the LC-water interface. Additionally, surfactant-free DNA molecule can adsorb non-specifically at the LC-water interface. The further washing with a salt

solution (0.1× SSC solution) removes more of the adsorbed DNA from the LC-water interface. We also observed a similar optical response using TAMRA tagged DNA (Figure 3.26) instead of FITC tagged DNA at the same hybridisation reaction condition.

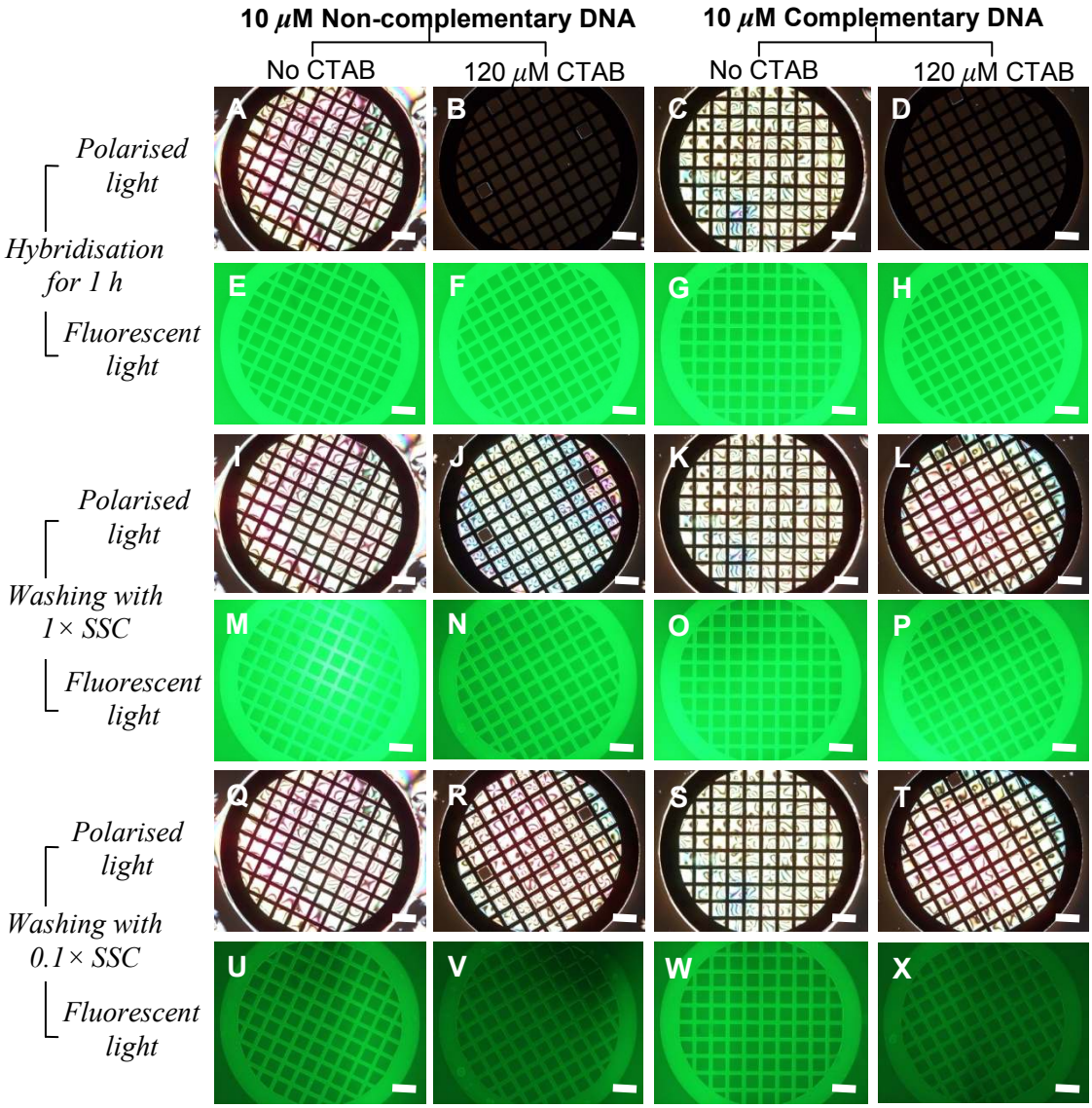

Figure 3.25: Optical images of 5CB between crossed polarisers after hybridisation with FITC tagged DNA. Complementary (5′-GGGGGGAAAAAA-3′)-CTAB complex or non-complementary DNA (5′-TTTTTTCCCCCC-3′)-CTAB complex and DNA alone were incubated at the LC-water interface and these adsorbed layers were hybridised with FITC-5′-TTTTTTCCCCCC-3′ DNA. DNA-CTAB complex changed the anchoring of LC to homeotropic (images B and D). All scale bars represent 300 μm.

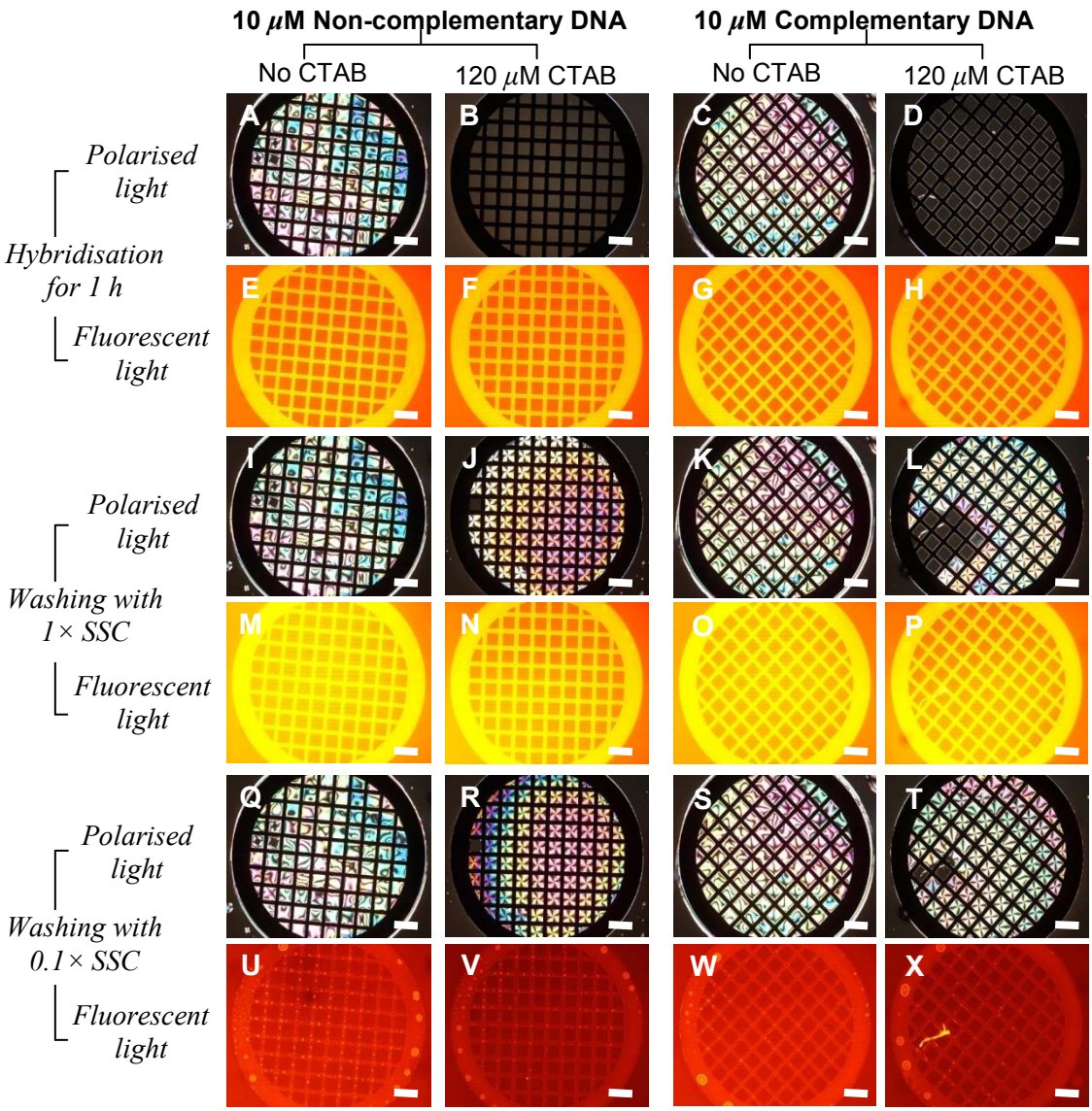

Figure 3.26: Optical images of 5CB between crossed polarisers after hybridisation with TAMRA tagged DNA. Complementary (5′-GGGGGGAAAAAA-3′)-CTAB complex or non-complementary DNA (5′-TTTTTTCCCCCC-3′)-CTAB complex and DNA alone were incubated at the LC-water interface and these adsorbed layers were hybridised with FITC-5′-TTTTTTCCCCCC-3′ DNA. DNA-CTAB complex changed the anchoring of 5CB to homeotropic (B and D). All scale bars represent 300 μm.

Therefore, the mixed DNA-CTA adsorbed layer at the 5CB-wtaer interface could not trigger the transition of LC alignment by the hybridisation with a complementary DNA because the adsorbed CTA^+ ion is easily desorbed from the interface by washing. Moreover, DNA molecule alone shows non-specific adsorption to the LC-water interface through the hydrophobic interactions between DNA and 5CB. It is also possible that the DNA molecules which are tightly packed with CTA^+ molecules in a

hexagonal structure[22] could not expose a DNA base structure to the aqueous phase to form a base pairing with a fluorescently tagged its complementary DNA. Leal *et al.* suggest a expected DNA-CTA structure that a central (near) cylindrical CTA (cetyltrimethylammonium) aggregate is surrounded by six DNA helices in the unit cell of the two-dimensional (2D) hexagonal structure shown in Figure 3.27 and the packing arrangement depends on the ratios of (DNA helices/CTA cylinder). [22]

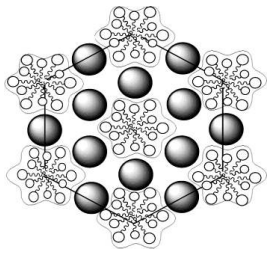

Figure 3.27: Schematic illustration of expected DNA-CTA packing for an electro-neutral complex consisting of a hexagonal arrangement of DNA helix (darker circles) around the central CTA distorted cylinder.[22]

However, this experimental system may prove very useful for studying the adsorption of DNA-cationic surfactant complex at the LC-water interface similar to ellipsometry. Using this system the structure of the adsorbed layer of DNA-cationic surfactant at the LC-water interface could be investigated depending on the DNA structure (e.g., single or double stranded) or molecular weight.

3.4 Adsorption of DNA-polymerisable cationic surfactant complex at the 5CB-water interface

3.4.1 Anchoring of 5CB by polymerisable cationic surfactants

The homeotropic anchoring of 5CB triggered by the adsorption of DNA-cationic surfactant complexes at the LC-water interface is reverted by washing with a salt solution (e.g., 10 mM NaBr). However, the DNA molecules sustained at the interface after exchanging the aqueous phases several times during the hybridisation reaction with its complementary DNA (e.g., washing step). Therefore, we considered a polymerisable cationic surfactant which can strongly adsorb at the interface as a carrier molecule instead of a normal cationic surfactant. Abbott *et al.* [23] established criteria for the surfactants that give rise to homeotropic anchoring of 5CB by comparing the influence of a series of surfactants. They proposed that interactions between the

aliphatic chains of the surfactant and 5CB, which are influenced by the conformations of the tails of the surfactants, largely dictate the orientation of the 5CB. Thus, we used two different cationic surfactants bearing a polymerisable methacrylate group in different positions and a primary hydrophobic chain length of 11 or more carbon atom (Figure 3.28). These polymerisable surfactants are expected to be difficult to desorb from at the LC-water interface because the cross-linked two-dimensional (2D) network is formed between surfactant molecules by polymerisation.[24]

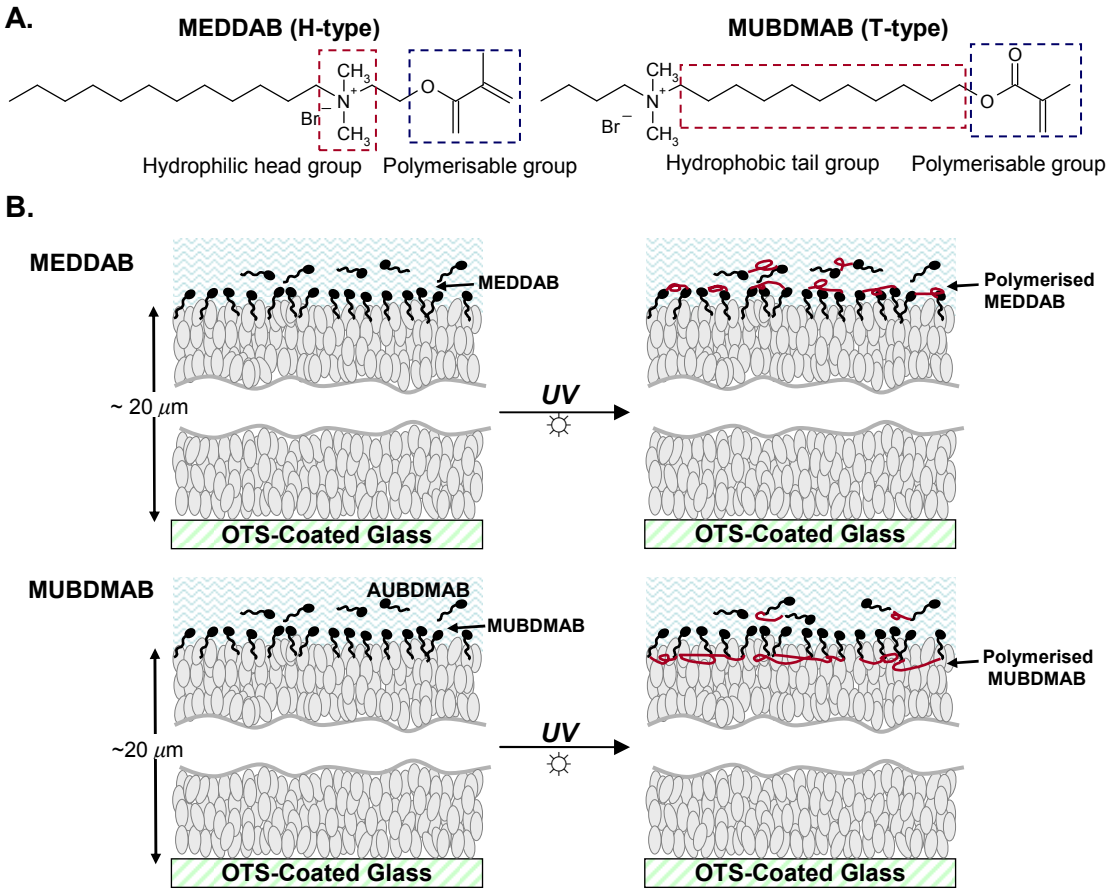

Figure 3.28: (A) Chemical structures of polymerisable cationic surfactant MEDDAB (H-type) and MUBDMAB (T-type). (B) Schematic representation of the adsorption of MEDDAB and MUBDMAB at the 5CB-water interface before and after UV polymerisation. Polymerised 2D network of MEDDAB could be formed in the aqueous phase otherwise that of MUBDMAB in the 5CB phase after UV irradiation.

Figure 3.29 shows the optical textures of 5CB when exposed to various concentrations of MEDDAB (H-type) and MUBDMAB (T-type) in pure water. An orientational change from planar to homeotropic anchoring of 5CB is observed in all cases.

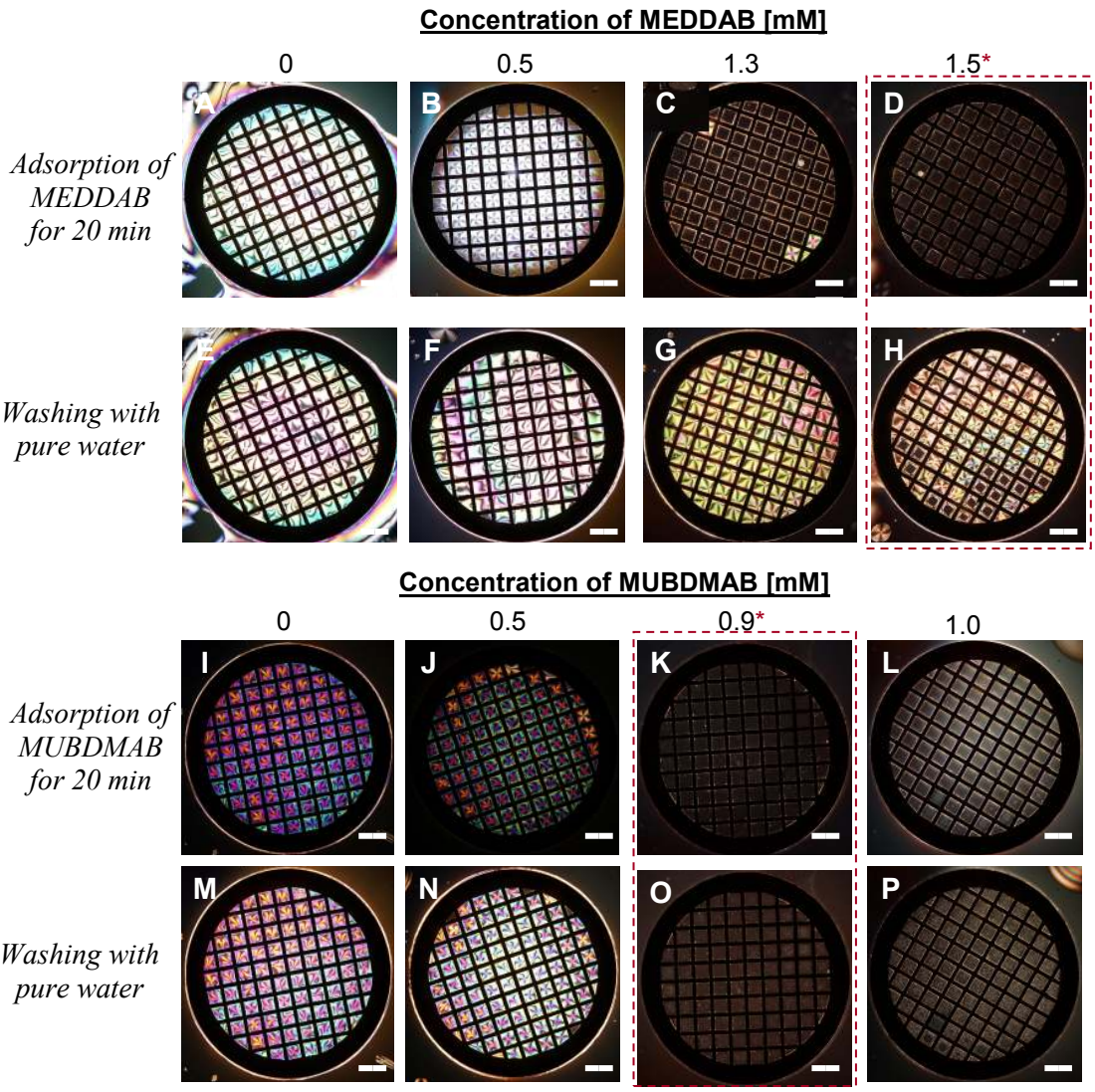

Figure 3.29: Optical images of 5CB between crossed polarisers of the LC cell (A-D) and (I-L) after incubation with MEDDAB and MUBDMAB aqueous solution for 20 min; (E-H) and (M-P) after washing with 6 perfusion chamber volumes of pure water. All scale bars represent 400 μm. Red dotted line shows a homeotropic transition point.

The concentrations over which all of the anchoring changes occurred (1.5 mM for MEDDAB, 0.9 mM for MUBDMAB) is explained by a combination of the high concentration of methacrylate groups in the interior of 5CB for the T-type surfactant, MUBDMAB and the electrostatic repulsion between adjacent head groups for the H-type surfactant, MEDDAB. For MEDDAB the triggered homeotropic anchoring of 5CB is reverted to planar (or possibly tilted) after washing with 6 perfusion chamber volumes of pure water. Meanwhile, MUBDMAB maintained the homeotropic anchoring of 5CB at the LC-water interface after rinsing with pure water several times via hydrophobic and electrostatic interactions with 5CB (Figure 3.29L and P). By comparing with the

anchoring change of 5CB by DTAB at 10 mM which has a C_{12} aliphatic chain, the results above suggest that MEDDAB with C_{12} aliphatic chain and MUBDMAB with C_{11} aliphatic chain are likely to have a higher surface excess concentrations and a higher penetration of 5CB into the surfactant monolayers by the methacrylate groups of these surfactants. Moreover, the aggregation behaviour of MEDDAB with the polymerisable moiety near to the ionic head group is more similar to that of the common *n*-alkyltrimethylammonium halide surfactants than the behaviour of MUBDMAB.

3.4.2 Adsorption of MUBDMAB and MEDDAB at the 5CB-water interfaces after UV polymerisation

Before UV polymerisation of MEDDAB and MUBDMAB adsorbed layer at the LC-water interface we examined UV polymerisation conditions (e.g., photoinitiator, UV source). Aqueous solution containing MUBDMAB and photoinitiator Darocur 1173 produced a yellowish thin polymerised film after UV irradiation as shown in Figure 3.30.

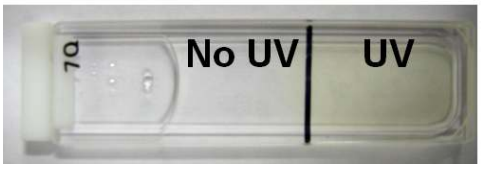

Figure 3.30: UV polymerisation of MUBDMAB. Aqueous solution of 1.2 mM MUBDMAB containing 0.2 vol% Darocur 1173 in UV spectrophotometer quartz cell was polymerised using UV SpotCure lamp (UVP) for 8 min at room temperature.

For the polymerisation of MUBDMAB we prepared a UV polymerisation cell which could not only reduce the effects of atmospheric oxygen on the polymerisation process but also efficiently produce polymerised surfactant network. An OTS-treated glass slide was used for the base of the cell coupled with a perfusion chamber. This could provide a reproducible method of preparing the polymerised network of polymerisable surfactants. As shown in Figure 3.31 a perfusion chamber absorbs a little of UV radiation emitted by the UV source, which is similar to a glass slide. The optical transmittance values of a perfusion chamber top cover (i.e. polycarbonate) at the main UV radiation wavelengths of the UV SpotCure lamp are ~0.08% at 254 nm, ~60% at 310 nm, ~84% at 360 nm, and 85% at 365 nm. Therefore, the perfusion chamber was used in the UV polymerisation cell without any modification.

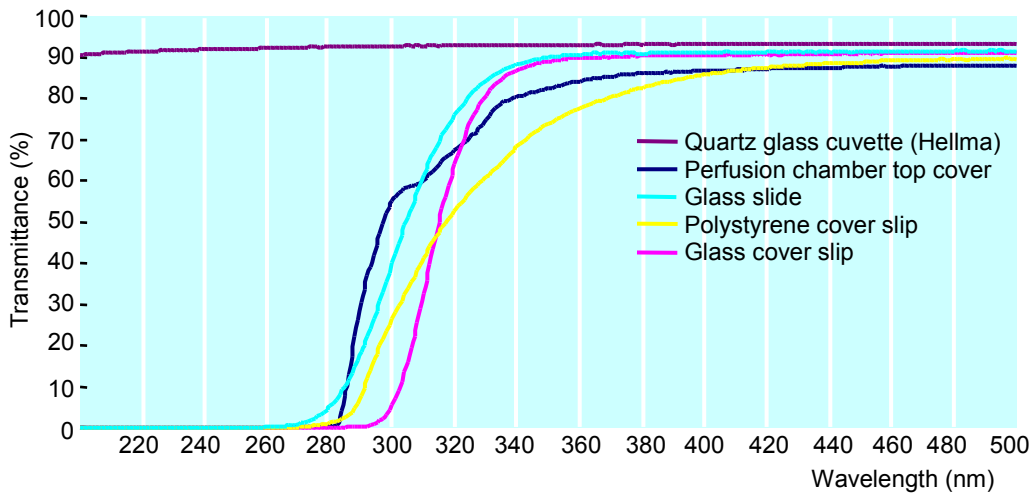

Figure 3.31: Light transmittance of various substrates for a UV polymerisation cell from 200 to 500 nm. Baselines were measured against air at room temperature.

We observed the effect of UV polymerisation of MUBDMAB adsorbed layer at the LC-water interface on the alignment of 5CB. Firstly, we prepared MUBDMAB monolayer at the LC-water interface by adsorption of MUBDMAB followed by removing excess of MUBDMAB in a perfusion chamber with washing. UV polymerisation of the MUBDMAB adsorbed monolayer at the interface changed the alignment of 5CB from homeotropic to planar anchoring (Figure 3.32M and N) compared with the case where no UV radiation was supplied (Figure 3.32L). A partial homeotropic anchoring of 5CB in Figure 3.32I and 3.32J is from the interaction between 5CB and Darocur 1173 at the LC-water interface but it was easily removed after washing with pure water. This partial homeotropic anchoring of 5CB is likely to occur by the partial quenching of the photo-initiators during UV irradiation. However, how polymerised MUBDMAB causes this transition of anchoring of 5CB is not clear yet. We assumed that desorption of polymerised MUBDMAB from the LC-water interface or the change of the interaction between the 5CB and polymerised MUBDMAB could make this transition of anchoring of 5CB.

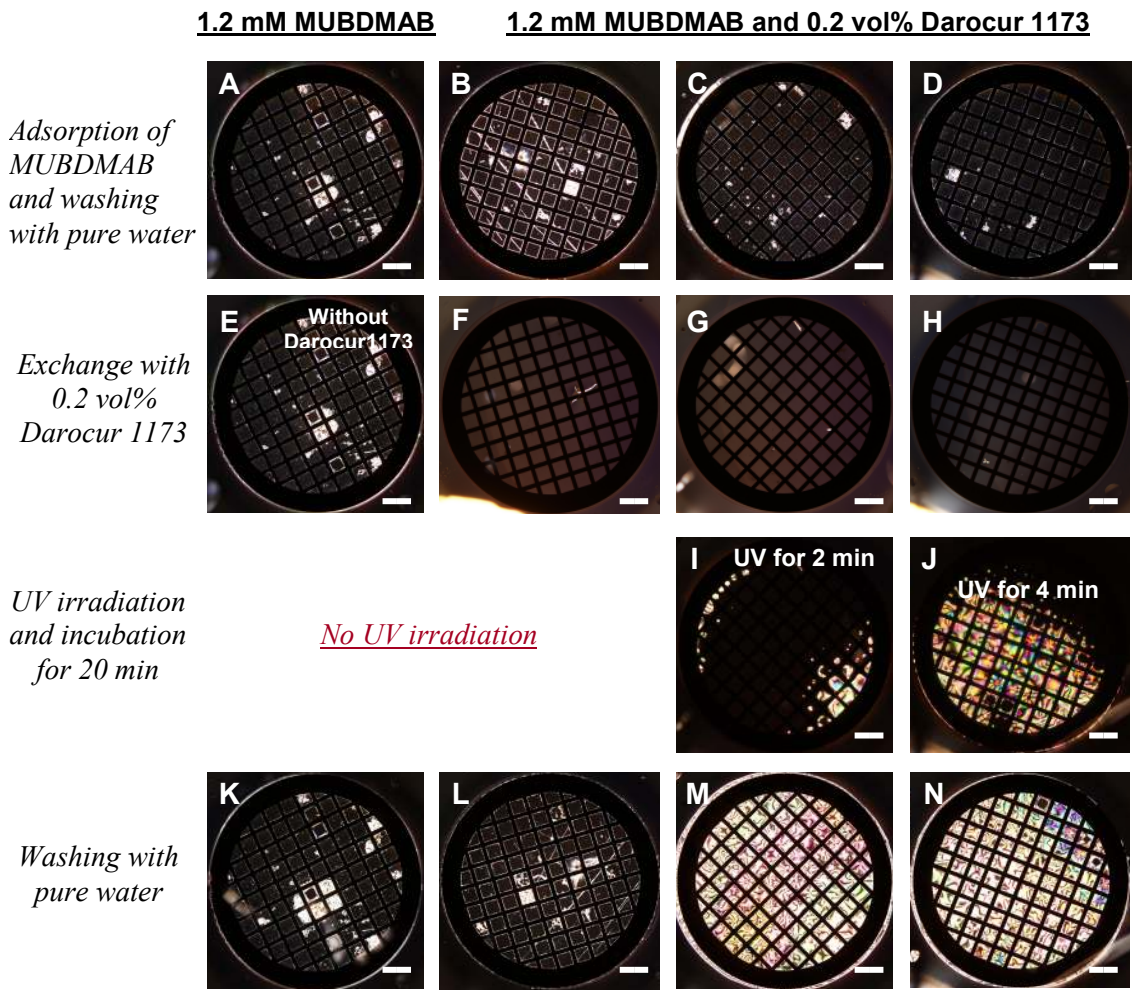

Figure 3.32: UV polymerisation triggered transition of anchoring of 5CB. Optical images of 5CB between crossed polarisers contacted with aqueous solution of 1.2 mM MUBDMAB and 0.2 vol% Darocur 1173, and irradiated using SpotCure lamp (UVP) according to the UV irradiation time. The LC cells were washed with 8 perfusion chamber volumes of pure water. All scale bars represent 400 μm.

To exclude the side effect of Darocur 1173 and UV light on the anchoring of 5CB in the above results, the influence of Darocur 1173 and UV light on the anchoring of 5CB at the LC-water interface was also investigated (Figure 3.33). Darocur 1173 on its own did induce a transition from planar to homeotropic anchoring of 5CB at 0.2 vol% concentration in aqueous solution (Figure 3.33C). However, this triggered transition was easily reverted to planar anchoring by washing with 8 chamber volumes of water (Figure 3.33I) similar to the Figure 3.32. Moreover, using only Darocur 1173 cannot change the optical texture of 5CB after UV irradiation (Figure 3.33F). UV radiation cannot produce any change of the LC optical textures in the absence of added surfactants (Figure 3.33E).

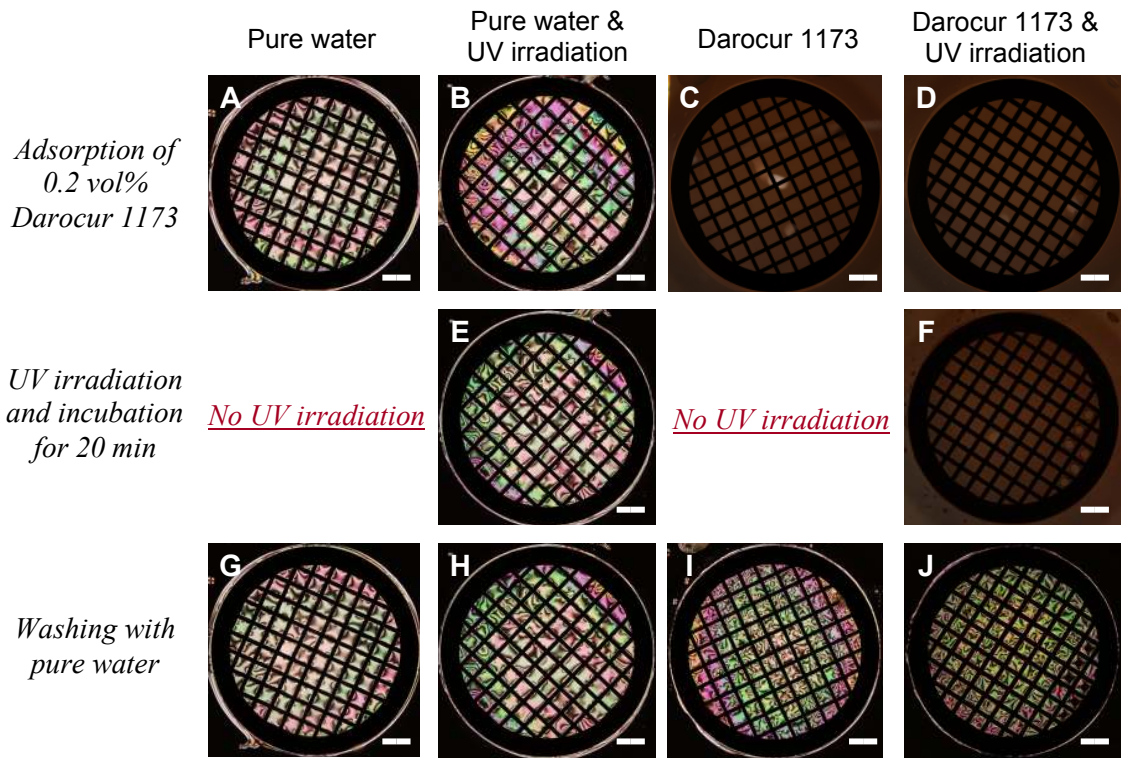

Figure 3.33: Optical images of 5CB between crossed polarisers after incubation with (A and B) pure water and (C and D) 0.2 vol% Darocur 1173 in pure water and irradiated using SpotCure (UVP) lamp for 2 min. All scale bars represent 400 μm.

In contrast, UV polymerisation of MEDDAB in which the polymerisable group is located in the head group region of the surfactant does not cause the transition of the LC texture. In order to exclude the possibility that the lack of optical transition might be a result of non-polymerisation of MEDDAB molecules, it was checked, using similar condition to Figure 3.30, that a bulk MEDDAB solution was polymerised by UV irradiation.

3.4.3 Anchoring of 5CB by DNA-polymerisable cationic surfactant complex

The interaction between DNA and polymerisable cationic surfactants, MEDDAB and MUBDMAB were investigated by the observation of the transition of alignment of 5CB and the adsorption of florescent DNA. Special attention was paid to the amount of desorption of the DNA-polymerisable cationic surfactant adsorbed layer from the LC-aqueous interface by washing with pure water. In this study, the concentrations of MUBDMAB and MEDDAB were fixed at 1.2 mM and 1.6 mM respectively over which

all of the anchoring transitions occurred. Then, surfactants were mixed with TAMRA-DNA (5`-GGCCAGTCACTG-3´-TAMRA) at the charge concentration mixing ratio R ≈ 12 because the precipitation of DNA-DTAB complexes reach the maximum amount near the charge neutralization and remains constant on the variation of R.[25] In Figure 3.34B, simultaneous addition of a premixed 10 μM DNA and 1.2 mM MUBDMAB could not make a homeotropic anchoring of 5CB unlike 1.2 mM MUBDMAB in the absence of DNA (Figure 3.34A) although some squares of the EM grid changed to the homeotropic anchoring after washing with pure water.

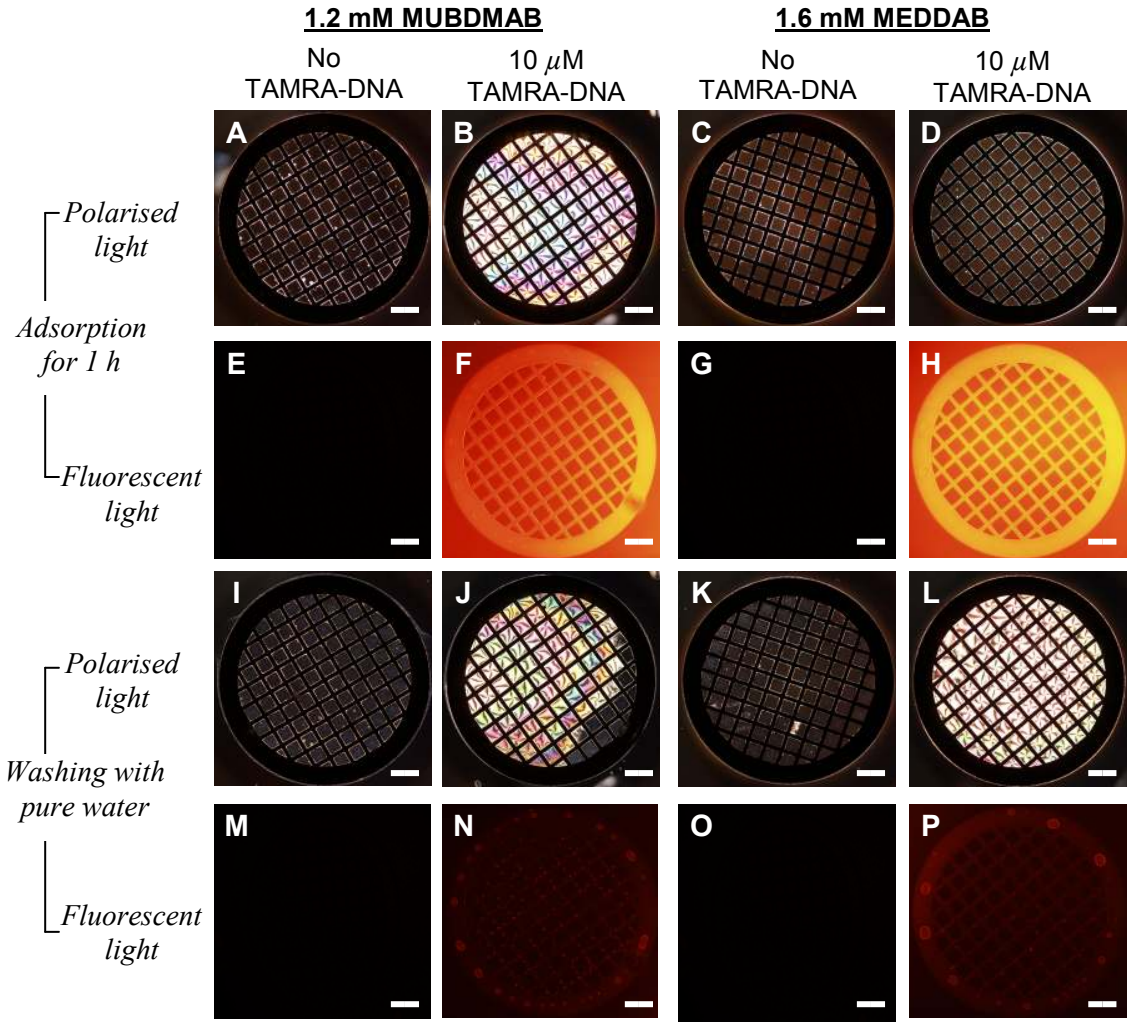

Figure 3.34: Optical images of 5CB between crossed polarisers contacted with aqueous solutions of (A) 1.2 mM MUBDMAB, (B) 1.2 mM MUBDMAB and 10 μM TAMRA-DNA (5´-GGCCAGTCACTG-3´-TAMRA), (C) 1.6 mM MEDDAB and (D) 1.6 mM MEDDAB and 10 μM TAMRA-DNA (5´-GGCCAGTCACTG-3´-TAMRA) in 1 mM NaBr. Fluorescence microscopy imaging was performed using tetramethylrhodamine isothiocynate (TRITC) filter. The perfusion chambers were washed with 8 perfusion chamber volumes of pure water. All scale bars represent 400 μm.

However, DNA-MEDDAB mixture produced a homeotropic anchoring of 5CB (Figure 3.34D), which was reverted back to a planar after washing with pure water (Figure 3.34L). MUBDAMB and MEDDAB are likely to make different types of complexes with DNA which show different adsorption behaviours at the LC-water interface. DNA-MEDDAB complex shows a similar behaviour with the adsorption of DNA-CTAB complex mentioned in the section 3.3.3. Moreover, DNA or DNA-polymerisable cationic surfactant complex preferentially adsorb at the metal surface of EM grids rather than the LC-water interface (Figure 3.34N and P).

The addition of DNA followed by the adsorption of MUBDMAB did not change the homeotropic anchoring of 5CB to planar (Figure 3.35C) unlike simultaneous addition of DNA and MUBDMAB (Figure 3.34B).

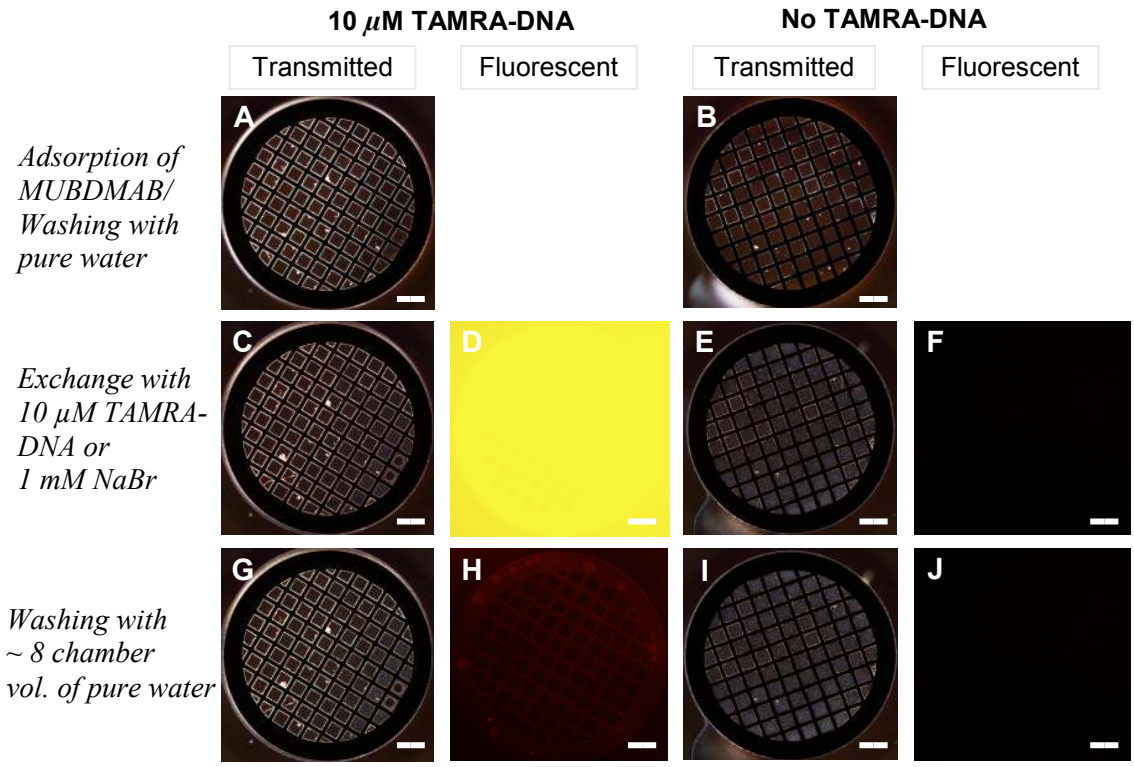

Figure 3.35: Optical images of 5CB between crossed polarisers contacted with aqueous solutions of 1.2 mM MUBDMAB and 10 μM TAMRA-DNA (5′-GGCCAGTCACTG-3′-TAMRA) in 1 mM NaBr by a serial addition. Optical examination was performed using tetramethylrhodamine isothiocynate (TRITC) filter for fluorescent images. All scale bars represent 400 μm.

However, DNA also did not form a complex with the MUBDMAB adsorbed layer at the LC-water interface (Figure 3.35H). Therefore, we conclude that DNA cannot adsorb

significantly enough on the MUBDMAB monolayer to change the anchoring of 5CB at the LC-water interface. It is also possible that DNA needs longer incubation time to form surface complex with MUBDMAB. In previous studies,[26,27] the equilibration time to make DNA-cationic surfactant complex is different ranging from 2 h to several days depending on the number of base pairs and the concentration of DNA. Additionally, from the above results, the addition order of DNA and surfactant (e.g., MUBDMAB) at the LC-water interface is also important to produce a mixed DNA-surfactant adsorbed layer at the LC-water interface.

3.4.4 Effect of UV polymerisation of mixed DNA-MEDDAB adsorbed layer at the LC-water interface

We further examined whether UV polymerisation of MEDDAB can prevent the desorption of mixed DNA-MEDDAB adsorbed layer from the LC-water interface as shown in Figure 3.34L as follows;

1) Simultaneous addition of MEDDAB and DNA at the LC-water interface.
2) UV irradiation for the polymerisation of MEDDAB of the mixed DNA-MEDDAB adsorbed layer at the LC-water interface.

The homeotropic alignment of 5CB was not changed by polymerisation of the mixed DNA-MEDDAB adsorbed layer (Figure 3.36B, C and D) similar to the non-polymerisation condition (Figure 3.36A). Moreover, the mixed DNA-MEDDAB adsorbed layer is likely to be desorbed from the LC-water interface in spite of UV polymerisation. After UV irradiation, the aqueous phase containing MEDDAB and DNA changed to a yellowish turbid solution which was easily removed by washing with pure water (data not shown). This suggests that DNA does not form enough surface complexes with the polymerised MEDDAB monolayer to change the anchoring of 5CB at the LC-water interface. Moreover, the alignment of 5CB was easily changed from homeotropic to planar anchoring and DNA was desorbed from the LC-water interface by washing with pure water. MEDDAB free-DNA or DNA-MEDDAB complexes slightly adsorb at the surface of metal EM grids. This suggests that water insoluble DNA-MEDDAB complexes are likely to be liberated from the LC-water interface rather than to remain at the interface similar to the adsorption and desorption of DNA-MUBDMAB complexes (Figure 3.35).

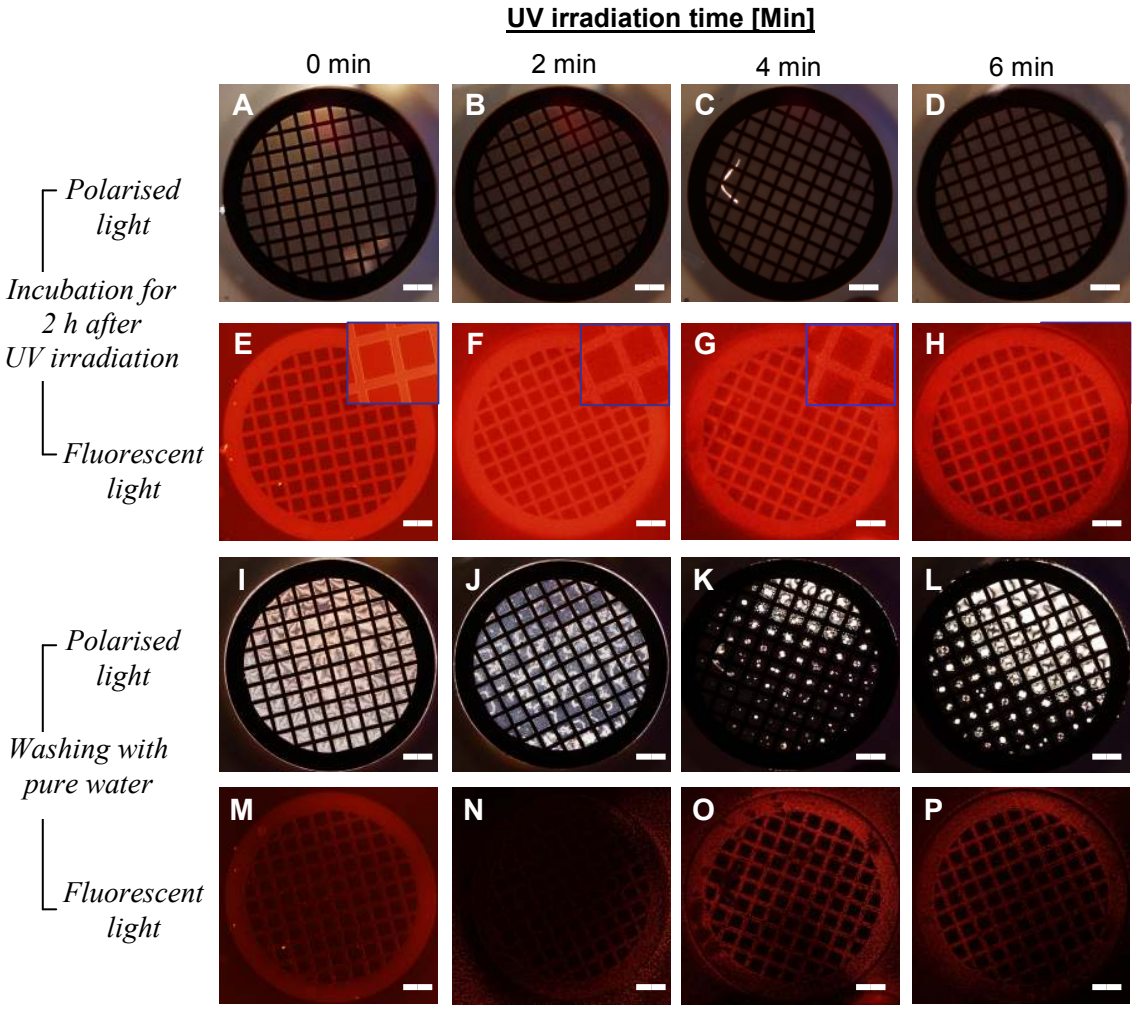

Figure 3.36: Optical images of 5CB after UV irradiation using SpotCure (UVP) lamp after contacted with 1.6 mM MEDDAB, 10 μM TAMRA-DNA (5′-GGCCAGTCACT G-3′-TAMRA) and 0.5 vol% Darocur 1173 in 1 mM NaBr according to the UV irradiation time. Optical microscopy was performed using crossed polarisers (A-D and I-L) and tetramethylrhodamine isothiocynate (TRITC) filter (E-H and M-P). The insects show the magnified images of E-H using a 50× objective. Each perfusion chamber was washed with 8 perfusion chamber volumes of pure water. All scale bars represent 400 μm.

3.5 Conclusions

In this chapter, we describe our attempt to produce a biosensor for DNA based on imaging of the adsorption of DNA moiety at the LC-water interface.

The main conclusions from this chapter are:

- The modified experimental system for imaging the adsorption of surfactants at the LC-water interface reproduces the direct detection of the interaction of LC with the adsorbed surfactant layer without the any other instruments.
- By performing a study of the anchoring of 5CB in contact with aqueous phase containing DNA-surfactants that possess different molecular architecture (e.g., DNA oligomer and a hydrophobic tail chain), DNA-surfactants do not cause a homeotropic anchoring of 5CB at any bulk concentrations of surfactants even at a high ionic strength.
- We conclude that the interaction between the hydrophobic moiety of the adsorbed DNA-surfactants and LC are not enough to change the alignment of LC. The results underlie the proposition that a combination of highly charged bulky head-groups of DNA-surfactant and a predicted looped configuration of $(C_{12}O)_n$ modified DNA-surfactant at the LC-water interface could not produce a sufficiently dense monolayer at the LC-water interface to change the orientation of 5CB.
- We studied the DNA-cationic surfactant mixed system to transit the planar anchoring of 5CB to homeotropic. The adsorption of cationic surfactants with a sufficient hydrophobic chain length (> C_{12} alkyl chain) changes the anchoring of 5CB from planar to homeotropic below their cmc. Surfactant-free DNA strongly adsorbs not only at the LC-water interface but also to hydrophobic OTS coated glass surface and the adsorbed DNA layer does not desorb from the interface after washing with a salt solution.
- Co-adsorption of cationic surfactants with DNA increases the adsorbed amount of DNA at the LC-water interface and leads to the transition of anchoring of LC depending on the mixing ratio of DNA and surfactant. Rinsing with a salt solution induce desorption of the cationic surfactant, leaving DNA layer at the LC-water interface.

- DNA-polymerisable cationic surfactant mixed system showed a similar behaviour to the DNA-cationic surfactant system. The adsorption of polymerisable cationic surfactants with a sufficient hydrophobic chain length (> C_{11} alkyl chain) triggers a transition from planar to homeotropic anchoring of 5CB. However, the triggered homeotropic anchoring by a polymerisable surfactant with a polymerisable group in the tail region is not reverted after washing with pure water in contrast with previously studied convenient surfactants (e.g., SDS and CTAB).
- UV polymerisation within the hydrophobic region of an adsorbed MUBDMAB layer triggers a change from homeotropic to planar anchoring otherwise the polymerisation within the hydrophilic region cannot do. However, DNA-polymerisable cationic surfactant mixed system showed desorption behaviour of adsorbed surfactant layer after washing with a salt solution with or without UV polymerisation, which is similar to DNA-cationic surfactant mixed system.
- Finally, these experimental systems could be useful to study DNA-cationic surfactant interactions for different structure DNA or differently mixed surfactants at the LC-water interface without any special technique (e.g., ellipsometry, differential scanning calorimetry etc.).

Recently, Price and Schwartz reported DNA hybridisation-induced reorientation of LC alignment at the LC-water interface.[7] They used octadecyltrimethylammonium-bromide (OTAB) and a nematic liquid crystal E7 (Merck Ltd.) which is a four-component LC mixture of cyanobiphenyls and a cyanoterphenyl instead of 5CB.[28] The main difference of their method from our approach is that OTAB is dissolved in the LC phase not in the aqueous phase to prevent desorption of OTAB from the interface by further exchanging with aqueous phases. Subsequent adsorption of single strand DNA to the surfactant-laden interface modified the interfacial structure, resulting in a transition of the LC from homeotropic to an intermediate tilted alignment. The hybridisation of complementary target ssDNA to the ssDNA/surfactant interfacial complex resulted in reverting to homeotropic LC alignment. The sensitivity of the LC anchoring to the interfacial structure allowed the detection of a one-base-pair mismatch between the probe and target with a lower limit of ~50 fmol.

3.6 References

1. V. K. Gupta and N. L. Abbott, "Design of surfaces for patterned alignment of liquid crystals on planar and curved substrates", *Science*, **1997***, 276*, 1533-1536.
2. V. K. Gupta, J. J. Skaife, T. B. Dubrovsky and N. L. Abbott, "Optical amplification of ligand-receptor binding using liquid crystals", *Science* **1998**, *279*, 2077-2080.
3. J. M. Brake and N. L. Abbott, "An experimental system for imaging the reversible adsorption of amphiphiles at aqueous-liquid crystal interfaces", *Langmuir* **2002**, *18*, 6101-6109.
4. J. M. Brake, A. D. Mezera, and N. L. Abbott, "Effect of surfactant structure on the orientation of liquid crystals at aqueous-liquid crystal interfaces", *Langmuir* **2003**, *19*, 6436-6442.
5. J. Hoogboom, K. Velonia, T. Rasing, A. E. Rowan and R. J. M. Nolte, "LCD-based detection of enzymatic action", *Chem. Commun.* **2006**, 434-435.
6. N. A. Lockwood, J. K. Gupta and N. L. Abbott, "Self-assembly of amphiphiles, polymers and proteins at interfaces between thermotropic liquid crystals and aqueous phases", *Surf. Sci. Rep.* **2008**, *63*, 255-293.
7. A. D. Price and D. K. Schwartz, "DNA hybridisation-induced reorientation of liquid crystal anchoring at the nematic liquid crystal/aqueous interface", *J. Am. Chem. Soc.* **2008**, *130*, 8188-8194.
8. L. A. Chrisey, C. E. O'Ferrall, B. J. Spargo, C. S. Dulcey and J. M. Calvert, "Fabrication of patterned DNA surfaces", *Nucleic Acids Res.* **1996**, *24*, 3040-3047.
9. C. Xu, P. Taylor, P. D. I. Fletcher and V. N. Paunov, "Adsorption and hybridisation of DNA-surfactants at fluid surfaces and liquid bilayers", *J. Mater. Chem.* **2005**, *15*, 394-402.
10. C. Xu, P. Taylor, M. Ersoz, P. D. I. Fletcher and V. N. Paunov, "Microcontact printing of DNA-surfactant arrays on solid substrates", *J. Mater. Chem.* **2003**, *13*, 3044-3048.
11. P. Taylor, **2005** *Self-recognizing surfaces using DNA surfactant* (PhD thesis) University of Hull.
12. J. M. Brake, A. D. Mezera and N. L. Abbott, "Active control of the anchoring of 4´-pentyl-4-cyanobiphenyl (5CB) at an aqueous-liquid crustal interface by suing a redox-active ferrocenyl surfactant", *Langmuir* **2003**, *19*, 8629-8637.

13. K. Eskilsson, C. Leal, B. Lindman, M. Miguel and T. Nylander, "DNA-surfactant complexes at solid surfaces", *Langmuir* **2001**, *17*, 1666-1669.
14. I. S. Kikuchi and A. M. Carmona-Ribeiro, "Interaction between DNA and synthetic cationic liposomes", *J. Phys. Chem. B* **2000**, *104*, 2829-2835.
15. K. Wagner, D. Harries, S. May, V. Kahl, J. O. Rädler and A. Ben-Shaul, "Direct evidence for counterion release upon cationic lipid-DNA condensation", *Langmuir* **2000**, *16*, 303-306.
16. A. V. Gorelov, E. D. Kudryashov, J-C. Jacquier, D. M. McLoughlin and K. A. Dawson, "Complex formation between DNA and cationic surfactant2, *Physica A* **1998**, *249*, 216-225.
17. M. Cárdenas, A. Braem, T. Nylander and B. Lindman, "DNA compaction at hydrophobic surfaces induced by a cationic amphiphile", *Langmuir* **2003**, 19, 7712-7718.
18. B. S. Gallardo, K. L. Metcalfe and N. L. Abbott, "Ferrocenyl surfactants at the surface of water: Principles for active control of interfacial properties", *Langmuir* **1996**, *12*, 4116-4124.
19. A. Jada, J. Lang, S-J. Candau and R. Zana, "Structure and dynamics of water-in-oil microemulsions", *Colloids Surf.* **1989**, *38*, 251-261.
20. S. Mel'nikov, V. Sergeyev and K. Yoshikawa, "Discrete coil-globule transition of large DNA induced by cationic surfactant", *J. Am. Chem. Soc*. **1995**, *117*, 2401-2408.
21. W. M. Gilbert, R. F. Bruinsma, P. A. Pincus, V. A. Parsegian, "DNA-inspired electrostatics", *Phys. Today* 2000, *53(9)*, 38-44.
22. C. Leal, L. Wadso, G. Olofsson, M. Miguel and H. Wennerström, "The hydration of a DNA-amphiphile complex", *J. Phys. Chem. B* **2004**, *108*, 3044-3050.
23. N. A. Lockwood and N. L. Abbott, "Self-assembly of surfactants and phospholipids at interfaces between aqueous phases and thermotropic liquid crystals", *Current Opinion in Colloid & Science* **2005**, *10*, 111-120.
24. A. Guyot, "Advances in reactive surfactants", *Adv. Coll. Int. Sci.* **2004**, *108-109*, 3-22.
25. R. Dias, S. Mel'nikov, V. Sergeyev, B. Lindman and M. G. Miguel, "DNA phase behaviour in the presence of oppositely charged surfactants", *Langmuir* **2000**, *16*, 9577-9583.

26. R. Dias, B. Lindman and M. G. Miguel, “DNA interaction with cationic vesicles”, *J. Phys. Chem.* B **2002**, *106*, 12600-12607.
27. M. Cardenas, T. Nylander, R. K. Thomas and B. Lindman, “DNA compaction onto hydrophobic surfaces by different cationic surfactants”, *Langmuir* **2005**, *21*, 6495-6502.
28. L. Bedjaoui, N. Gogibus, B. Ewen, T. Pakula, X. Coqueret, M. Benmouna and U. Maschke, “Preferential salvation of the eutectic mixture of liquid crystals E7 in a polysiloxane”, *Polymer* **2004**, *45*, 6555-6560.

Chapter 4

UV Sensors Based on the Polymerisable Surfactants Adsorption at the 5CB-Water Interface

Chapter 4

UV Sensors Based on the Polymerisable Surfactants Adsorption at the 5CB-Water Interface

In the chapter 3, we observed the transition of anchoring of 5CB by adsorption (homeotropic anchoring) of 11-(methacryloyloxy)undecylbutyldimethylammonium bromide (MUBDMAB) from an aqueous phase at the LC-water interface and UV polymerisation (planar anchoring) of interface bound layers at the interface. In this chapter we report the alignment changes of 5CB between crossed polarisers produced by adsorption and UV polymerisation of a range of polymerisable surfactants at the LC water interface at different pH and temperature conditions and finally suggest a possible application of these systems to simply sense the daily UV radiation.

4.1 Introduction

The radiation from the sun is essential for life on earth. Included within this radiation is ultraviolet (UV), which in small amounts is beneficial in human (e.g., vitamin D3 production) whereas causes skin cancers, cataracts, and other damaging effects to eyes are caused by prolonged exposure. In this section we briefly describe the background information about UV radiation, its effects and the global solar UV index (UVI).

4.1.1. Ultraviolet (UV) radiation

4.1.1.1 UV spectrum

UV radiation is part of the electromagnetic spectrum between x rays and visible light, i.e., with wavelengths between 40 and 400 nm (30–3 eV). There are several named regions of the UV spectrum corresponding to different wavelengths of the electromagnetic waves. Some of the regions overlap. Short wavelengths correspond to higher frequencies and higher energies, while longer waves oscillate at lower frequencies and carry less energy. Visible light and the start of the infrared (IR) spectrum are shown for comparison in Figure 4.1. The UV spectrum is divided into Vacuum UV (40–190 nm), Far UV (190–220 nm), UVC (220–290 nm), UVB (290–

320), and UVA (320–400 nm) (Figure 4.1).[1] Whereas wavelengths of 100–280 nm emited by the sun are absorbed by the atmospheric ozone, most radiation in the UVA range (315–400 nm) and about 10 % of the UVB rays (280–315 nm) reach the Earth's surface. Both UVA and UVB are of major importance to human health.

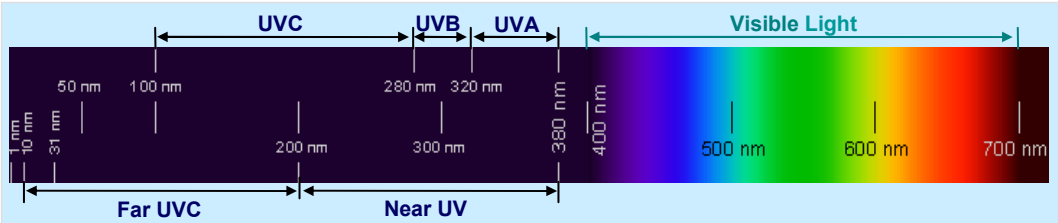

Figure 4.1: Ultraviolet (UV) electromagnetic spectrum.[2]

UVC is almost never observed in nature because it is absorbed completely in the atmosphere, as are Far UV and Vacuum UV. Germicidal lamps are designed to emit UVC radiation because of its ability to kill bacteria. In humans, UVC is absorbed in the outer dead layers of the epidermis. Accidental over-irradiation to UVC can cause corneal burns, commonly termed welders' flash, and snow blindness, a severe sunburn to the face. While UVC injury usually clears up in a day or two, it can be extremely painful.

UVB is typically the most destructive form of UV radiation because it has enough energy to cause photochemical damage to cellular DNA, yet not enough to be completely absorbed by the atmosphere. UVB is needed by humans for synthesis of vitamin D; however, harmful effects can include erythema (sunburn), cataracts, and development of skin cancer. Individuals working outdoors are at the greatest risk of UVB effects. Most solar UVB is blocked by ozone in the atmosphere, and there is concern that reductions in atmospheric ozone could increase the prevalence of skin cancer.

UVA is the most commonly encountered type of UV light. UVA radiation has an initial pigment-darkening effect (tanning) followed by erythema if the radiation exposure is excessive. Atmospheric ozone absorbs very little of this part of the UV spectrum. UVA is needed by humans for synthesis of vitamin D; however, over-exposure to UVA has been associated with toughening of the skin, suppression of the immune system, and cataract formation. UVA light is often called black light. Most phototherapy and tanning booths use UVA lamps.

4.1.1.2 Safety aspects of UV light

The sun is our primary natural source of UV radiation. Artificial sources include tanning booths, black lights, curing lamps, germicidal lamps, mercury vapor lamps, halogen lights, high-intensity discharge lamps, fluorescent and incandescent sources, and some types of lasers (excimer lasers, nitrogen lasers, and third harmonic Nd:YAG lasers). Unique hazards apply to the different source depending on the wavelength range and intensity of the emitted UV radiation.

The photochemical effects of UV radiation can be exacerbated by chemical agents including birth control pills, tetracycline, sulphathizole, cyclamates, antidepressants, coal tar distillates found in antidandruff shampoos, lime oil, and some cosmetics.[3] Protection from UV is provided by clothing, polycarbonate, glass, acrylics, and plastic diffusers used in office lighting. Sun-blocking lotions offer limited protection against UV radiation. Accidental UV over-irradiation can injure unaware victims due to the fact UV is invisible and does not produce an immediate reaction. Labeling on UV sources usually consists of a caution or warning label on the product or the bulb packaging cover or a warning sign on the entryway. Some type of emission indicator as required with laser products is rarely found. Reported UV accident scenarios often involve work near UV sources with protective coverings removed, cracked, or fallen off. Depending on the intensity of the UV source and length of radiation, an accident victim may end up with a lost-time injury even though totally unaware of the hazardous condition. Hazard communication training is especially important to help prevent accidental radiations in the workplace.

4.1.1.3 UV Index

UV index is a unit of measure of UV levels relevant to the effects on human skin (UV induced erythema). It is recommended as a parameter to raise the public awareness about the potential detrimental effects on health from solar UV exposure and to alert people of the need to adopt protective measures. It is expressed numerically as the equivalent of the wavelength-averaged irradiance (blue and red lines in Figure 4.2A) multiplied by the erythema action spectrum (grey line in Figure 4.2A) (W/m^2) by 40.[4]

It is also computed as[5]

$$UVI = (40m^2W^{-1})\int B(\lambda)I(\lambda)d\lambda \qquad [1]$$

where $I(\lambda)$ is the solar spectral irradiance (W/m^2nm^1) at the Earth's surface, $B(\lambda)$ is the McKinlay and Diffey action spectrum[6] for erythema induction in humans, and λ is wavelength (nm). The values of $I(\lambda)$ at depends mainly on location and time (particularly sun angle) and on the composition of the atmosphere (e.g., vertical profiles of ozone (O_3), pollutant and clouds).

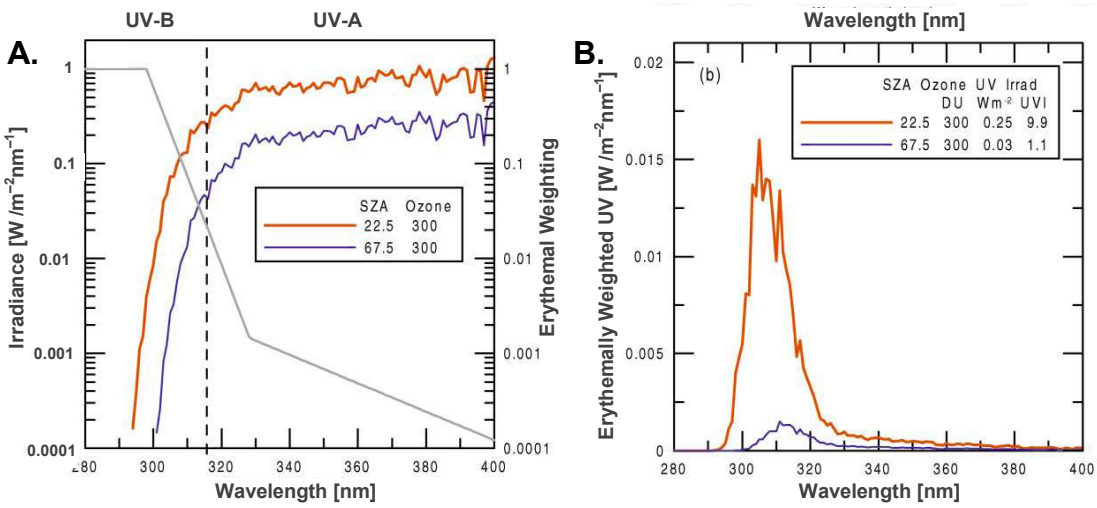

Figure 4.2: (A) Calculated spectra (1 nm resolution) and the erythemal weighting function plotted using a logarithmic *y*-axis for two solar zenith angle (SZA) and two ozone amounts (Dobson unit). (B) Erythemally weighted UV and UV index for these conditions.

For example, an erythemally weighted radiation of 0.2 W/m^2 corresponds to a UV Index of 8.0. Recently, operational UV Index forecasting has already been implemented in many countries. It would also allow more effective use of the UVI as an educational tool if standardised protective messages were associated with each range. Suggestions for category labels to standardise the UV index ranges are given in Table 4.1.[7]

Table 4.1: Suggestion of a universal set of category labels for the UV index[7]

Category label	UV index range
low	« 2
moderate	3 to 4
high	5 to 6
very High	7 to 8
extreme	above 9

In this chapter we investigated the effect of hydrophobic alkyl chain length and the position of a polymerisable group in the surfactant on the transition of alignment of 5CB induced by the adsorption of various polymerisable surfactants. Additionally, the optical transition reversals from homeotropic to planar anchoring caused by UV irradiation were also examined depending on various experimental conditions (e.g., UV exposure time, UV wavelength, and the surfactant structure etc.). Finally, we studied how these experimental systems can be used from the basis of a UV sensor which helps people to effectively protect themselves from solar UV radiation at various conditions (e.g., in the mountains in cold winter and on a beach in hot summer).

4.2 Influence of the molecular structure of polymerisable surfactants on the orientation of 5CB at the LC-water interface

In the section 3.4.1, we observed the 5CB alignment resulting from adsorption of the different polymerisable cationic surfactants (2-(methacryloyloxy)ethyl)dodecyl dimethylammonium bromide (MEDDAB) and 11-(methacryloyloxy)undecylbutyl dimethylammonium bromide (MUBDMAB) at the LC-water interface and the extent to which this was reversible by the flushing the perfusion chamber with pure water.

Figure 4.3 shows an illustrative set of the structures of two polymerisable surfactants MEDDAB and MUBDMAB and optical transition of 5CB from planar to homeotropic anchoring by their adsorption at the LC-water interface. For MUBDMAB, the homeotropic anchoring induced by the adsorption of MUBDMAB is not reverted after washing with 6 perfusion chamber volumes of pure water in contrast to the adsorption of SDS and CTAB at the LC-water interface in the chapter 3. However, for MEDDAB, the same washing condition causes almost complete reversal of the texture transition back to planar (or possibly tilted) similar to the adsorption of SDS and CTAB. However, the adsorbed MEDDAB monolayer was not desorbed by washing from the LC-water interface after incubation for > 1 h. We propose that the stable formation of a MEDDAB monolayer at the LC-water interface might need a longer incubation time (> 1 h) than that of MUBDMAB (20 min).

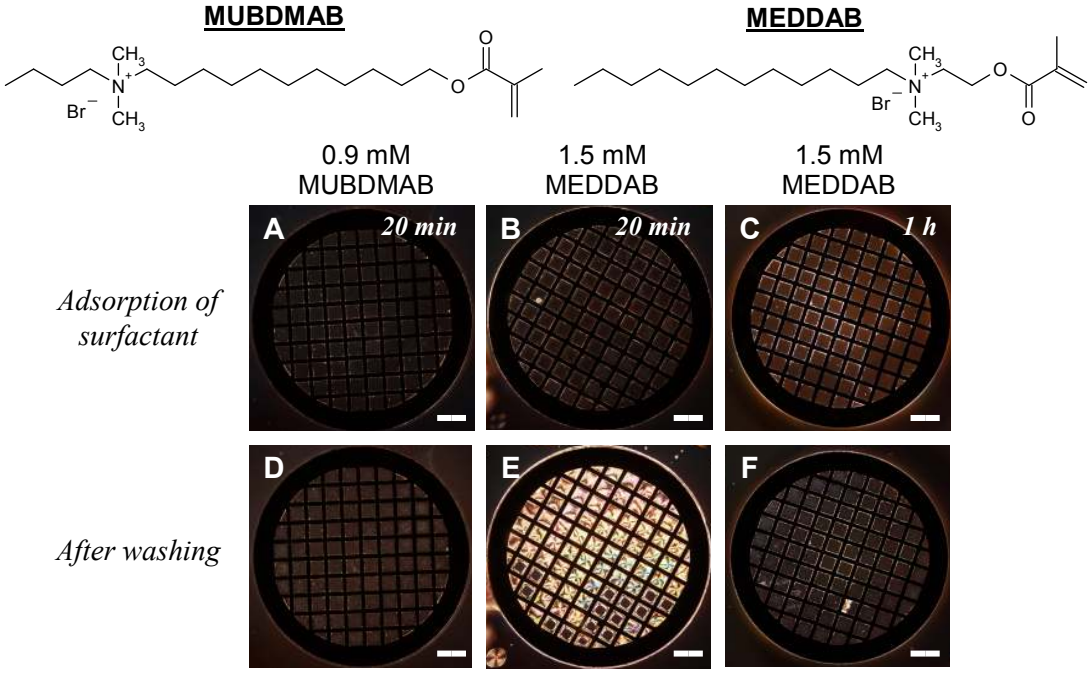

Figure 4.3: Influence of the position of a polymerisable group in the polymerisable surfactants on the anchoring of 5CB. Optical images of 5CB between crossed polarisers after incubation with 1.5 mM MEDDAB and 0.9 mM MUBDMAB solution in pure water (pH ~5.5). After the adsorption of surfactants the perfusion chambers were washed with 6 perfusion chamber volumes of pure water. All scale bars represent 400 μm.

We further examined the alignment of 5CB by the adsorption of other polymerisable surfactants including non-ionic and anionic polymerisable surfactants. Non-ionic polymerisable surfactant Noigen RN (Polyoxyethylene alkylphenyl ether) and anionic polymerisable surfactant Hitenol BC (Polyoxyethylene alkylphenyl ether ammonium sulphate) that contain a reactive propenyl group are generally used to improve the performance of conventional surfactants in emulsion polymers.[8] Therefore, these surfactants were considered as a substitute for MUBDMAB which is specially synthesised by Avecia Ltd. (Manchester, UK) and so is not commercially available.

The alignment of 5CB in contact with aqueous solutions of Noigen RN 10, 20 and Hitenol BC 10, 20 were determined (Figure 4.4). These surfactants with short alkyl chains (primary C_9 alkyl chain length) caused the orientation of 5CB to remain parallel to the interface up to concentrations at 100 mM of Hitenol BC and at which the 5CB began to be solubilised by the surfactant (e.g., 1 mM for Noigen RN 10).

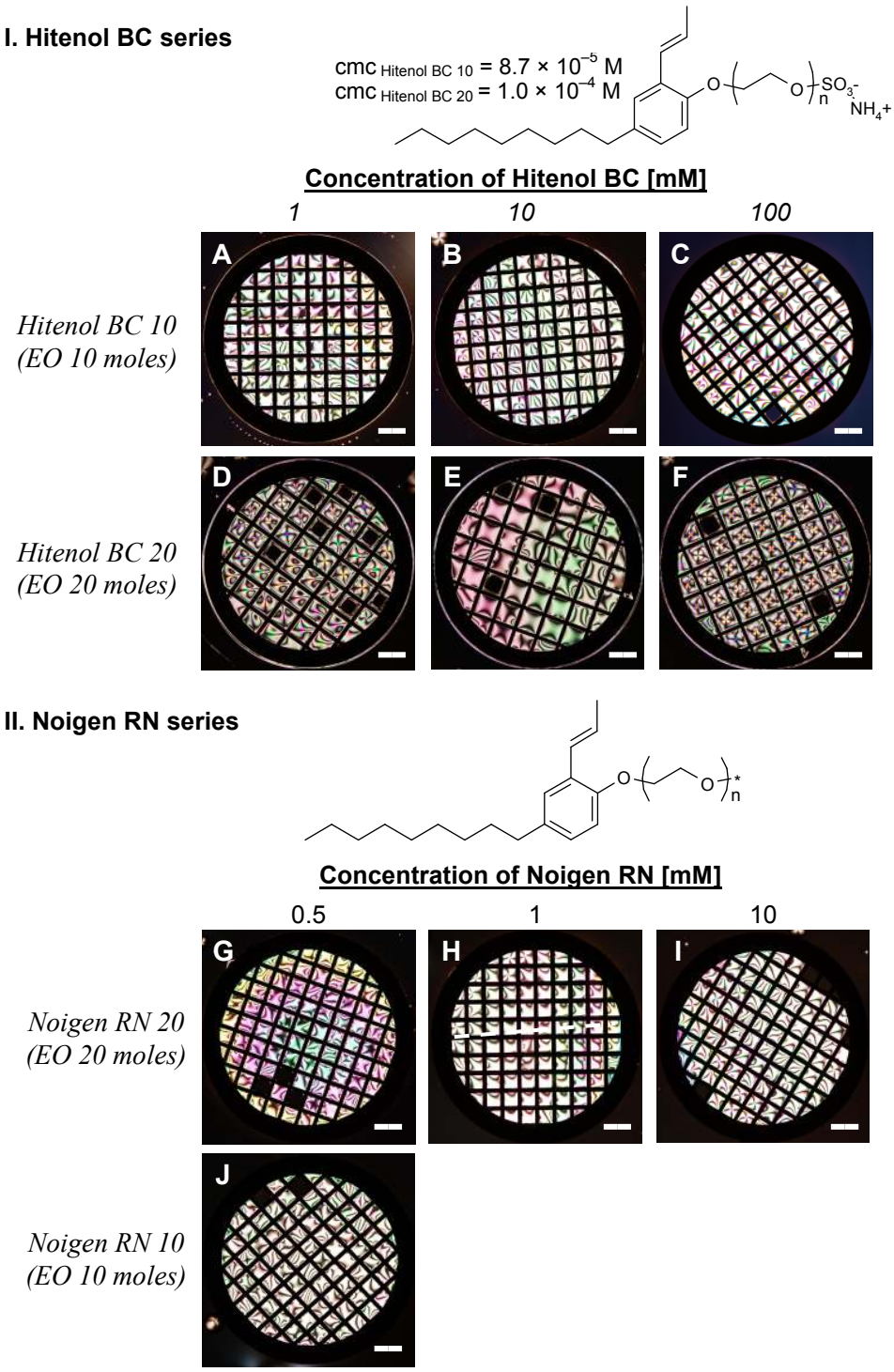

Figure 4.4: Optical images of 5CB between crossed polarisers after incubation with an aqueous solution containing Hitenol BC (anionic polymerisable surfactant) and Noigen RN (non-ionic polymerisable surfactant) (pH ~5.5) at various concentrations. All scale bars represent 400 μm.

These observations correlate with Brake's proposition[9] that the length of the aliphatic chains of surfactants (e.g., SDS, CTAB) at the LC-water interface mainly influence the alignment of the contacting 5CB. The orientation of the 5CB remained

planar when contacted with aqueous solutions of octyltrimethylammonium bromide (OTAB) with C_8 aliphatic chain up to limit of solubilisation of 5CB by OTAB (~300 mM). In contrast with OTAB, the adsorption of both DTAB (C_{12}) and CTAB (C_{16}) at the LC-water interface caused the orientation of 5CB to change from planar to homeotropic anchoring at 3 mM and 0.06 mM each.[10] We conclude that Noigen RN and Hitenol BC cause parallel alignment of 5CB at any bulk concentration of surfactants because of their short alkyl group. This is regardless of the length of EO group even though they have a benzene ring structure within the hydrophobic tail group.

Additional support for this conclusion was obtained in subsequent studies in which the effects of the adsorption of sodium oleate which has a C_{18} hydrophobic alky chain group on the anchoring of the LC were investigated. In past studies, considerable attention has been given to the preparation of unsaturated compounds suitable for use as monomers in polymerisation reactions. We choose sodium oleate, one of these unsaturated compounds as a cheap substitute for the polymerisable surfactant, MUBDMAB. Figure 4.5 shows the optical appearance of 5CB contacted with an aqueous solution containing sodium oleate.

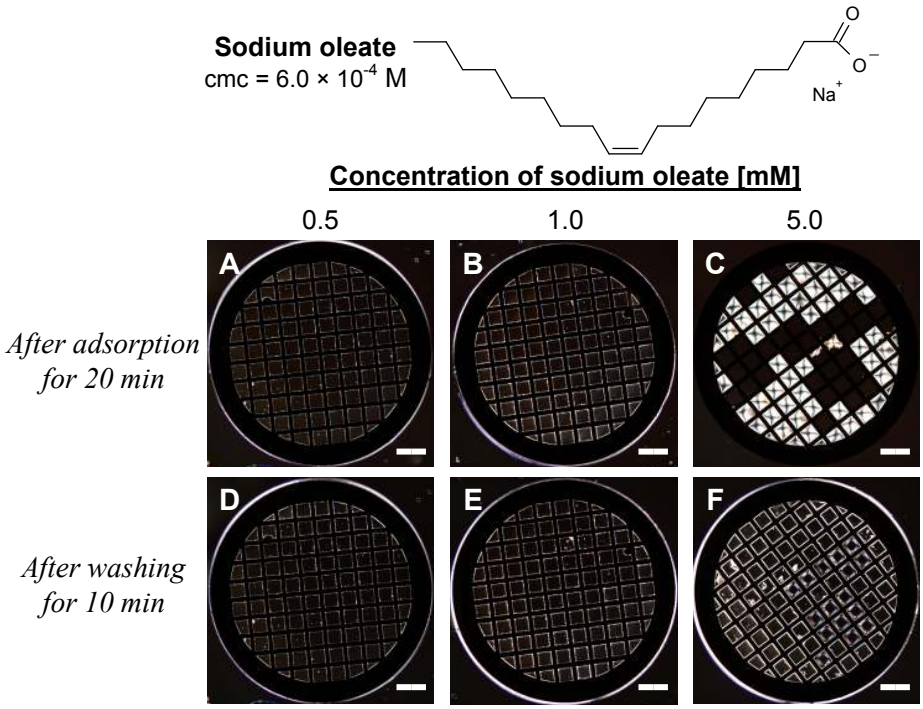

Figure 4.5: Optical images of 5CB between crossed polarisers after incubation with various concentrations of sodium oleate solutions in pure water (pH ~5.5). All scale bars represent 400 μm.

At 0.5 mM concentration sodium oleate resulted in homeotropic alignment of 5CB (Figure 4.5A) whereas the onset of solubilisation of 5CB by sodium oleate was observed to occur at 5.0 mM (Figure 4.5C). The concentration at which this optical change occurs is similar with that of TTAB with C_{14} hydrophobic alkyl chain group. From Figure 4.5D, the adsorbed sodium oleate monolayer is not removed from the LC-water interface by washing with pure water similar to the adsorption of MUBDMAB at the LC-water interface as shown in Figure 4.3D.

The results for the different polymerisable surfactants are summarized in Table 4.2 which lists the concentration at which the optical texture transformations occurs from planar to homeotropic anchoring, the cmc (where measured) and whether the texture transition is reversed by washing with water.

Table 4.2: Summary of the effects of adsorption of the different polymerisable surfactants from water to the 5CB-water interface on the optical textures of 5CB

Surfactant	cmc/mM	Anchoring of 5CB/mM	Effect on anchoring of washing with water
MUBDMAB	Not measured	• Planar at ≤ 0.5 • Homeotropic at ≥ 0.9	Not reversed after 6× volume wash
MEDDAB	4	• Planar at ≤ 0.5 • Homeotropic at ≥ 1.3	• Reversed by 6× volume wash after incubation for 20 min • Not reversed by 4× volume wash after incubation for 1 h
Sodium oleate	0.6	• Planar at ≤ 0.3 • Homeotropic at ≥ 0.5	Not reversed after 8× volume wash
Hitenol BC 10	0.087	• Planar up to 100	-
Hitenol BC 20	0.1	• Planar up to 100	-
Noigen RN 10	Not measured	• Planar up to 0.5	-
Noigen RN 20	Not measured	• Planar up to 10	-

From above results we conclude that polymerisable surfactants with primary hydrocarbon chain lengths of 11 or more carbon atoms such as MUBDMAB, MEDDAB, and sodium oleate induce a transition from planar to homeotropic anchoring of 5CB below their corresponding cmc values. For MEDDAB the alignment by adsorption of MEDDAB can be reverted by washing with 6 volumes if the incubation of the monolayer is short (20 min versus 60 min).

4.3 Effect of UV polymerisation of adsorbed polymerisable surfactants layer on the LC alignment

4.3.1 Effect of the position of polymerisable group in the surfactant

As shown in the section 3.4.2, UV polymerisation of an adsorbed MUBDMAB layer with homeotropic anchoring can cause the anchoring of 5CB to revert back to planar (Figure 4.6A and 4.6D). However, UV polymerisation of MEDDAB in which the polymerisable group is located in the head group region in the surfactant does not trigger the optical transition (Figure 4.6B and 4.6E).

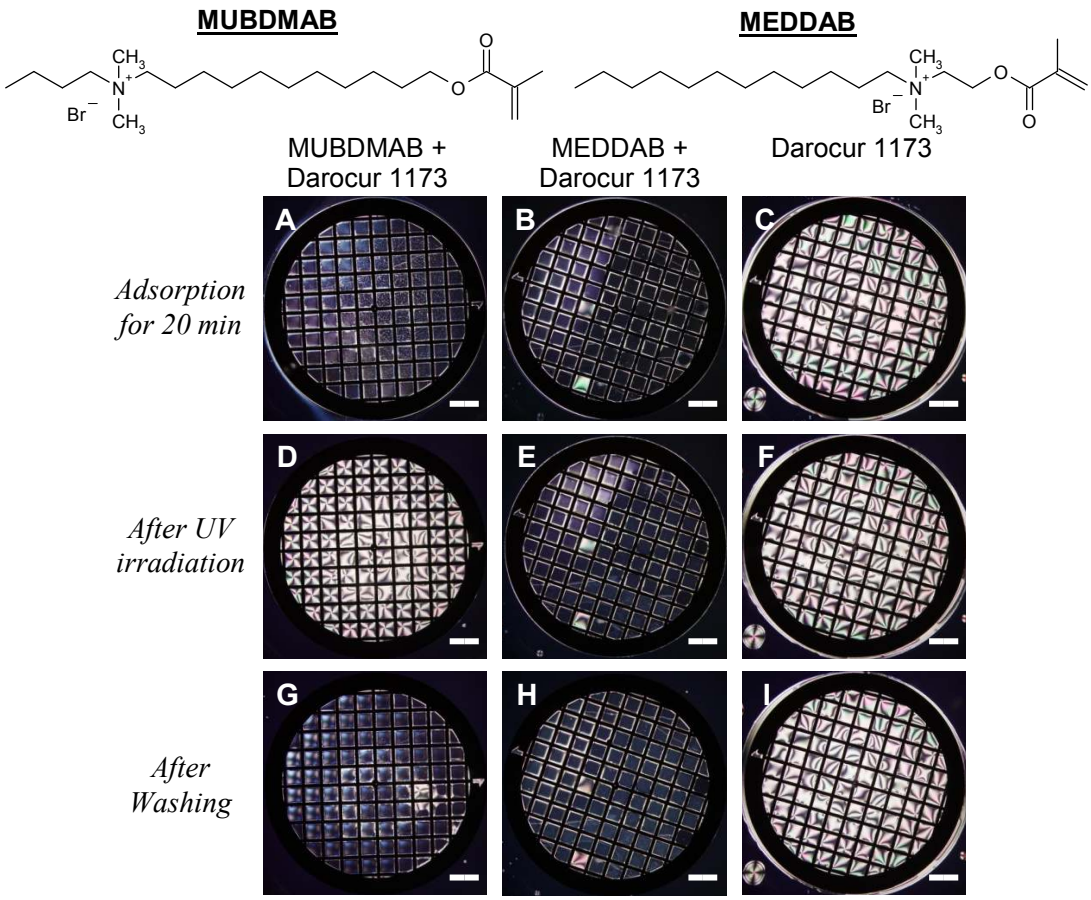

Figure 4.6: Optical images of 5CB between crossed polarisers after incubation with an aqueous surfactant solution of (A) 1.2 mM MUBDMAB and (B) 1.6 mM MEDDAB containing 0.1 vol% Darocur 1173. The optical cell was exposed by the UV curing lamp (Agar Scientific) for 30 min with height 30 mm without washing step. The optical cells were washed using 4 perfusion chamber volumes of pure water followed by 2 h incubation. All scale bars represent 400 μm.

We also confirmed that the UV irradiation of a sample containing Darocur 1173 alone with no polymerisable surfactant produced no change in the optical appearance of 5CB (Figure 4.6C and F). For the polymerisation of MUBDMAB in Figure 4.6 we used the UV curing lamp which has a fixed wavelength, 360 nm (UVA wavelength range) at room temperature to investigate the possibility of these systems detecting separate UVA, UVB wavelengths. The UV SpotCure lamp which was used in a previous experiment covers the range of UVA and UVB wavelengths (280–400 nm) (section 3.4).

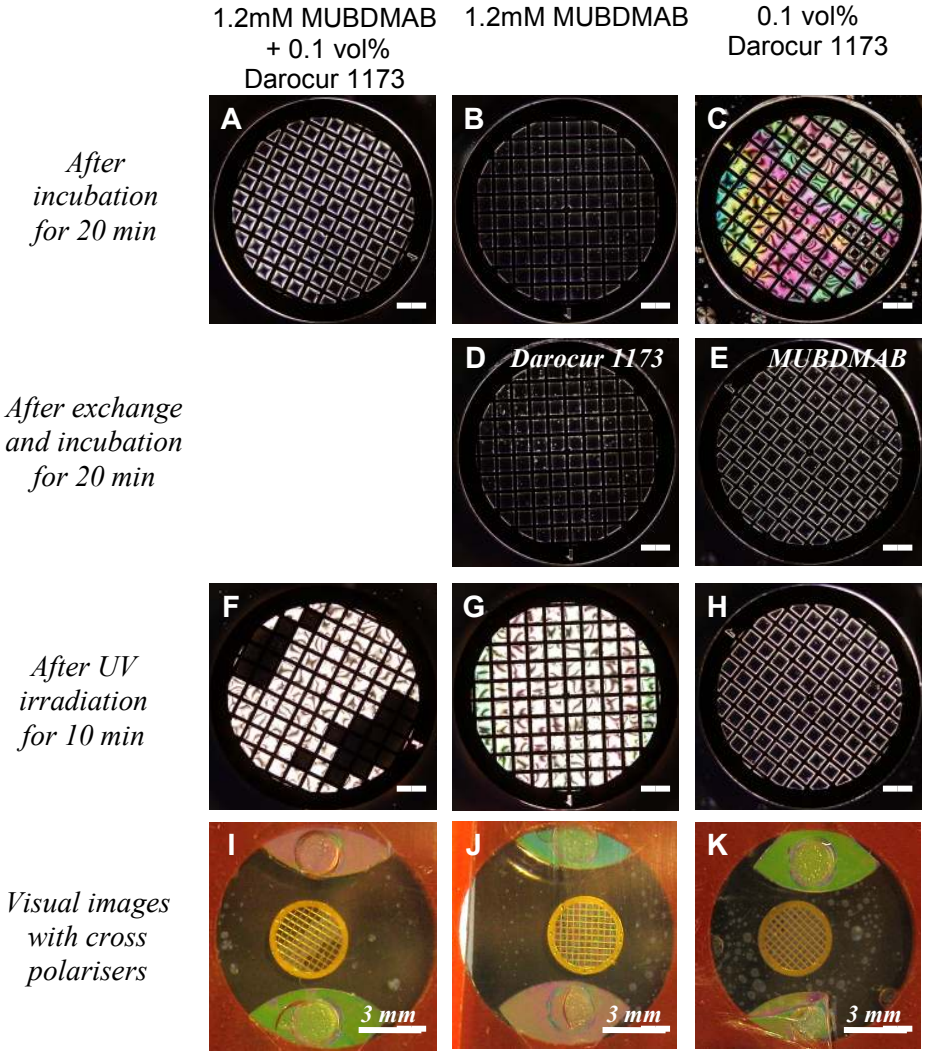

Figure 4.7: Optical images of 5CB between crossed polarisers after incubation with an aqueous solution containing 1.2 mM MUBDMAB with 0.1 vol% Darocur 1173 according to the order of addition of the MUBDMAB and Darocur 1173. All samples were irradiated using the UV curing lamp (Agar Scientific) for 10 min. Optical images (I-K) were captured using a digital camera (Canon IXUS 750). All scale bars represent 400 μm. For image F, the black squares in the grids correspond to a square which empty of 5CB.

Here, the UV triggered planar anchoring of 5CB can be detected by the naked eye under the room illumination using plastic crossed polarisers (Figure 4.7I and J). Darocur 1173 which interacts with 5CB (homeotropic anchoring) would easily be removed from the LC-water interface after washing with pure water (planar anchoring) (Figure 4.7E).

To investigate the effect of UV polymerisation of adsorbed sodium oleate on the alignment of 5CB at the LC-water interface, the sodium oleate was polymerised by UV irradiation after serial or simultaneous incubation with Darocur 1173. Figure 4.8 shows the planar anchoring of 5CB induced by UV polymerisation of the adsorbed sodium oleate monolayer with serial addition of 0.01 vol% Darocur 1173. At 0.3 mM, sodium oleate was partially washed off by replacing with an aqueous solution of Darocur 1173 (Figure 4.8D).

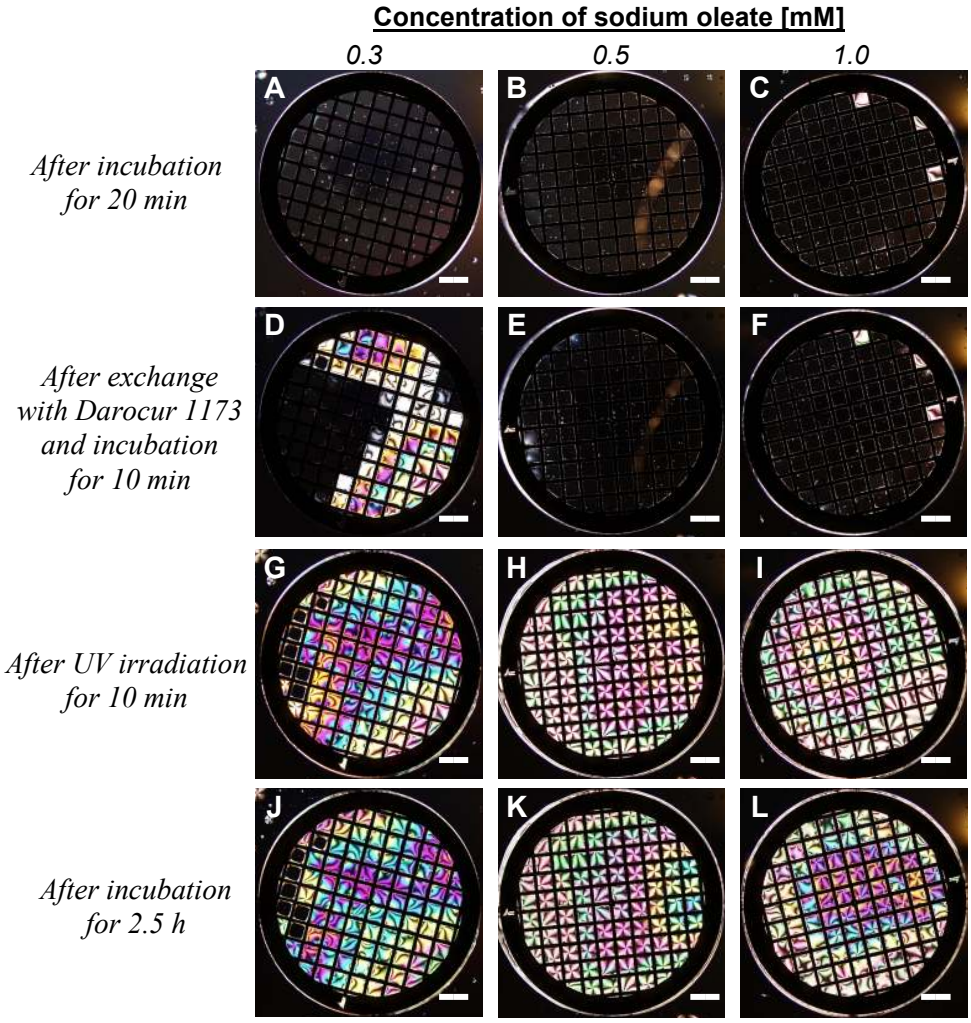

Figure 4.8: Optical images of 5CB between crossed polarisers after incubation with an aqueous solution containing various concentrations of sodium oleate and further replaced with an aqueous solution containing 0.1 vol% Darocur 1173. UV irradiation was performed using the UV curing lamp for 10 min. All scale bars represent 400 μm.

The co-adsorption of 0.5 mM sodium oleate and 0.01 vol% Darocur 1173 in pure water also produced homeotropic anchoring of 5CB at the LC-water interface and the homeotropic anchoring was changed to planar by UV irradiation (data not shown here). Following this procedure, the systems contain excess, non-adsorbed sodium oleate in the water phase. In principle, UV polymerisation may occur in both the adsorbed monolayer and in the water phase with possible subsequent adsorption of polymerised material leading to the LC anchoring transition. As shown in Figure 4.8, similar results were obtained when the excess, non-adsorbed sodium oleate (but not the adsorbed sodium oleate monolayer) is removed by washing prior to UV irradiation. Therefore, this comparison reveals that the polymerisation leading to the optical texture transition occurs within the adsorbed surfactant monolayer directly. From these results it appears that surfactants with polymerisable groups located in the hydrophobic tail regions of them (e.g., MUBDMAB and sodium oleate) exhibit the polymerisation induced transition of anchoring of 5CB. On the contrary, the polymerisation of MEDDAB in which the polymerisable group is located in the head group region of the surfactant can not induce the transition.

As shown in Figure 4.9 Noigen RN and Hitenol BC which have a short C_9 alkyl chain length and cannot change the alignment of 5CB from planar to homeotropic anchoring do not show any change of the alignment of 5CB after UV irradiation.

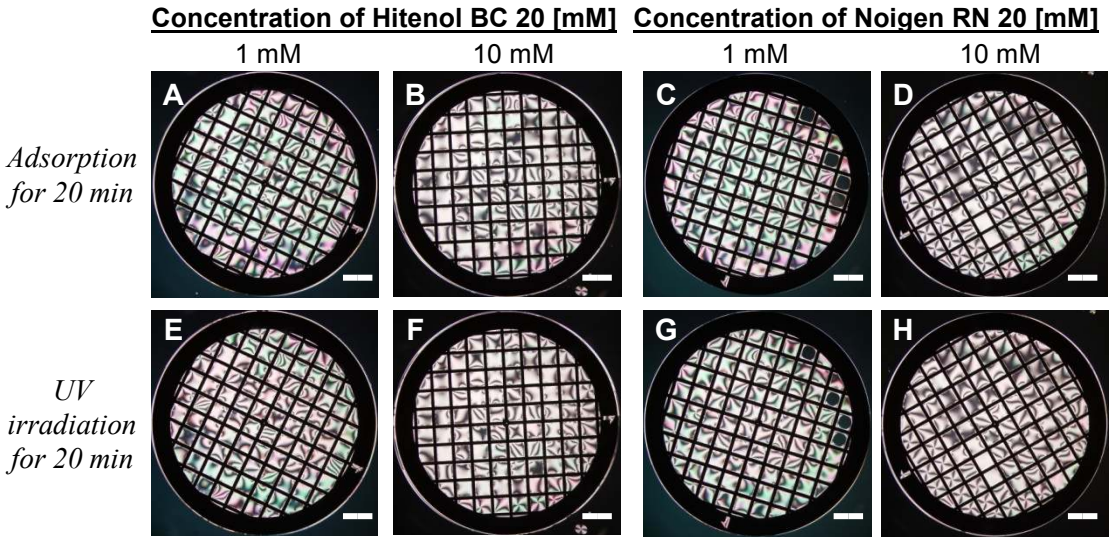

Figure 4.9: Optical images of 5CB between crossed polarisers after incubation with Hitenol BC 20 and Noigen RN 20 aqueous solution with 0.1 vol% Darocur 1173 and UV irradiation using the UV curing lamp (Agar Scientific) for 20 min. All scale bars represent 400 μm.

Furthermore, UV triggered planar anchoring of 5CB was reverted to homeotropic after a long incubation (≥ 3 h) at room temperature and the time stability of the UV triggered planar texture is proportional to the amount of UV radiation (Figure 4.10).

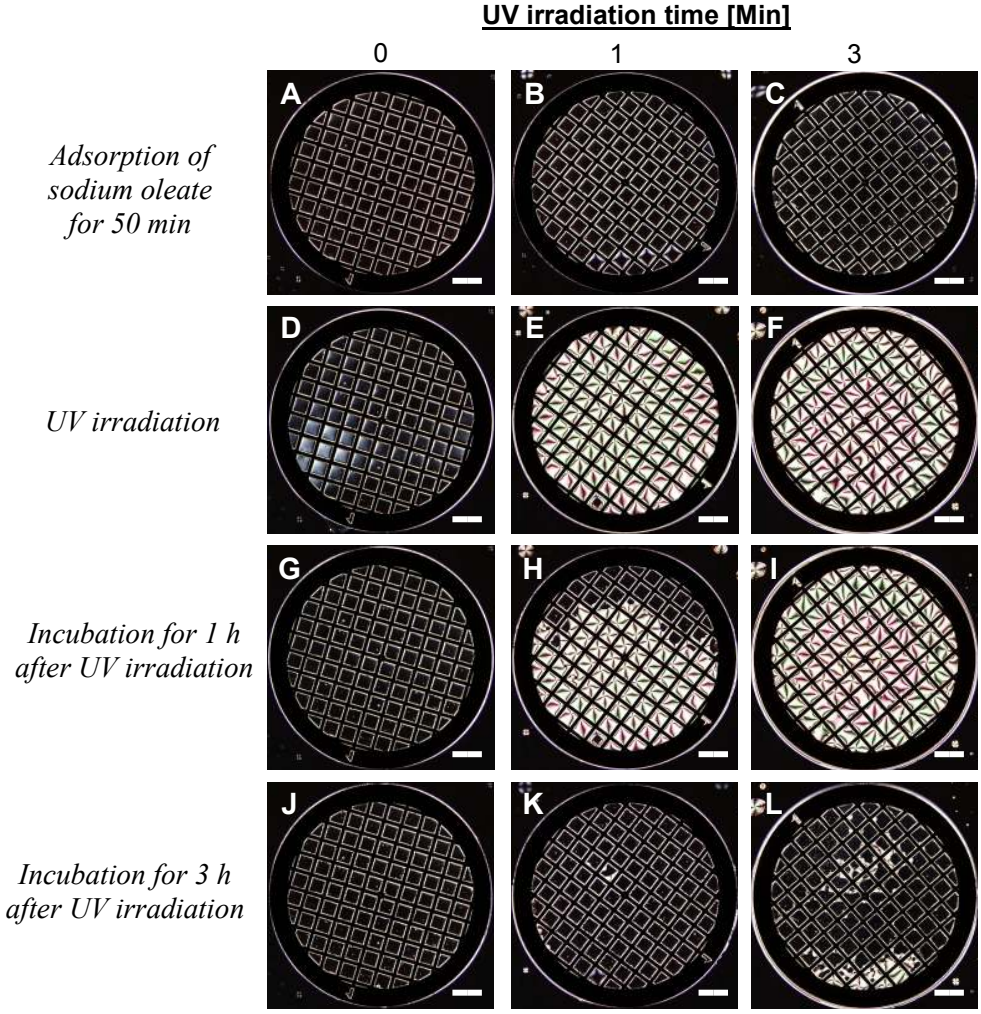

Figure 4.10: Optical images of 5CB between crossed polarisers after incubation with an aqueous solution containing 0.5 mM sodium oleate with 0.1 vol% Darocur 1173. UV irradiation was performed using the UV curing lamp (Agar Scientific) for various time intervals. All scale bars represent 400 μm.

This result likely reflects that the polymerised sodium oleate layer desorbed from the LC-water interface and then diffused to the aqueous phase or 5CB layer with the lapse of time.

4.3.2 Patterned polymerisation of adsorbed polymerisable surfactant layer at the LC-water interface

Experiments were made using UV irradiation through various substrates for a UV mask. First, we investigated the UV transmittance of various film substrates (e.g., photographic- or inkjet printable transparent film) for patterned UV masks with different shapes. Photographic film is a sheet of plastic (polyester, celluloid (nitrocellulose) or cellulose acetate) coated with an emulsion containing light-sensitive silver halide salts (bonded by gelatin) with variable crystal sizes that determine the sensitivity and resolution of the film. An overhead project (OHP) inkjet printable transparent film also is made of polyester. Both films inhibit the transmission of UV including the main adsorption wavelengths of Darocur 1173 regardless of their developed or printed colour, and therefore cannot trigger the transition of the alignment of 5CB by UV polymerisation of MUBDMAB at the LC-water interface in contrast to the cover of a perfusion chamber which is made of polycarbonate (Figure 4.11). Thus, these two kinds of materials are not suitable for UV patterning using MUBDMAB at the LC-water interface.

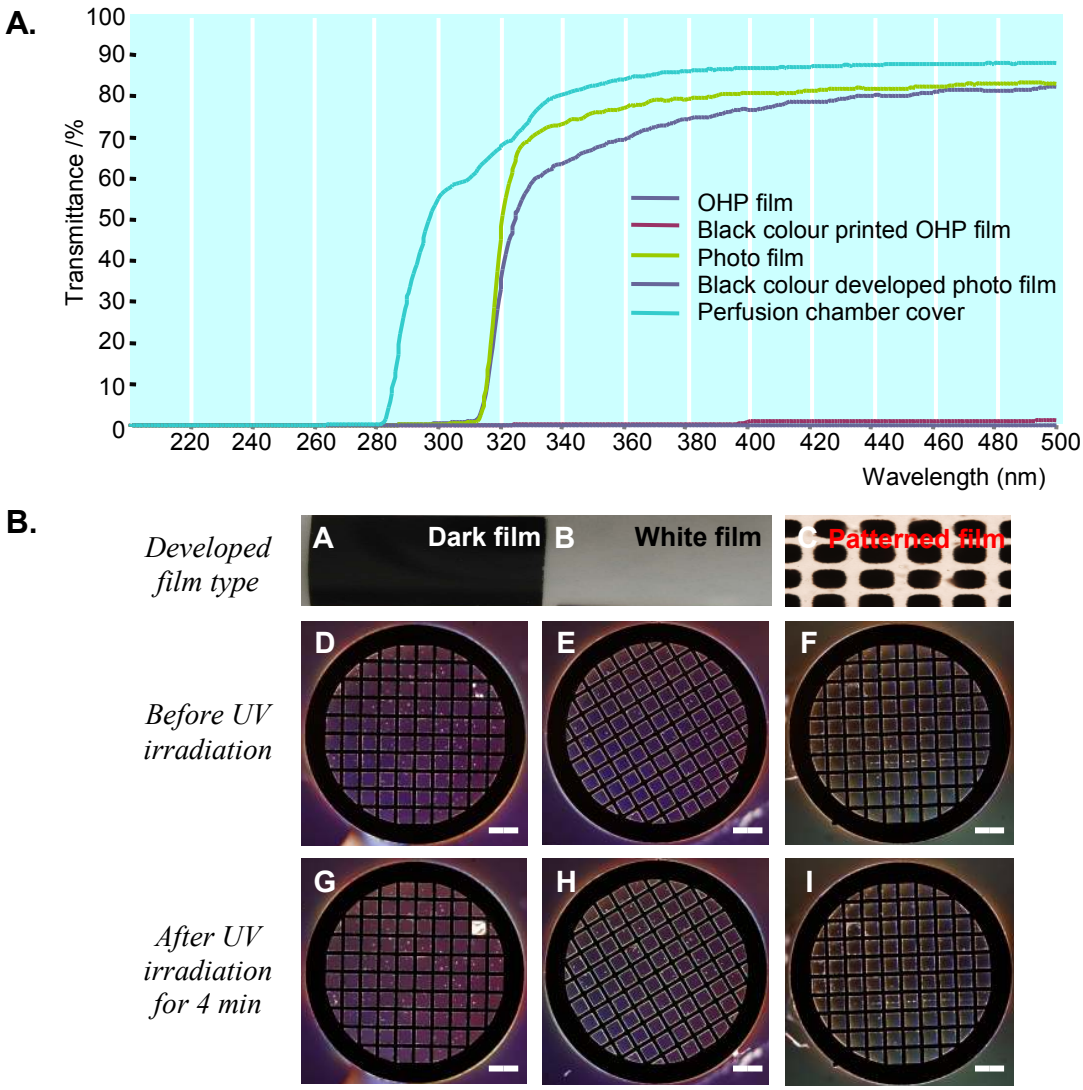

Figure 4.11: (A) Optical transmittance of photo film and inkjet printable overhead project (OHP) film from 200 to 500 nm. Baseline was measured against air. (B) Optical images of 5CB between crossed polarisers after incubation with an aqueous solution containing 1.2 mM MUBDMAB with 0.01 vol% Darocur 1173 and UV irradiation using the SpotCure lamp (UVP) covering with a photo film as a UV mask for 4 min. Patterned photo film is replicated with 50 μm × 50 μm dark region. All scale bars represent 400 μm.

Figure 4.12 shows some of the optical images of LC made using UV irradiation through an aluminium foil mask. MUBDMAB was polymerised using various concentrations of Darocur 1173 at fixed UV irradiation time. The planar anchoring of 5CB induced by UV irradiation was observed only in the UV irradiated region in the system with 0.01 vol% Darocur 1173 (Figure 4.12G). At above 0.01 vol% Darocur 1173, UV irradiation triggered planar anchoring of 5CB propagated into the dark, UV protected regions of the LC-water interface (Figure 4.12H).

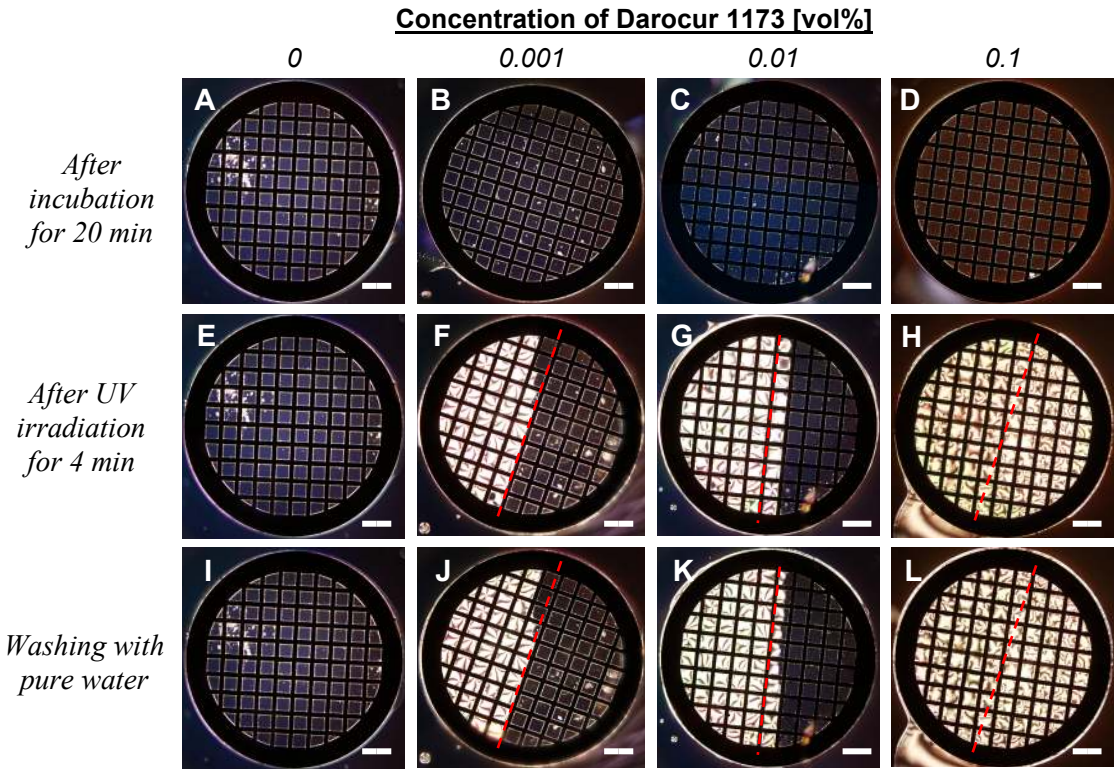

Figure 4.12: Optical images of 5CB between crossed polarisers after incubation with an aqueous solution containing 1.2 mM MUBDMAB and UV irradiation using the SpotCure lamp (UVP) for 4 min at various concentrations of Darocur 1173. The red dotted lines show the border of the aluminum foil cover used to mask UV radiation. The bright colour parts of images F and J are UV irradiated regions. The perfusion chambers were washed with 10 perfusion chamber volumes of pure water. All scale bars represent 400 μm.

As discussed in the Introduction, UV polymerisation of MUBDMAB is a radical chain reaction which involves two main radicals derived from Darocur 1173 after UV irradiation. Therefore, if UV irradiation occurs in a restricted area of the adsorbed surfactant monolayer at the LC-water interface and polymerisation cannot be terminated effectively, the polymerisation of surfactants can be propagated beyond the irradiated

area increasing the polymerisation area than the size of the pattern of a UV mask. From the results it is suggested that polymerisation is likely to be confined to only the adsorbed surfactant monolayer when the photoinitiator concentration is sufficiently small.

We examined the possibility to write a character at the LC-water interface with UV irradiation. Figure 4.13 shows some of the images made in this way using a punctured aluminium foil mask. A very low concentration of Darocur 1173 (e.g., 0.002 vol%) was used to avoid propagation of polymerisation beyond the illuminated edges of the mask as shown in Figure 4.12H. In Figure 4.13 close examination of the image obtained after 240 s after removal of the mask shows the presence of square area within the EM grid in which half of the square (the UV irradiated half) shows planar and half shows homeotropic anchoring of 5CB. However, the planar anchoring of 5CB at the borders slowly reverted to the homeotropic anchoring with loss of the sharpness of the boundary following washing and further incubation.

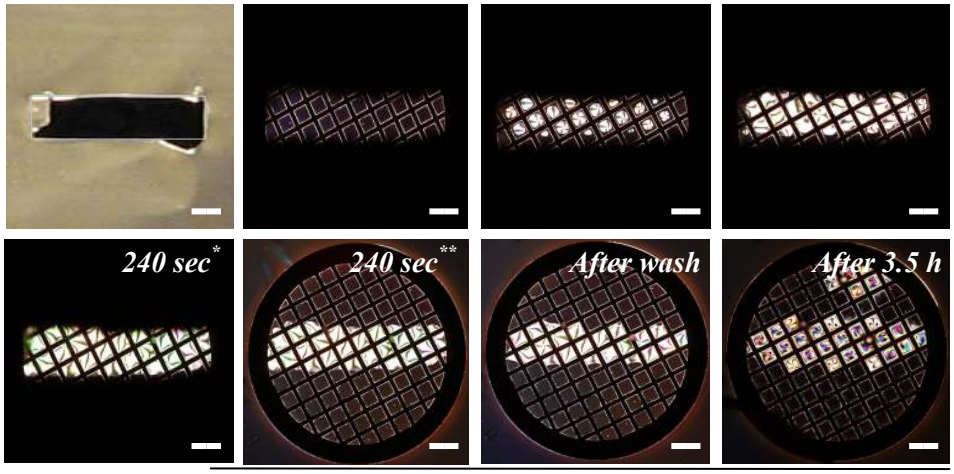

Before (*) and after (**) peeling off an aluminium foil mask.

Figure 4.13: Optical images of 5CB between crossed polarisers contacted with an aqueous solution containing 1.2 mM MUBDMAB with 0.002 vol% Darocur 1173 without washing. UV irradiation through punched aluminum foil as a UV mask was performed using the SpotCure lamp (UVP) for 240 sec. All scale bars represent 400 μm.

The LC optical cells for Figure 4.13 contained excess non-adsorbed sodium oleate in the water phase. The initial sharpness of the masked edge of the polymerised, planar texture region suggests that the polymerisation occurs directly in the adsorbed monolayer under the condition used here because the polymerisation occurring in the water phase might be expected to result in much more diffuse edges. The alternative

possibility of polymerisation in the water phase with subsequent adsorption of the polymerised species might be expected to result in much more diffuse edges. MUBDMAB was also polymerised using a punctured inkjet printable OHP film and nickel meshes (Agar Scientific, Stansted, Essex) as a UV mask with various concentrations of Darocur 1173 and UV irradiation time intervals (Figure 4.14).

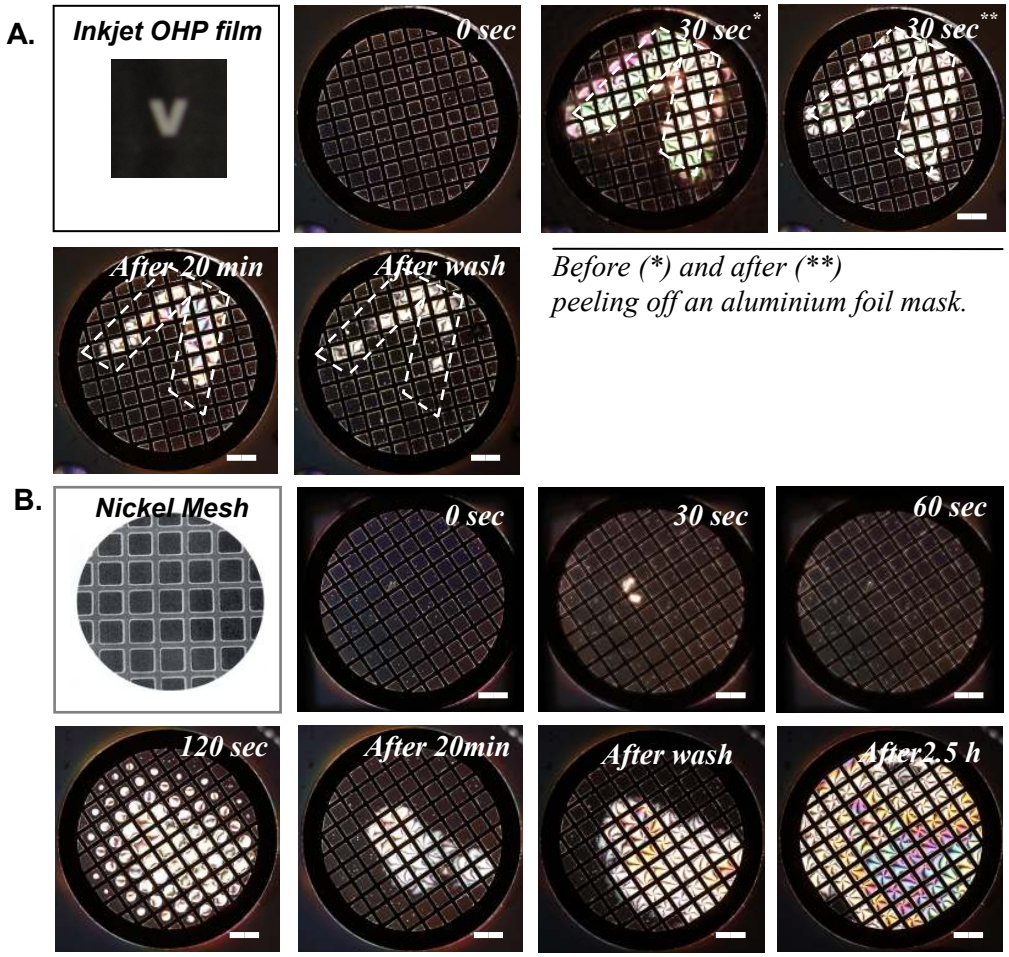

Figure 4.14: Optical images of 5CB between crossed polarisers after incubation with 1.2 mM MUBDMAB aqueous solution containing 0.002 vol% Darocur 1173 and covered with (A) a V shape-punched OHP film and (B) a nickel mesh (18.5 μm inner grid square side length and 7.5 μm bar width, Agar Scientific) as a UV mask and then UV irradiated using the SpotCure lamp (UVP) according to the UV irradiation time. All scale bars represent 400 μm.

Overall, it can be seen that this type of system containing a polymerisable species and photoinitiator could be used to "write with light" at the LC-water interface. For these systems containing polymerisable surfactant adsorbed from the water phase, it was observed that the planar texture obtained after polymerisation slowly reverted back to a homeotropic texture. The time taken for this reverse optical transition was typically

in the range of 1–4 h and was observed to depend on the experimental conditions including UV irradiation time and intensity, surfactant and photoinitiator concentrations, and incubation time after UV irradiation.

4.4 Polymerisation of oleic acid monolayer at the 5CB-water interface

The polymerisation experiments described in previous sections refer to systems in which the polymerisable surfactant was added into the aqueous phase. In this section, the behaviour of systems in which oleic acid was mixed with LC phase prior to loading in the LC optical cell and contact with an aqueous phase containing the photoinitiator is described. In this situation, the uncharged oleic acid will distribute between the LC and water phases and will also undergo deprotonation equilibrium in the water to produce oleate ion. Both oleic acid and oleate species can adsorb to the LC-water interface. Because the distribution and deprotonation equilibria will be coupled together, the formation of an adsorbed oleic/oleate monolayer and its composition at the LC-water interface is expected to depend strongly on the pH and the ionic strength of the aqueous phase. In this section this dependence was systematically determined using procedure 3 mentioned in the section 2.2.4.2 in which oleic acid was added initially in the 5CB phase.

4.4.1 Effect of oleic acid on the orientation and the nematic-isotropic transition temperature (T_{NI}) of 5CB

Before observing the anchoring of 5CB contacted with oleic acid at the LC-water interface, the effect of oleic acid on the alignment of 5CB within the copper EM grids which were sandwiched between OTS-treated glass microscope slides was investigated (Figure 4.15). At 5 vol% oleic acid in 5CB, the anchoring of 5CB is homeotropic at the LC-water interface. However, at 10 vol% oleic acid in 5CB, a coexistence of homeotropically and non-uniformly aligned regions of 5CB was consistently observed. In general, as the concentration of oleic acid was increase, the homeotropic anchoring of LC was unstable and highly nonuniform within the grids. We can speculate that processes of solubilisation of 5CB into oleic acid subsequently influence the behaviour of the system at high oleic acid concentrations which is also observed at high concentrations of SDS (e.g., 100 mM).

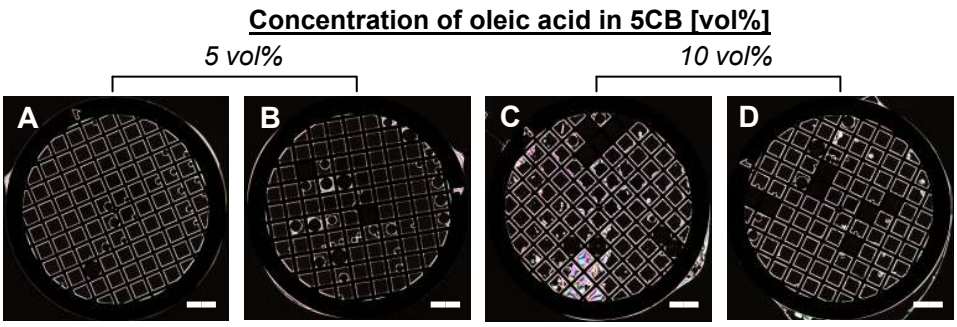

Figure 4.15: Optical images of 5CB and oleic acid mixtures between crossed polarisers after confined to copper EM grids and sandwiched between two OTS-coated glass slides. All scale bars represent 400 μm. The dark regions in C and D correspond to air trapped between the slides and not to the alignment of 5CB.

Pure 5CB shows a transition from crystal-nematic phase at ~24 °C and nematic-isotropic phase at ~36 °C[11,12] although it should be noted that it is common for 5CB to show supercooling of the nematic phase to temperatures well below 24 °C.[11] Addition of solutes such as oleic acid into 5CB is expected to reduce both transition temperatures. We examined the nematic-isotropic transition temperature (T_{NI}) of 5CB as a function of the concentration of oleic acid. The T_{NI} of 5CB decreases with increasing oleic concentration (Figure 4.16A).

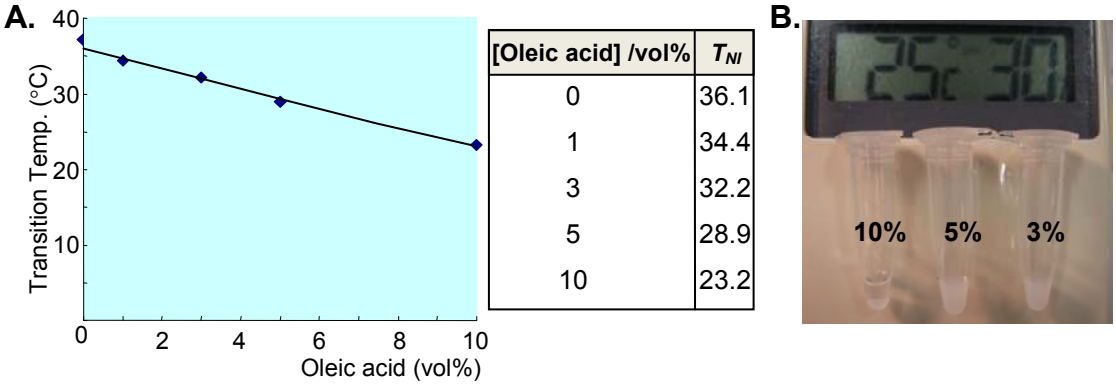

[Oleic acid] /vol%	T_{NI}
0	36.1
1	34.4
3	32.2
5	28.9
10	23.2

Figure 4.16: The change of nematic-isotropic transition temperatures (T_{NI}) of 5CB with oleic acid concentration. (A) T_{NI} of 5CB as a function of vol% oleic acid in 5CB. (B) Optical images of 5CB-oleic acid mixtures at 25 °C and 30% humidity condition. T_{NI} of 5CB was measured by observing the temperature to transit optical images of the 5CB-oleic acid mixtures confined to EM grids between crossed polarisers on OTS-coated slide glass controlled using cooling-heating stage.

Figure 4.16B shows that when 10 vol% of oleic acid is mixed with 5CB, the mixture is transparent and this result indicates the 5CB to be isotropic phase even at 25 °C.

However, at lower mixing ratios of oleic acid with 5CB (e.g., 3 vol%) the mixture appears opaque which means 5CB is nematic phase in the mixture (i.e. the director fluctuation in the bulk, non-aligned sample).

4.4.2 Anchoring of 5CB by oleic acid

The oleic acid which is initially dissolved in 5CB will be partitioned between the 5CB and aqueous phases when it contacts with an aqueous phase. Figure 4.17 shows the optical appearance of 5CB containing various concentrations of oleic acid contacted with pure water (pH ~5.5).

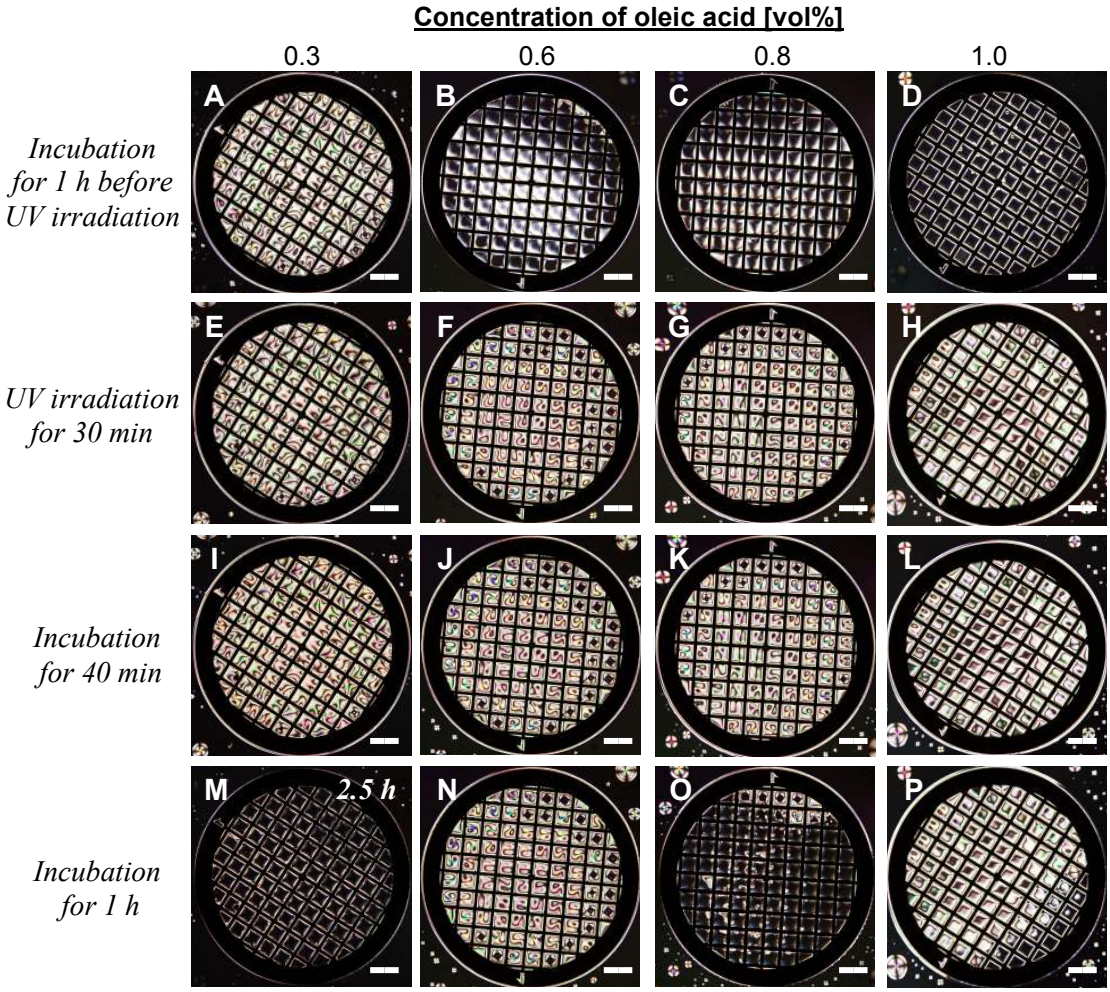

Figure 4.17: Optical images of 5CB between crossed polarisers after mixed with oleic acid and contacted with pure water (pH ~5.5) containing 0.1 vol% Darocur 1173. UV irradiation was performed using the UV curing lamp (Agar Scientific) for 30 min. All scale bars represent 400 μm.

For oleic acid concentration ranging from 0.6 to 1.0 vol% (Figure 4.17B, C and D), the observed optical texture is homeotropic anchoring of 5CB at the LC-water interface triggered by adsorption of oleic acid and oleate species. These optical textures of 5CB were transformed to planar anchoring by UV irradiation (Figure 4.17F, G, and H), similar to that seen in UV polymerisation of sodium oleate (Figure 4.8). At lower oleic acid concentrations (e.g., 0.3 vol %), the optical texture of the 5CB was found to be planar anchoring (Figure 4.17A). The partitioning of oleic acid depends on the solubility of oleic acid in aquoeus phase. For example, the solubility of oleic acid in 0.15 M Tris buffer (pH 8.5) is at least 1 mg/mL, whereas the solubility of oleic acid in phosphate buffered saline (pH 7.2) is less than 100 μg/mL.[13] From these results we speculate that 0.3 vol% oleic acid in 5CB could not make a critical surface density of oleic acid and oleate species (oleic acid/oleate) at the LC-water interface to transform the anchoring of 5CB from planar to homeotropic. In the literature[14], the partition coefficient of oleic acid between octanol and water is approximately $10^{7.64}$. Therefore, only a very small amount of the oleic acid initially dissolved in the 5CB phase is likely to move to the aqueous phase leading to a low adsorption of oleic acid/oleate at the LC-water interface.

We performed a series of UV polymerisations using different concentrations of photoinitiator Darocur 1173 to examine the effect of Darocur 1173 on the adsorption of oleic acid/oleate at the LC-water interface. Figure 4.18 shows the optical appearance of 5CB containing 0.8 vol% oleic acid when contacted with aqueous solutions containing various concentrations of Darocur 1173. At 0.05 vol% Darocur 1173, we did not observe any optical transition of anchoring of 5CB after UV irradiation (Figure 4.18E). At above 0.1 vol% Darocur 1173 (Figure 4.18F, G, and H) UV irradiation triggered transition of anchoring of 5CB from homeotropic to planar anchoring. At higher concentrations of Darocur 1173, the retention time of UV triggered planar anchoring of 5CB is longer than at lower concentrations (~1 h at 0.15 vol%; >1.5 h at 0.2 vol%).

Thus, we conclude that the extent of UV triggered planar anchoring of 5CB at the LC-water interface and the reversal time to homeotropic anchoring are dependent on the concentration of photoinitiator at fixed concentration of oleic acid in 5CB phase and the polymerisation of mixed oleic acid/oleate adsorbed layer at the LC-water interface is likely to induce the transition of anchoring of 5CB.

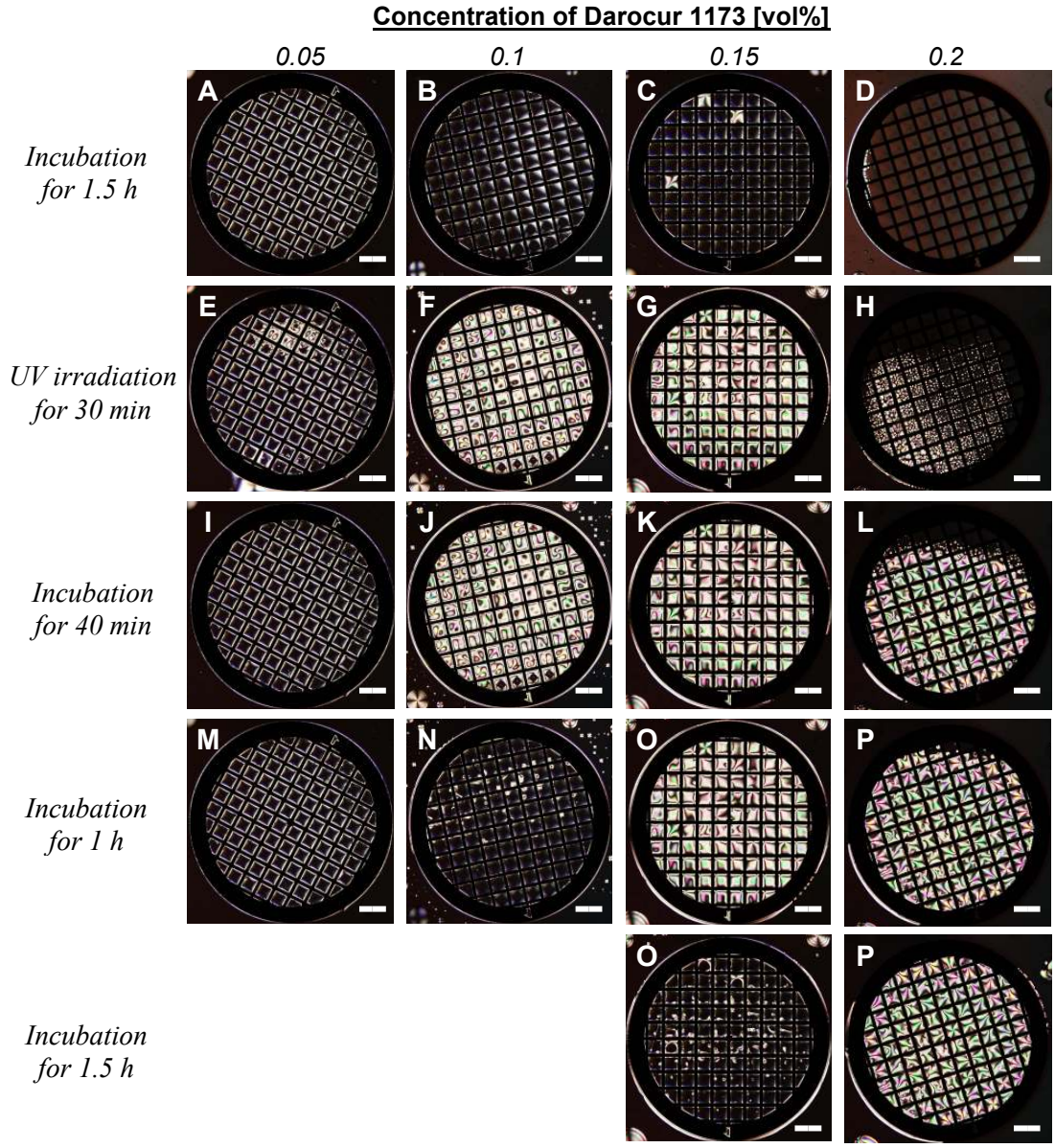

Figure 4.18: Optical images of 5CB containing 0.8 vol% oleic acid between crossed polarisers after incubation with aqueous solutions with various concentrations of Darocur 1173. UV irradiation was performed using the UV curing lamp (Agar Scientific) for 30 min. All scale bars represent 400 μm.

4.4.3 Effect of pH and ionic strength on the adsorption of oleic acid at the 5CB-water interface

In the oleic acid systems, the uncharged oleic acid may distribute between the 5CB and water phase and also undergo deprotonation equilibrium in the water to produce oleate ions which can also adsorb at the LC-water interface (Figure 4.19).

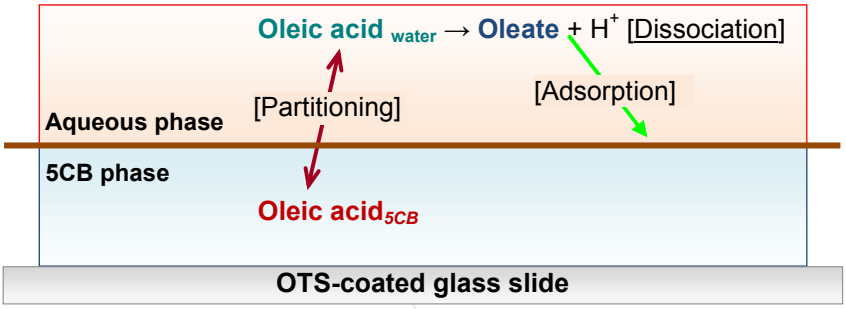

I. Partitioning of oleic acid according to pH: $P_{high\ pH} > P_{low\ pH}$
II. Dissociation of oleic acid according to pH: $[Oleate]_{high\ pH} > [Oleate]_{low\ pH}$
III. Adsorption of oleate according to ionic strength: $Repulsion_{low\ salt} > Repulsion_{High\ salt}$

❖ **At high pH and high ionic strength: High surface density of oleic acid/oleate**

Figure 4.19: Schematic illustration of the adsorption of oleic acid and oleate ions at the LC-water interface after being contacted with an aqueous solution.

Because the distribution and deprotonation equilibria will be coupled together as shown in Figure 4.19, the formation of an adsorbed oleic and oleate monolayer and its composition at the LC-water interface is expected to depend strongly on the pH and ionic strength of the aqueous phase. Therefore, we systematically observed the alignment of 5CB at the LC-water interface with various combinations of pH and ionic strength of the aqueous solutions before and after UV irradiation.

4.4.3.1 Effect of pH

Figure 4.20 shows the anchoring of 5CB mixed with 5 vol% oleic acid at the LC-water interface according to the pH of an aqueous phase. At pH 4 and 7 LC optical cells show a homeotropic anchoring of 5CB whereas the film of 5CB-oleic acid mixture confined to EM grids was disrupted at pH 10 (Figure 4.20D). Because the pK_a value of oleic acid is 4.8, oleic acid exists as oleate which adsorbs at the LC-water interface at high pH. After long incubation (≥ 3 h), the homeotropic anchoring of 5CB in some holes of EM grids slightly was reverted to planar anchoring at pH 4 and 7 (Figure 4.20M, N) in contrast to pure water (Figure 4.20L).

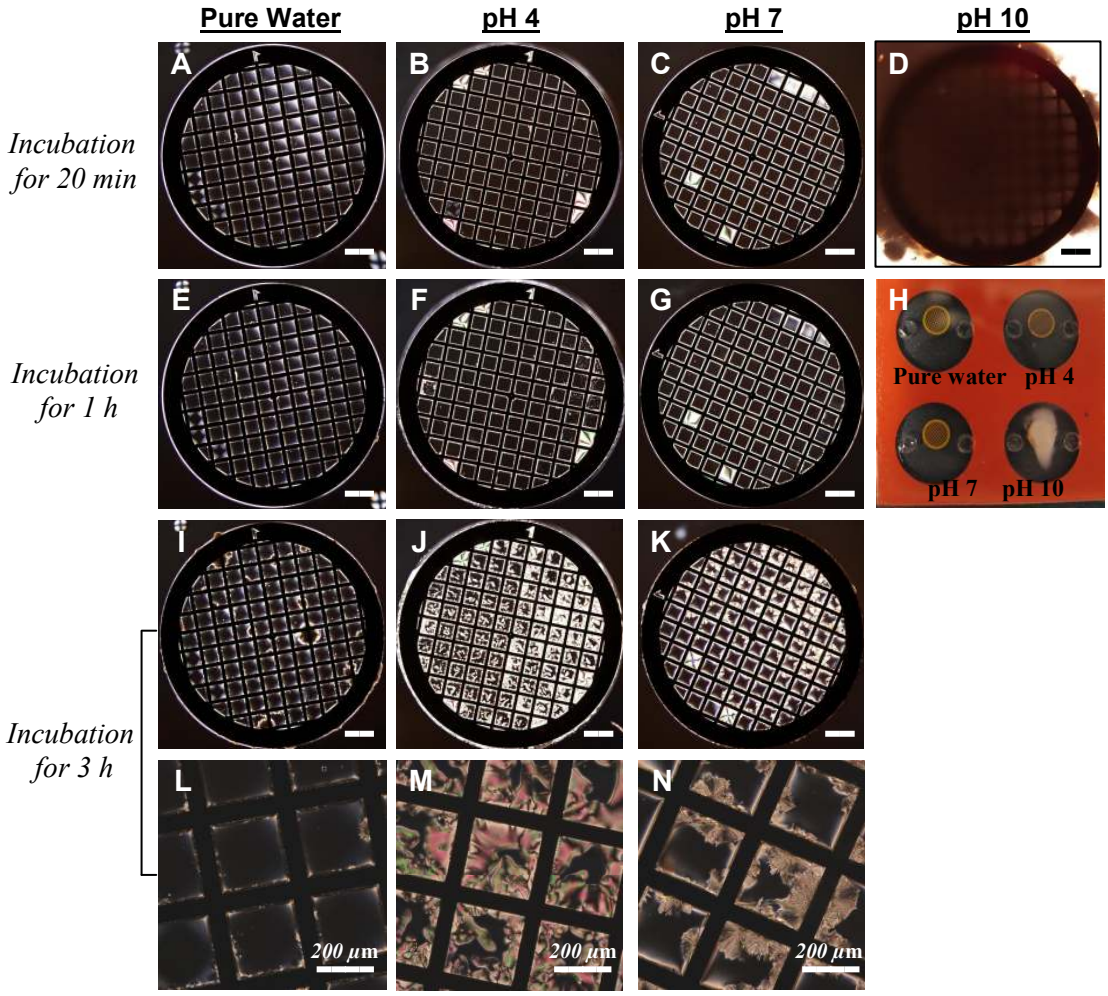

Figure 4.20: Optical images of 5CB containing 5 vol% oleic acid between crossed polarisers after incubation with various aqueous solutions: (A) pure water (pH ~5.5); (B) pH 4 buffer; (C) pH 7 buffer; (D) pH 10 buffer. For image H, the 5CB film confined within the EM grid is disrupted and forms a white precipitate in the aqueous phase at pH 10 in contrast to pH 4–7. The image (H) was obtained using a digital camera (Canon IXUS 750). All scale bars represent 400 μm except (L-M).

The disruption of the film of 5CB at a high pH was thought to be caused by the addition of oleic acid into 5CB because the film of pure 5CB is very stable after long incubation (≥ 3 h) in pH 10 aqueous solution (Figure 4.21A-C) compared with that of 5CB containing 3 vol% oleic acid (Figure 4.21D).

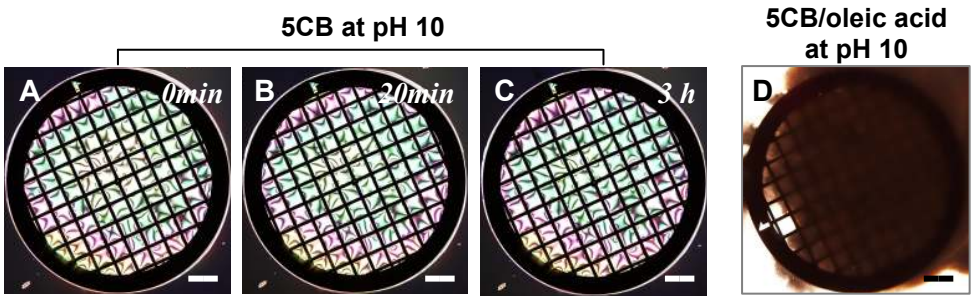

Figure 4.21: Optical images of 5CB between crossed polarisers after incubation with pH 10 buffer. The LC film containing 3 vol% oleic acid was disrupted immediately after adding pH 10 buffer (D) compared to pure LC film (A-C). All scale bars represent 400 μm.

Figure 4.22 shows that the extent of unstable and nonuniform 5CB alignment is less with 3 vol% oleic acid in 5CB compared with 5 vol% oleic acid in 5CB (Figure 4.20).

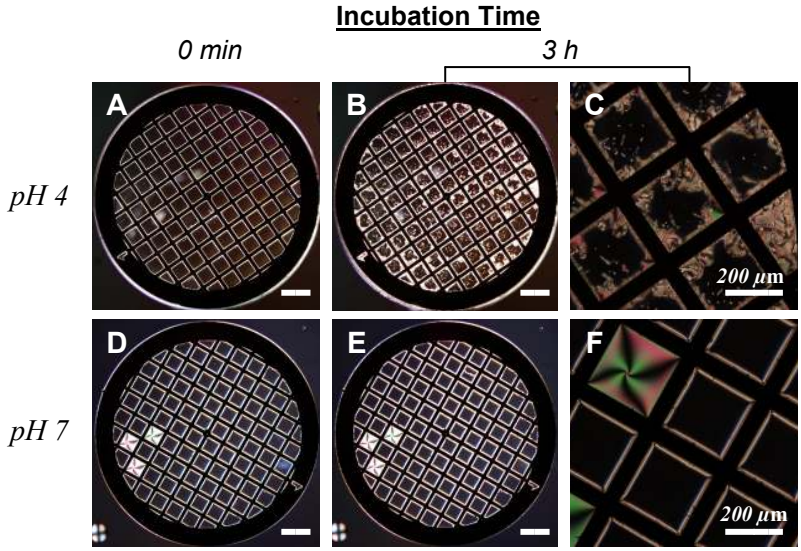

Figure 4.22: Optical images of 5CB containing 3 vol% oleic acid between crossed polarisers after incubation with buffer solutions at (A) pH 4 and (D) pH 7. All scale bars represent 400 μm except images C and F.

This result likely reflects that most of the oleic acid in the 5CB phase converts to oleate, hence disrupting the LC-water interface at pH 10. Furthermore, the triggered homeotropic anchoring of 5CB by adsorption of oleic acid/oleate at pH 7 was maintained for longer than at pH 4. This difference is also likely due to differences in the dissociation of oleic acid depending on pH of aqueous phases.

We also investigated the effect of UV irradiation on the adsorption/desorption equilibrium of oleic acid/oleate at the 5CB-water interface in aqueous solutions at

various pH values at fixed ionic strength. At 0.1 mM ionic strength, the 5CB in the EM grids exposed at aqueous solutions at pH ranging from pH 5 to 8 shows the planar anchoring of 5CB after UV irradiation (Figure 4.23). However, the reversal time of induced planar anchoring of LC decreases with increasing the pH of contacted aqueous solutions (Figure 4.23I, J, K, and L). This relationship between ionic strength and pH of aqueous phases are consistent at different ionic strength conditions (Figure 4.24).

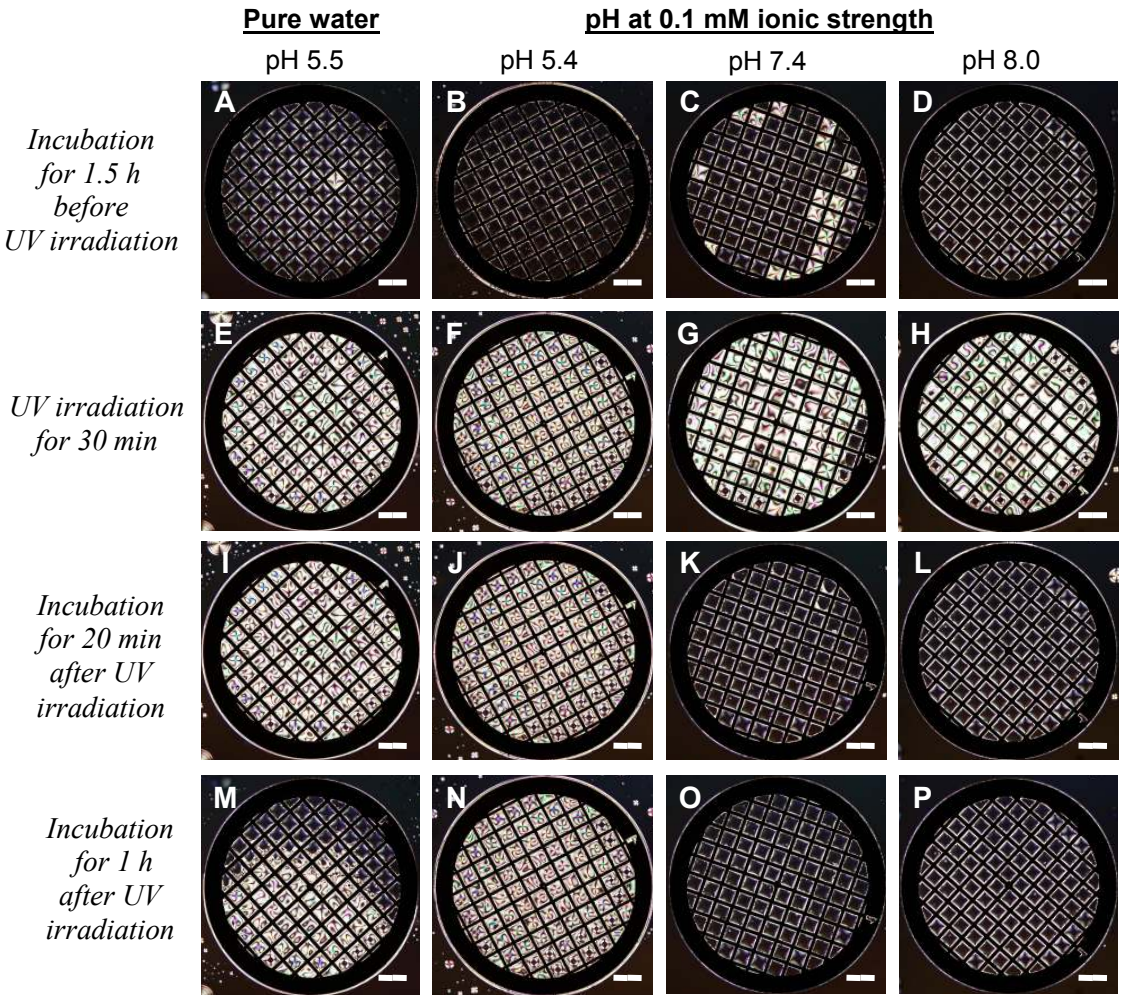

Figure 4.23: Optical images of 5CB containing 0.8 vol% oleic acid between crossed polarisers after incubation with 0.1 mM buffer solutions containing 0.1 vol% Darocur 1173 at various pH values. UV irradiation was performed using the UV curing lamp (Agar Scientific) for 30 min. All scale bars represent 400 μm.

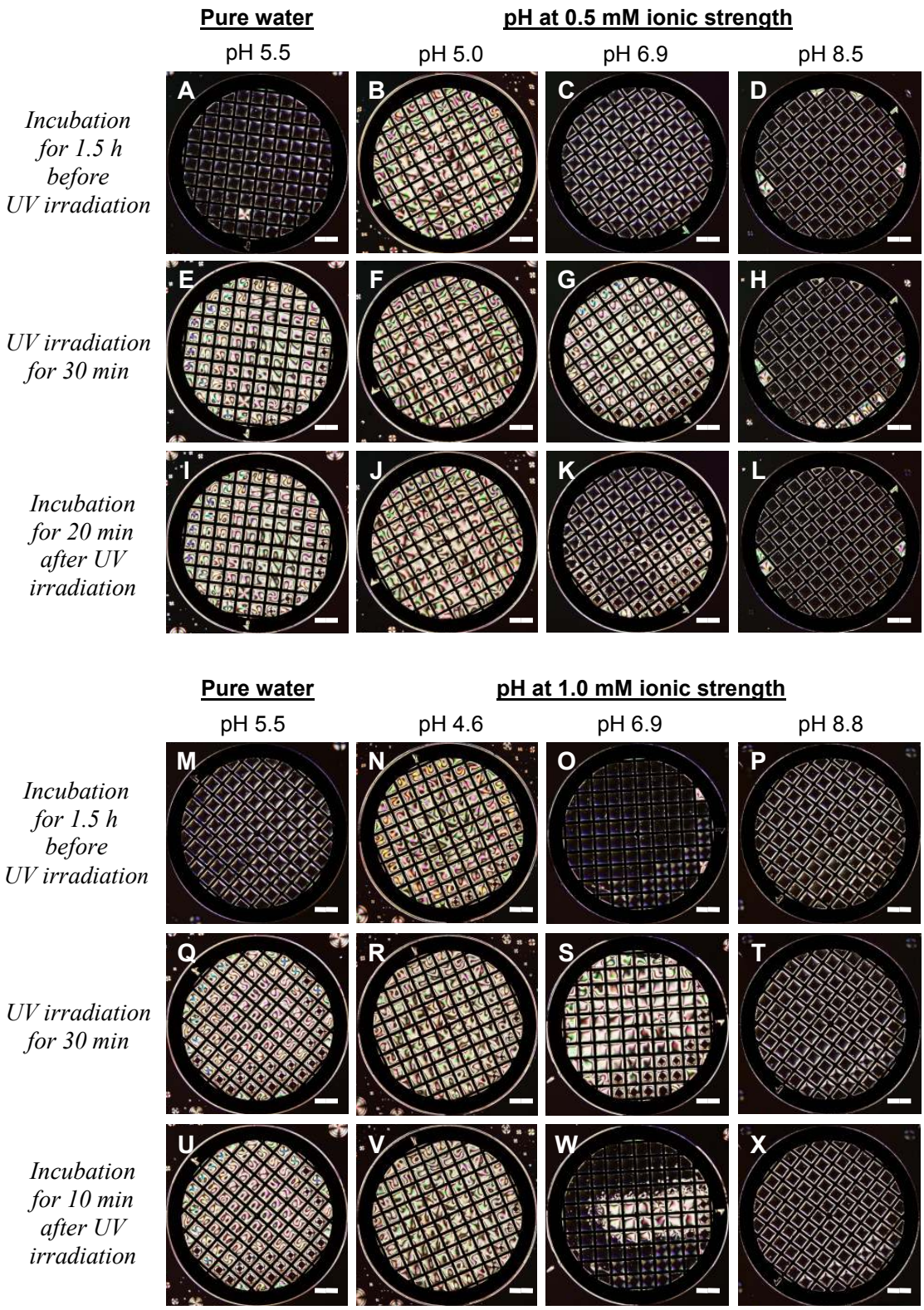

Figure 4.24: Optical images of 5CB containing 0.8 vol% oleic acid between crossed polarisers after incubation with in 0.5 and 0.1 mM buffer solutions containing 0.1 vol% Darocur 1173 at various pH values. UV irradiation was performed using the UV curing lamp (Agar Scientific) for 30 min. All scale bars represent 400 μm.

4.4.3.2 Effect of the ionic strength

We also examined the effect of ionic strength on the transition of anchoring of 5CB triggered by UV irradiation at a fixed concentration of oleic acid in 5CB. Figure 4.25 shows that the transition of UV triggered planar anchoring of 5CB to homeotropic was too fast (~5 sec) to capture the image in case of pH 7 buffer solution containing 0.1 M NaH_2PO_4 (Figure 4.25H) whereas in pure water the UV triggered planar anchoring was maintained for >30 min (Figure 4.25F). It is expected that the adsorption and desorption of mixed oleic acid/oleate and polymerised oleic acid/oleate layer is mainly controlled by the ionic strength in the aqueous phase.

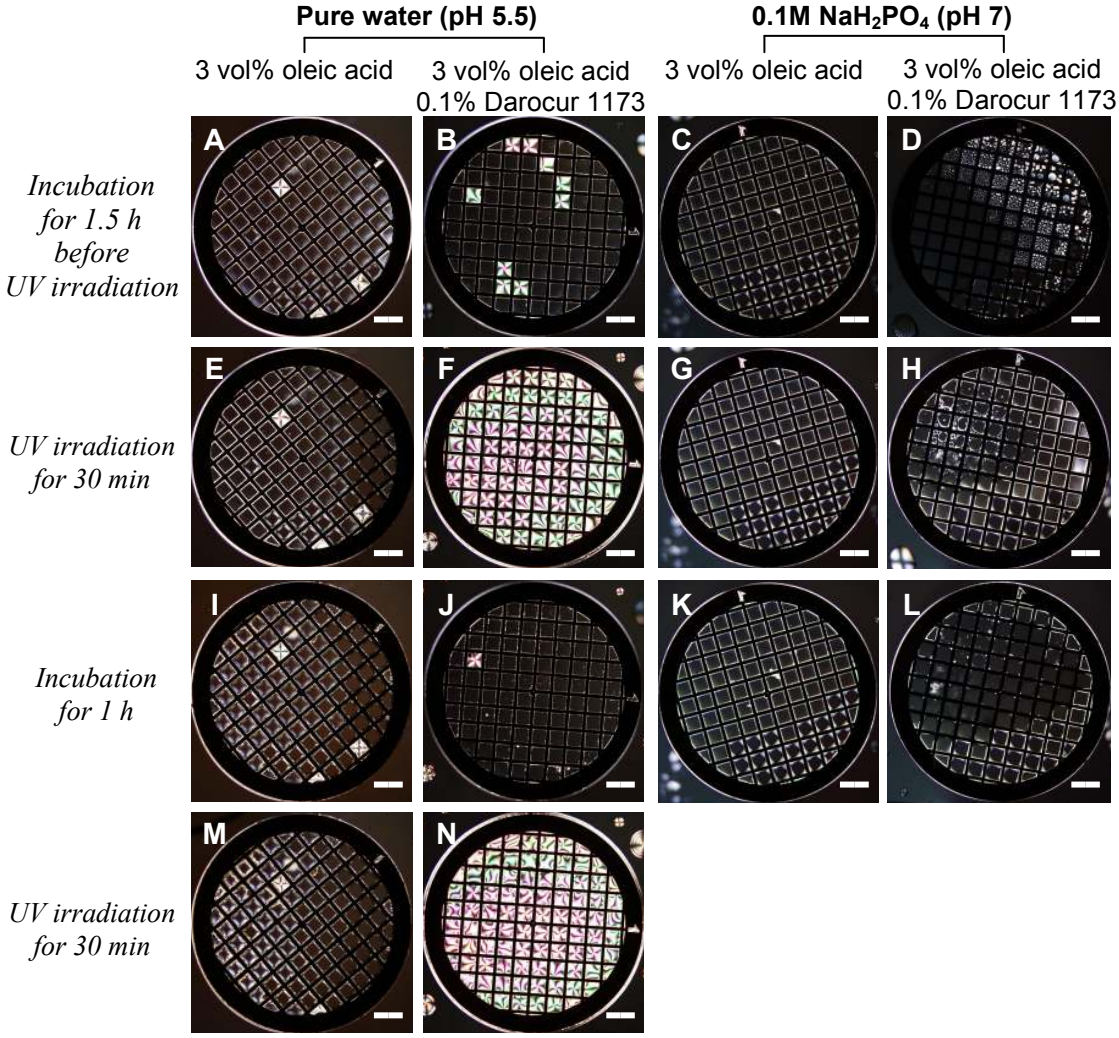

Figure 4.25: Optical images of 5CB containing 3 vol% oleic acid between crossed polarisers after incubation in pure water (pH ~5.5) or pH 7 buffer solution without Darocur 1173 (A and C) and with 0.1 vol% Darocur 1173 (B and D). UV irradiation was performed using the UV curing lamp (Agar Scientific) for 30 min. All scale bars represent 400 μm.

Moreover, the reverted homeotropic anchoring of 5CB (Figure 4.25J) was returned again to planar (Figure 4.25N) by the second UV irradiation. It means that a portion of mixed oleic acid/oleate adsorbed layer at the LC-water interface are polymerised by UV irradiation then, the polymerised oleic acid/oleate layer could be replaced with oleic acid in 5CB phase which reestablishes a homeotropic anchoring of 5CB.

We further investigated the influence of ionic strength on the adsorption of oleic acid/oleate at the LC-water interface at a fixed pH. At pH 5, only the 5CB which was exposed at low ionic strength (0.1 mM) showed the homeotropic anchoring of 5CB at the LC-water interface (Figure 4.26B) and UV irradiation induced planar anchoring of 5CB (Figure 4.26F).

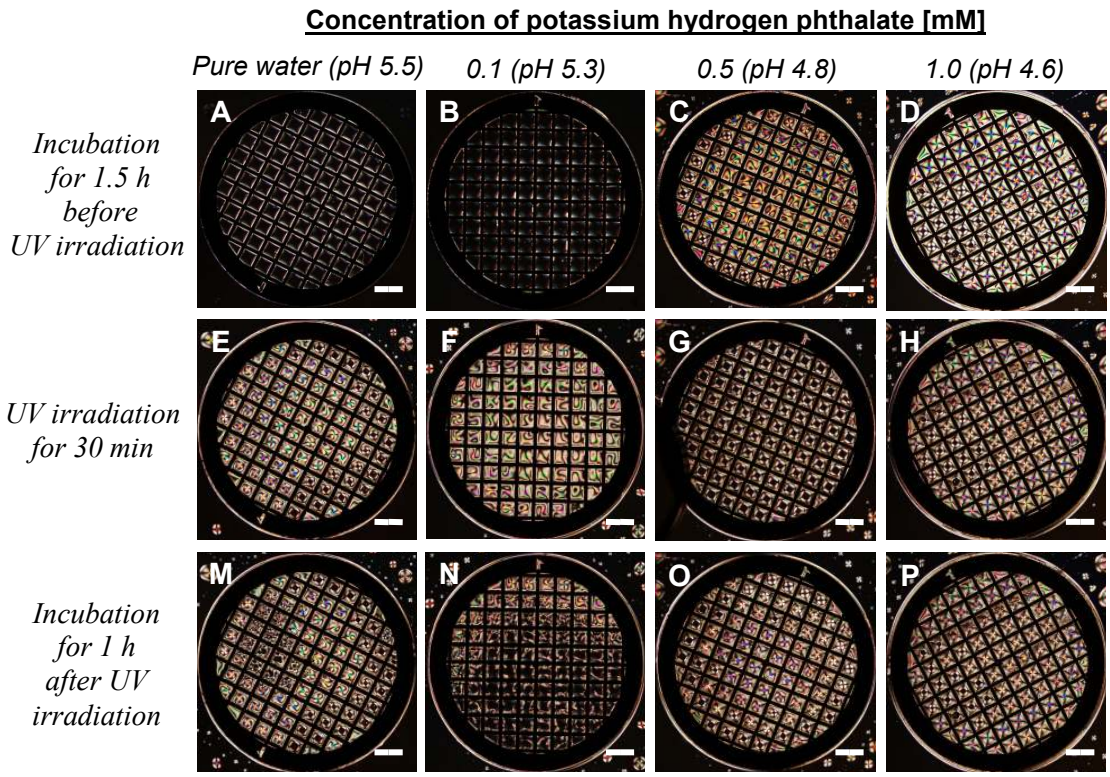

Figure 4.26: Optical images of 5CB containing 0.8 vol% oleic acid between crossed polarisers after incubation with buffer solutions with 0.1 vol% Darocur 1173 at about pH 5 with various ionic strengths. Figures in parenthesis refer to the actual pH values of the buffer solutions. UV irradiation was performed using the UV curing lamp (Agar Scientific) for 30 min. All scale bars represent 400 μm.

At pH 7, all the LC samples show the homeotropic anchoring of 5CB at the LC-water interface and also show UV triggered planar anchoring of 5CB at ionic strengths up to 1 mM (Figure 4.27). The reversal time of induced planar anchoring of 5CB to homeotropic decreases with increasing the ionic strengths of aqueous solutions.

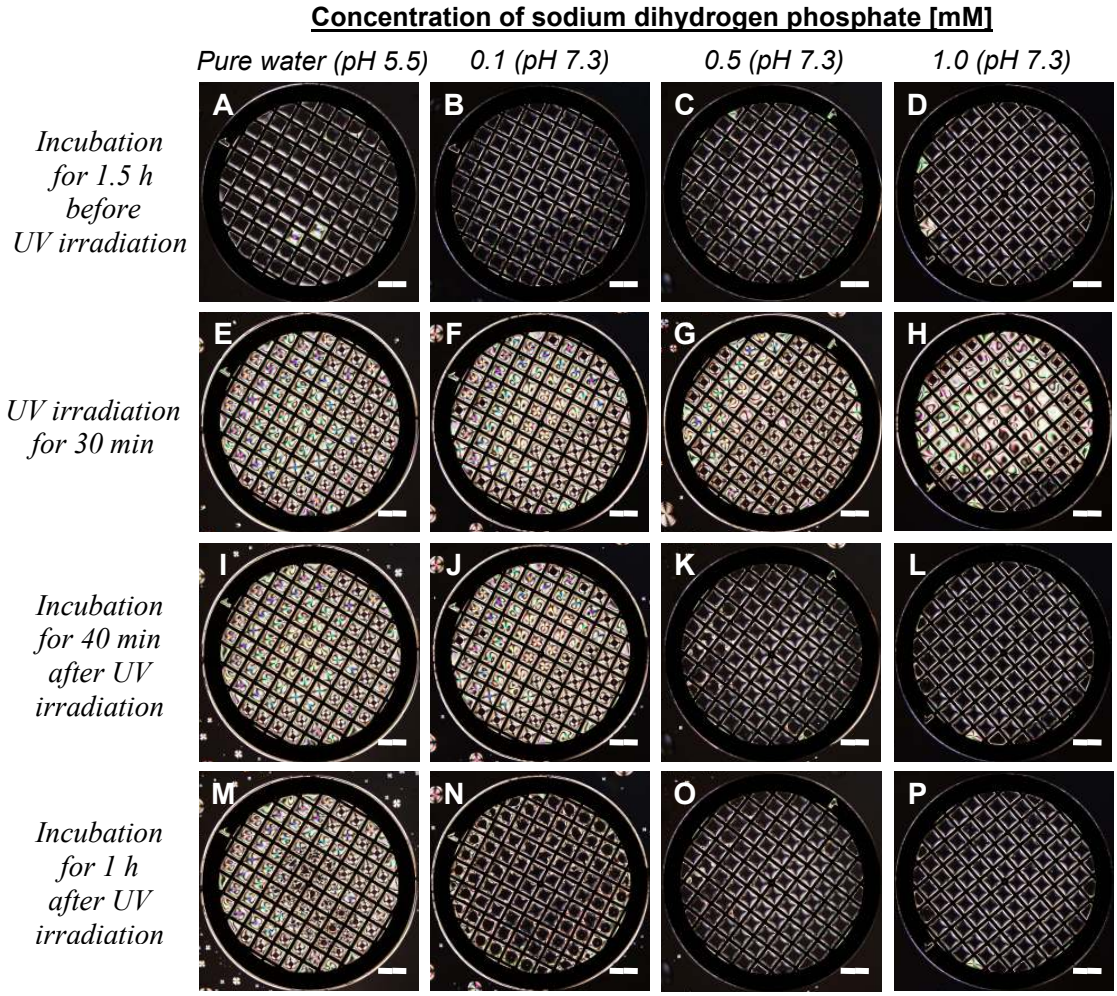

Figure 4.27: Optical images of 5CB containing 0.8 vol% oleic acid between crossed polarisers with buffer solutions containing 0.1 vol% Darocur 1173 at around pH 7 according to various ionic strengths. Figures in parenthesis refer to the actual pH values of the buffer solutions. UV irradiation was performed using the UV curing lamp (Agar Scientific) for 30 min. All scale bars represent 400 μm.

This tendency is the same at pH 8 (Figure 4.28) with different ionic strengths.

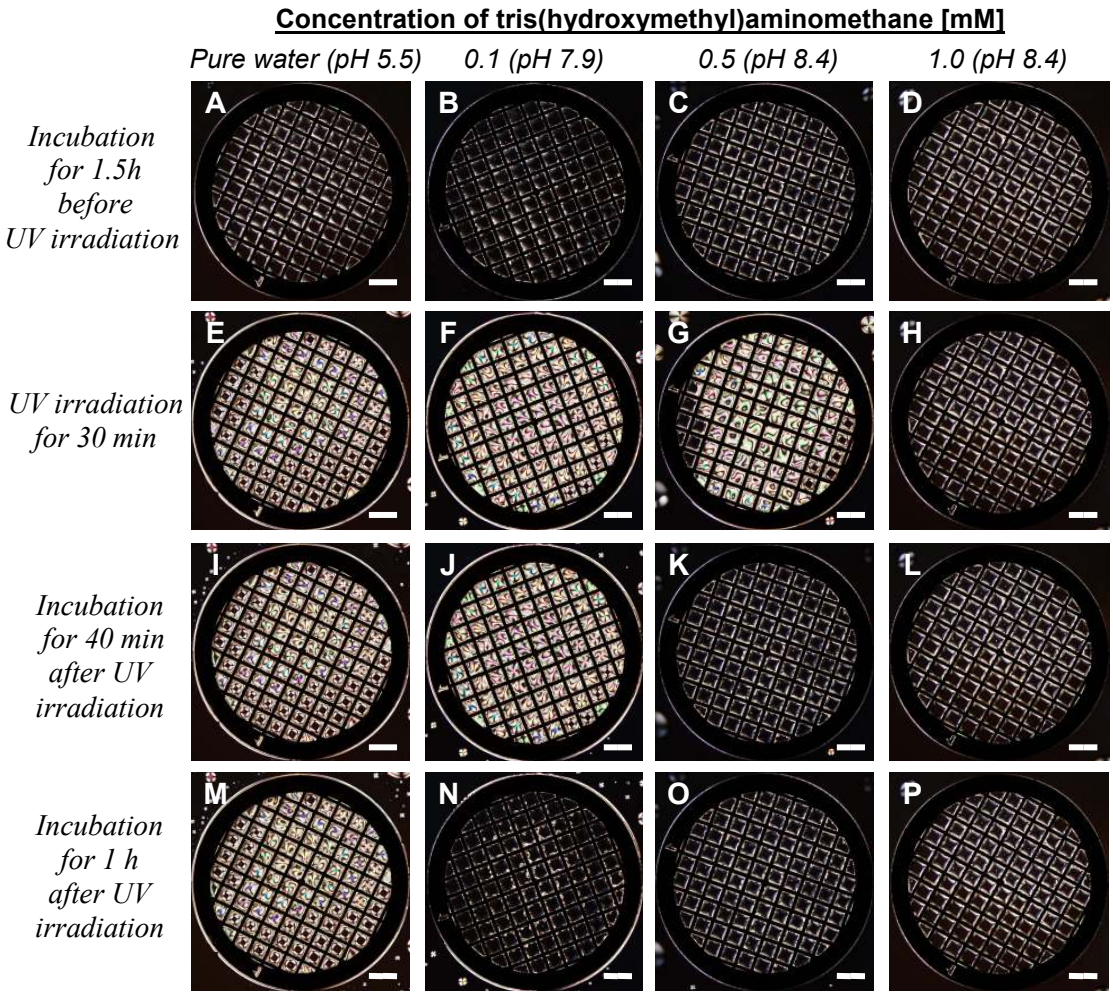

Figure 4.28: Optical images of 5CB containing 0.8 vol% oleic acid between crossed polarisers after incubation with buffer solutions containing 0.1 vol% Darocur 1173 at around pH 8 with various ionic strengths. Figures in parenthesis refer to the actual pH values of buffer solutions. UV irradiation was performed using the UV curing lamp (Agar Scientific) for 30 min. All scale bars represent 400 μm.

The homeotropic anchoring of 5CB in Figure 4.24T after UV irradiation might have resulted from the fast desorption of polymerised oleic acid/oleate and adsorption of oleic acid/oleate at high ionic strength (1 mM) and high pH (pH 8.8). Hence, we did not observe the UV triggered planar anchoring of 5CB after UV irradiation at the condition. Figure 4.29 shows another example to prove this proposition. 5CB and oleic acid mixture confined in the EM grid shows a homeotropic anchoring of 5CB in 1.0 mM aqueous solution pH 8.8 after UV irradiation (Figure 4.29H). The samples were washed with pure water to remove the polymerised oleic acid/oleate layer from the

interface and re-establish oleic acid/oleate monolayer at the interface. Finally, after the second UV irradiation we observed the UV triggered planar anchoring of 5CB in all LC cell samples (Figure 4.29N, O, and P) corresponding to that shown in pure water (Figure 4.29A) and the induced planar anchoring of 5CB was maintained for > 1 h.

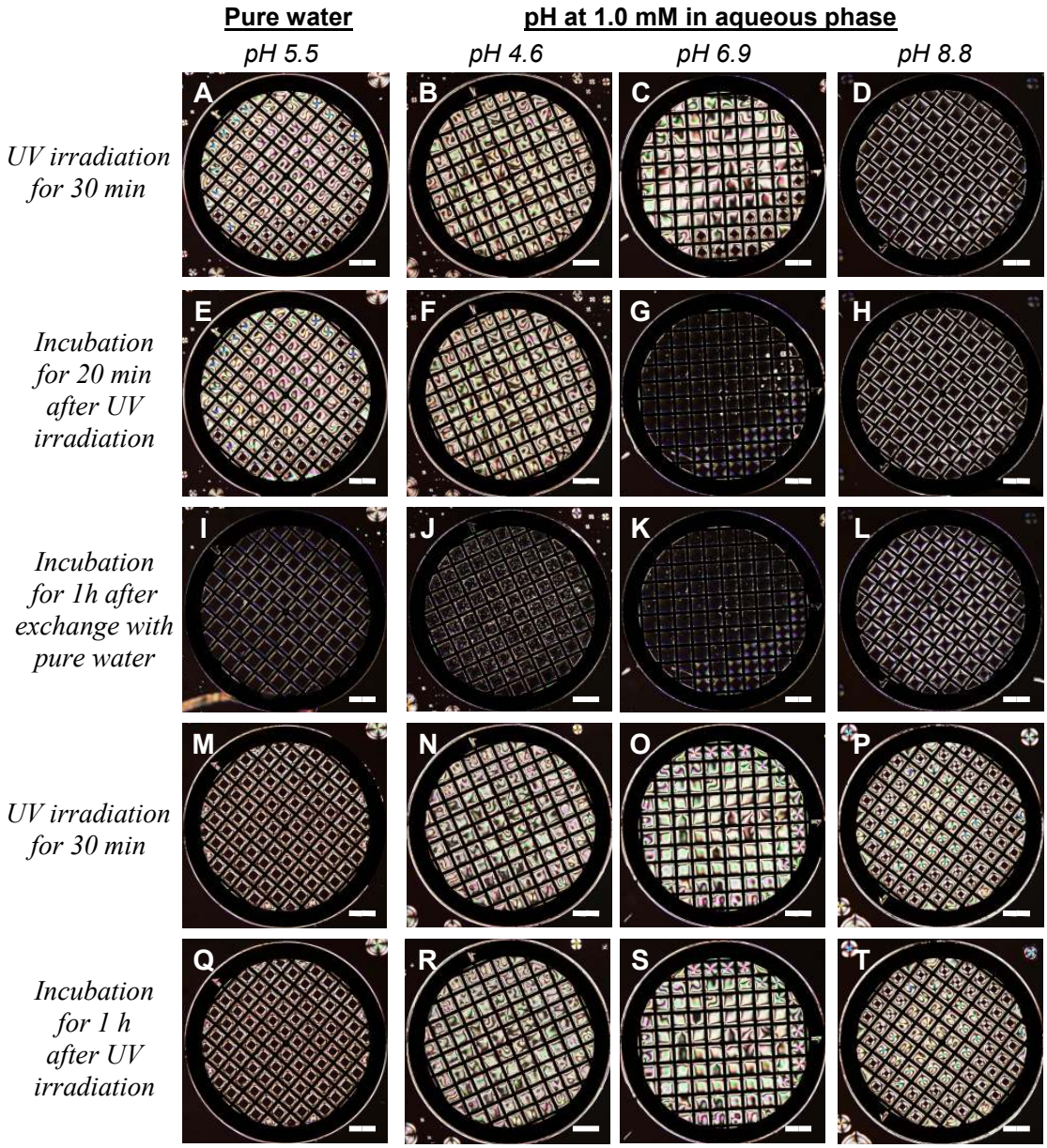

Figure 4.29: Optical images of 5CB containing 0.8 vol% oleic acid between crossed polarisers after incubation with in 1.0 mM buffer solutions containing 0.1 vol% Darocur 1173 at various pH values. UV irradiation was performed using the UV curing lamp (Agar Scientific) for 30 min. All scale bars represent 400 μm.

This result reflects the effect of ionic strength and pH of an aqueous phase on desorption of polymerised oleic acid/oleate from the LC-water interface and adsorption of oleic acid/oleate from 5CB and aqueous phases to the interface.

As shown in Figure 4.29H, 0.8 vol% oleic acid in 5CB does not make a UV triggered planar anchoring of 5CB at 1 mM, pH 8. However, a higher UV radiation energy produced by a twice UV irradiation can trigger the transition of anchoring of 5CB from homeotropic to planar anchoring at a higher ionic strength and pH 8 conditions (Figure 4.30).

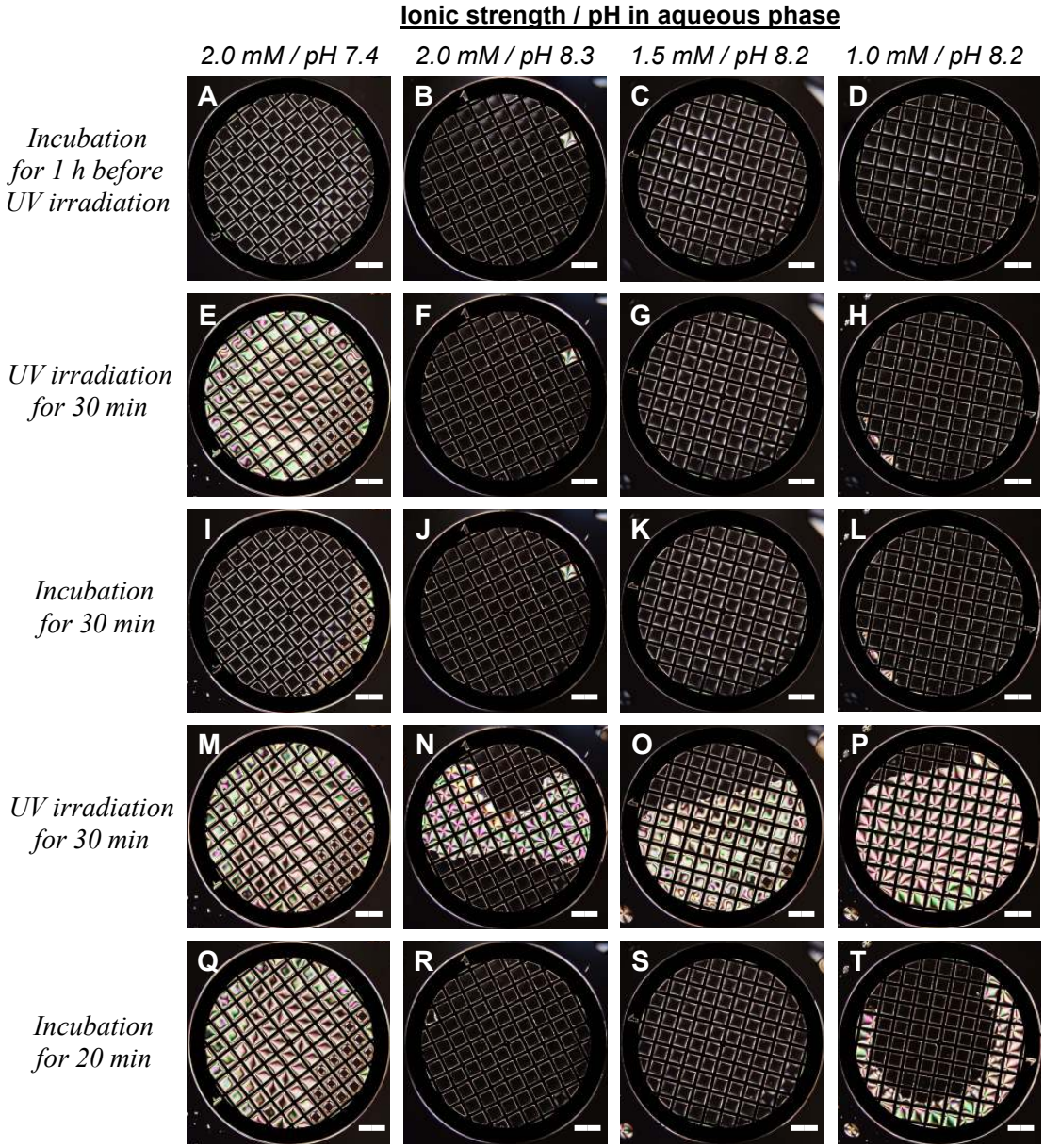

Figure 4.30: Optical images of 5CB containing 0.8 vol% oleic acid between crossed polarisers after incubation with buffer solutions containing 0.1 vol% Darocur 1173 at various pH and ionic strengths. UV irradiation was performed using the UV curing lamp (Agar Scientific) for 30 min. All scale bars represent 400 μm.

We also examined the effect of the concentration of oleic acid in 5CB on the anchoring of 5CB at high ionic strength and high pH (at 2 mM, pH 8). In 2 mM aqueous solution at pH 8.3, 0.5 vol% oleic acid triggered the transition of anchoring of 5CB from homeotropic to planar anchoring by UV irradiation (Figure 4.31E). The result is similar to the optical response of 5CB at 0.8 vol% oleic acid in an aqueous solution 2 mM at pH 7.4 (Figure 4.30E). However, at higher concentrations of oleic acid (> 0.5 % vol) the LC optical cell needs a higher UV radiation energy to induce the transition of anchoring of 5CB at the same conditions.

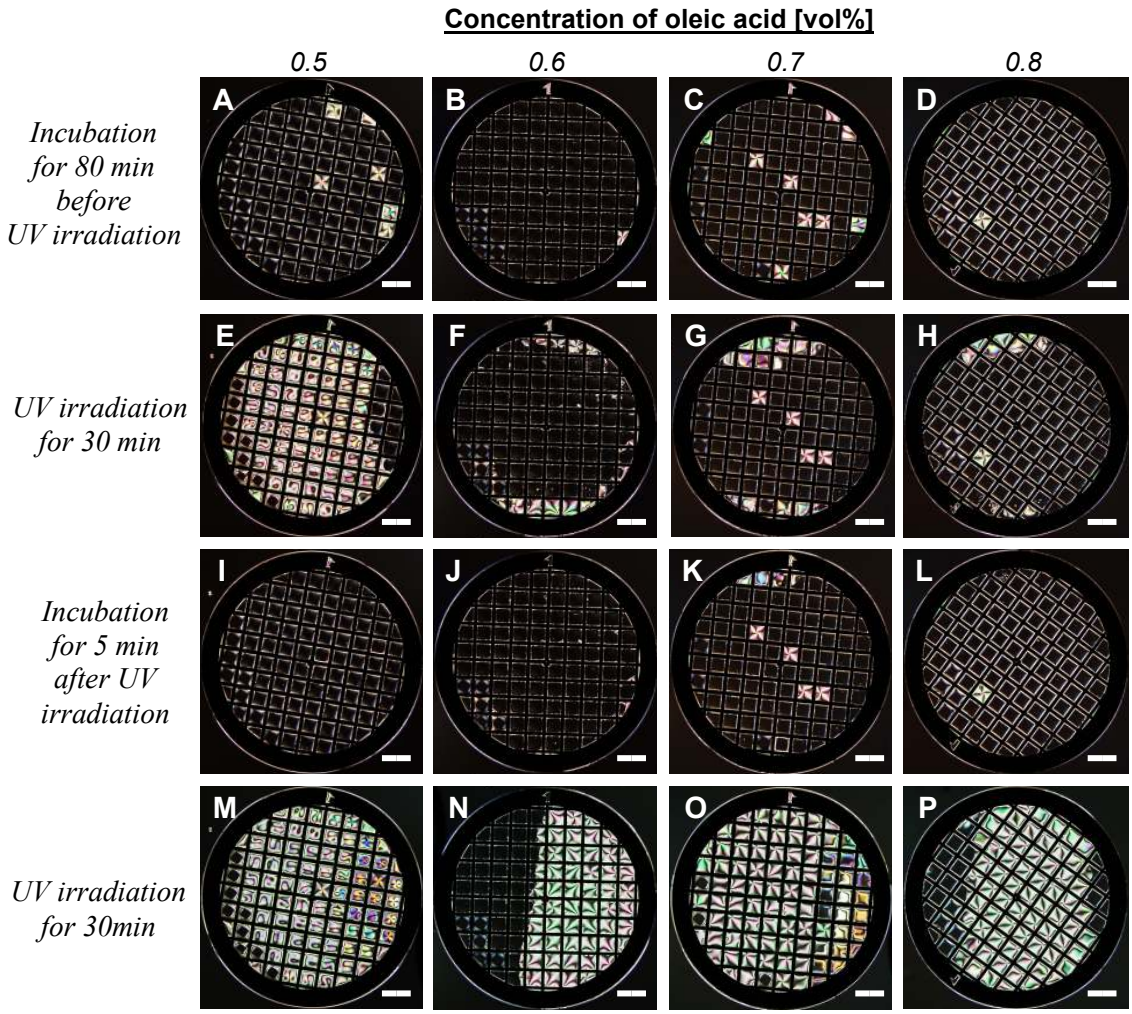

Figure 4.31: Optical images of 5CB containing various concentrations of oleic acid between crossed polarisers after incubation with 2 mM Tris buffer solution pH 8.3 containing 0.1 vol% Darocur 1173. UV irradiation was performed using the UV curing lamp (Agar Scientific) for 30 min. All scale bars represent 400 μm.

We further investigated the dependence of anchoring of 5CB on the concentration of oleic acid according to pH at a fixed 2 mM ionic strength (Figure 4.32). We note that the amount of polymerised oleic acid/oleate layer at the LC-water interface is very

important to the anchoring of 5CB at the interface. At higher concentrations of oleic acid in 5CB, more oleic acid/oleate molecules might quickly re-adsorb at the LC-water interface after UV triggered desorption of polymerised oleic acid/oleate layer from the interface than at lower oleic acid concentrations in 5CB. Thus, at lower concentrations of oleic acid in 5CB, UV triggered planar anchoring of 5CB is maintained for longer than at higher concentrations.

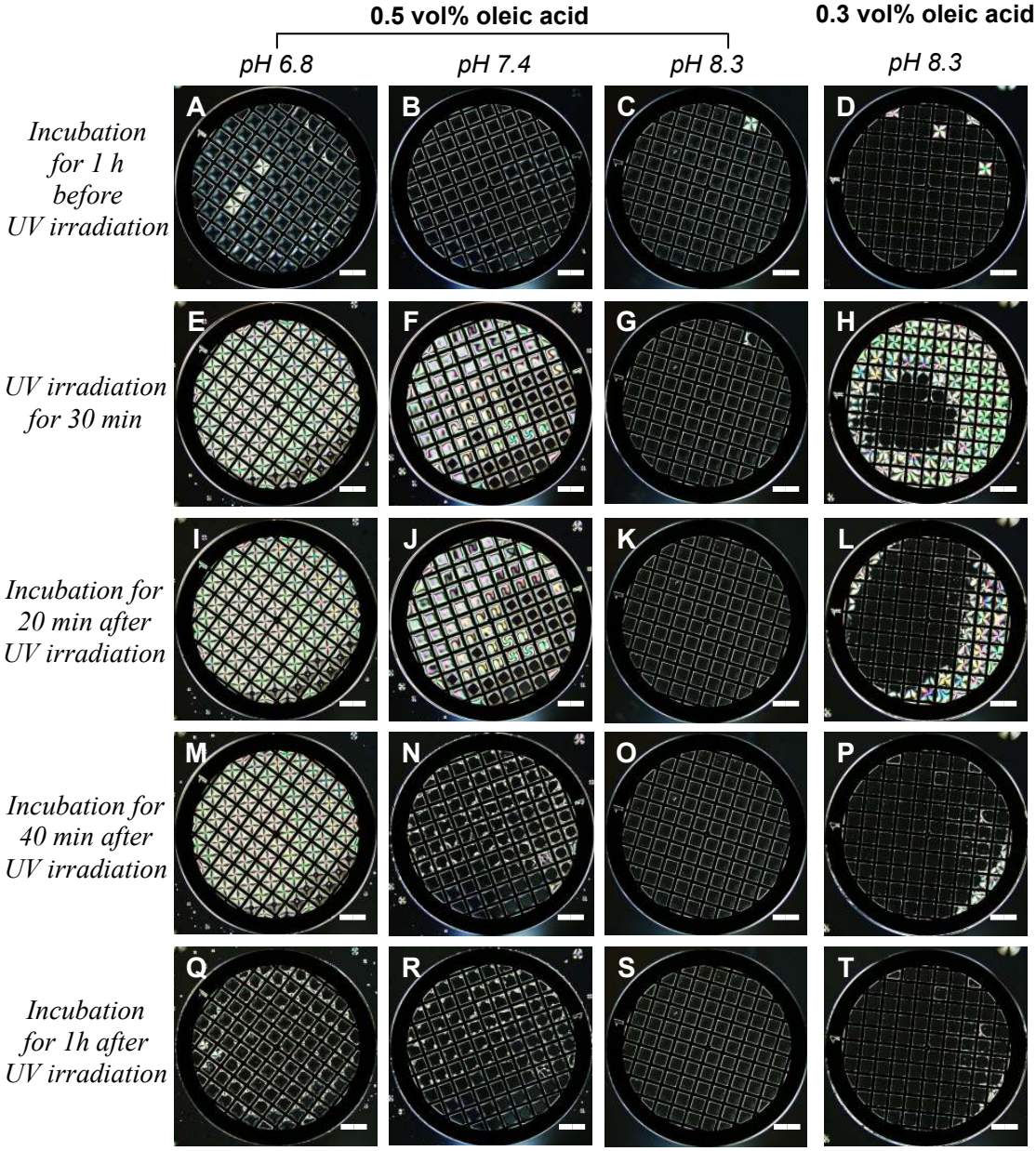

Figure 4.32: Optical images of 5CB containing various concentrations of oleic acid between crossed polarisers after incubation with 2 mM buffer solutions at various pH values. UV irradiation was performed using the UV curing lamp (Agar Scientific) for 30 min. All scale bars represent 400 μm.

4.4.3.3 Summary

From the results presented in the previous sections, three major patterns of anchoring of 5CB at the LC-water interface emerge, which are summarised as shown in Figure 4.33.

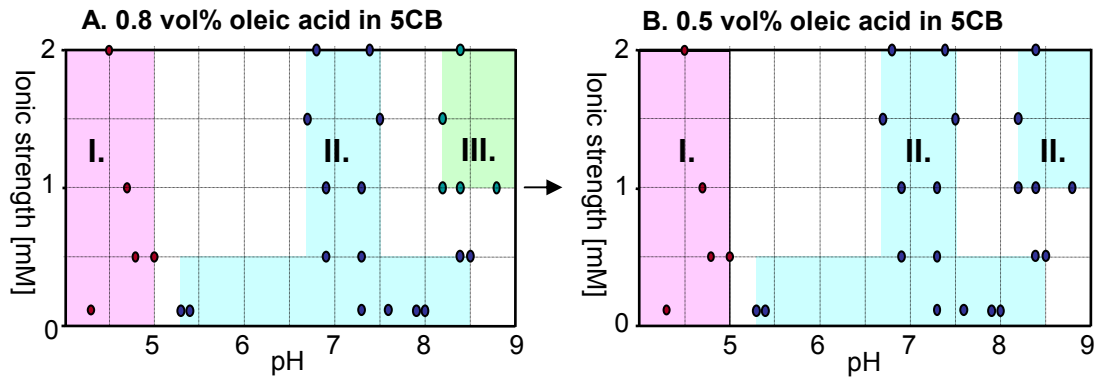

. No adsorption of the oleic acid/oleate at the LC-water interface.
. Adsorption, polymerisation and desorption of oleic acid/oleate at the LC-water interface.
. Adsorption, polymerisation and desorption/fast re-adsorption of oleic acid/oleate at the LC-water interface.

Figure 4.33: Summary of the variation with pH and ionic strength of the adsorption and polymerisation behaviour of systems containing oleic acid added initially to the 5CB phase contacted with aqueous phases containing 0.1 vol% Darocur 1173. In regions *III*, the interfacial behaviour is similar to that in region *II* except for the fast reversal of the UV triggered planar anchoring of 5CB at the LC-water interface (less than 10 min).

In region *I* (at low pH) the optical texture of 5CB remains planar anchoring regardless of the concentration of oleic acid in 5CB, ionic strength, and UV irradiation. This means that there is not enough adsorption of oleic acid/oleate species to induce homeotropic anchoring of 5CB at the LC-water interface by a full protonation of oleic acid. In region *II* (intermediate pH and particularly low ionic strength), homeotropic anchoring of 5CB is observed by the adsorption of oleic acid/oleate species and UV irradiation causes a planar anchoring of 5CB. Moreover, this planar anchoring triggered by the polymerised monolayer reverts back to homeotropic anchoring slowly (1–4 h). It appears that the maximum stability of the planar anchoring of 5CB induced by the polymerised film occurs at intermediate pH where the adsorbed film is likely to be a mixture of oleic acid/oleate species. This happens when the pH of the aqueous phase is not high enough to produce an excess of non-adsorbed oleate ions capable of displacing the polymerised layer or to sufficiently ionise the polymerised film and render it

hydrophilic and capable of rapid desorption. The high pH of region *III* presumably enables either the formation of sufficient excess of oleate ions or the ionization of the polymerised layer so as to cause the polymerised layer to be either displaced or desorbed and cause the texture to revert from planar to homeotropic anchoring. The polymerised film is likely to be desorbed faster at higher initial concentration of oleic acid because the Region *III* at 0.8 vol% oleic acid transfers to Region *II* at 0.5 vol% oleic acid in 5CB.

4.5 Preparation of prototype UV sensor

In all of the experiments described above, the UV triggered planar anchoring of 5CB is reverted back to homeotropic after a few hours of incubation. Hence, the time stability of the planar anchoring texture needs to be increased for detecting the amount of exposure to UV radiation. In this section we describe the enhanced time stability of UV triggered planar textures of 5CB in oleic acid/oleate system by the addition of a cross-linker and the temperature dependence of UV induced transition of anchoring of 5CB during UV irradiation periods. We also developed a simple UV sensor for UV radiation based on the UV triggered polymerisation and resultant optical texture change from homeotropic to planar anchoring.

4.5.1 Anchoring of 5CB by cross-linked oleic acid/oleate species

For the systems containing polymerisable surfactants adsorbed at the LC-water interface it was observed that UV triggered planar anchoring of 5CB was reverted to the homeotropic after incubation for several hours. We investigated the effect of a cross-linker divinylbenzene (DVB) to inhibit the reversibility of UV triggered planar anchoring of 5CB to homeotropic in order to make a permanent UV sensor. DVB is an extremely versatile cross-linking agent that also improves polymer properties. It is used in the synthesis and manufacture of many resins, plastics, composites, and latexes used in coatings. Effective in small amounts, DVB can increase physical strength properties (hardness, tensile strength, and impact resistance) without hindering other properties. [15, 16] We expected to determine whether insoluble, infusible copolymers could be obtained, in order to produce films which retain the alignment of 5CB and sustain after long incubation and washing with pure water.

DVB was mixed together with 0.8 vol% oleic acid in 5CB phase at various mixing ratios and these premixtures were placed in EM grids. As shown in Figure 4.34, DVB inhibited the optical transition reversal of 5CB from planar to homeotropic anchoring at 0.1 vol% for 1 h incubation after UV irradiation. The UV triggered planar anchoring of 5CB was also retained after further long time incubation (≥ 7 h) above 0.1 vol% DVB. For 0.3 vol% DVB, no transition of the planar texture back to the homeotropic texture was seen after incubation for longer than one day.

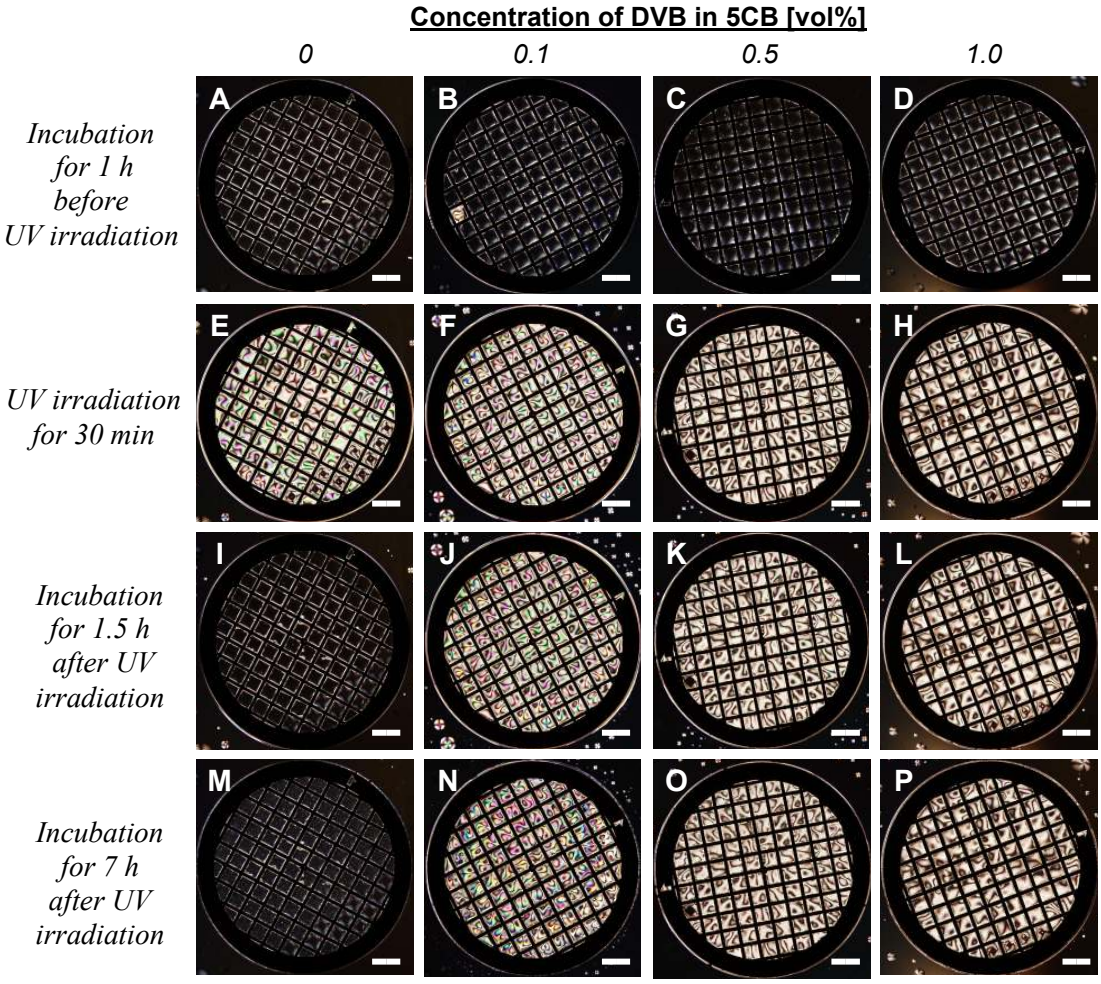

Figure 4.34: Optical images of 5CB containing 0.8 vol% oleic acid and various concentrations of cross-linker divinyl benzene (DVB) between crossed polarisers after incubation with an aqueous solution containing 0.1 vol% Darocur 1173 (pH ~5.5). UV irradiation was performed using the UV curing lamp (Agar Scientific) for 30 min. All scale bars represent 400 μm.

DVB is expected to prevent the desorption of polymerised oleic acid/oleate layer and the re-adsorption of oleic acid/oleate species after UV irradiation even at high ionic strength and pH conditions (Region *III* mentioned in section 4.4.3.3). As previously

shown in Figure 4.31H, at 0.8 vol% oleic acid the UV triggered planar anchoring of 5CB is very quickly reverted to homeotropic at high ionic strength and high pH (2 mM, pH 8.3). However, by addition of 0.5 vol% DVB the UV triggered planar anchoring of 5CB was maintained for > 2 h at the same condition (Figure 4.35G). From the results it proposes that we can capture the alignment of 5CB to detect the amount of UV radiation at the time of UV irradiation. We also confirmed that an unsaturated oleic acid can be copolymerised readily with a highly reactive unsaturated vinyl monomer (e.g., DVB) although it is obvious that oleic acid is much less reactive than homologous, short chain compounds.

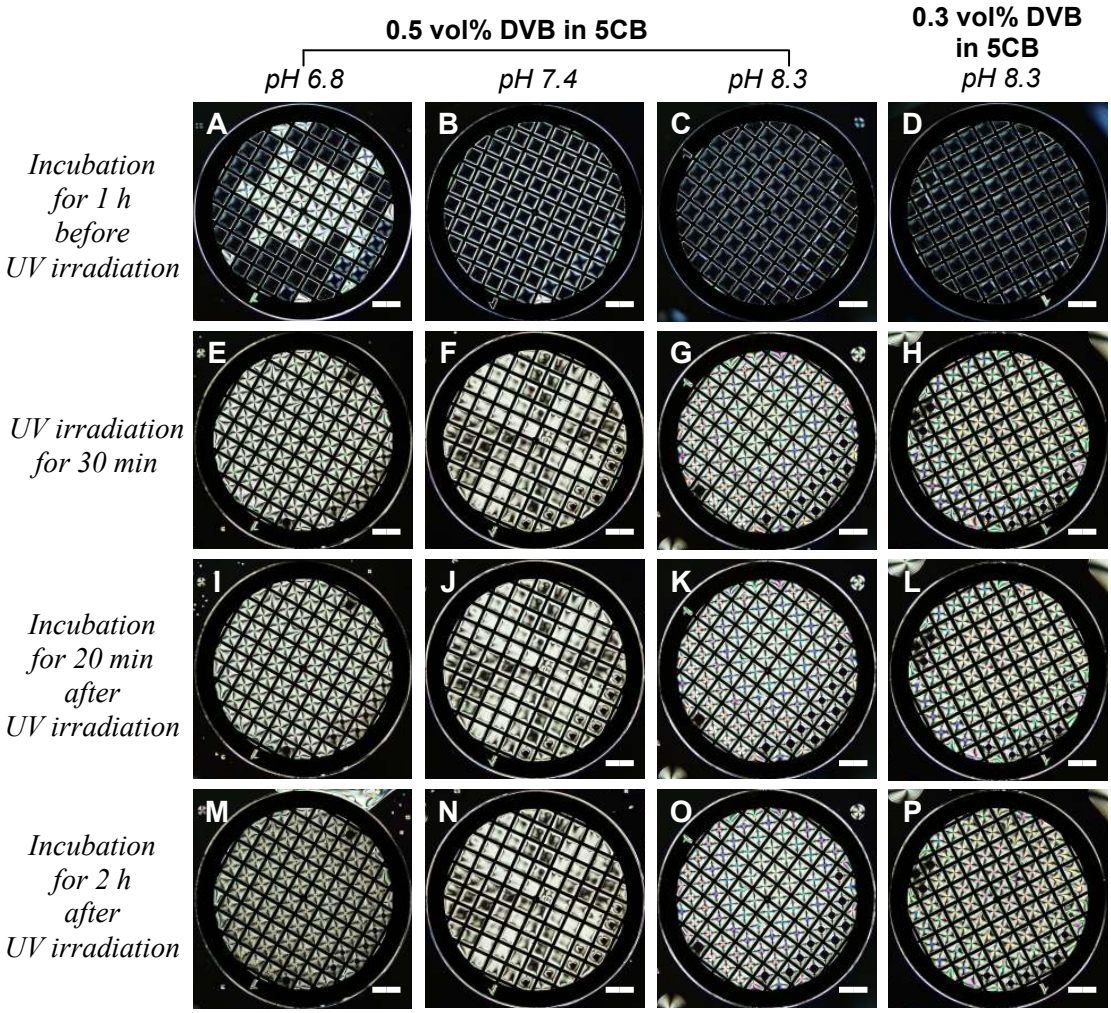

Figure 4.35: Optical images of 5CB containing 0.8 vol% oleic acid and various concentrations of DVB between crossed polarisers after incubation with 2 mM various pH buffer solutions. UV irradiation was performed using the UV curing lamp (Agar Scientific) for 30 min. All scale bars represent 400 μm.

It was also checked that addition of either DVB or Darocur 1173 at their highest concentrations used here (up to 0.5 and 0.1 vol% for DVB and Darocur 1173

respectively) did not produce a change in the anchoring of 5CB from planar to homeotropic (Figure 4.36).

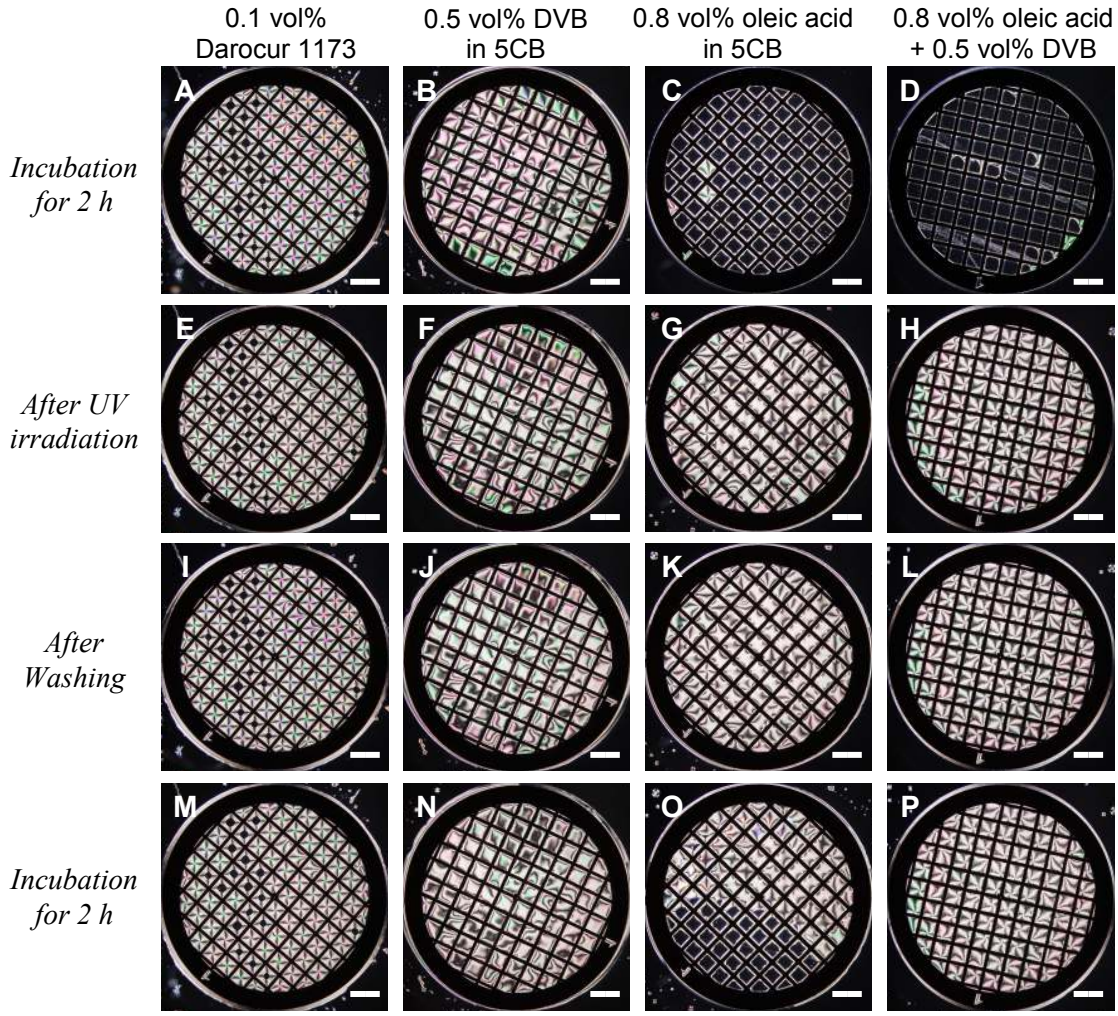

Figure 4.36: Optical images of 5CB containing 0.8 vol% oleic acid and 0.5 vol% DVB between crossed polarisers after incubation with an aqueous solution with 0.1 vol% Darocur 1173. UV irradiation was performed using the UV curing lamp (Agar Scientific) for 30 min. The chambers were washed with 4 perfusion chamber volumes of pure water. All scale bars represent 400 μm.

4.5.2 Effect of temperature on the UV polymerisation of an adsorbed oleic acid/oleate and DVB mixtures at the LC-water interface

As discussed in the section 4.4.1, the addition of solutes (e.g., oleic acid and DVB) into 5CB decreases the nematic-isotropic transition temperature (T_{NI}) of 5CB. We investigated the effect of temperature on the LC optical textures observed during adsorption and polymerisation of oleic acid/oleate and DVB complex at the LC-water

interface. The adsorption of oleic acid/oleate species at the LC-water interface is fluctuated by changing the order of 5CB above T_{NI} of the 5CB (pure 5CB: 36 °C; 5CB containing 1.0 vol% oleic acid: ~34 °C). If UV triggered planar anchoring of 5CB is not reverted to homeotropic above T_{NI}, this experimental system could be used as a UV sensor at various temperature conditions (e.g., summer daytime at 40 °C).

As shown in Figure 4.37, 5CB which was mixed with oleic acid and DVB contacted with an aqueous phase containing Darocur 1173 showed a homeotropic anchoring texture (Figure 4.37A-D) at room temperature. When the UV sensors were heated to ~30 °C the UV triggered planar anchoring of the 5CB in the EM grids disappeared (no optical signal between crossed polarisers) due to the transition of the nematic phase of 5CB to the isotropic in EM grids. It means that the T_{NI} of the 5CB was decreased from 36 to ~30 °C by adding of 0.8 vol% oleic acid and 0.5 vol% DVB into 5CB. However, the original UV triggered planar anchoring of the 5CB returned when the sensors were cooled down to room temperature again (Figure 4.37M, O). These results lead us to propose that if the oleic acid/oleate adsorbed layer is cross-linked with DVB at the LC-water interface once, it still adsorbs at the interface and memorise the UV triggered planar anchoring of 5CB in spite of heating above the T_{NI} of 5CB (~30 °C) after further long time incubation ($\geq$ 2 h) (Figure 4.37O).

We also investigated the effect of the temperature during UV irradiation on the anchoring of 5CB at various temperatures (e.g., UV radiation in summer season). The 5CB-oleic acid system was equilibrated at various temperatures ranging from 5 to 40 °C before UV irradiation. After UV irradiation at the equilibrated temperature the UV sensors were incubated at room temperature for imaging optical response of 5CB. At 5 °C, the optical texture of the 5CB appears to be different from that observed at room temperature (Figure 3.38A-D.). As the sensors were cooled down to 10 °C, a mixed homeotropic and nonuniform planar anchoring of 5CB were consistently observed in EM grids. This optical texture of 5CB may be explained by the crystallisation of 5CB and the low solubility of oleic acid in water phase at low temperature. This inhomogeneous anchoring of 5CB was fully transformed uniform planar anchoring after UV irradiation at the temperatures (Figure 3.38E and G).

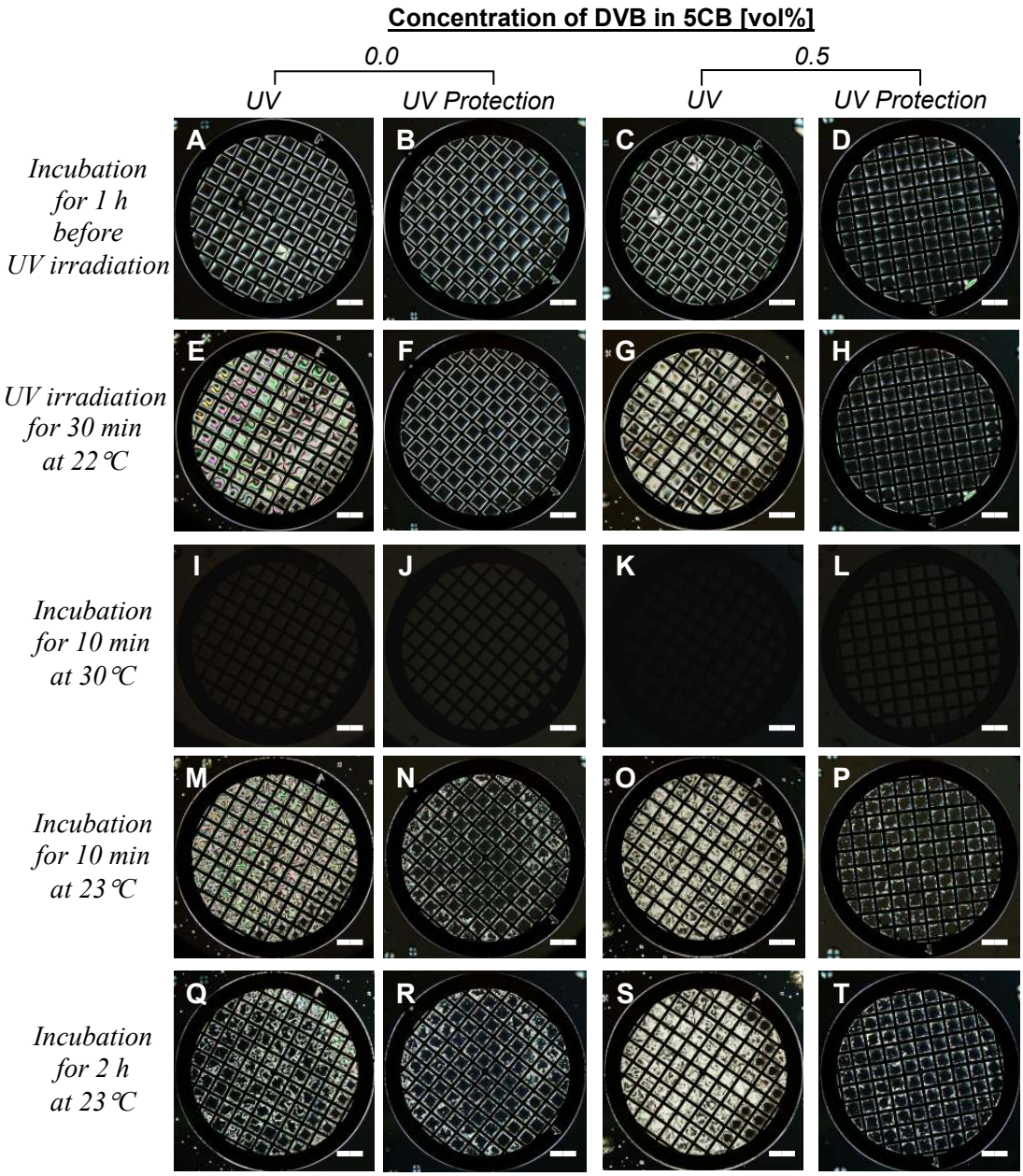

Figure 4.37: Optical images of 5CB containing 0.8 vol% oleic acid and various concentrations of DVB between crossed polarisers after incubation with an aqueous solution containing 0.1 vol% Darocur 1173. The sensors were irradiated using the UV curing lamp (Agar Scientific) for 30 min at 22 °C, then heated up to 30 °C and finally cooled down to 23 °C. For images I-L, the dark colour corresponds to the isotropic phase of 5CB at 30 °C. All scale bars represent 400 μm.

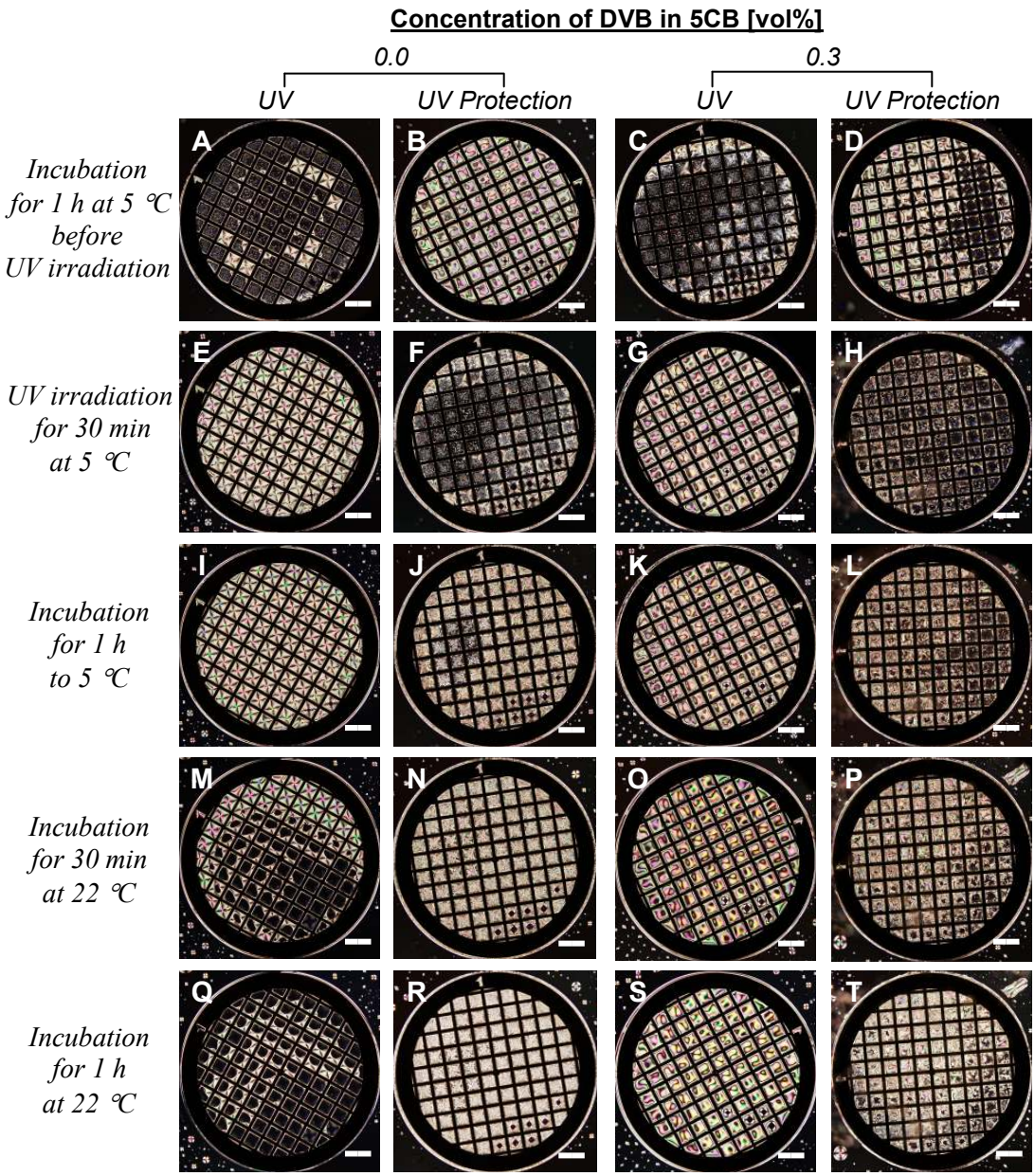

Figure 4.38: Optical images of 5CB containing 0.8 vol% oleic acid and various concentrations of DVB between crossed polarisers after incubation with an aqueous solution containing 0.1 vol% Darocur 1173 at 5 °C. The sensors were irradiated using the UV curing lamp (Agar Scientific) for 30 min at 5 °C and then equilibrated at 22 °C. All scale bars represent 400 μm.

Raising the temperature of UV sensors to 40 °C causes the transition of 5CB from nematic to isotropic phase and all the spaces of the EM grids appear dark (i.e. no optical signal) between crossed polarisers (Figure 4.39A-D). After UV irradiation at 40 °C and then equilibration at 22 °C, the anchoring texture of 5CB was same as that observed after UV irradiation at room temperature (Figure 4.39I and K). The UV triggered planar

anchoring of 5CB was only maintained in the sensor containing DVB (Figure 4.39O) after a longer incubation (> 1.5 h).

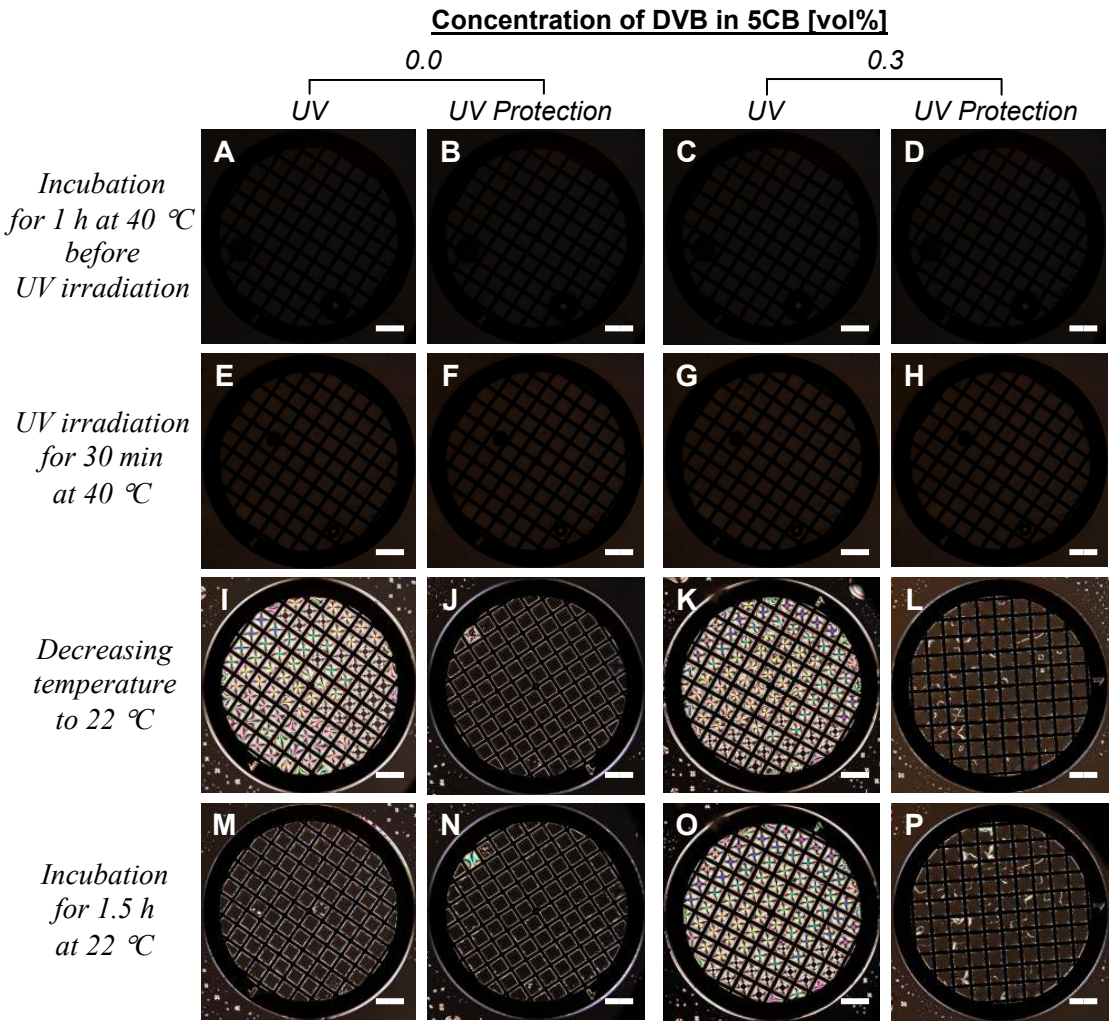

Figure 4.39: Optical images of 5CB containing 0.8 vol% oleic acid and 0.3 vol% DVB between crossed polarisers after incubation with an aqueous solution containing 0.1 vol% Darocur 1173 at 40 °C. The sensors were irradiated using the UV curing lamp (Agar Scientific) for 30 min at 40 °C, then cooled down to 22 °C. All scale bars represent 400 μm. For images A-H, the dark colour corresponds to the isotropic phase of 5CB at 40 °C. All scale bars represent 400 μm.

We also observed similar optical response of 5CB at 10 and 35 °C conditions followed by the same procedure used for 5 and 40 °C (Figure 4.40).

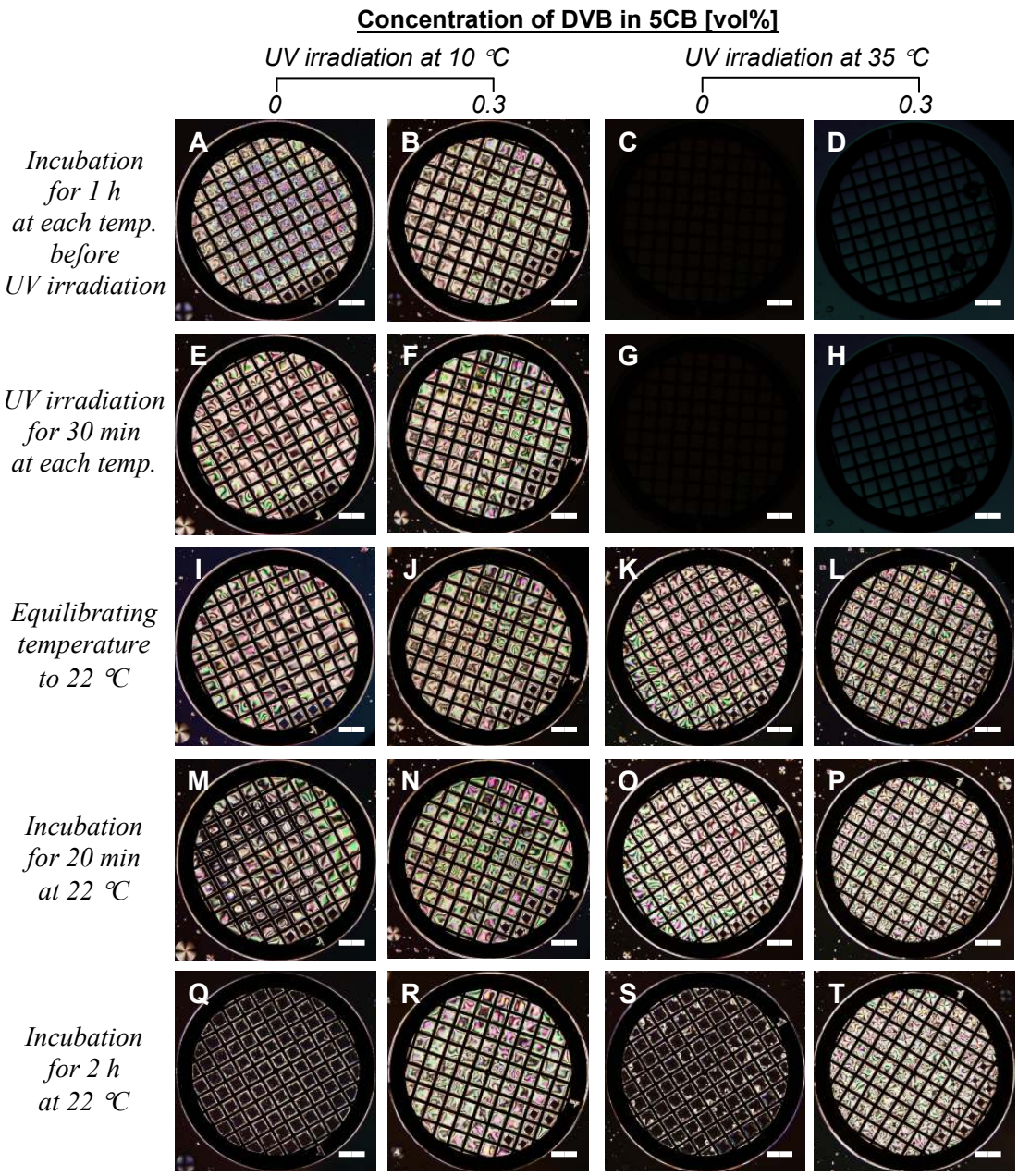

Figure 4.40: Optical images of 5CB containing 0.8 vol% oleic acid and 0.3 vol% DVB between crossed polarisers after incubation with an aqueous solution containing 0.1 vol% Darocur 1173 at 10 and 35 °C. The sensors were irradiated using the UV curing lamp (Agar Scientific) for 30 min at interest temperatures, and then adjusted to 22 °C. All scale bars represent 400 μm.

From this set of experiments we conclude that the textures and stabilities of the polymerised oleic acid/oleate and DVB film at 22 °C are independent of the temperature at which sensors are incubated and UV irradiated. Thus, 5CB in EM grids can detect UV radiation in either at a crystalline or isotropic liquid state.

4.5.3 Possible UV sensor visible to the naked eye

The UV triggered polymerisation and resultant optical texture change of 5CB from homeotropic to planar anchoring forms the basis of a simple sensor for UV radiation. For applications such as avoiding sunburn and risk of skin cancer, we envisage that such a sensor might take the form of a skin adhesive patch in which the sensor response would need to be visible to the naked eye. From this background we mounted a 5CB-filled EM grid into a perfusion chamber which was sandwiched between crossed plastic film polarisers (Agar Scientific, Essex). The EM grids used here had a larger grid inner length of 423 μm which was found to improve visibility than a smaller grid (261 μm) used before. The images in Figure 4.41 show the appearance in normal ambient lighting of a control grid which was not exposed to UV (Figure 4.41C) and an identical grid exposed to UV radiation for 10 min by using UV curing lamp (Figure 4.41G). The optical images between crossed polarisers under a microscope are exactly matched with the digital camera images of the prototype under ambient lighting conditions.

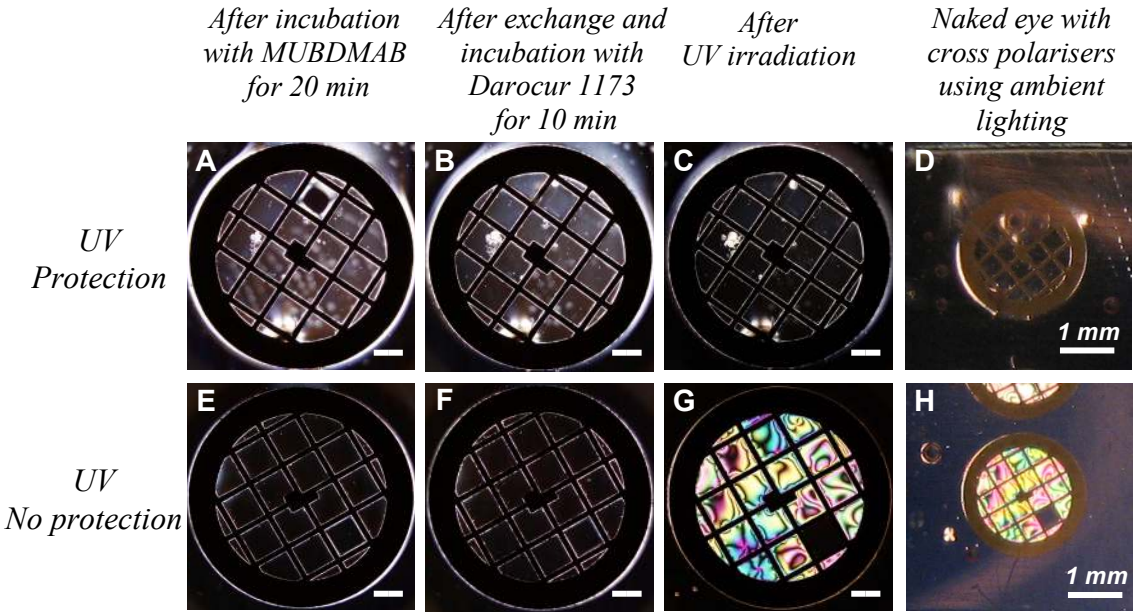

Figure 4.41: Optical images of 5CB between crossed polarisers after incubation with an aqueous solution containing 1.2 mM MUBDMAB and 0.1 vol% Darocur 1173. UV irradiation was performed using UV curing lamp (Agar Scientific) for 10 min. The perfusion chamber in (A) was covered with aluminum foil during UV irradiation. All scale bars represent 400 μm. Optical images (D and H) were captured using a digital camera (Canon IXUS 750). For image G, the black square in the grid corresponds to a square which was empty of 5CB.

To convert the intensity of UV radiation to induce a transition from homeotropic to planar anchoring of 5CB to UV index units we measured a UV index units using a Maplin UV meter (code N11FT) as a function of the distance between a UV lamp and the detector.

The UV light intensity from the wand tip of SpotCure lamp (UVP) located 20 mm above the LC optical cell was also estimated to be about 41 UV index units by extrapolating to the distance used for UV irradiation [UV index = 163.97 × $(1/2^2)$ = 41] as shown in Figure 4.42.The UV intensity to trigger a transition of anchoring of 5CB in Figure 4.41 which is irradiated with the UV curing lamp (Agar Scientific) located 30 mm above a UV sensor is measured to be about 1.75 UV index units. The UV index corresponds to the average intensity over the wavelength range 280–400 nm weighted by erythemal weighting factor. On this scale, a UV index of 10 corresponds approximately to the UV intensity from the sun at mid-day in summer time on a cloudless day.[17] In some cities near equator (e.g., Hong Kong), the UV light intensity goes up to ~300 mW/m^2 (UV index 12–13) at noon during the summer season.[18] Hence, the UV irradiation conditions used in this work span the range of intensities relevant to potential UV sensor usage condition.

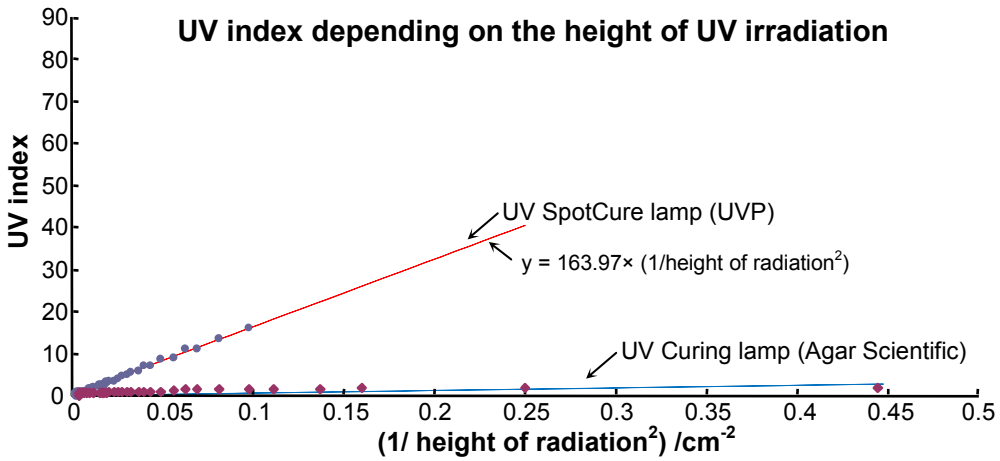

Figure 4.42: Relationship of the distance between UV sources and Maplin UV meter with UV index. UV index at 20 mm distance from UV SpotCure lamp (UVP) is extrapolated using the fitted graph equation [UV index = 163.97 × (1/height of radiation^2)].

The response of the LC sensing system to the UV doses is clearly visible to the naked eye without any special lighting requirement (e.g., back lighting). Moreover, the combination of polymerisable surfactant and a cross-linker could provide dual usability of a UV sensor such as: (i) a reusable (e.g., only polymerisable surfactant) and (ii) an

accumulative type (e.g., polymerisable surfactant and cross-linker). Although it remains to be seen whether fabrication, storage stability, UV dose, wavelength response, cost, ease-of-use, and other considerations could be optimized to yield a marketable device, we consider that the systems described here offer an approach towards a cheap device capable of signalling and avoiding over-exposure to potentially harmful UV radiation.

4.6 Conclusions

In this chapter we show that the planar-homeotropic transition can be induced by the adsorption of various UV polymerisable surfactants and that, in some cases, UV polymerisation of the adsorbed polymerised monolayer triggers a homeotropic-planar transition.

The main conclusions from this chapter are:

- It can be seen that the adsorption of polymerisable surfactants with a sufficient hydrophobic chain length from either the water or 5CB phase to the LC-water interface triggers a change from planar to homeotropic anchoring as seen in already published results.[10]
- UV polymerisation of an adsorbed monolayer within the hydrophobic chain region results in a change from homeotropic to planar anchoring. Polymerisation within the hydrophilic head group region of the monolayer does not produce the anchoring transition.
- UV polymerisation triggered anchoring transition from homeotropic to planar anchoring of 5CB occurs irrespectively of the presence of an excess non-adsorbed polymerisable surfactant present in the aqueous phase. This suggests that the anchoring transition of 5CB occurs directly within the adsorbed monolayer at the LC-water interface.
- The planar anchoring induced by the polymerised film slowly reverts back to homeotropic anchoring over some hours. The UV triggered planar anchoring can be sustained over a least a day by incorporation of a cross-linker during the polymerisation.
- Using masked irradiation, it is possible to reproduce mask shaped within the 5CB-water interface that is, “writing with light” on liquid surface.
- These experimental systems form the basis of a UV sensor device whose response is visible to the naked eye and which have potential applications in the signalling and avoidance of over-exposure to harmful UV radiation.

4.7 References

1. F. J. Barbero, G. López, and F. J. Batlles, "Determination of daily solar ultraviolet radiation using statistical models and artificial neural networks", *Ann. Geophys.* **2006**, *24*, 2105-2114.
2. *Ultraviolet (UV) electromagnetic spectrum*: http://www.windows.ucar.edu/ physical_science/magnetism/images/uv_spectrum_regions_big.gif. [Accessed 1 June 2007]
3. *Ultraviolet (UV) Radiation Protection and the Science of UV Exposure from the Sun and Sky*: http://chppm-www.apgea.army.mil/documents/FACT/25-008-0697.pdf [Accessed 15 July 2007]
4. R. McKenzie, D. Smale and M. Kotkamp, "Relationship between UVB and erythemally weighted radiation", *Photochem. Photobiol. Sci.* **2004**, *3*, 252-256.
5. S. Madronich, "Analytic formula for the clear-sky UV index", *Photochem. Photobiol. Sci.* **2007**, *83*, 1537-1538.
6. A. F. McKinlay and B. L. Diffey, "A reference action spectrum for ultraviolet induced erythema in human skin", In Human Exposure to Ultraviolet Radiation: Risks and Regulations, ed. W. R. Passchier and B. F. M. Bosnjakovic, Elsevier, Amsterdam **1987**, *83-87*.
7. M. H. Repacholi, "Global solar UV index", *Radiation Protection Dosimetry* **2000**, *91*, 307-311.
8. M. Li and K. Matyjaszewski, "Reverse atom transfer radical polymerisation in miniemulsion", *Macromolecules* **2003**, *36,* 6028-6035.
9. J. M. Brake, A. D. Mezera, and N. L. Abbott, "Effect of surfactant structure on the orientation of liquid crystals at aqueous-liquid crystal interface", *Langmuir* **2003**, *19*, 6436-6442.
10. J. M. Brake and N. L. Abbott, "An experimental system for imaging the reversible adsorption of amphiphiles at aqueous-liquid crystal interfaces", *Langmuir* **2002**, *18*, 6101-6109.
11. P. J. Collings and M. Hird, *Introduction to Liquid Crystals Chemistry and Physics*, Taylor & Francis, London, 1997.
12. V. Kitaev and E. Kumacheva, "Thin films of liquid crystals confined between crystalline surfaces", *J. Phys. Chem. B* **2000**, *104*, 8822-8829.

13. *Specification of Oleic acid from Cayman Chemicals*: http://www.caymanchem.com/pdfs/90260.pdf [Accessed 2 June 2007]
14. T-Y. Lim, J-L. Li, and B-H. Chen, "Solubilization of selected free fatty acids in palm oil by biodegradable ethoxylated surfactants", *J. Agric. Food Chem.* **2005**, *53***,** 4476-4483.
15. K. H. Park, R. J. Twieg, R. Ravikiran, L. F. Rhodes, R. A. Shick, D. Yankelevich, and A. Knoesen, "Synthesis and nonlinear-optical properties of vinyl-addition poly(norbornene)s", *Macromolecules* **2004**, *37*, 5163-5178.
16. K. Sunaga, M. Kim, K. Saito, and K. Sugita, "Characteristics of porous anion-exchange membranes prepared by cografting of glycidyl methacrylate with divinylbenzene", *Chem. Mater.* **1999,** *11,* 1986-1989.
17. WHO *Global Solar UV Index*, Publication WHO/S-DE/OEH/02.2, World Health Organization, Geneva, Switzerland, 2002, pp. 1-28.
18. *Hong Kong Observatory: Weather* Information (UV Index for Hong Kong): http://www.weather.gov.hk/wxinfo/uvindex/english/euvtodayminus1.htm [Accessed 15 July 2007]

Chapter 5

Designing Self-propelling Particles Using Stimuli-responsive Gels

Chapter 5

Designing Self-propelling Particles Using Stimuli-responsive Gels

5.1 Strategies to develop self-propelling hydrogel particles

Many applications for stimuli-responsive gels exhibiting abrupt volume phase transition in response to external stimuli have been explored for industrial and biomedical fields. One of the goals in these applications is to achieve a novel system in which a biomimetic intelligent gels sense environmental changes by themselves and go into action. If a self-cyclic reaction such as heartbeat and peristaltic motion in the digestive tract is achieved for gels, new possibilities will be created (e.g., a self-walking microactuator or a micropump with peristaltic motion like worms). In this chapter we present the attempts to prepare an "intelligent" hydrogel particle that undergoes an autonomous propelling in a liquid without or with reliance on an alternation in external conditions. The mechanical oscillations in these systems are expected to be driven by 1) the chemical energy of self-oscillation reaction, called the Belousov-Zhabotinsky reaction (BZ) in a closed system without external stimuli, or 2) an electric field in an electrolyte solution. The oscillating behaviour depends on the gel geometry because the volume oscillation is isotropic. Therefore, by changing the shape of the gel, the direction of mechanical motion could be changed. Moreover, the period of chemical oscillation and the velocity of the chemical waves can be controlled by changing the condition of the inner gel composition and the outer solution. Thus, if the anisotropic shaped microgels showing a very fast swelling–deswelling motion to spout out water into a liquid are prepared, a self-propelling actuator with a peristaltic motion like worms might be possible by using the gel. If such self-propelling is achieved for gels, new possibilities will be created, such as novel biomimetic intelligent materials exhibiting rhythmic drug release synchronised with cell cycles.

5.1.1 Self-oscillating hydrogels in the BZ and BR reaction solutions

In this section we describe the concepts and previous studies for the preparation of spontaneous mechanical oscillation of polymer gels by (1) setting up of an oscillatory

chemical reaction such as the BZ reaction within the gel, and (2) adsorbing electrolyte onto a gel network coupled with an electric field.

5.1.1.1 Self-oscillation of poly(NIPAAm-co-(Ru(bpy)$_3$) gel in the BZ reaction

Yoshida *et al.*[1, 2, 3] have developed a novel gel system in which swelling-deswelling change repeats autonomously and periodically in a closed solution without on-off switching of an external stimulus using the BZ reaction (Figure 5.1).

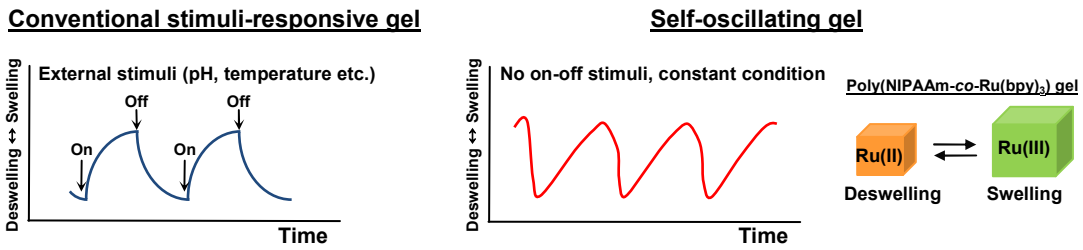

Figure 5.1: Conventional stimuli-responsive gel and novel self-oscillating gel.[2]

Such a system could show characteristic behaviour as if it were alive, similar to the beating of a heart muscle. In the BZ reaction, metal catalysts with higher redox potential, such as cerium ion, ferroin, or ruthenium tris(2,2´-bipyridine) [Ru(bpy)$_3$] are widely used. They prepared a copolymer gel of temperature-responsive *N*-isopropylacrylamide (NIPAAm) in which Ru(bpy)$_3$ is covalently bound to the polymer chain (Figure 5.2).

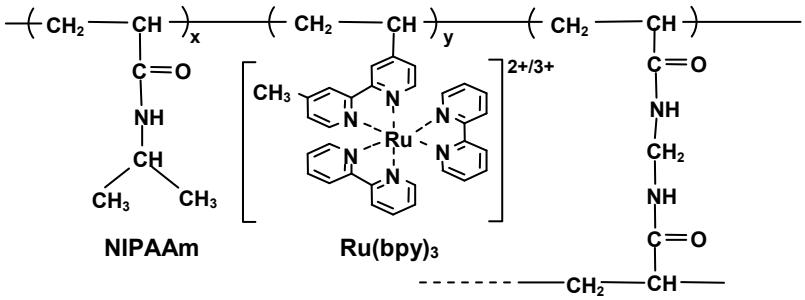

Figure 5.2 Chemical structure of poly(NIPAAm-*co*-Ru(bpy)$_3$) gel.[3]

In their studies, the polymerisable catalytic monomer, ruthenium(4-vinyl-4´-methyl-2,2´-bipyridine)bis(2,2´-bipyridine)bis(hexafluorophosphate) [Ru(bpy)$_2$(mvbpy)$_2$(PF$_6$)$_2$] has been used as a polymerisable ruthenium catalyst of the BZ reaction.[1, 4] The prepared poly(NIPAAm-*co*-Ru(bpy)$_3$) gel is transparent and tinged with orange in pure water, based on the colour of a reduced state of Ru(bpy)$_3^{2+}$. In a solution of powerful oxidizing agent such as cerium sulphate (Ce^{4+}), the catalyst is oxidized to Ru(bpy)$_3^{3+}$ with the

corresponding green colour. When the gel is immersed in the BZ substrates solution at 20 °C, the chemical oscillation was generated within the gel matrix based on the redox changes of the catalyst moiety: $Ru(bpy)_3^{2+} \leftrightarrow Ru(bpy)_3^{3+}$ with a period of about 5 min (Figure 5.3). The redox changes of $Ru(bpy)_3$ induce swelling/deswelling changes of the gel because the hydrophilicity of the polymer increases and the gel expands in the oxidized state. The locally swollen and shrunken parts move to the direction of the gel length with the propagating chemical waves. The propagation of the chemical waves makes the free end of the gel move back and forth at a rate corresponding to the wave propagation speed. Therefore, the gel changes its total size and shape periodically by the BZ reaction. However, it was difficult to recognise the change in size from the optical images since the change of gel size was only a few percent.

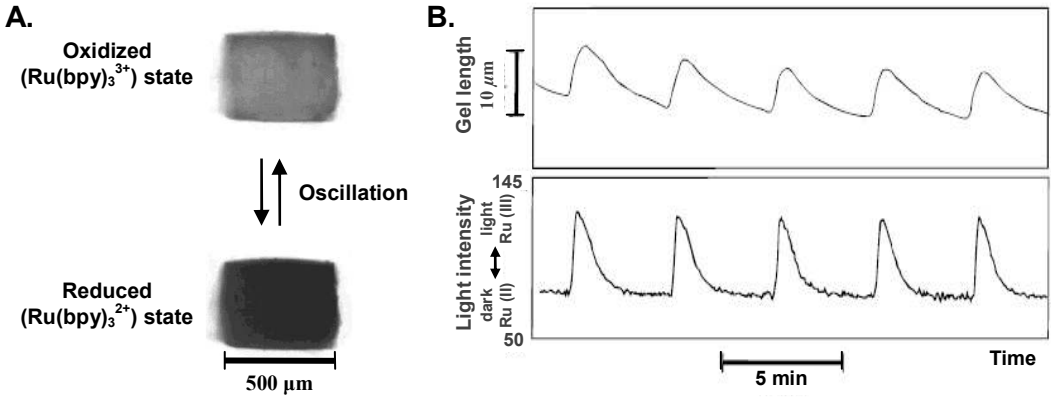

Figure 5.3: (A) Images of poly(NIPAAm-*co*-$Ru(bpy)_3$) gel undergoing redox changes. (B) Periodic redox changes of the gel (lower) and the swelling-deswelling oscillation (upper) in the mixture of reactants of the BZ reaction (0.0625 M malonic acid, 0.084 M $NaBrO_3$, 0.6 M HNO_3) at 20 °C. Transmitted light intensity of the gel is converted to an 8-bit grey scale value.[5] Data are from the Ref.5.

In a previous study by Yoshida *et al.*, [5] a good empirical relation between the concentrations of substrates consisting of malonic acid (MA), $NaBrO_3$, HNO_3, and $Ru(bpy)_3Cl_2$ and the oscillation period (T in second) of the BZ reaction has been obtained with the power law

$$T_s = 2.97\ [MA]^{-0.414}[NaBrO_3]^{-0.796}[HNO_3]^{-0.743} \qquad [1]$$

Initial molar concentrations of substrates leading to stable oscillation is 0.05 M < [MA] < 2 M; 0.05 M < $[NaBrO_3]$ < 1 M; 0.2 M < $[HNO_3]$ < 1 M. It is also known that the sulfuric acid concentration is an important parameter of the classical BZ reaction: the higher the sulfuric acid concentration, the higher the frequency of the oscillations.[6] For

the catalyst concentration usually the opposite relationship holds: the higher the catalyst concentration, the lower the frequency. In this study both the catalyst and the acid are bound to the same polymer chain; thus their concentrations cannot be varied independently.

5.1.1.2 Self-oscillation of polyacrylamide (PAA) gel in the BR reaction

We also used another well-known oscillating chemical reaction, the Brigg-Rauscher (BR) reaction to produce the mechanical oscillation of polyacrylamide (PAA) gel. Bishop *et al.*[7] demonstrated an oscillating system which can give rise to chemical waves based on the BR reaction. The PAA gel film (thickness of 400 μm) containing 3% (w/v) a soluble starch indicator thyodene was equilibrated with an aqueous solution containing 2.15% (w/v) KIO_3, 0.25% (v/v) H_2SO_4, 0.78% (w/v) malonic acid, and 0.18% (w/v) $MnSO_4$. Chemical waves were initiated by contacting with a micropatterned agarose stamp containing 30% (w/v) hydrogen peroxide solution. The frequencies of the waves are regulated by local concentrations of the reactants that trigger the waves (Figure 5.4). The first wave (Figure 5.4B) appears ~30 sec after the stamp is applied and propagates radially outward from the features as a blue band whose colour is due to the formation of a complex $2I_2$, I^-, and thyodene.[8] Moreover, waves influenced one another at large separations.[9]

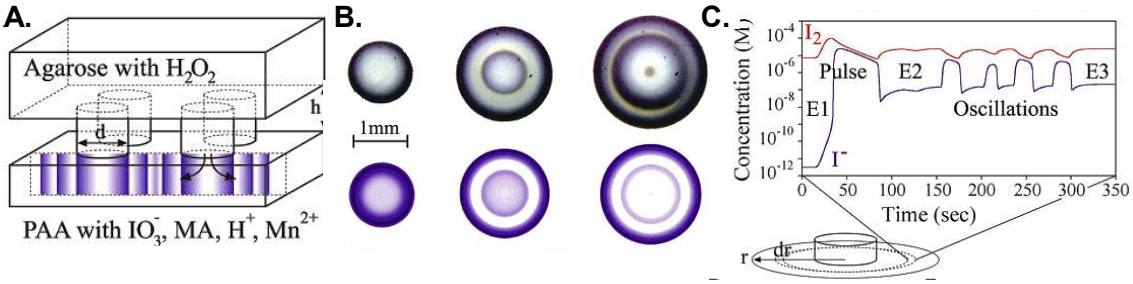

Figure 5.4: (A) Illustrates the experimental arrangement. (B) Chemical waves emitted from isolated, circular features: experimental images (top) and reaction-diffusion model (bottom). (C) Temporal variations in I^- and I_2 concentrations at a fixed distance from a circular feature as calculated.[7]

5.1.2 Electro-responsive polyelectrolyte gels

Deformable robots, such as slug, eel, and snake-like robots can adapt to situations in which conventional constructions consisting of rigid links and joints often fail. Electro-active polymer gels are a type of candidate material for building deformable

mollusc-like robots because their shapes and sizes are controllable by an electric field. Such gels represent an "open system," capable of exchanging matter and energy with the external environment.

5.1.2.1 Electrical contraction of polyelectrolyte gels

If the water-swollen cross-linked polyelectrolyte gel (e.g., poly(acrylic acid) gel) is inserted between a pair of planar electrodes and a direct current (*dc*) voltage is applied, it undergoes anisotropic contraction and concomitant (water) extrusion. [10,11] The electrically induced contraction of the gel is caused by the transport of hydrated ions and water in the network and the contractile behaviour is essentially an electrochemical phenomenon. When an external electric field is applied across the gel, the macro- and microions receive electrical forces in the opposite direction. However, the macroions are stationary since they are chemically fixed to the polymer network, while the counterions are mobile, capable of migrating along the electric field and dragging water molecules with them. According to the capillary model system, the contraction efficiency is inversely proportional to the charge density of the network and increases with an increase of the degree of swelling.[12] The theoretical analysis also predicts that the speed of gel contraction depends only on the amount of charge being transported through the gel (i.e. the quantity of electricity), and is independent of the electric field. Thus, the electrically induced contraction of the gel is dominated by electrokinetic processes of hydrated ions and water in the polymer gels.

In this chapter, we have designed self-propelling hydrogel actuators under an applied electric field as an alternative driving force instead of a self-oscillating reaction. We selected a typical electro-active polymer gel, poly(2-acrylamido-2-methylpropane sulfonic acid) (PAMPS) gel[13,14] and its co-polymer gel combined with a various electrolytic monomers because of its ability to undergo large transformations. The PAMPS gel strongly bends in a surfactant solution when *dc* electric field is applied. In general, electro-active polymer systems consist of a polymer and electrodes either separate or composite. Both types can be modelled by considering the local electrical and chemical interactions of the polymer, the solution, and the electric field.

5.1.2.2 Electro-response of polyelectrolyte gel in an oppositely charged surfactant solution

Surfactant binding to solvated and cross-linked polyelectrolytes having charges on the side chains as well as chain backbones has been extensively studied using various kinds of oppositely charged surfactants.[16,17,18] It has been proposed that there are three categories of surfactant binding; 1) cooperative and stoichiometric,[15] 2) non-cooperative and stoichiometric,[16] and 3) cooperative and non-stoichiometric.[17,18] The modes of these categories are predominantly determined by the three dimensional chemical structure of the surfactant, hydrophobicity, and the charge density of the polyelectrolyte. For example, *n*-alkylpyridinium chloride (C_nPyCl) stoichiometrically binds to PAMPS gel. The binding is cooperative through the side-by-side hydrophobic packing of *n*-alkyl groups. In the binding isotherms for C_nPyCl-PAMPS gel complex formation, the steep increase in binding at a critical surfactant concentration clearly demonstrates the cooperative binding (Figure 5.5).

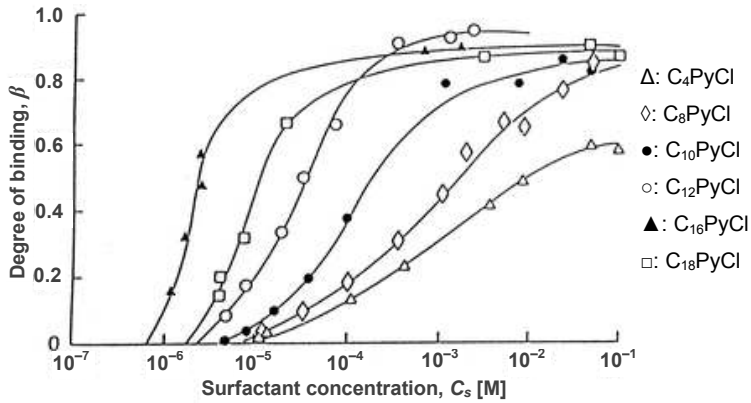

Figure 5.5: Binding of isotherms of the surfactant *n*-alkylpyridinium chloride molecules with the PAMPS gel in 30 mM Na_2SO_4 at 25 °C. Equilibration time is 30 days. The degree of binding (β) is defined as the molar ratio of bound surfactant to the total sulfonate groups in the gel. Data are from Ref. 19.

Moreover, the hydrophobic interaction between the alkyl chain of the surfactant and the backbone of PAMPS favors the binding equilibrium and stabilizes the complex. With the binding of surfactant, the PAMPS gel loses its electrostatic energy, leading to a contraction in its volume. A supramolecular structure is formed in the surfactant-bound gel. As described above, positively charged surfactant, C_nPyCl molecules bind to anionic polymer gels (PAMPS) through electrostatic interactions and bring about contraction of the gel.[20,21,22] The degree of the bending and volume expansion, and the

shape of the gel depend on its spatial position in the electric field as shown in Figure 5.6.[23]

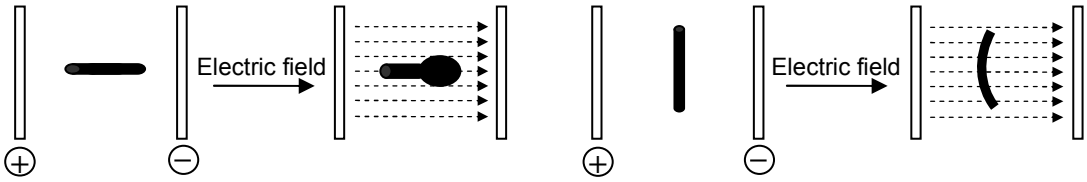

Figure 5.6: Schematics of the effect of the electric field on the shrinking, swelling and bending of the polyelectrolyte gel.

Using this phenomenon, an electrically driven artificial "worm-like muscle" and a swinging pendulum made of water-swollen synthetic polymer gel possessing motility in water have been reported.[13]

5.2 Self-oscillation of hydrogels using the BZ or BR reactions

5.2.1 Swelling behaviour of hydrogel in the BZ or BR reactions

5.2.1.1 Self-oscillation of ruthenium catalyst $[Ru(bpy)_3]^{2+}$ in the BZ solution

Before the preparation of a self-propelling hydrogel particle, we firstly investigated the self-oscillation of ruthenium catalyst in the BZ substrates solution. $Ru(bpy)_3Cl_2$ was used instead of a polymerisable catalyst $Ru(bpy)_2(mvbpy)_2(PF_6)_2$. The chloride ions ($Cl^-$) inhibit the BZ reaction, and therefore the Cl^- ions were removed before the experiment was run using a single-replacement reaction.[24] In brief a nearly saturated solution of $Ru(bpy)_3^{2+}$ was prepared by dissolving 48.66 mg of $Ru(bpy)_3Cl_2$ in 0.65 mL of pure water. 0.31 mL of 0.4272 M $AgNO_3$ is added slowly to the $Ru(bpy)_3Cl_2$ aqueous solution with vigorous mixing. The Ag^+ ions from the $AgNO_3$ complex with the Cl^- ions from the $Ru(bpy)_3Cl_2$ to form AgCl, which is insoluble in water and forms a precipitate. The precipitate was removed by centrifugation several times until there was no precipitate. A small excess of Ag^+ ions which remained after the AgCl precipitation and could cause spontaneous Ru^{3+} production was removed by slowly adding 0.04 mL of 1 wt% NaBr aqueous solution with vigorous mixing. The AgBr precipitate was removed completely by centrifugation. The resulting solution contains approximately 65 mM $Ru(bpy)_3^{2+}$. The prepared ruthenium catalyst showed an orange colour originating from the Ru^{2+} state in the reducing agent and light green colour originating from the Ru^{3+} state in the oxidizing agent (Figure 5.7A). The

reduced form of ruthenium showed an intense fluorescence when it was illuminated with UV light in a dark place. Figure 5.7B shows a self-oscillating behaviour of the $Ru(bpy)_3$ catalyst in the BZ substrate solution at room temperature.

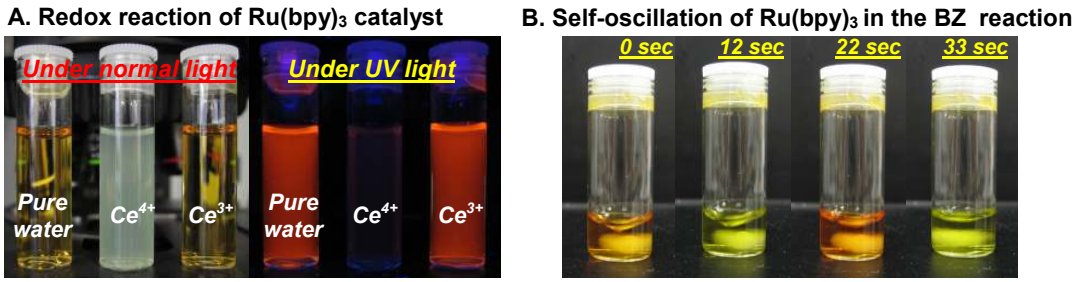

Figure 5.7: (A) Colours of 0.05 mM $Ru(bpy)_3$ catalyst in the oxidizing agent (1 mM $Ce(SO_4)_2$) and reducing agent (1 mM $Ce_2(SO_4)_3$) at room temperature. (B) The self-oscillating behaviour of 0.6 mM $Ru(bpy)_3^{2+}$ as a catalyst in the mixture of reactants of the BZ reaction (0.75 M malonic acid, 0.18 M $NaBrO_3$, 3 M H_2SO_4) at room temperature.

The chemical oscillation of the BZ reaction depends on both the BZ substrate concentrations and the catalyst concentration as shown in Figure 5.8.

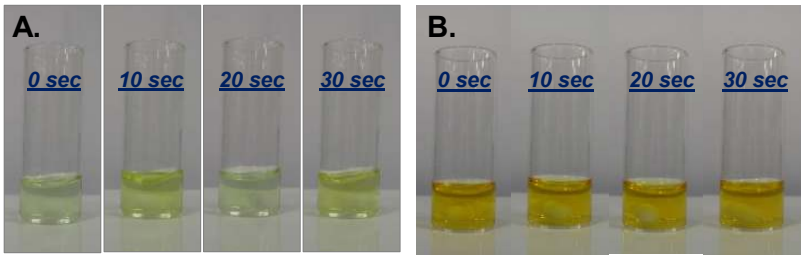

Figure 5.8: Self-oscillating behaviour of 0.2 mM $Ru(bpy)_3^{2+}$ as a catalyst in the BZ substrates solution (A) 0.75 M malonic acid, 0.18 M $NaBrO_3$, 3 M H_2SO_4 and (B) 0.0625 M malonic acid, 0.084 M $NaBrO_3$, 0.894 M HNO_3 at room temperature. Both images from left to right are at 10 sec intervals

The chemical oscillation of the BZ reaction was also observed using 0.013 M $MnSO_4$ as a catalyst instead of ruthenium into the aqueous solution containing 0.104 M malonic acid, 0.057 M potassium bromate, and 1.671 M sulfuric acid in a petri-dish (data not shown here) and a glass tube (Figure 5.9) at room temperature.[25] In a glass tube with mixing the period of colour oscillation is about 10 sec. Spiral waves were developed in a thin unstirred layer of reacting solution in a test tube.

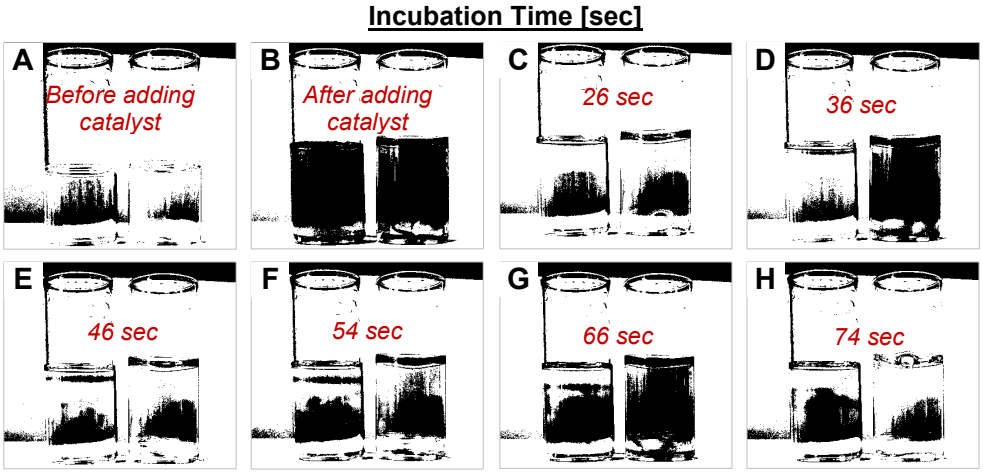

Figure 5.9: Self-oscillating behaviour with 0.013M $MnSO_4$ as a catalyst in the BZ substrates solution (0.104 M malonic acid, 0.057 M $KBrO_3$, and 1.671 M H_2SO_4) in a glass tube at 23 °C. The images were converted to the grayscale using Microsoft PowerPoint software. (A): Before adding of $MnSO_4$ as a catalyst; (B-D): After adding of $MnSO_4$. For each image the right hand-side sample tube was mixed by stirring compared with the left hand-side sample without mixing.

5.2.1.2 Swelling behaviour of poly(N-isopropylacrylamide) (PNIPAAm) gel containing $Ru(bpy)_3^{2+}$ in the BZ or BR reactions

The chemical waves and swelling behaviour of PNIPAAm gel containing ruthenium catalyst $Ru(bpy)_3^{2+}$ in the BZ solution was evaluated according to the procedure described in a previous study.[26] The gelation was carried out in a glass capillary tube with 0.5 mm inner diameter at 60 °C as described in section 2.2.4.1 and cut into cylinders or disc shapes and then immersed in an aqueous solution containing 33 mM $Ru(bpy)_3^{2+}$ for several hours.

The change of size and colour of the gel containing absorbed $Ru(bpy)_3^{2+}$ was then determined as a function of time in the BZ substrates solution containing 0.0625 M malonic acid, 0.084 M $NaBrO_3$, 0.3 M HNO_3, and 25 mM $Ru(bpy)_3^{2+}$ at room temperature. The cylindrical gel samples showed a decrease in the total length and diameter after incubation in the BZ solution. This total deswelling is due to an increase in ionic strength after the gel is transferred from pure water to the BZ solution (Figure 5.10). However, at steady state after 1 h the gels did not show any further deswelling behaviour. This initial deswelling behaviour of the gel in the BZ solution could be observed in all our experiments.

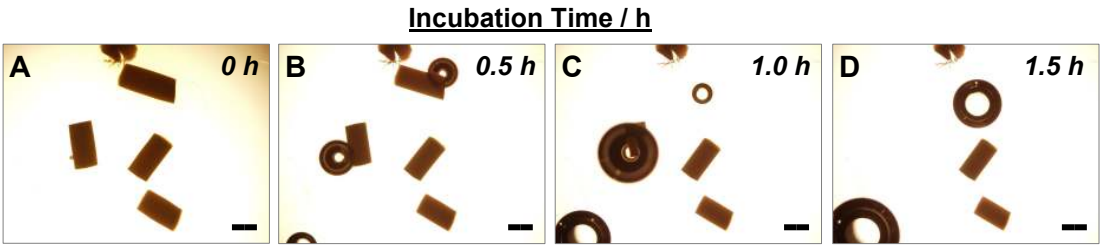

Figure 5.10: Optical images of cylindrical PNIPAAm gels (19.2% (w/v) NIPAAm, 0.8% (w/v) *N,N′*-methylenebisacrylamide (MBAAm)) pre-soaked in 0.033M $Ru(bpy)_3^{2+}$ for 3 h in the BZ solution (0.0625 M malonic acid, 0.15 M $NaBrO_3$, 0.3 M HNO_3 according to the reaction time at 23 °C. The spherical objects (images B, C, and D) are gas bubbles formed during the incubation. All scale bars represent 400 μm.

We synthesized poly(NIPAAm-*co*-AAc) gel with acidic comonomer acrylic acid (AAc) to enhance the swelling-deswelling behaviour of PNIPAAm gel using the same polymerisation method described above. The gel showed a deswelling behaviour after 1 h incubation but no oscillation in all experiments (Figure 5.11).

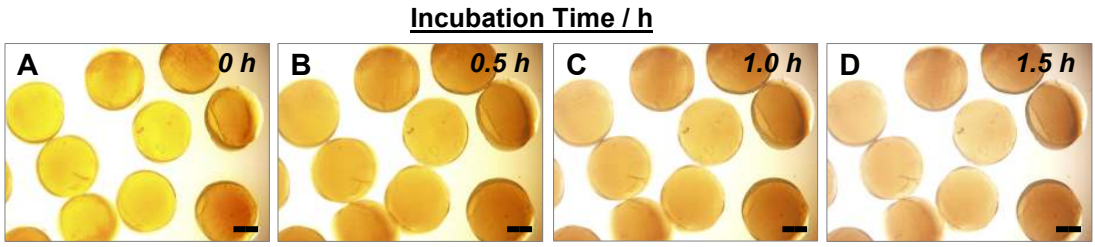

Figure 5.11: Optical images of disc shaped poly(NIPAAm-*co*-AAc) gels (15.4% (w/v) NIPAAm, 0.7% (w/v) AAc, and 0.66% (w/v) MBAAm) pre-soaked in 0.033 M $Ru(bpy)_3^{2+}$ for 3 h in the BZ solution (0.0625 M malonic acid, 0.15 M $NaBrO_3$, 0.3 M HNO_3 according to the reaction time at 23 °C. All scale bars represent 400 μm.

We also measured the self-oscillating behaviour of PNIPAAm gel by coupling with the BR reaction instead of the BZ reaction as a driving energy for the mechanical oscillation. We observed the deswelling behaviour of PNIPAAm gel after 1 h incubation but could not detect any oscillating behaviour over 2 h periods (Figure 5.12). Additionally, in the BR reaction, oxygen gas was produced and formed bubbles and this gas formation perturbed the observation of oscillation under a microscope.

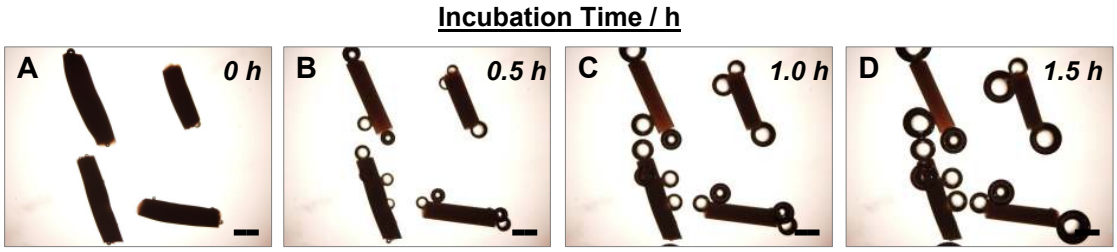

Figure 5.12: Optical images of deswelling behaviour of cylindrical PNIPAAm gels (9.5% (w/v) NIPAAm, 0.5% (w/v) MBAAm, and 3% (w/v) starch) in the BR solution (2.15 wt% KIO_3, 0.25 vol% H_2SO_4, 0.78 wt% malonic acid, and 0.18 wt% $MnSO_4$) according to the reaction time at 21°C. The spherical objects (images B, C, and D) are gas bubbles formed during the incubation. All scale bars represent 400 μm.

The PNIPAAm gel contained pre-absorbed BR substrates showed a bending-stretching motion in hydrogen peroxide solution, however the contraction rate was too slow to prepare a self-propelling hydrogel particle (e.g., the cyclic period is longer than 1 h) (Figure 5.13). This behaviour might be caused by the inhomogeneous distribution of the BR substrate in the gel, which could cause the different charge distribution of the gel network during the BR oscillating reaction.

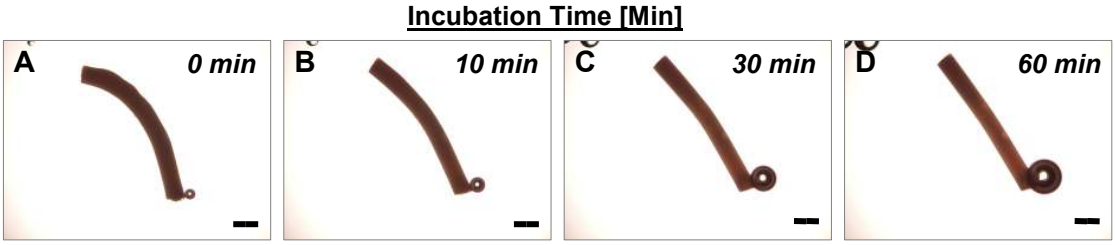

Figure 5.13: Optical images of the bending-stretching motion of a cylindrical PNIPAAm gel (19.2% (w/v) NIPAAm, 0.8% (w/v) MBAAm) pre-soaked in the BR solution (2.15 wt% KIO_3, 0.25 vol% H_2SO_4, 0.78 wt% malonic acid, 0.18 wt% $MnSO_4$, and 0.03 wt% starch) and incubated in 12 vol% H_2O_2 solution according to the incubation time at 23 °C. All scale bars represent 400 μm.

In the next step, we initially examined the swelling-deswelling behaviour of the poly(NIPAAm-*co*-AMPS) gel which was polymerised together with $Ru(bpy)_3Cl_2$ under reduced and oxidized states by using 10 mM $Ce(SO_4)_2$ as an oxidizing agent and 10 mM $Ce_2(SO_4)_3$ as a reducing agent, respectively. The prepared disc shaped poly(NIPAAm-*co*-AMPS) gel containing $Ru(bpy)_3$ is transparent and orange colour in pure water, based on the colour of $Ru(bpy)_3^{2+}$. In $Ce(SO_4)_2$ solution, however, the $Ru(bpy)_3$ is oxidized to $Ru(bpy)_3^{3+}$ with a corresponding green colour (Figure 5.14). From

Yoshida's result,[1,2,3] the extent of swelling in the oxidized state is relatively larger than that in the reduced state all over the temperature range because the hydrophilicity of the polymer increases and the gel expands in the oxidized state. However, the prepared poly(NIPAAm-*co*-AMPS) was more shrunken in the oxidized state than in the reduced state as shown in Figure 5.14. This result suggests that the swelling-deswelling behaviour of the gels might be independent of the redox reaction of $Ru(bpy)_3^{2+}$ in the oxidizing and reducing agents but related with the pH of the solutions.

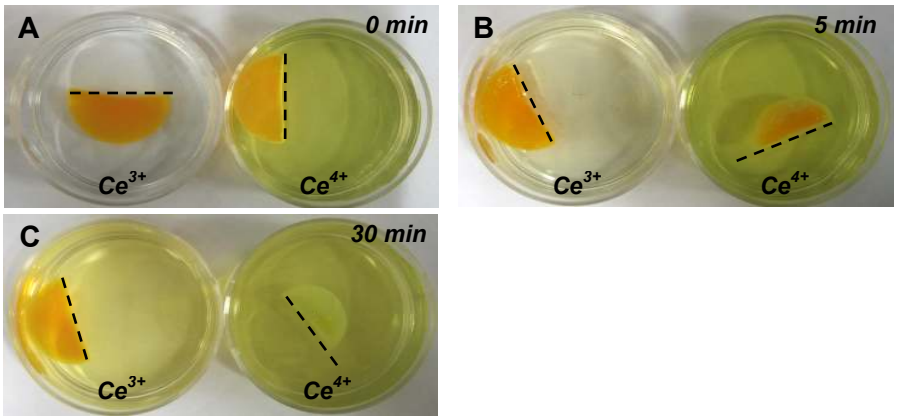

Figure 5.14: Swelling-deswelling behaviour of thermally synthesised poly(NIPAAm-*co*-AMPS) semi-circular disc shaped gel (15.6% (w/v) NIPAAm, 0.28% (w/v) MBAAm) containing 1.62% (w/v) $Ru(bpy)_3^{2+}$ in the reduced and oxidized states at room temperature. The dotted line in each image indicates the initial size of the semicircle of the gel disc. The size of the disc gel decreases only in the oxidized state of ruthenium not in the reduced state.

From all the above results the mechanical oscillating behaviour of the PNIPAAm based gel was not produced via the energy of the BZ and BR reactions using $Ru(bpy)_3^{2+}$ catalyst which was just physically absorbed in the PNIPAAm gel network. For constructing a gel system capable of energy conversion from chemical oscillation of the BZ reaction to mechanical oscillation of polymer chains, the catalyst of the BZ reaction $Ru(bpy)_3^{2+}$ should be covalently bonded to the polymer chain of NIPAAm in the gel.

5.2.2 Preparation of anisotropic poly(NIPAAm-*co*-Ru(bpy)$_3$-*co*-AMPS) gels

Maeda *et al.* developed "self-walking" poly(NIPAAm-*co*-Ru(bpy)$_3$-*co*-AMPS) gel strip which produces a self-oscillating anisotropic contraction similar to the walk motion in the BZ substrate solution.[29] For an asymmetrical swelling-deswelling they introduced the hydrophilic monomer 2-acrylamide-2-methylpropane sulfonic acid (AMPS) into the poly(NIPAAm-*co*-Ru(bpy)$_3$) gel network as shown in Figure 5.15.

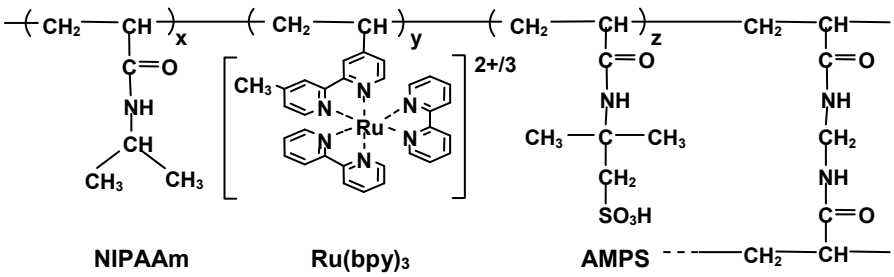

Figure 5.15: Chemical structure of poly(NIPAAm-*co*-Ru(bpy)$_3$-*co*-AMPS) gel.[27]

During the polymerisation, the monomer solution faces two different surfaces of plates: a hydrophilic glass surface and a hydrophobic Teflon surface as shown in Figure 5.16. Since the hydrophobic $Ru(bpy)_3^{2+}$ monomer easily migrates to the hydrophobic surface side a nonuniform distribution along the height is formed by the content of each component in the polymer network. At the surface of the side where the content of hydrophilic AMPS is higher, the swelling ratio of the gel membrane in water becomes larger than that at the opposite side in the same gel where the content of hydrophobic $Ru(bpy)_3^{2+}$ is higher. Consequently, in water, the gel strip always bends in the direction of the surface that faces the hydrophobic Teflon plate as shown in Figure 5.16.

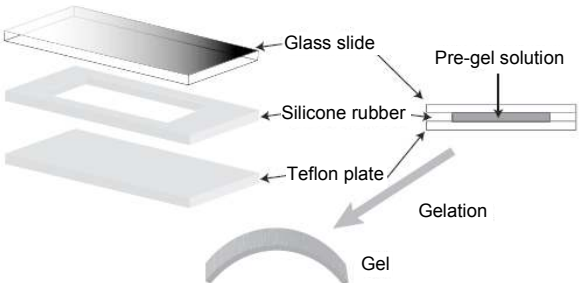

Figure 5.16: Preparation of the poly(NIPAAm-*co*-Ru(bpy)$_3$-*co*-AMPS) gel membrane undergoing anisotropic contraction in pure water.[29]

Based on this idea we attempted to create biomimetic soft actuators which can swim in a liquid like a live snake or worm. To produce a repeated anisotropic contraction in a gel strip, a pattern of hydrophobic-hydrophilic surfaces on a glass slide was prepared using a silanizing agent and adhesive tape for the masking of silanization. After the tape-masked glass slide was hydrophobized with a silanizing agent dichlorodimethylsilane (DCDMS), the masked region remained hydrophilic otherwise the unmasked region became hydrophobic (Figure 5.17). We confirmed the nature of the hydrophilic-hydrophobic surfaces of the patterned glass side using contact angle measurements of pure water drops in air. The contact angle of water on DCDMS coated glass slide is 103 ± 2 ° otherwise ~10 ± 1 ° for a piranha cleaned glass slide. According

to Maeda's results,[29] the gel strip always bends in the direction of the surface that faces the hydrophobic Teflon plate surface in pure water after polymerisation according to an inhomogeneous distribution of monomer as shown in Figure 5.17.

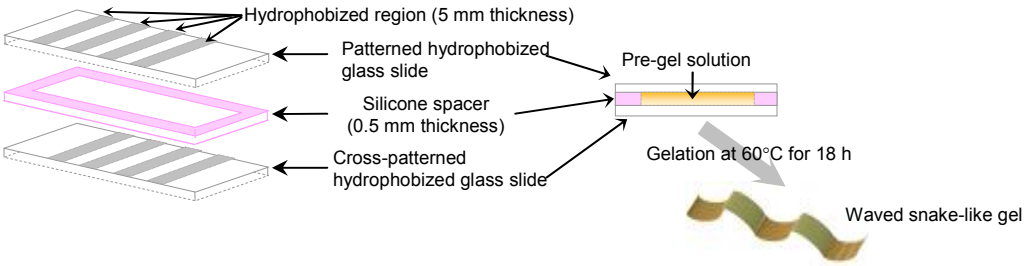

Figure 5.17: Preparation of the poly(NIPAAm-*co*-Ru(bpy)$_3$-*co*-AMPS) gel strips having a patterned bending wave such as a snake in the BZ substrate solution using cross-patterned hydrophobized glass slides.

Therefore, when the monomer solution containing NIPAAm, AMPS, and a polymerisable ruthenium monomer (Ru(bpy)$_2$(mvbpy)(PF$_6$)$_2$) are polymerised, the gel is expected to show a waved shape in pure water when formed in a sandwich between a fully silanised glass surface and a glass slide, and a curved shape using two patterned silanised glass slides. However, the gel strips which were polymerised using a silanised glass slide instead of a Teflon plate did not bend strongly enough after polymerisation as shown in Figure 5.18.

Hydrophobic surface	Teflon plate (from Ref. 29)	Patterned silanised glass slide	Fully silanised glass slide
Dimension of gel (width ×length × thickness)	3 mm × 6 mm × 0.5 mm	4 mm × 10 mm × 0.5 mm	4 mm × 10 mm × 0.5 mm
Gel shapes	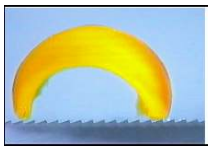		

Figure 5.18: Swelling behaviour of poly(NIPAAm-*co*-Ru(bpy)$_3$-*co*-AMPS) gels in pure water depending on the hydrophobic substrate for polymerisation. The gels are composed of 15.6% (w/v) NIPAAm, 1.6% (w/v) Ru(bpy)$_2$(mvbpy)(PF$_6$)$_2$, 0.56% (w/v) AMPS, and 0.28% (w/v) MBAAm.

The probable reason for this is that the Ru(bpy)$_3^{2+}$ could not easily migrate to the silanised glass slide compared to the Teflon plate and could not produce a gradient distribution of each component in the polymer network (especially Ru(bpy)$_3^{2+}$

monomer). Because of the uneven distribution of orange colour in the gel we also observed the random distribution of $Ru(bpy)_3^{2+}$ in the gel strip. To confirm the difference between our and Maeda *et al.*'s results, a Teflon plate was used together with a silanised glass slide under the same polymerisation conditions. Although the extent of the bending of the gel was increased compared to the silanised glass, we could not obtain enough strongly bended gels as shown in their study (Figure 5.18).

Figure 5.19 shows the textures and swelling behaviour of the synthesised poly(NIPAAm-*co*-$Ru(bpy)_3$-*co*-AMPS) gels in aqueous solutions containing Ce^{3+} and Ce^{4+} respectively. The gels show the redox transitions of the catalyst moiety: $Ru(bpy)_3^{2+}$ (orange colour) ↔ $Ru(bpy)_3^{3+}$ (green colour) by serial incubation in Ce^{3+} and Ce^{3+} solutions. However, drastic volume changes were not induced between the oxidised and reduced states of $Ru(bpy)_3$ and the anisotropic contraction was not observed (data not shown).

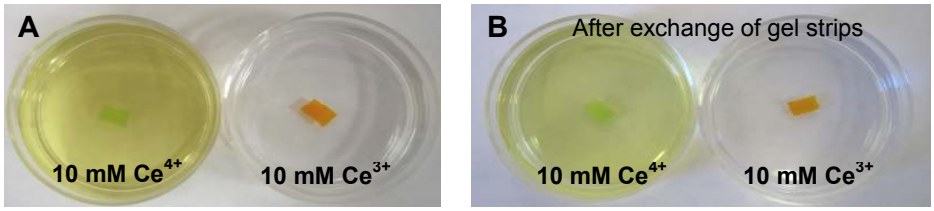

Figure 5.19: The redox changes of the poly(NIPAAm-*co*-$Ru(bpy)_3$-*co*-AMPS) gel. (A) Images after incubation in the reducing agent (10 mM $Ce_2(SO_4)_3$, 78 mM H_2SO_4) and the oxidizing agent (10 mM $Ce(SO_4)_2$, 78 mM H_2SO_4). (B) The redox transition caused by exchanging the gels strips into another solution and incubated for more than 12 h.

However, the gel shows the redox transition continually without the loss of the ruthenium catalyst into an aqueous solution. Therefore, it suggests that the polymerisable catalyst $Ru(bpy)_2(mvbpy)(PF_6)_2$ is properly copolymerized into the poly(NIPAAm-*co*-AMPS) gel network and shows a redox reaction between in Ce^{3+} and Ce^{3+} solutions.

The gel prepared as described above was cut into a rectangular shape pieces (~3 mm × 4 mm × 0.5 mm) and then immersed into an aqueous solution containing 62.5 mM malonic acid, 84 mM sodium bromate, and 0.8924 M nitric acid in a petri dish at room temperature as mentioned in a previous study.[29] The outer solution is composed of the reactants in the BZ reaction, with the exception of catalyst, and the redox oscillation does not take place in the solution. According to their results, as the BZ substrates

penetrate into the gel, the BZ reaction would take places within the gel phase with the $Ru(bpy)_3^{2+}$ catalyst. However, as shown in Figure 5.20, it was difficult to observe the repeated changes of the catalyst between the oxidized ($Ru(bpy)_3^{2+}$) and the reduced ($Ru(bpy)_3^{3+}$) states by the colour changes (orange ↔green) at the condition.

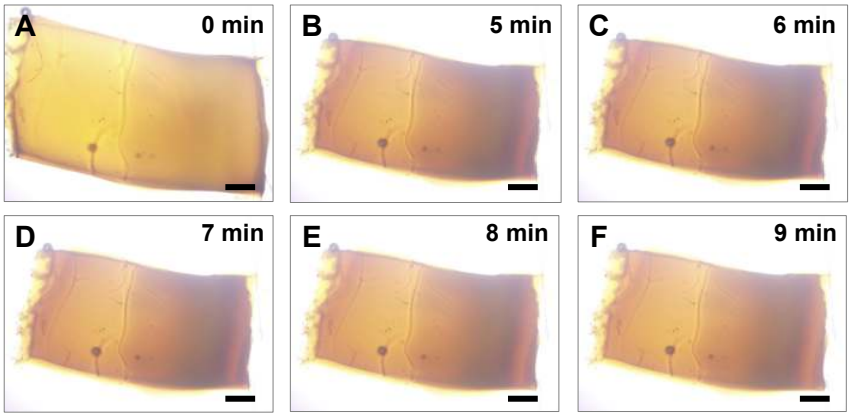

Figure 5.20: Snapshots of swelling-deswelling of the poly(NIPAAm-*co*-$Ru(bpy)_3$-*co*-AMPS) gel strip in the BZ solution (0.1 M malonic acid, 0.25 M $NaBrO_3$ and 0.3 M HNO_3) at room temperature every 1 min. The initial shrinking of the gel strip was observed in the BZ solution (pH <1) until 5 min. All scale bars represent 500 μm.

Even at a concentration of the BZ substrates (0.1875 M malonic acid and 0.2520 M sodium bromate) which is three times higher than Maeda *et al.*'s condition,[29] the very slow self-oscillations of the immobilised $Ru(bpy)_3^{2+}$ (i.e. colour oscillation between orange and green) were only observed without a periodical swelling-deswelling transition of the gel. The gel strip was shrunken until 5 min (Figure 5.20B) and this might be caused by the full protonation of AMPS which is incorporated into the polymer as a pH control site at low pH condition. In general under strongly acidic conditions like the BZ reaction solution (pH < 1), the decrease of the polymer hydrophilicity causes the deswelling of the gel.[28]

Figure 5.21 shows the redox transition of the $Ru(bpy)_3^{2+}$ of the gel strip under Ce^{3+} and Ce^{4+} solutions. The oxidation of ruthenium tends to take place at the edge of the gel and moves to the centre of the gel showing the moving pattern shown in Figure 5.21B. Since the change of gel size is only a few percent, it is difficult to observe the changes of the size from the image.

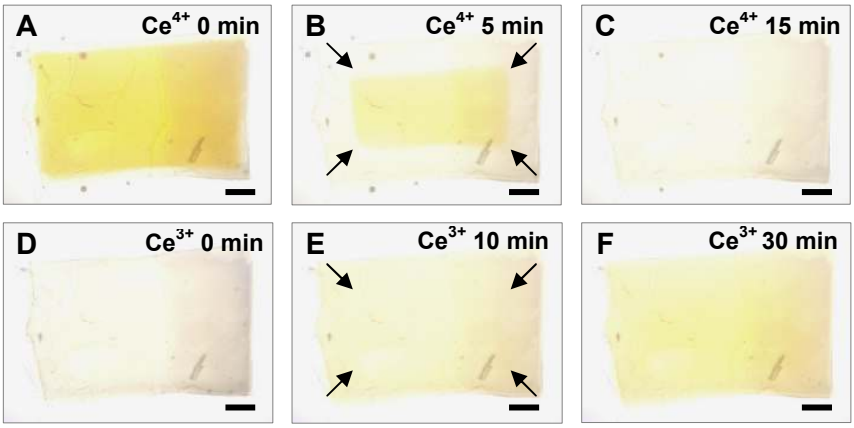

Figure 5.21: A spatial-temporal pattern of the redox reaction of $Ru(bpy)_3^{2+}$ in the rectangular poly(NIPAAm-*co*-$Ru(bpy)_3$-*co*-AMPS) gel in the reducing agent (Ce^{3+}) and the oxidizing agent (Ce^{4+}). Images A, B, and C are taken after soaking the gel in Ce^{3+} solution. Images D, E and F are taken after exchanging the Ce^{4+} solution with Ce^{3+}solution. The arrow indicates the direction of chemical wave propagation. All scale bars represent 500 μm.

The propagation of the redox reaction of $Ru(bpy)_3^{2+}$ in the gel were also observed under a microscope by using monochromic light passed through a blue filter on the halogen light source, and colour changes on the gel surface were converted on a Image Pro Plus software to 8-bit gray scale changes as shown in Figure 5.22.

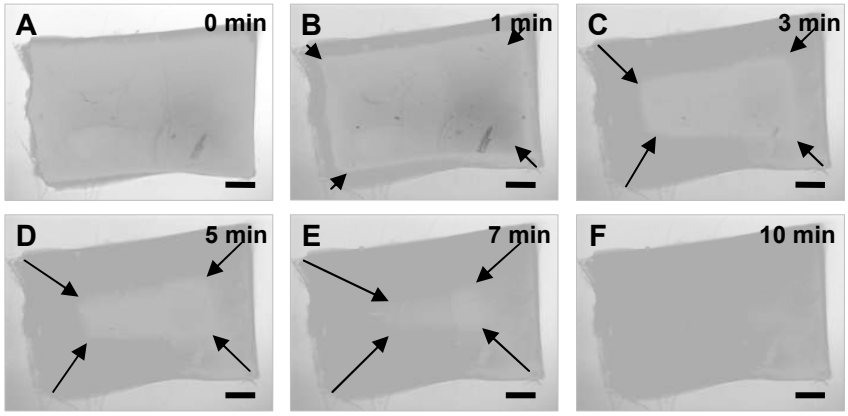

Figure 5.22: A spatial-temporal propagation of a rectangular poly(NIPAAm-*co*-$Ru(bpy)_3$-*co*-AMPS) gel in Ce^{4+} solution. The arrow indicates the direction of wave propagation. All scale bars represent 500 μm.

From Yoshida's previously study,[2] the poly(NIPAAm-*co*-$Ru(bpy)_3$) rectangle (1 mm width and 20 mm length) shows a cyclic extension-contraction change within ca. ± 50

μm in the BZ solution containing 0.0625 M malonic acid, 0.084 M sodium bromate and 0.3 M nitric acid, and maintained at 20 °C

5.2.3 UV polymerisation of poly(NIPAAm-*co*-Ru(bpy)$_3$-*co*-AMPS) gels

In all experiments discussed above we have prepared the poly(NIPAAm-*co*-Ru(bpy)$_3$-*co*-AMPS) gel using a thermal polymerisation method (section 2.4.1.1) as mentioned in a previous study[29]. However, after a polymerisation at 60 °C for 18 h, sharply-defined edges of polymerised gels were not obtained due to bubble formation from the edge of the silicone gasket. Therefore, we examined a thermal polymerisation at low temperature using ammonium persulfate (APS) as an initiator instead of 2,2´-azobis(2-methyl-propionitrile) (AIBN) for gel synthesis.[30] As shown in Figure 5.23, at low temperature, more even edges of poly(NIPAAm-*co*-Ru(bpy)$_3$-*co*-AMPS) gels were obtained than at high temperature. However, APS tends to react with Ru(bpy)$_3^{2+}$ to produce a precipitate in a monomer solution and finally produce a opaque gel with a uneven distribution of the Ru(bpy)$_3^{2+}$.

Polymerisation method	Hot process	Cold process
Initiator	AIBN	APS
Accelerator	-	TEMED
Reaction condition	60 °C for 18 h	0 °C for 1 h
Polymerised gel textures	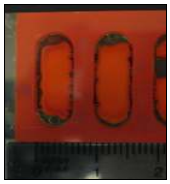	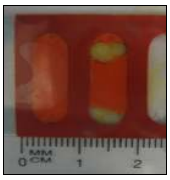

Figure 5.23: Polymerisation of poly(NIPAAm-*co*-Ru(bpy)$_3$-*co*-AMPS) gels depending on two different thermal polymerisation conditions.

Therefore, we considered other methods for polymerising poly(NIPAAm-*co*-Ru(bpy)$_3$-*co*-AMPS) gel instead of a thermal polymerisation. In the next section we describe a simple and convenient method to prepare various anisotropic bigels using UV radiation and a photoinitiator.

5.2.3.1 Effect of photoinitiator Darocur 1173 on the polymerisation of poly(NIPAAm-co-AMPS) gels

To minimize the defects of the structure of a gel caused by a bubble formation during the polymerisation and reduce the reaction time, we have used UV polymerisation as used for the polymerisation of surfactants (chapter 4). Firstly, we have polymerised poly(NIPAAm-*co*-AMPS) gel using 2,2-dimethyl-2-hydroxy-acetophenone (Darocur 1173) as a photoinitiator and the UV curing lamp (Agar Scientific) as a UV source in a perfusion chamber at room temperature. Figure 5.24 shows that the extent of the polymerisation and the swelling behaviour of the gels are likely to depend on the concentration of Darocur 1173 at a fixed UV irradiation time. Higher concentration of the photoinitiator produced more swelling of the gels in pure or ethanol solution.

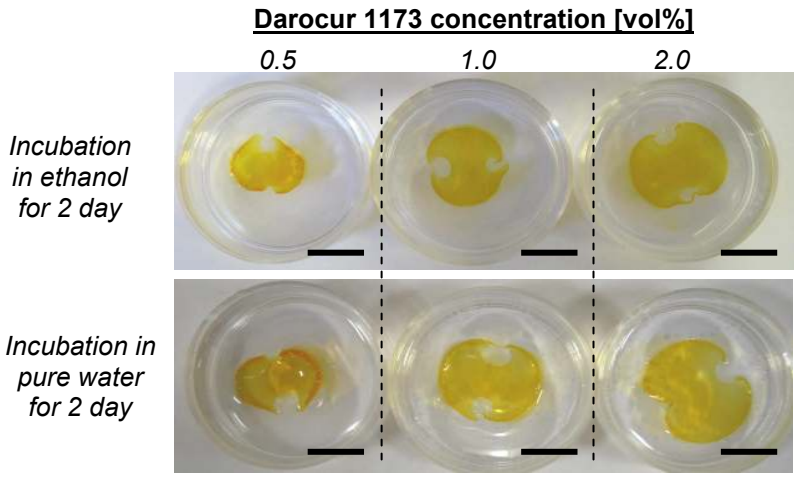

Figure 5.24: The effect of the concentration of Darocur 1173 on the swelling behaviour of poly(NIPAAm-*co*-AMPS) gel. The gel was composed of 15.6% (w/v) NIPAAm, 0.083% (w/v) AMPS, 0.47% (w/v) MBAAm, and 0.83% (w/v) $Ru(bpy)_3^{2+}$ and polymerised in a perfusion chamber (10 mm diameter, 1 mm depth) by UV irradiation using UV curing lamp (Agar Scientific) for 30 min at 21 °C. All scale bars represent 10 mm.

Recently, Yoshida *et al.* have also used 2,2-dimethoxy-2-phenylacetophenone (Darocur 692, 5 mol%) as a photoinitiator to prepare the micro sized patterned hydrogel which was polymerised using UV light from a mercury lamp (100 W, peak wavelength 365 nm) which was focused by a 10× objective lens for 9 sec.[31]

5.2.3.2 Synthesis of anisotropic PNIPAAm/poly(NIPAAm-co-AMPS)bigels with a double UV polymerisation

For the preparation of poly(NIPAAm-*co*-Ru(bpy)$_3$-*co*-AMPS) gel showing a strong anisotropic contraction, we synthesised a class of gels based on the spatial modulation of the chemical nature of gels. The modulated gel strip is achieved by allowing only part of the first gel network [e.g., poly(NIPAAm-*co*-Ru(bpy)$_3$] to interpenetrate with the second gel network [e.g., poly(NIPAAm-*co*-AMPS)] as shown in Figure 5.25.

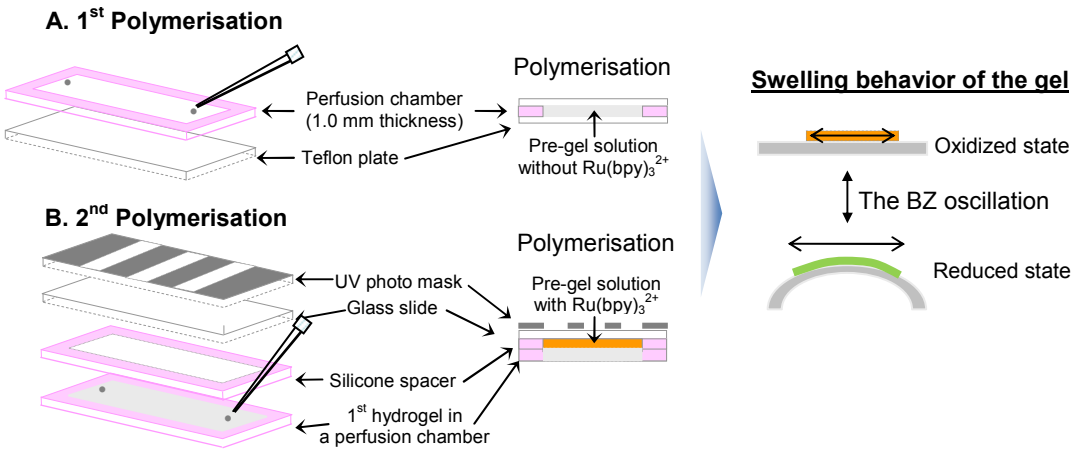

Figure 5.25: Schematic of the preparation of an anisotropic poly(NIPAAm-*co*-AMPS)/ poly(NIPAAm-*co*-Ru(bpy)$_3$) bigel membrane by a double UV polymerisation in a perfusion chamber.

In this section we propose a novel bigel having an modulated and heterogenous structure which could create an anisotropic elbow shaped gel based on the different swelling behaviours of the two gel parts in response to external enviornmental changes (e.g., solvent, pH). In particular, if the BZ self-oscillation of the poly(NIPAAm-*co*-Ru(bpy)$_3$) gel is the controlling mechanism, we can expect the self-propelling of the elbow shaped gel by repeating bending motions in the BZ substrates solution. A perfusion chamber as a polymerisation cell is very useful to prevent the shrinkage of the first polymerised hydrogel through exposure to the atmosphere before the second polymerisation.

We synthesised the anisotropic bigel strip by first polymerising a poly(NIPAAm-*co*-AMPS) gel slab and then a poly(NIPAAm-*co*-Ru(bpy)$_3$) gel slab. However, the two gels were easily and quickly separated immediately after being immersed in ethanol

solution as shown in Figure 5.26A. In contrast, a parallel asymmetrical bigel with different compositions could be prepared by a serial UV polymerisation in a perfusion chamber shown as in Figure 5.26B. After the first polymerisation in a half masked perfusion chamber with aluminum foil, the unreacted monomer solution in the UV protected side was flushed with ethanol solution and dried for a few seconds. Then the second monomer solution was filled and polymerised under the same polymerisation conditions. Finally, we obtained the bigel in which the two different gels were polymerised in parallel. The prepared gel was very stable in ethanol and pure water for longer than a week.

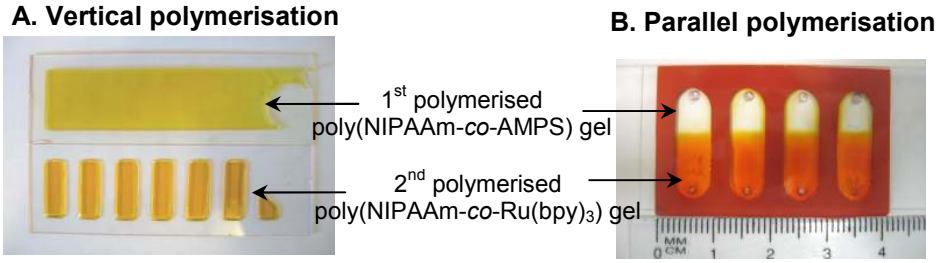

Figure 5.26: (A) Unstable vertical hybridized bigel through the poor interpenetration of a poly(NIPAAm-*co*-Ru(bpy)$_3$) gel into a poly(NIPAAm-*co*-AMPS) gel after the second UV polymerisation. (B) Stable parallel bigel consisting of poly(NIPAAm-*co*-AMPS) gel and poly(NIPAAm-*co*-Ru(bpy)$_3$) using a perfusion chamber. Each monomer solution was polymerised by UV irradiation using the UV curing lamp (Agar Scientific) and 2 vol% Darocur 1173 as a photoinitiator for 10 min at room temperature.

From these all results we can conclude that the contact area of interface between the two monomer solutions and the UV intensity at the interface between two gels during the second UV polymerisation are important to the interpenetration of the second gel into the first gel along with the concentration of a cross-linker in the gels. Therefore, we investigated the effect of the path for UV radiation on the formation of stable bigels as illustrated in Figure 5.27.

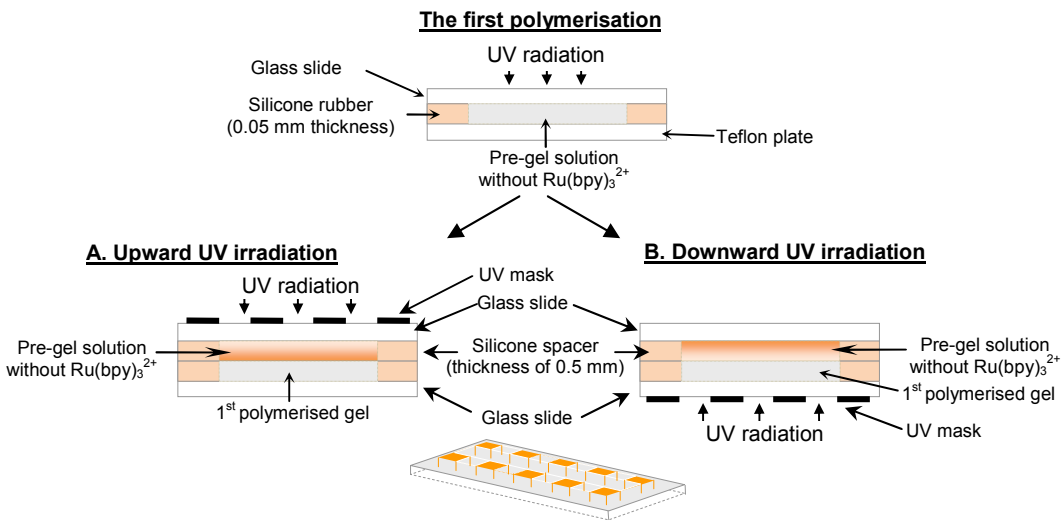

Figure 5.27: Schematic illustration of the synthesis of an anisotropic bigel consisting of poly(NIPAAm-*co*-AMPS) and poly(NIPAAm-*co*-Ru(bpy)$_3$) depending on the direction of the second UV irradiation.

Figure 5.28 shows that the direction of the second UV irradiation decides whether the second gel can interpenetrate into the first gel to form a stable linkage between them or not. The downward polymerisation in which UV radiation is passed through the first polymerised gel to reach to the second monomer solution is likely to produce a stable bigel structure rather than the upward polymerisation.

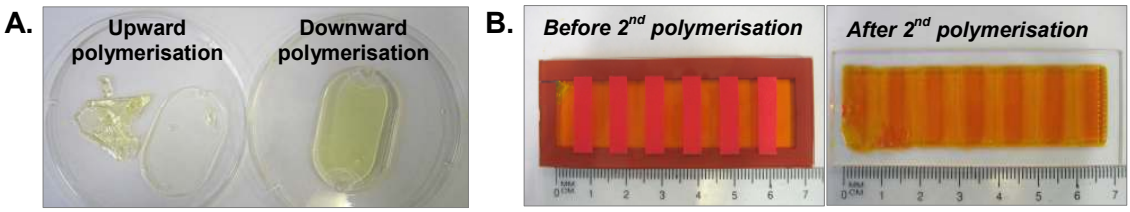

Figure 5.28: (A) Effect of the direction of UV irradiation for the second polymerisation of a bigel comprising of PNIPAAm and poly(NIPAAm-*co*-AMPS) on the stability of the bigel. (B) Synthesis of a ladder shaped bigel comprising of PNIPAAm and poly(NIPAAm-*co*-AMPS) containing Ru(bpy$_3$)$^{2+}$ (the red part of the bigel) using a downward double polymerisation method with a red colour sticky tape as a UV mask. The second monomer solution was only polymerised in the unmasked regions. Monomer solutions were polymerised in (A) the perfusion chambers (thickness of 0.5 mm) and (B) between glass slide and Teflon plate separated by a silicone spacer (thickness of 0.5 mm) by UV irradiation for 5 min for the first polymerisation and for 30 min for the second polymerisation at room temperature.

In order to determine whether the intensity of a UV radiation decides the different interpenetration of the second gel into the first gel, we measured UV transmittance at each interface of the polymerisation at 360 nm which is main wavelength emitted by the UV curing lamp used for UV polymerisation. Results are summarised in Table 5.1.

Table 5.1 UV transmittances of various samples used for UV polymerisation at 360 nm which is main wavelength emitted by the UV curing lamp (Agar Scientific).

Measured samples	A_{360nm}	Transmittance (%)
Glass slide	0.043	90.6
0.5 mm spacer between glass slides	0.084	82.4
1.0 mm spacer between glass slides	0.083	82.6
NIPAAm monomer between 0.5 mm spacer	0.062	86.7
NIPAAm monomer between 1.0 mm spacer	0.078	83.6
1.0 mm spacer with 0.5 mm polymerised NIPAAm gel	0.284	52.0
0.5 mm spacer with NIPAAm monomer with Darocur 1173	0.203	62.7
1.0 mm spacer with NIPAAm monomer with Darocur 1173	0.355	44.2
1.0 mm spacer with 0.5 mm polymerized NIPAAm gel and 0.5 mm NIPAAm monomers with Darocur 1173	0.419	38.1

* *All NIPAAm solution were sandwiched with two glass slides*

From the results, the UV transmittance of NIPAAm monomer solutions decreases as the thickness of monomer solutions increases. The polymerised PNIPAAm gel (thickness of ~0.5 mm) shows a less UV transmittance than NIPAAm monomer solution containing Darocur 1173 with the same thickness. In summary the UV intensities at interfaces of two NIPAAm layers are very different according to the direction of UV irradiation as shown in Figure 5.29 (Upward polymerisation: 69.2%; downward polymerisation: 57.4%).

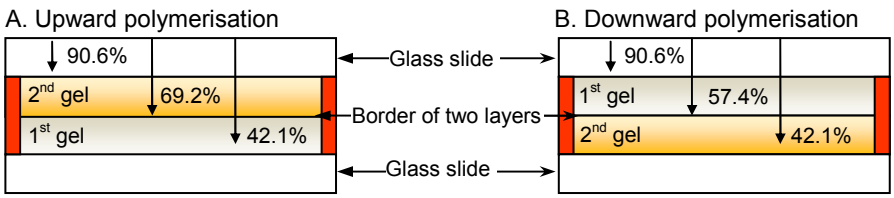

Figure 5.29: The UV transmittance at interfaces between the first polymerised PNIPAAm gel and a NIPAAM monomer solution according to the direction of UV irradiation for the second polymerisation.

In addition, we changed the distance between UV source and the polymerisation cell for the synthesis of the second gel at fixed UV irradiation time. In our previous results the synthesised bigel was unstable after UV polymerisation directly onto the second monomer solution at the distance 20 mm for 30 min (Figure 5.30A). When the distance between UV source and the polymerisation cell was increased from 20 to 60 mm, the second polymerised gel is likely to be more interpenetrated into the first gel as shown in Figure 5.30B. However, this polymerisation condition is not strong enough to produce a stable bigel product.

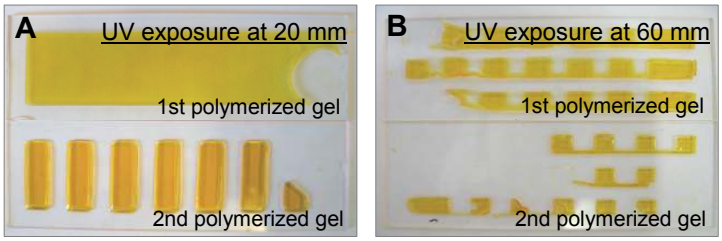

Figure 5.30: Synthesis of PNIPAAm/poly(NIPAAm-*co*-AMPS) bigel. The first polymerised PNIPAAm gel was polymerised with 2 vol% Darocur 1173 by UV irradiation for 5 min and UV was irradiated directly onto the second poly(NIPAAm-*co*-AMPS) gel containing $Ru(bpy)_3^{2+}$ (i.e. upward method) for 30 min at room temperature.

At low UV intensity, NIPAAm monomers in the second polymerised solution are likely to produce a stronger polymer network with the first polymerised gel than at high intensity. As shown in Figure 5.31, at strong UV irradiation condition, the monomers in the second polymerised solution are consumed very fast to produce a polymer network in the upper layer than the bottom layer which is the interface between two gels.

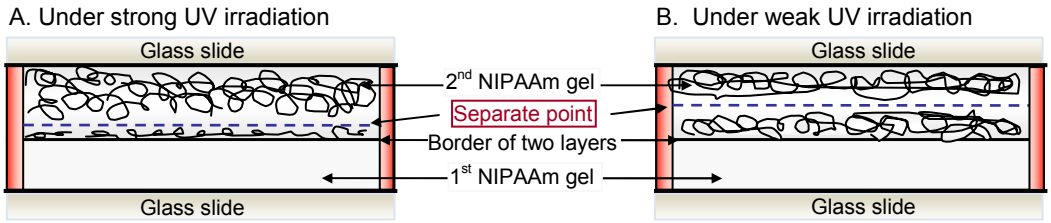

Figure 5.31: Schematic illustration of the effect of UV intensity on the stability of a bigel comprising of two polymerised solutions with different monomer compositions. (A) Strong UV irradiation in Figure 5.30A. (B) Weak UV irradiation in Figure 5.30B.

The best condition for strong cross-linking between the two gels was obtained by UV irradiation through the first polymerised gel (i.e. a downward method) at 40 mm height from a polymerisation cell for 30 min for the second polymerisation.

In order to prepare a snake-like, self-propelling gel in the BZ substrates solution, various structured bigels were synthesised using different combinations of monomer solutions and the differently fabricated silicone spacers. Firstly, PNIPAAm/ poly(NIPAAm-*co*-AMPS) bigel strips were prepared as shown in Figure 5.32. $Ru(bpy)_3^{2+}$ was included in the second NIPAAm monomer solution to distinguish the first polymerised gel from the second polymerised gel.

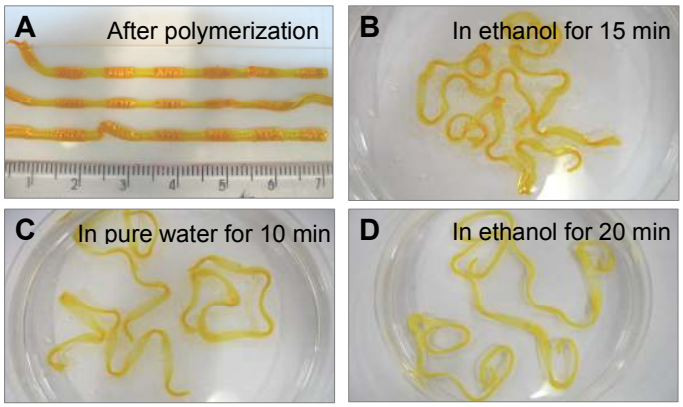

Figure 5.32: Anisotropic poly(NIPAAm-*co*-AMPS)/PNIPAAm bigel. The second monomer solution containing $Ru(bpy)_3^{2+}$ was polymerised using UV irradiation through the first poly(NIPAAm-*co*-AMPS) gel (downward method) for 30 min at room temperature.

As shown in Figure 5.32, the asymmetrical poly(NIPAAm-*co*-AMPS)/PNIPAAm bigel was curved in the yellow coloured hybrid region between the two gels in ethanol and pure water. The swelling ratio of the first polymerised poly(NIPAAm-*co*-AMPS) in water becomes larger than the second polymerized PNIPAAm gel at the opposite side in the hybrid regions because the hydrophilic component AMPS of the polymer chain prevents the detachment of water molecules from the gel network. From the results, we speculate that if we synthesise an asymmetrical poly(NIPAAm-*co*-$Ru(bpy)_3$)/poly (NIPAAm-*co*-AMPS) bigel it might show a circular or a non-circular coiled shape (Figure 5.32D) rather than a snake-like shape as we expected before.

When the order of the polymerisation of two gels of the bigel was changed, the prepared bigel showed a different structure based on the swelling behaviour of poly(NIPAAm-*co*-AMPS) and PNIPAAm gel (Figure 5.33). In the poly(NIPAAm-*co*-AMPS)/PNIPAAm bigel (Figure 5.33A), the linker region between the curved hybrid regions shows a higher swelling ratio than the hybrid regions and the bigel was more curved than PNIPAAm/poly(NIPAAm-*co*-AMPS) bigel (Figure 5.33B). Therefore, the

bigels with different swelling ratios could be obtained at the same gel composition depending on the order of UV polymerisation of monomer solutions.

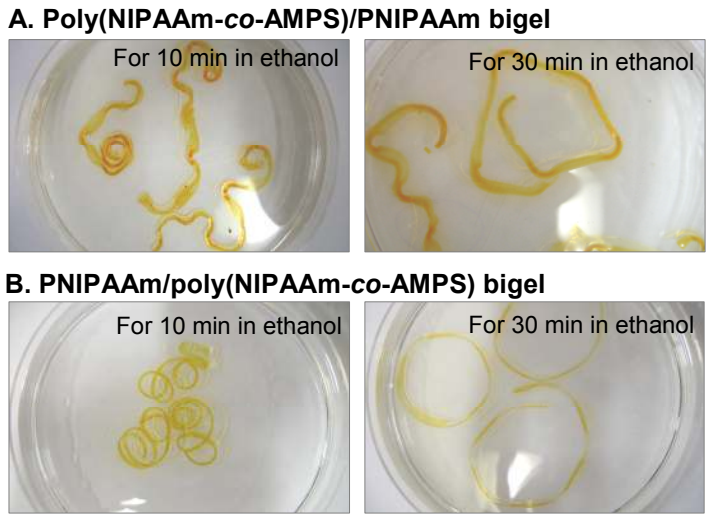

Figure 5.33: Different swelling behaviours of bigels composed of poly(NIPAAm-*co*-AMPS) gel and PNIPAAm gel according to the order of UV polymerisation. The compositions of poly(NIPAAm-*co*-AMPS) and PNIPAAm gels are same in two bigels synthesis.

From the difference in the curvature between the $Ru(bpy)_3^{2+}$ and $Ru(bpy)_3^{3+}$ states, it is anticipated that the bigel will undergo periodical bending and stretching changes when the $Ru(bpy)_3$ moiety is oxidized and reduced periodically in the BZ substrates solution at constant temperature (Figure 5.34).

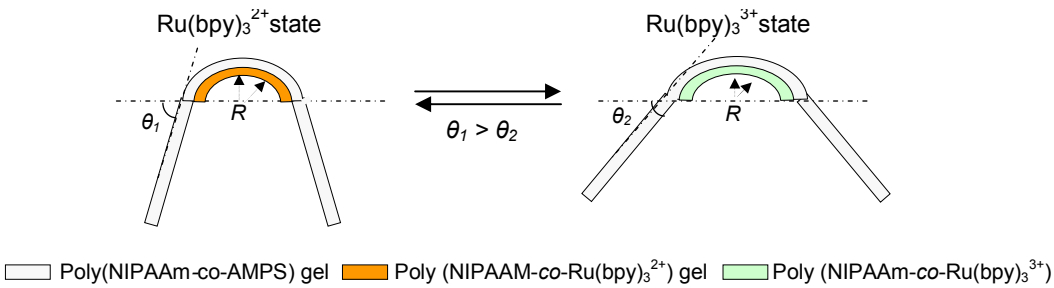

Figure 5.34: Schematic illustration of asymmetrical contraction of the poly(NIPAAm-*co*-AMPS)/poly(NIPAAm-*co*-$Ru(bpy)_3$) bigel in the BZ substrates solution. The bigel is expected to propagate in the liquid by a cyclic bending-straightening motion driven by the chemical energy of the BZ reaction.

5.2.3.3 Preparation of asymmetrical elbow-shaped PNIPAAm/poly(NIPAAm-co-Ru(bpy)$_3$-co-AMPS) bigels

In order to prepare the elbow shaped bigel showing a self-bending and straightening motion in the BZ substrates solution, asymmetrical PNIPAAm/ poly(NIPAAm-*co*-Ru(bpy)$_3$-*co*-AMPS) gel was produced using two differently fabricated silicone spacers as shown in Figure 5.35.

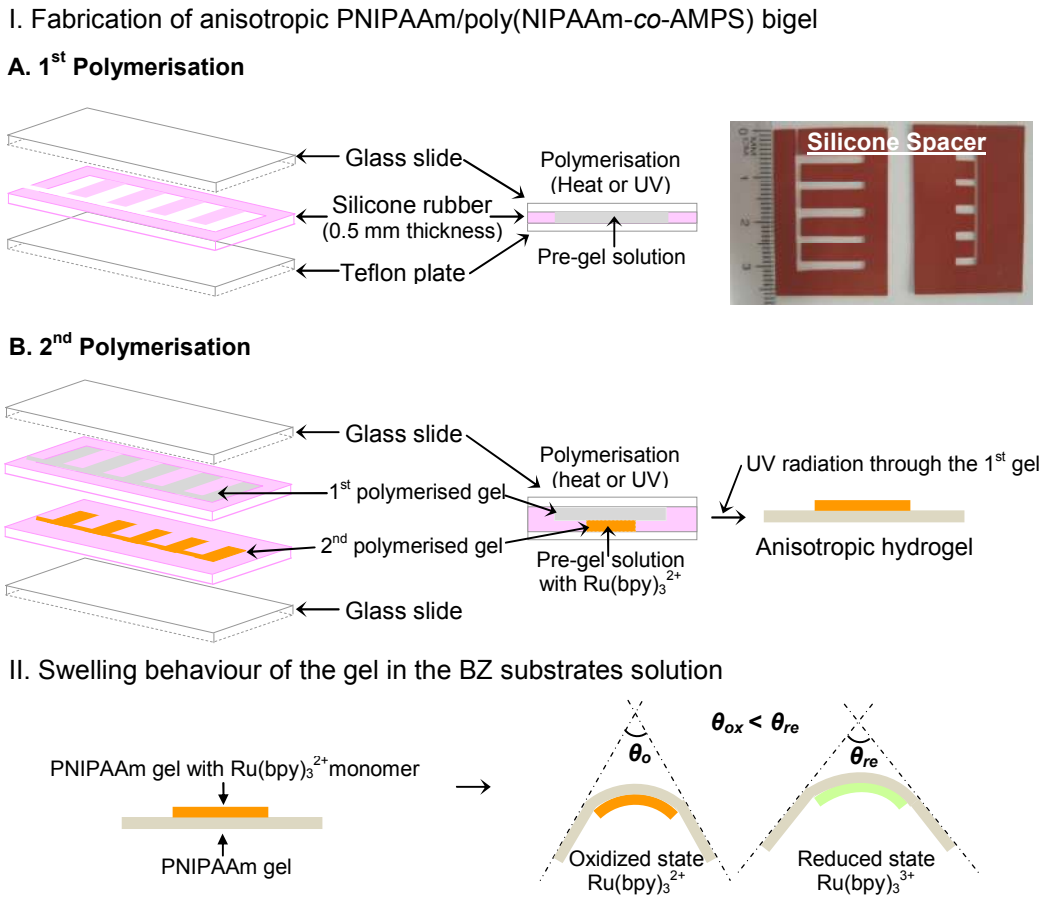

Figure 5.35: I. Preparation of anisotropic elbow-shaped PNIPAAm/poly(NIPAAm-*co*-Ru(bpy)$_3$) bigel. II. Schematic illustration of expected swelling behaviour of anisotropic PNIPAAm/poly(NIPAAm-*co*-Ru(bpy)$_3$) bigel in the BZ substrates solution.

The elbow-shaped anisotropic bigel was obtained as shown in Figure 5.36. We confirmed that the curved structure is mainly caused by the different swelling behaviour (Figure 5.37D) not by the different gel thickness (Figure 5.37B) in the hybrid regions. From Figure 5.36, the all bigel samples are denoted by the previously given abbreviations for components together with their compositions.[32] The content of an acidic comonomer, AMPS is its mol% with respect to NIPAAm (NIPA) and the content of MBAAm (BIS) its mol% with respect to total monomers. For example in the

hydrogel NIPA/AMPS2/BIS1, 100 × (number of moles of AMPS/number of moles of NIPAAm) = 2 and 100 × [(number of moles of MBAAm)/ (number of moles of AMPS + number of moles of NIPAAm)] = 1.

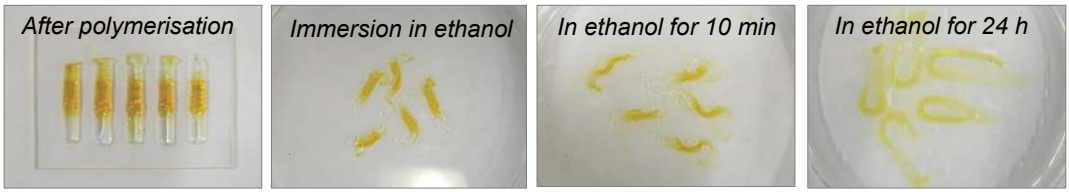

Figure 5.36: Elbow-shaped poly(NIPAAm-*co*-AMPS)/PNIPAAm bigels. The first gel composition is NIPA/AMPS2/BIS1 and the second is NIPA/BIS1 including $Ru(bpy)_3^{2+}$.

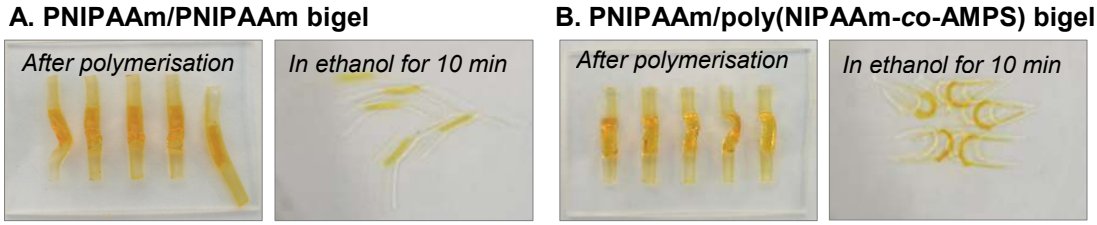

Figure 5.37: Different swelling behaviour of anisotropic elbow-shaped bigels depending on the composition of the second polymerised gels. A. 1st gel = NIP/BIS1; 2nd gel = NIP/BIS1. B. 1st gel = NIP/BIS1; 2nd gel: NIP/AMPS5/BIS1. The yellow hybrid region of the bigel is caused by $Ru(bpy)_3^{2+}$ included in the second gel.

When changing the direction of UV irradiation from the first gel to the second gel at the same composition, the formation of a bigel was poor and the curvature of the second polymerised gel was reversed. Finally, the second polymerised gel was separated from the first gel after incubation in ethanol for 1 h (Figure 5.38).

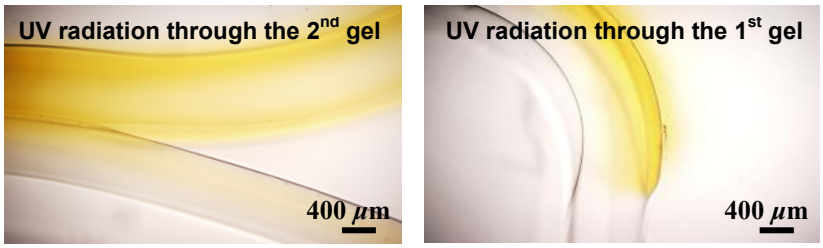

Figure 5.38: Stability of anisotropic elbow-shaped PNIPAAm/poly(NIPAAm-*co*-AMPS) bigel in ethanol according to the direction of the second UV irradiation. The yellow region of the bigel is the hybrid region between two hydrogels. The composition of the first polymerised gel is NIPA/BIS 1.5 and the second is NIPA/AMPS5/BIS1 including $Ru(bpy)_3^{2+}$.

It means that the gradient of AMPS or NIPAAm in the second polymerised gel is likely to be different depending on the direction of UV irradiation. At a higher concentration of AMPS in poly(NIPAAm-*co*-AMPS) gel (e.g., 5 mol% AMPS), we obtained a very similar unstable formation of bigel products.

5.2.3.4 Effect of the concentration of cross-linker on the formation of a bigel

The lower concentration of a cross-linker, the more flexible is the gel formed. We examined the formation of PNIPAAm/poly(NIPAAm-*co*-AMPS) bigel and its swelling behaviour with different concentrations of the cross-linker. At a low concentration of MBAAm (< 1 mol%) the bigel was produced at low rate (≤ 10%) regardless of the AMPS concentration (0–10 mol%). However, when the concentration of MBAAm was increased to 1.5 mol% the adhesiveness between the two gels was increased and formed a stable bigel as shown in Figure 5.39.

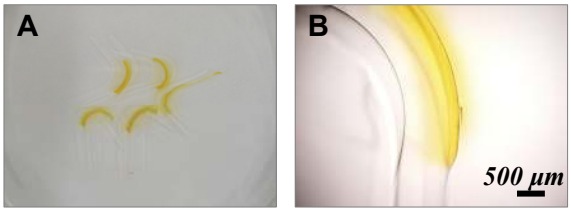

Figure 5.39: Anisotropic elbow-shaped PNIPAAm/poly(NIPAAm-*co*-AMPS) bigel in ethanol. The yellow region of the bigel is the hybrid region between two hydrogel. The composition of the first gel is NIPA/BIS 1.5 and the second gel is NIPA/AMPS5/BIS1.5.

We finally synthesised an anisotropic poly(NIPAAm-*co*-Ru(bpy)$_3$)/PNIPAAm bigel as shown in Table 5.2.

Table 5.2: The compositions of PNIPAAm/poly(NIPAAm-*co*-Ru(bpy)$_3$) bigel

Components	Maeda *et al.*'s gel[29]	poly(NIPAAm-*co*-Ru(bpy)$_3$) gel	PNIPAAm gel
NIPAAm	0.156 g	0.156 g	
MBAAm	2.8 mg	3.2 mg	3.1 mg
Ru(bpy)$_2$(mvbpy)(PF$_6$)$_2$	16.2 mg	16.2 mg	-
AMPS	5.5 mg	-	-
DMSO	0.1 mL	0.1 mL	
Methanol/Ethanol	0.5 mL	0.488 mL	
Water	0.4 mL	0.4 mL	
AIBN/Darocur 1173	AIBN 6.6 mg	Darocur 1173 12 μL	
Final composition	NIPA/Ru(bpy)$_3$1.3/ AMPS1.9/BIS 1.3	NIPA/Ru(bpy)$_3$1.3/BIS 1.5	NIPA/BIS1.5

The composition was the same as the one used in Maeda *et al.*'s study[29] for preparation of a self-walking gel except for the concentration of a cross-linker to increase the adhesiveness between the two gels. In Figure 5.40, the prepared bigel was very slightly curved in the hybrid region between the PNIPAAm and poly(NIPAAm-*co*-Ru(bpy)$_3$) gels in ethanol and pure water. The bigel strip did not show more well-curved shapes compared to the PNIPAAm/poly(NIPAAm-*co*-AMPS) bigel and it was similar to the PNIPAAm/ PNIPAAm bigel (Figure 5.37B).

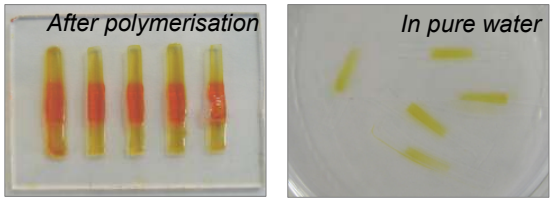

Figure 5.40: Anisotropic poly(NIPAAm-*co*-Ru(bpy)$_3$)/PNIPAAm bigels. The compositions of the gels are NIPA/BIS1.5 and NIPA/Ru(bpy)$_3$1.3/BIS 1.5. The bigel does not show a large bending motion in pure water.

Figure 5.41 shows the redox state dependence of swelling ratio for the bigel. The oxidation of the Ru(bpy)$_3^{2+}$(orange colour) to Ru(bpy)$_3^{3+}$ (green colour) in Ce^{4+} solution (Figure 5.41C and D) caused an increased swelling degree to straighten the bigel relative to its shape in Ce^{3+} solution (Figure 5.41A). However, the bigel did not show drastic changes of its swelling behaviour depending on the redox reaction of the Ru(bpy)$_3$ moiety.

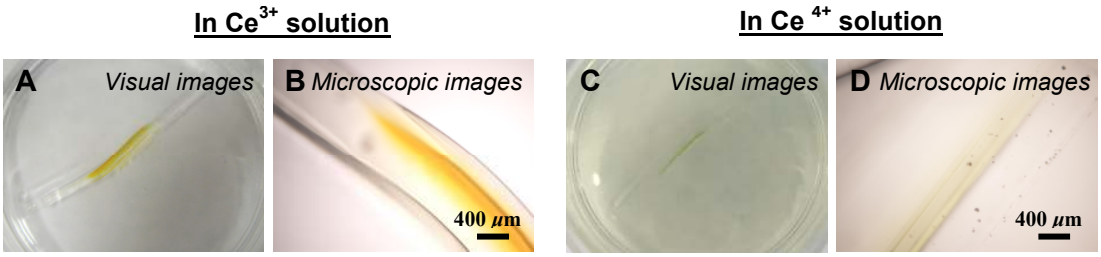

Figure 5.41: Swelling behaviour of asymmetrical PNIPAAm/poly(NIPAAm-*co*-Ru(bpy)$_3$) bigel. The poly(NIPAAm-*co*-Ru(bpy)$_3$) gel was equilibrated in the oxidizing agent 5 mM $Ce(SO_4)_2$ and the reducing agent 5 mM $Ce_2(SO_4)_3$ for 1 h .

We could not observe any straightening-bending cyclic motion in the BZ substrates solution at room temperature. However, the bigel in the BZ solution (Figure 5.42A) was more curved than in pure water (Figure 5.42B). This bending motion might be induced by the acidic condition of the BZ reaction not by the self-oscillating BZ

reaction. The curved gel strips (Figure 5.42A) in the BZ solution reversibly returned to the straight shape after exchanging with pure water (Figure 5.42B).

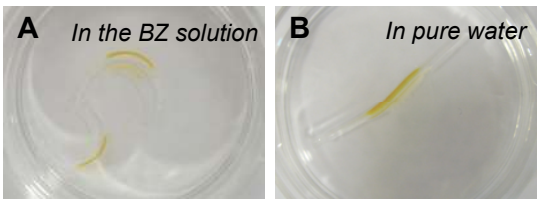

Figure 5.42: Swelling behaviour of asymmetrical PNIPAAm/poly(NIPAAm-*co*-Ru(bpy)$_3$) bigel in the BZ substrates solution (62.5 mM malonic acid, 84 mM sodium bromate, 0.894 M nitric acid) at 21 °C.

After the polymerisation of the second gel of the bigel, the ruthenium catalytic monomer [Ru(bpy)$_2$(mvbpy)(PF$_6$)$_2$] was slightly washed off during the ethanol washing step and the extent of bending of the bigel in pure water was different from batch to batch. This suggests that the ruthenium catalyst was not fully incorporated into the PNIPAAm gel network at the present polymerisation condition. We investigated the extent of the polymerisation of the poly(NIPAAm-*co*-Ru(bpy)$_3$) gel at various polymerisation conditions (e.g., different UV intensity, the concentration of ruthenium catalyst etc.).

At 16.2 mg ruthenium catalyst the poly(NIPAAm-*co*-Ru(bpy)$_3$) gel was not fully polymerised (NIPA/Ru 1.3/BIS 1.3) at any condition even at a high concentration of a photoinitiator and for a longer UV irradiation time. However, when the concentration of ruthenium catalyst was decreased to 8.1 mg, partial polymerisation was observed. We found that the higher extent of a polymerisation could be obtained at lower concentrations of ruthenium catalyst (Figure 5.43A) and the swellability of the bigel depends on the concentration of the Ru(bpy)$_3^{2+}$ moiety in the gel network (Figure 5.43B). Because the ruthenium catalyst Ru(bpy)$_2$(mvbpy)(PF$_6$)$_2$ (molecular weight: 899.61) is a larger and bulkier molecule than NIPAAm monomer (molecular weight: 113.16), a fast polymerisation condition might prevent the fast incorporation of ruthenium monomers into the NIPAAm network. However, at this concentration, the incorporated Ru(bpy)$_3^{2+}$ monomers were unevenly distributed into the gel which was correlated with a inhomogeneous yellow colour in the gel (Figure 5.43A). The bigel showed the maximum bending motion in pure water when 0.4 mol% Ru(bpy)$_3^{2+}$ is incorporated into the PNIPAAm gel network (Figure 5.43B).

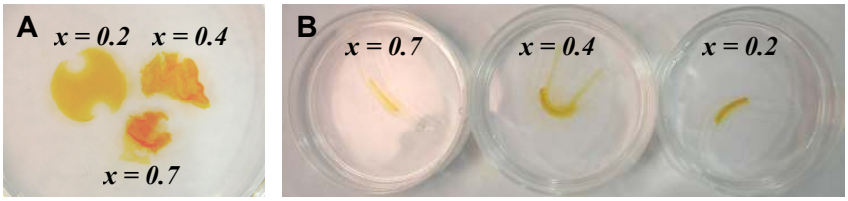

Figure 5.43: (A) Effect of concentration of ruthenium catalyst on the gel shape of poly(NIPAAm-*co*-Ru(bpy)$_3$) gels. The gel was polymerised in a perfusion chamber (diameter of 1.0 cm and thickness of 0.5 mm). (B) The swelling behaviour of the PNIPAAm/poly(NIPAAm-*co*-Ru(bpy)$_3$) bigel depending on the concentration of the Ru(bpy)$_3^{2+}$ moiety in the gel. *x* is the mole% of ruthenium catalyst Ru(bpy)$_2$ (mvbpy)(PF$_6$)$_2$ of the NIPA/Ru *x*/BIS1.3 gel.

Additionally, the photoinitiator Darocur 1173 might also react with ruthenium monomers at high concentrations and may not properly function as an initiator. 2,2-dimethoxy-2-phenylacetopheone which was used as a photoinitiator in Yoshida *et al.*'s recent UV polymerisation study [31] could be considered as a substitutes for Darocur 1173.

When a lower concentration of ruthenium monomer was used in the second polymerisation of poly(NIPAAm-*co*-Ru(bpy)$_3$) gel, the prepared bigel was thicker and more curved than a higher concentration of ruthenium catalyst (Figure 5.44). In the Ce^{4+} solution the Ru(bpy)$_3^{2+}$ moiety is oxidized to Ru (bpy)$_3^{3+}$ and showed the colour change from orange to the green shown in Figure 5.44B. The elbow-shaped gel was less curved in Ce^{3+} and Ce^{4+} solution rather than in pure water by pH difference.

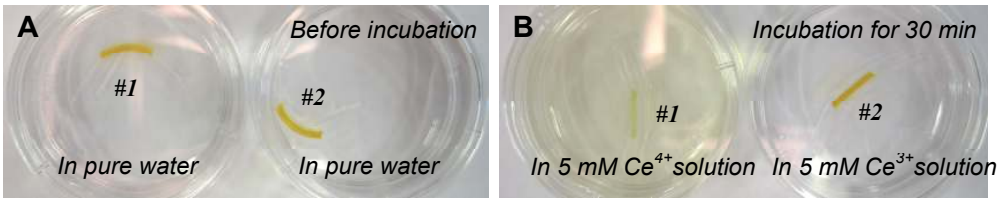

Figure 5.44: Swelling behaviour of the PNIPAAm/poly(NIPAAm-*co*-Ru(bpy)$_3$) bigels in Ce^{3+} and Ce^{4+} solution. In the reducing agent (5 mM $Ce_2(SO_4)_3$ solution in 0.04 M H_2SO_4), the gel keeps a orange tinge colour originating from the Ru(bpy)$_3^{2+}$ state. In the oxidizing agent (5 mM $Ce(SO_4)_2$ solution in 0.04 M H_2SO_4) on the other hand, the gel keeps a tinge of light green colour originating from the Ru(bpy)$_3^{3+}$ state. The gel straightens up more in Ce^{3+} and Ce^{4+} solution than in pure water at a low pH.

The curved bigel did not show self-oscillation behaviour in the two different BZ solutions; (i) 62.5 mM malonic acid, 84 mM sodium bromate, 0.894 M nitric acid, (ii) 0.75 M malonic acid, 0.18 M sodium bromate, 3 M H_2SO_4 at room temperature.

5.2.3.5 Effect of pH and solvent on the swelling behaviour of anisotropic bigels comprising of poly(NIPAAm-co-AMPS)and PNIPAAm

When various acidic comonomers (e.g., acrylic acid) are cross-linked with NIPAAm, 2-acrylamide-2-methylpropane sulfonic acid (AMPS) exhibits the highest swelling ratios in pure water rather than other comonomers under comparable conditions of composition. Huglin *et al.* have studied the effect of pH on the swelling behaviour of these gels in Table 5.3 where it can be seen that the swelling is sensitive to pH.[33]

Table 5.3: Degree of swelling, *r*, and $R^{a)}$ at 20 °C for poly(NIPAAm-*co*-AMPS) gels according to pH. The content of AMPS is in mol% with respect to NIPAAm and the content of a cross-linker MBAAm is its mol% with respect to monomer or total monomers. $^{a)}$ Values of *R* tabulated under pH = 1 and pH = 12 are denoted in the original text by R_1 and R_{12}, respectively. Data are from Ref. 33.

pH	1	5.7	12	1	5.7	12	1	5.7	12
	NIPA/AMPS/BIS1			NIPA/AMPS5/BIS1			NIPA/AMPS10/BIS1		
r	15.7	16.2	16.7	17.3	49.6	36.8	23.7	68.6	54.6
R	0.97	1	1.03	0.35	1	0.74	0.35	1	0.79
r	19.6	45.7	24.2	21.7	117	50.8	28.8	206	72.3
R	0.43	1	0.53	0.19	1	0.43	0.14	1	0.35
	NIPA/AMPS1/BIS0.25			NIPA/AMPS5/BIS0.25			NIPA/AMPS10/BIS0.25		
r	25.3	76.7	33.3	29.3	326	69.3	32.5	444	111
R	0.33	1	0.43	0.09	1	0.21	0.07	1	0.25

Therefore, we investigated the bending-straightening motion of the poly(NIPAAm-*co*-AMPs)/PNIPAAm bigels at different pH values. When the poly(NIPAAm-*co*-AMPS)/PNIPAAm bigel was equilibrated in pure water for two days, the hybrid region of the bigel showed slightly different swelling behaviors (i.e. different curved shape) as shown in Figure 5.45A. When the bigels were immersed in various 10 mM pH buffer solutions to examine the effect of pH on their swelling behaviours, the curved bigel strips were deswelled and straightened at pH 4, 9 (Figure 5.45B). In these gel strips, the content of AMPS is 1.8 mol% with respect to NIPAAm and the content of MBAAm is 1.2 mol% with respect to total monomers.

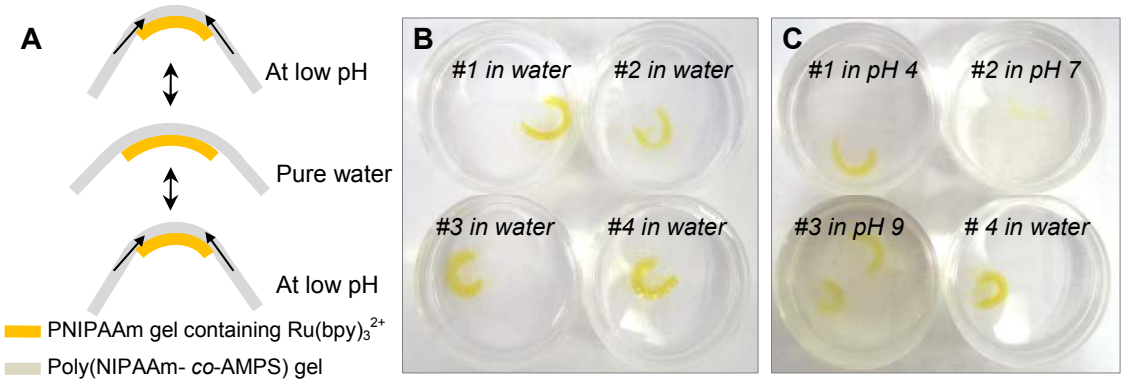

Figure 5.45: Swelling behaviour of the curved poly(NIPAAm-*co*-AMPS)/PNIPAAm bigels according to various pH. (A) Schematic illustration of the expected swelling behaviour of the bigel depending on pH. The bigel was equilibrated in (B) pure water for two days and then immersed in (C) pH 4, 7 and 9 bu ffer solutions for 1 h.

We expected that if the bigel shows a fast bending-straightening motion depending on the pH so that we could prepare self-propelling particles using the bigel coupled with a pH oscillating reaction. However, the bigel shows only very slow straightening-bending motion depending on the pH and the response was not fast enough to move it in the aqueous phase.

Here, we discuss the results of observations on the swelling behaviour of PNIPAAm gel containing $Ru(bpy)_3^{2+}$ in a mixture of ethanol and pure water. The NIPAAm polymer behaves as a flexible coil in ethanol which is a good solvent for it. In pure water, on the other hand, the polymer is elongated and stiffer than in ethanol. Hydrogen bonding occurs between water molecules and the amide groups of the polymer, triggering the formation of a layer of highly organised water molecules around the polymer. PNIPAAm copolymers containing ionisable groups (e.g., acrylic acid) undergo discontinuous transitions between swollen and collapsed states in response to the changes in solvent composition. For instance, the gels underwent a reentrant phenomenon where gels, once collapsed, can swell again when the ratio of water to dimethylsulfoxide in mixed solvent was varied systematically.[34] To gain the same dimension between the gels, PNIPAAm gels were prepared by UV polymerisation in a perfusion chamber which can produce a cylinder shaped gel (height: 1.0 mm, diameter: 9 mm) at room temperature (Figure 5.46). $Ru(bpy)_3^{2+}$ was polymerised together with a NIPAAm monomer to easily measure the swelling behaviour of the gel. Figure 5.46

shows the swelling ratio of the PNIPAAm gels containing $Ru(bpy)_3^{2+}$ in different ethanol-water mixed solvents.

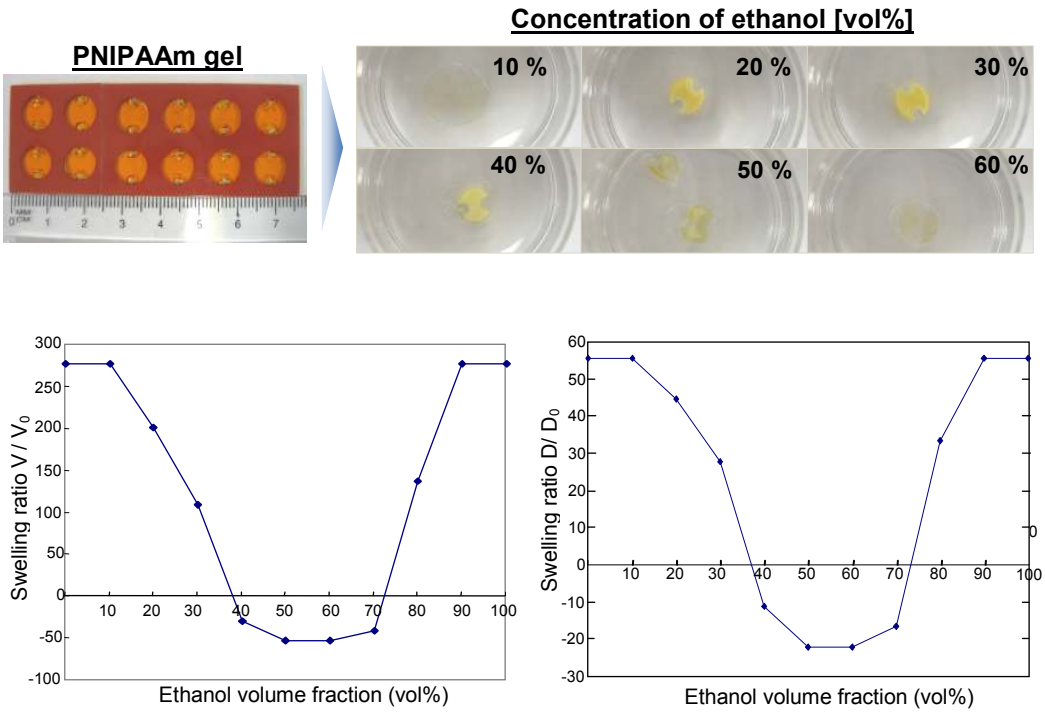

Figure 5.46: Dependence of the swelling ratio for the PNIPAAm gel on the solvent composition of ethanol-water mixtures at room temperature. The gels were equilibrated in these solvents for 3 days. The volume of PNIPAAm gel is calculated based on the assumption that the swelling ratio of the height of the gel cylinder is the same as the swelling ratio of the diameter of the gel. V_0 and D_0 are the initial volume and diameter of the gel respectively.

These patterns of behaviour are consistent with previous studies by Amiya *et al.*[35] on the behaviour of cross-linked PNIPAAm gels in mixed alcohol-water solvents. Such gels respond to changes in solvent composition by reversible shrinking and swelling. For example, at 22 °C a PNIPAAm gel containing 8 mM sodium acrylate is swollen for methanol composition ranging from 0 to 30 vol% (mole fraction of methanol (x_m) = 0.16). At a methanol composition of 30 vol% the gel undergoes a discrete volume collapse by 10 times. The gel volume remains constant with further increase of the methanol content up to 57 vol% (x_m = 0.37). At this concentration the gel "reswells discontinuously". To account for the occurrence of the two transitions, they present a model that requires the free energy of the methanol-water interaction to become negative in a given methanol-water composition range in Figure 5.47. In the absence of polymer, the interaction parameter between alcohol and water is always positive.

Addition of PNIPAAm to water-methanol mixtures enhances the attractive interaction for water and methanol.

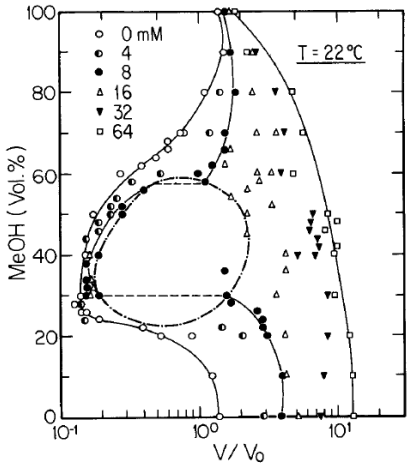

Figure 5.47: Swelling ratio (final to initial equilibrium volume) of PNIPAAm gels in mixtures of methanol and water at 22 °C. The numerical values shown in the figure indicate the concentrations of sodium acrylate incorporated within the polymer network at gelation. Data are from Ref 35.

For solvent composition of methanol mole fraction (x_m) < 0.05, the methanol molecules are kept apart each other by the formation of hydrogen cages around each molecule. Under these circumstances the polymer-solvent interactions are essentially undisturbed by the presence of methanol molecules. As the methanol mole fraction increase, there is no longer sufficient water to provide clathrate cavities for all the methanol molecules. These are now free to interact with polymer segments. In solutions of higher methanol content, the methanol-polymer interaction becomes predominant. In this work the reentrant phenomenon was also observed in the PNIPAAm gel containing $Ru(bpy)_3^{2+}$. In addition, we can expect this phenomenon if we can immobilise the $Ru(bpy)_3^{2+}$ catalyst in the gel network more easily.

5.3 Preparation of electro-responsive anisotropic polyelectrolyte gels

In section 5.2 we have designed a self-propelling hydrogel driven by the energy of the BZ or BR reaction. However, the prepared gels show too slow swelling-deswelling oscillating behaviour to propel the gel in the aqueous phase. Therefore, we have investigated the application of an electric field as a driving force for a fast and reversible electroactuation of a polyelectrolyte gel.

When a water-swollen cross-linked polyelectrolyte gel is inserted between a pair of electrodes and a direct current (*dc*) electric field is applied, it undergoes anisotropic contraction and concomitant fluid (water) exudation.[10,11] Figure 5.48 shows the schematic illustration of the shape change of an anionic polyelectrolyte gel such as cross-linked poly(acrylic acid) gel with time under an electrical field.[12] An anionic gel slightly swells near the cathode and extensively contracts near the anode, the reverse occurs for the cationic gel (not shown in here). The rate of contraction is proportional to the applied electrical current and the contraction of the gel is reversible; that is, it swells in water after the electricity is turned off.

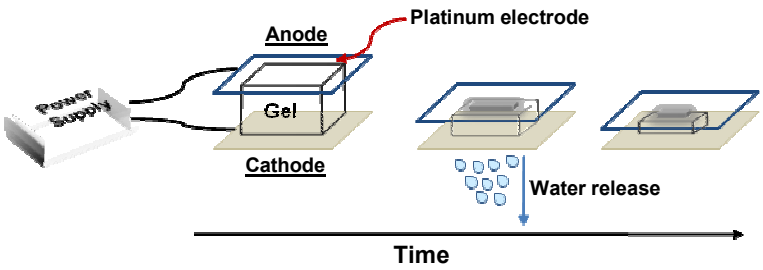

Figure 5.48: Schematic view of the shape change of an anionic gel with time under an electric field. The dark region to the anode electrode is the shrunken area of the anionic hydrogel.

In this section, we describe some of our results that attempts to develop anisotropic self-propulsion hydrogel particles driven by an electrical field (e.g., electroactuation). Polyelectrolyte gels show an anisotropic swelling in a salt solution under the influence of an electric field.[36] The swelling deformation produces bending of rectangular gels with large deflection. The swelling, or bending, is found to be induced by an increase in the osmotic pressure due to ionic drift in the electric field. Thus, if the gel is in a salt solution under *ac* electric field, the gel is expected to repeat the swelling-deswelling behaviour and to propel in the salt solution. We present two types of behaviour of the poly(2-acrylamido-2-methyl-1-propanesulfonic acid) (PAMPS) gel associated with an electric field: one is the deformation of the PAMPS gel induced by *ac* electric field and another concern is the electrical motility of the PAMPS gel induced by *dc* electric field.

5.3.1 Preparation of electroactuating polyelectrolyte gels

5.3.1.1 Bending motion of PAMPS gel in an electrolyte solution

Cross-linked water swollen PAMPS gels were prepared by UV polymerisation of 5.0 mol% of AMPS monomers in oxygen free water in the presence of 5×10^{-2} mol% *N,N'*-methylene bisacrylamide (MBAAm) as a cross-linker and 5×10^{-2} mol% of Darocur 1173 as a photoinitiator. UV polymerisation was carried in a glass capillary tube with an inner diameter 0.45 mm under UV curing lamp (Agar Scientific, UK) which was positioned at 20 mm height for 10 min at room temperature. The polymerised gel was then immersed in pure water at least for a day to remove unreacted monomers. The gels were then coloured by incubating in an aqueous solution containing 1 mM of methylene blue, followed by washing with pure water several times. This facilitated the observation of the deformation of the gel more easily under a microscope.

For measuring the rate of bending motion, a piece of water-swollen cylindrical gel (e.g., 10 mm long and 1 mm in diameter) was incubated in 10 mM hexadecyl pyridinium chloride ($C_{16}PyCl$) aqueous solution containing 30 mM lithium sulphate (Li_2SO_4) between a pair of parallel 0.2 mm diameter platinum wire electrodes. A *dc* voltage (2–15 V/cm) was applied across the electrodes set 1 cm or 2 cm apart, using a Trek 610C high voltage power amplifier (Trek Inc., NY) in conjunction with a Agilent 33220A signal generator (Agilent Technologies, CA) as shown in Figure 5.49. When applying *ac* electric field into an electrochemical cell we have usually used a capacitor to remove any *dc* component. We also measured the applied electric field between the electrodes using a digital voltmeter (Meterman 27XT, Wavetek).

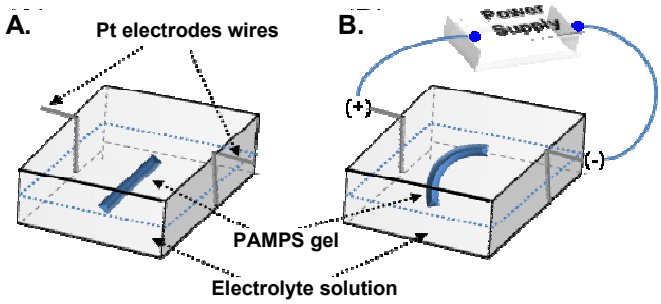

Figure 5.49: Cylindrical PAMPS gel placed between two platinum (Pt) electrodes in an electrolyte solution shows (A) no electroactuation and (B) electroactuation by application of *dc* electric field during a time period of 20 sec.

The influence of applied electric field on the bending motion of the PAMPS gel was firstly examined according to the concentration of $C_{16}PyCl$ and Li_2SO_4. At 5 V/cm the PAMPS gel started bending very slowly towards the anode. The bending rate was increased with increasing *dc* voltage and the bending was easily observed at 10 V/cm. When *ac* electric field with 1–5 V/cm of 0.1–10 Hz were applied across the gel between platinum electrodes with a separation of 1 or 2 cm, no bending motion of the gel was observed. We could not observed any electro-response at the maximum applied *ac* electric field (5 V/cm) in an aqueous solution containing 10 mM $C_{16}PyCl$ and 30 mM Li_2SO_4 using our generator and amplifier.

Table 5.4: Summary of the bending motion of the PAMPS gel in *dc* and *ac* electric fields in an aqueous solution containing 10 mM $C_{16}PyCl$ and 30 mM Li_2SO_4

Electric field (V/cm)	Bending motion of the PAMPS gel	
	dc electric field	*ac* electric field (from 0.1 to 10 Hz)
2	No bending	No bending
5	Slow bending	No bending
10	Fast bending	Not available
15	Fast bending	Not available

To increase the applied *ac* voltage using the same generator and amplifier, we increased the resistance of the electrochemical cell in two ways: 1) decreasing of the exposed surface area of Pt electrode in an electrolyte solution, 2) decreasing of the dimensions of the electrochemical cell.

Firstly, the Pt electrode was coated with nail polish leaving ~ 1 mm of uncoated area at the end of the electrode. Using these coated Pt electrodes, we obtained a higher *ac* electric field (~10 V/cm) at 1 Hz in 10 mM Li_2SO_4, 10 mM $C_{16}PyCl$ solution. However, no electro-response of the PAMPS gel (e.g., bending or propulsion) was observed. In a previous study,[37] the polyvinyl alcohol-polyacrylic acid gel film shows bending-straightening motion when subjected to electric field of less than 1 Hz at 15 V/cm in 10 mM Na_2CO_3 aqueous solution however they wave or vibrate under signals from 2–5 Hz. Therefore, we should generate a higher *ac* electric field to observe the electro-response of the PAMPS gel at the above condition.

Secondly, the applied *ac* electric field and the electro-response of the PAMPS gel were measured according to the distance between Pt electrodes (i.e. the dimension of the cell). Changing the dimension of an electrochemical cell had little effect on the applied *ac* electric field even after decreased to a quarter of the original dimension. We summarise all these results in Figure 5.50.

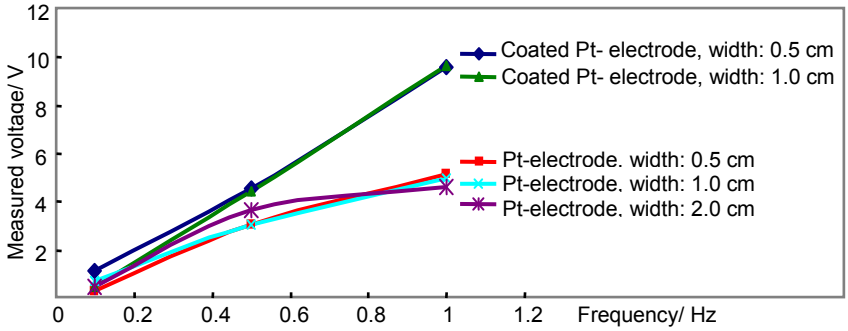

Figure 5.50: Effect of the dimension of an electrochemical cell and the partial coating of the Pt electrode under *ac* electric field at various frequencies. The *ac* electric field was measured in 10 mM $C_{16}PyCl$ and 30 mM Li_2SO_4 at 10 V set voltage of the generator (Agilent Model 33220A, Agilent Technologies).

We examined the electro-response of the elbow-shaped PNIPAAm /poly(NIPAAm-*co*-AMPS) gel bigel strip which was expected to change the gel shape (e.g., elbow shape ↔ straight shape) by applying an electric field. However, the bigel did not show any response to either the *ac* or *dc* electric field in all conditions. It was assumed that this is due to an insufficient amount of ionisable groups in the AMPS in the part of poly(NIPAAm-*co*-AMPS) gel and the thickness of the gel (~2 mm) compared to the cylindrical PAMPS gel (~1 mm). Whereas the bigel was shrunken and showed straighten shape at a higher ionic strength aqueous solution (e.g., 10 mM $C_{16}PyCl$) very slowly after long incubation for > 12 h at room temperature without an electric field.

To find the optimal ionic strength to induce a fast electroactuation of the PAMPS gel using our electrical equipment set-up, the electric response of the PAMPS gel was examined by measuring the bending angles of cylindrical gel at a fixed interval (e.g., 20 sec) according to the concentration of $Li_2SO_4$and $C_{16}PyCl$ as shown in Figure 5.51.

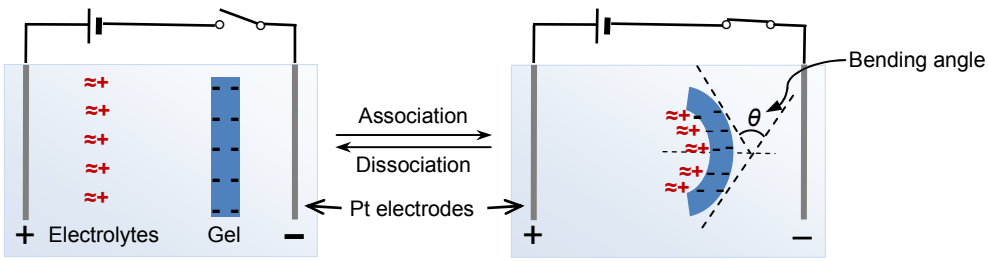

Figure 5.51: The electro-response of the PAMPS gel measured by the bending angle (θ) in an electrolyte solution under electric field.

Table 5.5 shows the electrical bending motion of the PAMPS gel under *dc* electric field. The measured *dc* electric field between Pt electrodes was not drastically changed by increasing the setting voltage of the generator from 1 to 5 V.

Table 5.5: Electro-deformation of the PAMPS gel as a function of the concentration of Li_2SO_4 and $C_{16}PyCl$ under *dc* electric field

Aqueous solution	Setting *dc* voltage of the generator	Measured voltage (V/cm)	Measured maximum Bended angle/ degree
Pure water		200 V	No bending
30 mM Li_2SO_4 10 mM $C_{16}PyCl$	1 V_{DC}	16.3 V	60 degree
	5 V_{DC}	15.5 V	
100 mM Li_2SO_4	1 V_{DC}	8.4 V	No bending
	5 V_{DC}	8.3 V	
30 mM Li_2SO_4	1 V_{DC}	13 V	14 degree
	5 V_{DC}	14.9 V	30 degree
10 mM Li_2SO_4	1 V_{DC}	20 V	Slow bending and straightening
	5 V_{DC}	24 V	
10 mM $C_{16}PyCl$	0.5 V_{DC}	63 V	52 degree
	1.0 V_{DC}	64 V	
1 mM $C_{16}PyCl$	0.5 V_{DC}	100 V	Vibration and fast collapsed
	5 V_{DC}	150 V	

We also measured the electro-response of the PAMPS gel under *ac* electric field without a capacitor which is likely to drastically decrease the applied *ac* field in polyelectrolyte solutions. Under this condition the *ac* electric field from the generator and amplifier generated the oscillating *dc* component as well as the *ac* component, thus we measured the applied *ac* and *dc* voltage separately at the set *ac* voltage of the generator (Table 5.6).

Table 5.6: Bending angles of the PAMPS gel under *ac* electric field without a capacitor connection between a generator and amplifier and a Pt electrode as a function of the frequency of the *ac* electric field

Setting *ac* voltage (V_{ac})	Frequency	Measured square wave of *dc* component (V/cm)	Measured *ac* voltage (V/cm)	Bending response
1 V	1 Hz	+ 38.5 ↔ – 46.5	~ 0	Weak
	0.5 Hz	+ 45.0 ↔ – 41.5	~ 0	Weak
	0.1 Hz	+ 47.5 ↔ – 43.0	~ 0	Strong
2 V	1 Hz	+ 50.5 ↔ – 49.5	~ 0	Weak
5 V	1 Hz	+ 55.0 ↔ – 36.0	~ 0	Weak
	0.1 Hz	+ 60.5 ↔ – 45.5	~ 0	Strong

At these conditions, the PAMPS gel (1 cm length and 1 mm diameter) showed a bending-straightening motion when subjected to *ac* electric fields of less than 1 Hz (Figure 5.52).

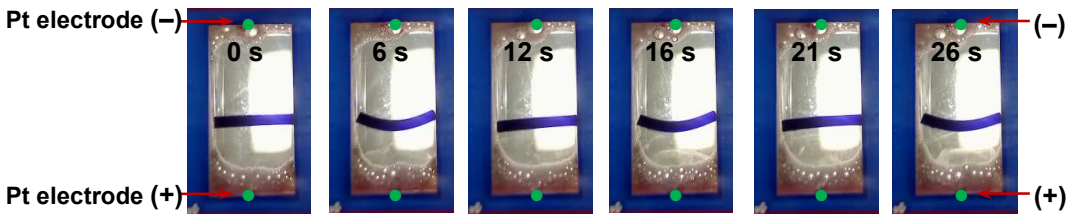

Figure 5.52: Oscillatory bending-straightening motion of the PAMPS gel under *ac* electric field (1 V, 0.5 Hz) in 10mM $C_{16}PyCl$ and 30 mM Li_2SO_4 according to the time scale without a capacitor connection. The dimension of an electrochemical cell is 1 cm × 2 cm and all images were captured using Logitech Quickcam Pro 9000.

The bending-straightening behaviour was induced by the square wave of potential of the *dc* component generated at these conditions and not by the *ac* electric field which was measured to be almost zero. The piece of gel moved slowly from the cathode to the anode under high setting *ac* electric field of low frequency (e.g., at 5 V, 0.1 Hz), which is likely to be due to electrophoresis of the charged particles under *dc* electric field.

The deformation speed of the gel is proportional to the frequency of the applied electric field. It also depends on the thickness of the gel and the flexibility of the gel mainly determined by the concentrations of AMPS and a cross-linker MBAAm in the gels (data not shown here).

5.3.1.2 The motility of PAMPS gel in dc electric field

When a high *dc* electric field (e.g., 100 V/cm) was applied in 1 mM $C_{16}PyCl$ aqueous solution (without a capacitor), the cylindrical PAMPS gel sample showed a rotation or propulsion depending on its dimension. Therefore, the propulsion of a small cylindrical PAMPS gel (3 mm length and 1 mm diameter) was examined in detail at various conditions. The PAMPS gel moved from the cathode to the anode with a rate of ~0.1 cm/s at applied 50 V/cm and the direction was changed oppositely by alternating the direction of *dc* voltage. At a high *dc* electric field (e.g., 100 V/cm) the PAMPS gel was slowly shrunk and deformed, whereas the gel swelled and returned to the cylindrical shape after the applied electric field was switched off. Figure 5.53 shows one of the examples of the propulsion of the PAMPS gel in *dc* electric field.

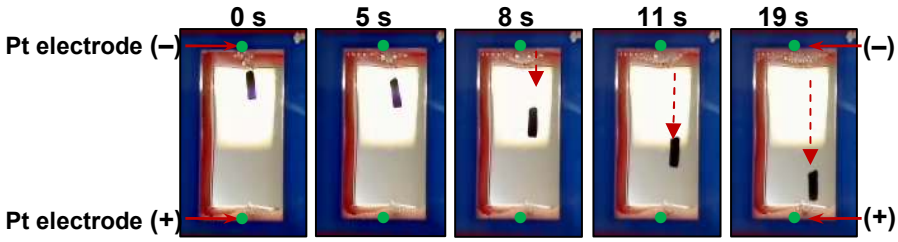

Figure 5.53: The propulsion of the PAMPS gel driven by *dc* electric field in 1 mM $C_{16}PyCl$ aqueous solution without a capacitor connection according to the time scale. The cylindrical gel (3 mm length, 1 mm diameter) was moved from cathode to anode electrode. The dimension of the cell is 1 cm × 2 cm and all images were captured using Logitech Quickcam Pro 9000.

At high *dc* electric field the gas which was formed at the surface of Pt electrodes inhibited the propulsion of the PAMPS gel, therefore care should be taken to prevent the gas formation at the electrode to observe accurate propulsions (e.g., covering the electrode with a dialysis membrane).

5.4 Conclusions

In this chapter, we designed novel biomimetic self-propelling hydrogel particles made of synthetic polymer. Either chemical self-oscillation reactions or an electric field were used to generate autonomous swelling-deswelling oscillations of the gels in an aqueous solution.

The main conclusions from this chapter are:

- We developed a new bigel synthesis method by UV polymerisation. The bigels having a different hydrophilicity shows the anisotropic contraction in water and ethanol. The anisotropic contractions observed from these bigels are based on the fact that the volumes of two different gels are sensitive to different aspects of the same external environment.
- Using this method we prepared the bigel which has a part of the gel with covalently bonded ruthenium catalyst $Ru(bpy)_3^{2+}$ which participates in a redox reaction in oxidising and reducing conditions. However, the bigel did not show a drastic enough oscillatory bending-straightening motion to propel the gel in the BZ substrates solution. We observed a very slow propagation of the chemical waves onto the gel surface coupled with the BZ reaction.
- For a preparation of an electro-actuating particles, weakly cross-linked poly(2-acrylamido-2-methyl-propanesulfonic acid) (PAMPS) gels were synthesised and its electro-mechanical behaviour of the particles in the presence of cetylpyridinium chloride and lithium sulphate solution was observed under *ac* and *dc* electric fields.
- Without a capacitor connection between the generator and the platinum (Pt) electrodes of the electrochemical cell, the PAMPS gel shows the oscillatory bending-straightening motion by the square wave of potential of the *dc* component. However, under *ac* field with a capacitor connection to cut-off the *dc* component, the oscillatory motion was not observed due to the insufficient magnitude of the applied *ac* field. Under high *dc* electric fields, the small cylindrical PAMPS gel particle (< 3 mm length) shows a directional movement from the cathode to the anode consistent with an electrophoresis.
- For all these results, we conclude that the rate of volume change should be a function of the initial size of the particles. Therefore, we need to decrease the size of the gel particle to submillimetres to drive it in a liquid using chemical and electrical driving forces used in this chapter.

5.5 References

1. R. Yoshida, T. Takahashi, T. Yamaguchi and H. Ichijo, "Self-oscillating gel", *J. Am. Chem. Soc.* **1996**, *118*, 5134-5135.
2. R. Yoshida, E. Kokufuta and T. Yamaguchi, "Beating polymer gels coupled with a nonlinear chemical reaction", *Chaos* **1999**, *9*, 260-266.
3. R. Yoshida, T. Takahashi, T. Yamaguchi and H. Ichijo, "Self-oscillating gels", *Adv. Mater.* **1997**, *9*, 175-178.
4. P. K. Gosh and T. G. Spiro, "Photoelectrochemistry of tris(bipyridyl)ruthenium(II) covalently attached to n-type SnO_2", *J. Am. Chem. Soc.* **1980**, *102*, 5543-5549.
5. R. Yoshida, M. Tanaka, S. Onodera, T. Yamaguchi and E. Kokufuta, "In-phase synchronisation of chemical and mechanical oscillations in self-oscillating gels", *J. Phys. Chem. A* **2000**, *104*, 7549-7555.
6. M-L. Smoes, "Period of homogenous oscillations in the ferroin-catalysed Zhabotinskii system, *J. Chem. Phys.* **1979**, *71*, 4669-4679.
7. K. J. M. Bishop, M. Fialkowski and B. A. Grzybowski, "Micropatterning chemical oscillations: Waves, autofocusing, and symmetry breaking", *J. Am. Chem.* **2005**, *127*, 15943-15948.
8. R. C. Teitelbaum, S. L. Ruby and T. J. Marks, "On the structure of starch-iodine", *J. Am. Chem. Soc.* **1978**, *100*, 3215-3217.
9. P. Foerster, S. C. Müller and B. Hess, "Curvature and propagation velocity of chemical waves", *Science* **1988**, *241*, 685-687.
10. Y. Osada and M. Hasebe, "Electrically activated mechanochemical devices using polyelectrolyte gels", *Chem. Lett.* **1985**, 1285-1288.
11. R. Kishi and Y. Osada, "Reversible volume change of microparticles in an electric field", *J. Chem. Soc., Faraday Trans. 1* **1989**, *85*, 655-662.
12. J. P. Gong, T. Nitta and Y. Osada, "Electrokinetic modelling of the contractile phenomena of polyelectrolyte gels. One-dimensional capillary model", *J. Phys. Chem.* **1994**, *98*, 9583-9587.
13. Y. Osada, H. Okuzaki and H. Hori, "A polymer gel with electrically driven motility", *Nature* **1992**, *355*, 242-244.
14. Y. Osada, H. Okuzaki, J. P. Gong and T. Nitta, "Electro-driven gel motility on the base of cooperative molecular assembly reaction", *Polymer Sci.* **1994**, *36*, 340-351.

15. H. Okuzaki and Y. Osada, “Electro-driven chemomechanical polymer gel as an intelligent soft material”, *J. Biomater. Sci. Polymer Ed.* **1994**, *5*, 485-496.
16. N. Isogai, J. P. Gong and Y. Osada, “Thermosensitve polymer gels by reversible surfactant binding”, *Macromolecules* **1996**, *29*, 6803-6806.
17. S. Y. Yu, M. Hirata, L. Chen, S. Matsumoto, M. Matsukata, J. P. Gong and Y. Osada, “Formation of soluble complexes by two-step surfactant binding”, *Macromolecules* **1996**, *29*, 8021-8023.
18. L. Chen, S. Y. Yu, J. P. Gong and Y. Osada, “Surfactant binding of polycations carrying charges on the chain backbone: Cooperaticity, stoichiometry and crystallinty”, *Macromolecules* **1998**, *31*, 787-794.
19. H. Okuzaki and Y. Osada, “Electro-driven polyelectrolyte gel with biomimetic motility”, *Electrochimica Acta*. **1995**, *40*, 2229-2232.
20. H. Okuzaki and Y. Osada, “Effect of hydrophobic interaction on the cooperative binding of a surfactant to a polymer network”, *Macromolecules* **1994**, *27*, 502-506.
21. H. Okuzaki and Y. Osada, “Ordered-aggregate formation by surfactant-charged gel interaction”, *Macromolecules* **1995**, *28*, 380-382.
22. H. Okuzaki and Y. Osada, “Role and Effect of cross-linkage on the polyelectrolyte-surfactant interaction”, *Macromolecules* **1995**, 28, 4554-4557.
23. E. Jabbari, J. Tavakoli and A. S. Sarvestani, “Swelling characteristics of acrylic acid polyelectrolyte hydrogel in a dc electric field*”, Smart Mater. Struct.* **2007**, *16*, 1614-1620.
24. M. S. Paoletti, T. H. Solomon, “Front propagation and mode-locking in an advection-reaction-diffusion system”, *Phys. Rev. E* **2005**, *72*, 046204:1-046204:10
25. http://neon.chem.ox.ac.uk/vrchemistry/FilmStudio/oscillating/HTML/page01.htm [Accessed 12 July 2007].
26. R. Yoshida, G. Otoshi, T. Yamaguchi and E. Kokufuta, “Traveling chemical waves for measuring solute diffusivity in thermosensitive poly(N-isopropylacrylamide) gel”, *J. Phys. Chem. A* **2001**, *105*, 3667-3672.
27. Y. Hara and R. Yoshida, “Self-oscillation of polymer chains induced by the Belousov-Zhabotinsky reaction under acid-free conditions”, *J. Phys. Chem. B* **2005,** *109*, 9451-9454.
28. I. Varga, I. Szalai, R. Mészaros and T. Gilányi, “Pulsating pH-responsive nanogels”, *J. Phys. Chem. B.* **2006**, *110*, 20297-20301.

29. S. Maeda, Y. Hara, T. Sakai, R. Yoshida and S. Hashimoto, “Self-walking gel”, *Adv. Matter.* **2007**, ***0000***.*00*. 1-5.
30. Y. Ogawa, K. Ogawa, B. Wang and E. Kokufuta, “A biochemo-mechanical system consisting of polyampholyte gels with coiommobilised glucose oxidase and urease”, *Langmuir* **2001**, *17*, 2670-2674.
31. S. Tateyama, Y. Shibuta and R. Yoshida, “Direction control of chemical wave propagation in self-oscillating gel array”, *J. Phys. Chem. B* **2008,** *112,* 1777-1782.
32. M. B. Huglin, Y. Liu, J. L. Velada, “Thermoreversible swelling behaviour of hydrogels based on N-isopropylacrylamide with acidic comonomers”, *Polymer* **1997**, *38*, 5785-5791
33. J. L. Velada, Y. Liu and M. B. Huglin, “Effect of pH on the swelling behaviour of hydrogels based on N-isopropylacrylamide with acidic comonomers”, *Macromol. Chem. Phys.* **1998**, *199*, 1127-1134.
34. S. Katayama, Y. Hirokawa and T. Tanaka, “Reentrant phase transition in acrylamide-derivative copolymer gels”, *Macromolecules* **1984**, *17*, 2641-2643.
35. T. Amiya, Y. Hirokawa, Y. Hirose, Y. Li and T. Tanaka, “Reentrant phase transition of *N*-isopropylacrylamide gels in mixed solvents*”, J. Chem. Phys.* **1987**, 86, 2375-2379.
36. T. Shiga, “Deformation and viscoelastic behaviour of polymer gels in electric fields”, *Proc. Japan Acad. B* **1998**, *74*, 6-11.
37. T. Shiga, Y. Hirose, A. Okada and T. Kurauchi, “Deformation of ionic polymer gel films in electric fields”, *J. Mater. Sci.* **1994**, *29*, 5715-5718.

Chapter 6

Designing Self-propelling Janus Particles

Chapter 6

Designing Self-propelling Janus Particles

6.1 Strategies to develop self-propelling Janus particles based on osmotic pressure gradient

The studies of autonomous nano- and micron-sized motors that can convert stored chemical to mechanical energy may help us not only to understand chemomechanical transduction found in various kinds of motilities in living organisms but also to design novel artificial motors that mimic them. However, it is difficult to make self-propelling particles which swim by themselves in liquids. The flagella and ciliar motions of bacteria are the best known natural self-propelling mechanism on the microscale. There were many reports about the development of self-propulsion on the microscale such as bimetal-particle propulsion via catalytic decomposition of hydrogen peroxide,[1,2] the self-motion of camphene disc on water surface driven by the convection and the surface tension of the camphene layer[3] and self-propelling semiconductor diode powered by an external electric field.[4] Mallouk and co-workers reported the autonomous, non-Brownian movement of platinum/gold (Pt/Au) nanorods, 370 nm in diameter and consisting of 1 μm long Pt and Au segments as shown in Figure 6.1A.[6]

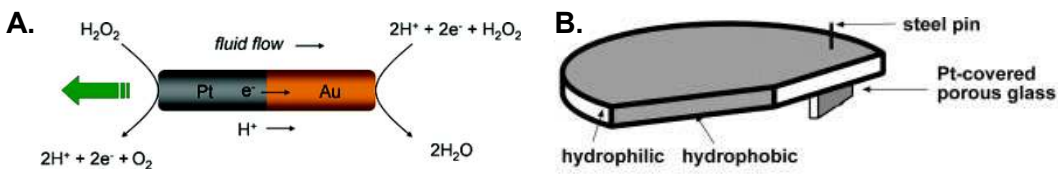

Figure 6.1: Schematic illustrations of self-propelling objects (A) 1 μm long and 370 nm in diameter Pt and Au bimetallic nanorod[5] and (B) a thin hemicylindrical polydimethylsiloxane (PDMS) plate (< 1 cm) with 2 mm × 2 mm Pt-covered glass filter propelled by the catalytic decomposition of hydrogen peroxide to oxygen and water.[1]

These bimetallic nanorods catalyse the spontaneous decomposition of hydrogen peroxide to oxygen and water at the Pt end in 2–4 wt% hydrogen peroxide solution. For the Pt-Au nanorods, the experimentally determined rate of oxygen evolution from 3.7 wt% hydrogen peroxide was 9.7×10^{-16} mol of O_2/sec per rod and they move predominantly along their axis in the direction of the Pt end at a speed of 7.9 ± 0.7 μm/s.[6]

Whitesides *et al.* have used the impulse of oxygen bubbles generated by the catalytic decomposition of hydrogen peroxide to propel cm/mm-scale objects on the surface of a 1–3 wt% hydrogen peroxide aqueous solution with velocities of up to 1–2 cm/s (Figure 6.1B).[1] There are many other chemical systems that can generate a motion, such as self-propulsion of tetrahydrofuran swollen hydrogels,[7,8] but most cases are limited to movement on the surfaces of liquids, in the duration over which they can move and in the constancy of that motion.

We have studied systems to develop metal coated Janus particles moving autonomously by osmotic pressure in an aqueous solution. A Janus particle has an asymmetrical shape divided in two parts, which have different surface properties such as surface charges and functional groups. The energy to move the particle will be provided by the osmotic pressure gradient generated by two different ways: 1) the catalytic decomposition of a "fuel" contained in the environment by an enzyme immobilised on the surface of the particle, and 2) the diffusion of a chemical (e.g., glucose, ethanol) from the particle interior into the environment as shown in Figure 6.2. The two particles are expected to move in the opposite direction with respect to the Au-coated surface of the Janus particles.

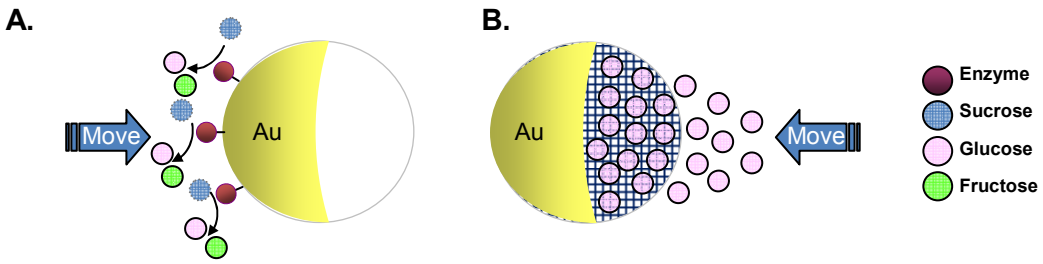

Figure 6.2: Schematic illustrations of self-propulsion Au-coated Janus particles driven by (A) invertase reaction and (B) glucose diffusion.

The velocity and duration of motion of the particle are expected to be strongly dependent on the shape, size, and morphology. Therefore, we first designed asymmetric Janus spherical particles using various well-established preparation methods such as the gel trapping technique (GTT) and then partly coating with metal (e.g., Au and Pt) to cover the exposed surface of the particle for anisotropic surface modification. The metal coating functions not only to produce a surface to immobilise enzymes but also as a barrier to promote an asymmetric dissolution of chemicals from the particle into the aqueous phase.

We first describe some theoretical considerations relevant to the propulsion of particles using an osmotic pressure gradient. If we simplify the reaction condition in which an enzyme immobilised spherical particle is propelled by the osmotic gradient which is generated by the catalytic activity of the enzyme in water we can estimate the minimum diameter of the particle to move in the water and its velocity as follows. We consider four forces acting on a particle in a liquid: gravity, osmotic pressure, friction, and buoyancy as shown Figure 6.3.

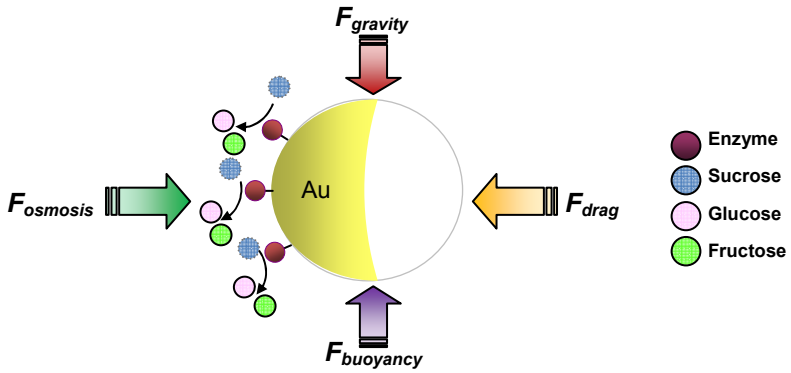

Figure 6.3: A schematic illustrating of four forces acting on the invertase immobilised Au-coated Janus particle.

For a spherical Janus particle propelling through a liquid, the various forces acting on the particle are given by the following equations:

$$F_{gravity} = m_p \times g \qquad [1]$$

$$F_{buoyancy} = \frac{4\pi \times r^3 \times \rho_p \times g}{3} \qquad [2]$$

where m_p is the particle mass, g is the acceleration due to gravity (g = 9.81 m/s^2), ρ_p is the density of the particle (e.g., ρ_p = 1.05 g/cm^3 for polystyrene latex liquid), r is the particle radius. If we balance the $F_{gravity}$ and $F_{buoyancy}$ by matching the densities between the liquid and the particle, we avoid the gravity force effect and consider only the rest two forces $F_{osmosis}$ and F_{drag}.

The osmotic pressure ($\Delta\Pi$) exerts the following force ($F_{osmosis}$) on the particle:

$$F_{osmosis} = \pi \times r^2 \times \Delta\Pi \qquad [3]$$

$$\Delta\Pi = \Delta C_m \times R \times T \qquad [4]$$

$$F_{osmosis} = \pi \times r^2 \times \Delta C_m \times R \times T \qquad [5]$$

where ΔC_m is the concentration difference of molecules between the Au surface of the particle and bulk liquid phase and is related with the activity of the enzyme immobilised

on the Au-coated part of the particle surface. T is the temperature of the liquid phase, R is the gas constant (R = 8.314 J/K mol)

For the particle propelling by osmotic pressure through a liquid, it initially accelerates. As the velocity increases, the drag force (F_{drag}) acting in the opposite direction to the acceleration force increases. Eventually, it reaches a constant velocity called the terminal velocity (v_t) at which the drag force exactly balances the net acceleration force. The drag force acting on the particle is

$$F_{drag} = 6\pi \times \eta \times r \times v_t \qquad [6]$$

where v_t is the terminal velocity of a particle and η is the viscosity of liquid (e.g., η_{water} = 1.002 cp at 20 °C [9]).

So, finally the terminal velocity of the particle (v_t) is

$$v_t = \left(\frac{R \times T}{6\eta}\right) \times r \times \Delta C_m \qquad [7]$$

If the sub-surface concentrations of glucose, fructose, and sucrose can be expressed as [*Glucose*], [*Fructose*] and [*Sucrose*] and invertase is immobilised on the surface of the particle and is active. $\Delta\Pi$ is always positive because ΔC_m is positive (ΔC_m = [*Glucose*] + [*Fructose*] − [*Sucrose*] > 0). ΔC_m depends on the rate of the catalytic reaction of immobilised enzyme and the diffusion rate of the molecule which is produced by the enzyme on the surface of the particle. If the time for reactant and product diffusion over a distance r is τ, the catalytic reaction rate of the immobilised enzyme must be bigger than τ^{-1} to propel the particle in a liquid

$$\tau^{-1} \approx \frac{2D}{r^2} \qquad [8]$$

where D is the diffusion coefficient of the reactant and products (e.g., D for sucrose in water = 0.5212×10^{-9} m^2/s at 25 °C[9]).

6.2 Enzymatic reactions driven Janus particles

6.2.1 Preparation of invertase reaction driven Janus particles

Enzymes are often immobilised onto or into solid supports[10] and entrapped into capsules[11]to increase their stability by protecting the active materials from deactivation. Many methods are available for enzyme immobilisation but may be subdivided into two

general classes: 1) chemical methods, where covalent bonds are formed with the enzyme, and 2) physical method, where weak interactions between support and enzyme exist. Many inorganic and organic materials are used for the preparation of immobilised enzymes such as a porous glass,[12] silica gels, gold particle[10] and hydrogels.[11,13]For a covalent enzyme immobilisation, a surface modification or activation steps is needed such as the activation of amine groups of surface by glutaraldehyde.[14] In this chapter, we immobilised two different enzymes onto the Au-coated hemisphere of a Janus particle and the enzymes immobilised on the surface of the particle (e.g., invertase) generate the concentration difference of a soluble substrate in the proximity of both hemispheres to create the osmotic pressure gradient for propulsion shown in Figure 6.2.

Invertase, from *Saccharomyces cerevisiae,* is an enzyme catalysing the hydrolysis of sucrose to glucose and fructose as following reaction:

$$\text{Sucrose} + H_2O \rightarrow \text{Glucose} + \text{Fructose}$$

The resulting imbalance of the sugar concentration creates the osmotic pressure gradient and induces a motion of the particle relative to the fluid and finally propels the particle toward the Au-coated side with respect to the stationary fluid. The direction of movement of the particles is expected as opposite to previous results[1] in which the platinum (Pt) catalyst is at the trailing end of the moving PDMS plates (Figure 6.1B).

6.2.1.1 Immobilisation of invertase on Au-coated Janus particles

In this section we describe the method for invertase immobilisation at the Au surface of spherical Janus particles. The Au-coated polystyrene latex and polymethyl methacrylate (PMMA) Janus particles were produced by Au evaporation onto the partially embedded particle monolayer on PDMS by the gel trapping technique (GTT) or on a glass slide for the glass sliding technique (GST) with a vacuum thermal evaporator. The Au-coated Janus particles were isolated from the solid supports by subsequent mechanical elution with pure water descried in section 2.2.5. We observed the structures of the Au-coated Janus particles using SEM as shown in Figure 6.4.[15] Most particles were not damaged after isolating from the glucose layer on the glass slide. In the backscattered electron images of the Au-coated Janus particles we can easily see some white crescents corresponding to the metal surface. However, the thickness of a metal layer is too thin to see the obvious border between the two hemispheres of the particles.

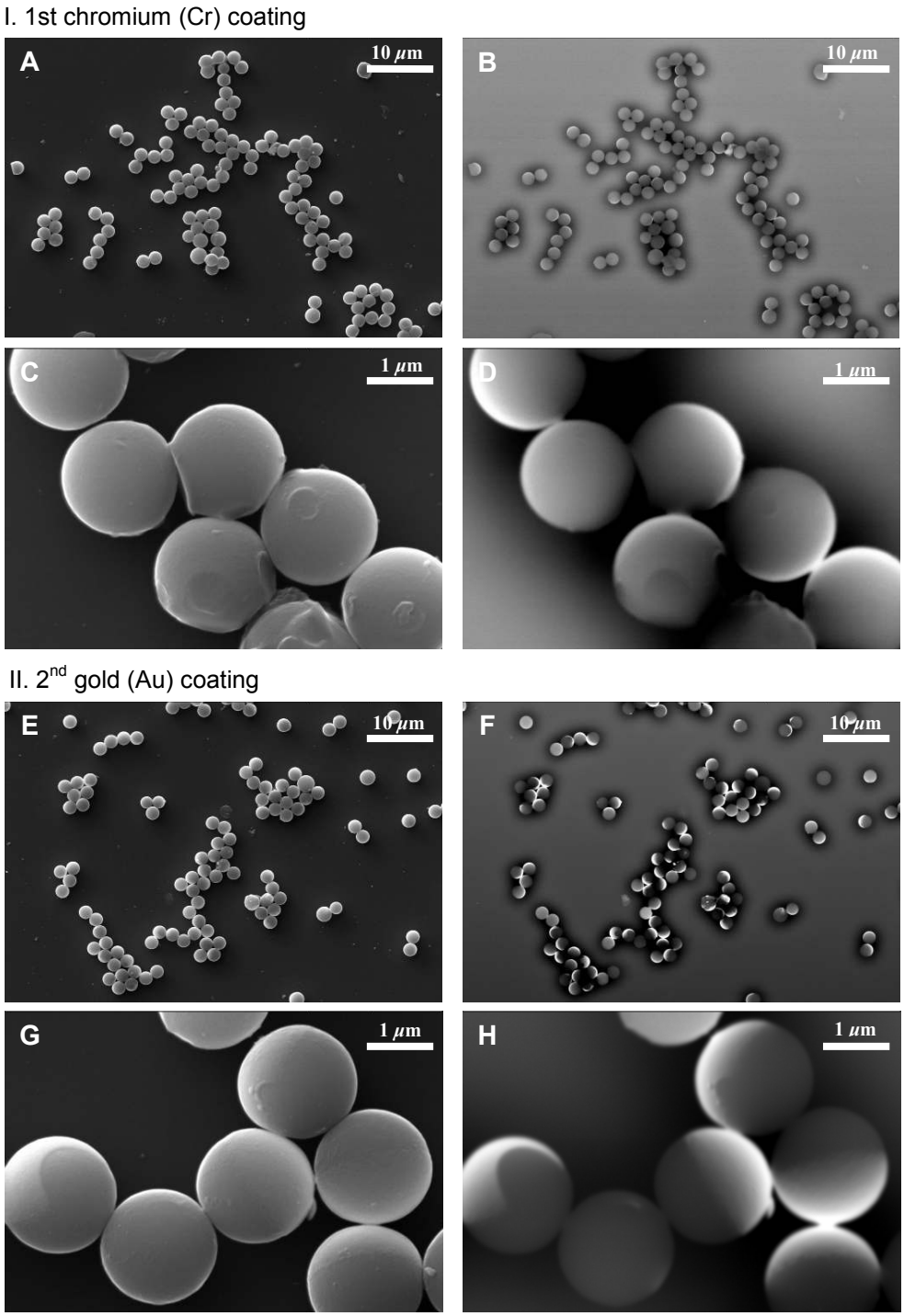

Figure 6.4: Scanning electron microscope (SEM) photographs of Au coated polystyrene latex Janus particles with diameter 2 μm prepared by the glass sliding technique (GST). Images A, C, E, and G are the secondary electron images. Images B, D, F, and H are backscattered electron images.

In previous studies,[16,17] the amino acid cysteine (H_2N-$CH(CH_2SH)$-$COOH$) which bears three functional groups, the amino, carboxyl and terminal thiol groups is water

soluble and would readily bind to the surface of Au nanorods via an Au-S linkage between and SH-group of cysteine in a solution as shown Figure 6.5.

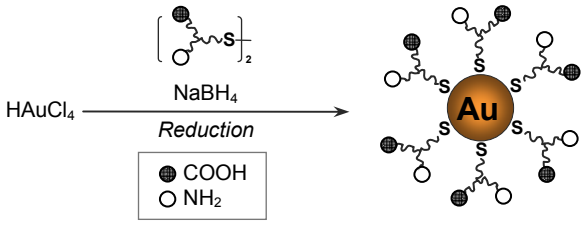

Figure 6.5: Illustration of oligomerisation of L-cysteine onto Au nanoparticles. L-cystine transforms to L-cysteine by $NaBH_4$[17].

Therefore, we immobilised an enzyme containing cysteine such as invertase on the Au-coated solid surface of the particle in an aqueous solution.

Invertase was immobilised on the Au layer of Au coated Janus particles as follows. The isolated Au coated Janus particles were washed thoroughly in pure water several times. 4 mg of solid invertase (401 units/mg of solid) was mixed with 0.2 mL of Au coated polystyrene (3 μm diameter) or carboxylated polystyrene latex Janus particles (15.47 μm diameter) in 1 mM Tris-buffer (pH 7.0) to finally 8020 units/mL and incubated at 25 or 4 °C[11] water bath for 3 h. The invertase immobilised particles were precipitated by centrifugation (14,500 rpm) for 20 min at room temperature using MiniSpin Plus centrifuge (Eppendorf, Hamburg, Germany) and then washed with 0.5 mL of pure water three times. Finally, the sample was stored at 5 °C before use. At the reaction condition (pH 7.0) invertase is expected to interact with the Au layer of the Janus particles not with negatively changed opposite carboxylate surface of the particles because the carboxylic group ($pK_a \approx 4.7$) is deprotonated at pH 7.0. The existing electrostatic repulsion between the surface of the Janus particle and invertase is likely to prevent the adsorption of invertase to the uncoated carboxylate surface.

6.2.1.2 Fluorescent detection of the immobilised invertase on the particles

To confirm the invertase immobilisation on the Au coated Janus particle as shown in Figure 6.2, we carried out two experiments: 1) fluorescent labelling and 2) the enzyme activity measurement. First, we used fluorescent labelling reagent fluorescent isothiocyanate (FITC) to detect the immobilised invertase at the surface of Janus particle. FITC isomer *I* is the most widely used fluorescent labelling reagent due to the flourophore's high quantum efficiency and conjugate stability. FITC reacts with free

amino groups of proteins to form stable conjugates as shown Figure 6.6. FITC-protein conjugates, in particular FITC labelled antibodies, are used as specific probes in immunocytochemistry and flow cytometry applications.[18]

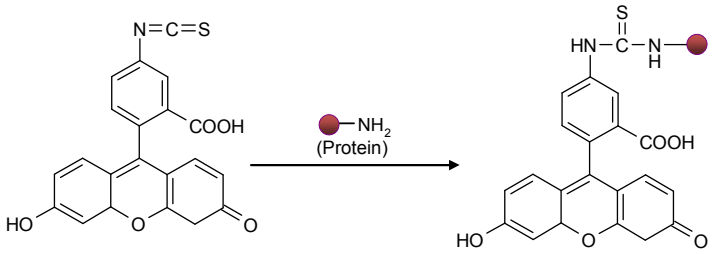

Figure 6.6: Schematic illustration of FITC labelling reaction: FITC conjugation occurs through the free amino group of proteins or peptides, forming a stable thiourea bond.

The FITC labelling reaction was followed the procedure described in the manual of Fluoro Tag™ FITC Conjugation Kit (Sigma-Aldrich, Missouri, US). Invertase immobilised Janus particle was dissolved in 0.2 mL of FITC solution at 2 mg/mL in 0.1 M carbonate-bicarbonate buffer, pH 9.1 and incubated for 3 h at 25 °C water bath with frequent shaking. The FITC labeled particles were precipitated by centrifugation (14,500 rpm) for 10 min at room temperature using MiniSpin Plus centrifuge (Eppendorf, Hamburg, Germany) and then washed with 0.2 mL of pure water three times. In a control experiment, we also incubated two other particles, invertase incubated and native polystyrene latex particles under the same experimental conditions. Fluorescent images were obtained with refractive mode on an Olympus microscope at 460-490 nm excitation wavelength and fluorescein isothiocyanate (FITC) filter.

Although it shows a strong adsorption to the invertase immobilised Au coated Janus particles (Figure 6.7A) FITC also shows a non-specific binding to the non-modified (Figure 6.7C) and the invertase incubated (Figure 6.7B) polystyrene latex particles. Moreover, the fluorescent intensity of the invertase incubated particles is higher than that of invertase immobilised Au coated Janus particles. The non-specific binding of FITC on the particles was not removed after several washing with pure water (Figure 6.7F). The Au deposited area (dark colour) of the Au coated Janus particle did not show any fluorescent intensity (green colour) (Figure 6.7A) compared to the opposite uncoated surface of the same particle (Figure 6.7B).

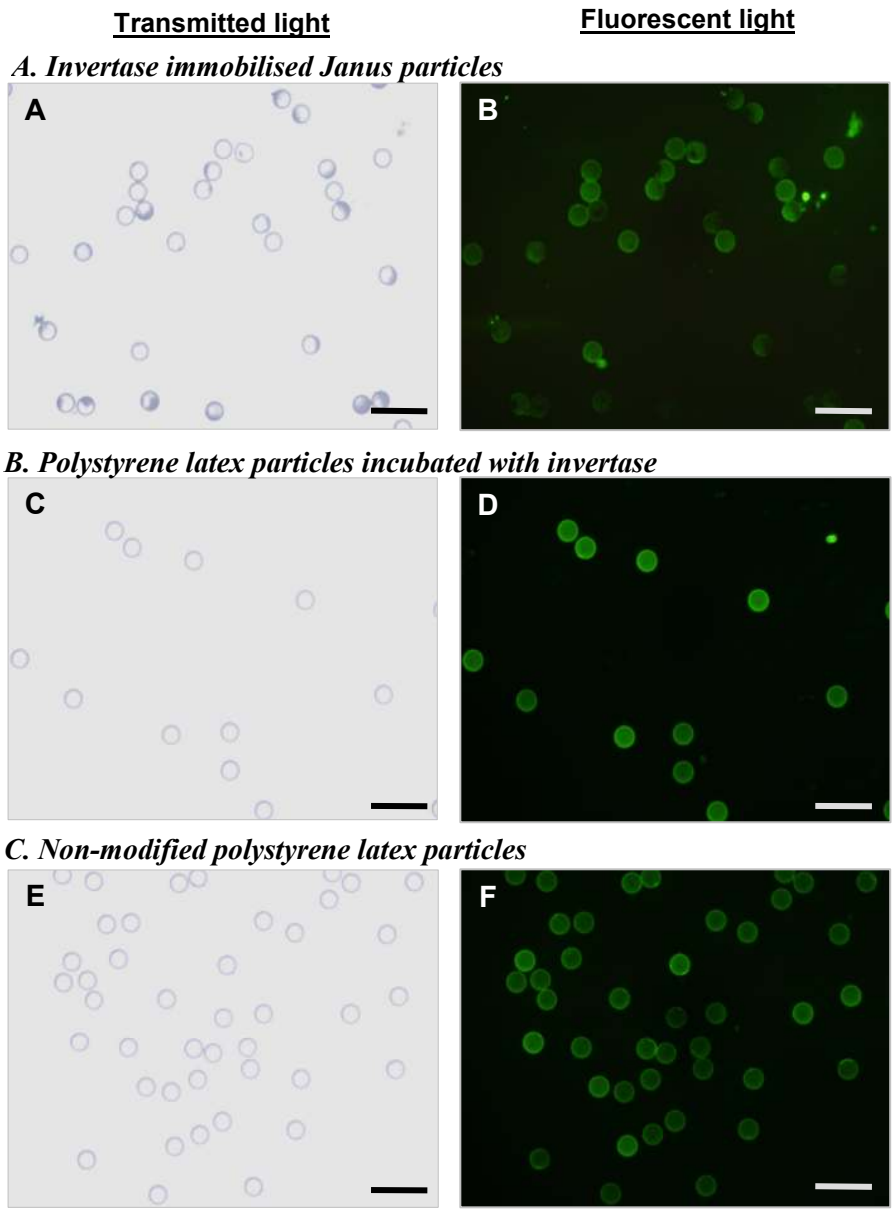

Figure 6.7: Optical images of carboxylated polystyrene latex particles (15.47 μm, diameter) labeled with fluorescein isothiocyanate (FITC). Optical examination was performed using FITC filter for fluorescent images and a 50× objective at room temperature. All scale bars represent 30 μm.

Furthermore, we proved that FITC does not adsorb to the gold (Au) and chromium (Cr) surface at the same FITC conjugation condition used above using the Au-coated (Figure 6.8) or Cr-coated (not shown here) glass slide samples.

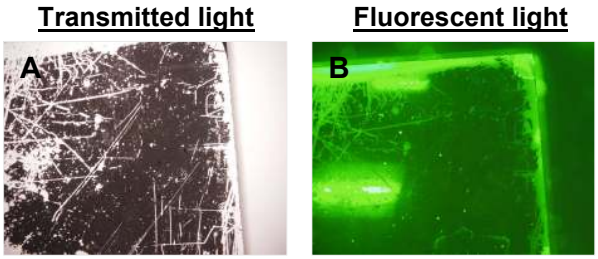

Figure 6.8: Optical images of the Au-coated glass slide after incubation with FITC solution at the same conditions used in Figure 6.7. Optical examination was performed using FITC filter for fluorescent imaging. For image A, the black area corresponds to the Au coated surface on the glass slide. FITC adsorbs stronger to the uncoated glass surface than to the Au coated glass surface.

These results indicate that FITC strongly adsorbs on the non-modified polystyrene latex surface but not on the invertase immobilised Au surface of the Janus particles. Thus, we could not confirm the immobilisation of invertase on the Au layer of the Janus particles using FITC labelling reaction. Finally, we conclude that we need to conjugate invertase with FITC firstly, purify the FITC labeled invertase from the unconjugated FITC by Sephadex® G-25 column (Sigma-Aldrich) and then incubate the Au-coated Janus particles with the labeled invertase to exclude non-specific FITC adsorption.

6.2.1.3 Measurement of catalytic activity of the immobilised invertase

For the non-specific binding of FITC to the polystyrene latex particles we performed a measurement of the catalytic activity of the immobilised invertase at the Au coated Janus particles using 3, 5-dinitrosalicylic acid (DNS) to confirm its immobilisation. DNS reagent provides a sensitive test for determining reducing sugars in a variety of biological fluids.[19,20] The reagent is composed of DNS, potassium sodium tartrate, phenol, sodium metabisulfite, and sodium hydroxide. Basically, this method detects the presence of free carbonyl groups (C=O), the so-called reducing sugars. This involves the oxidation of the aldehyde functional group present in, for example, glucose and the ketone functional group in fructose. Simultaneously, DNS is reduced to 3-amino-5-nitrosalicylic acid under alkaline conditions, as illustrated in Figure 6.9. During the reaction, the colour development of DNS is stabilised by potassium sodium tartrate and enhanced by phenol, and sulfite protects the reagent and reducing sugar from oxidation. The determination of invertase activity was based on the hydrolytic release of glucose from sucrose[21] and the colour change produced by the DNS method is proportional to the invertase activity present in the sample.

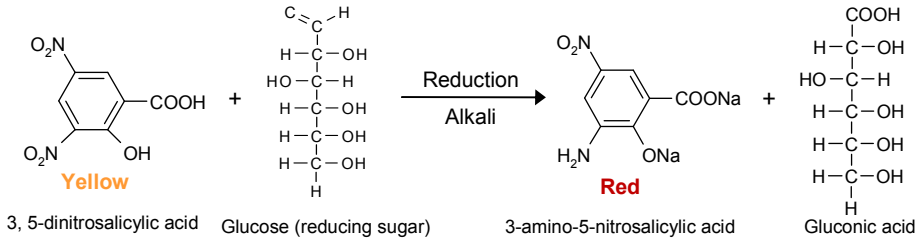

Figure 6.9: Schematic illustration of 3, 5-dinitrosalicylic acid reaction with glucose.

For an assay the reaction mixture was prepared by mixing 0.1 M sucrose and free invertase or invertase immobilised polystyrene latex particles in 0.6 mL of 8.3 mM Na-acetate buffer (pH 4.7). The reaction mixtures were incubated at 30 °C for 3 h, and the reaction was terminated by the addition of 0.4 mL of modified DNS reagent (22 mM dinitrosalicylic acid, 253 mM sodium hydroxide, 42 mM phenol, 28 mM sodium metabisulfite, and 520 mM sodium potassium tartrate tetrahydrate in water) and immersing in a boiling water bath for 10 min. The final volume of the samples was adjusted to 2 mL with pure water. After the samples were cooled down to room temperature, the absorbance was measured at 575 nm. The amount of produced glucose was calculated from the calibration curve using standard glucose samples under the same reaction conditions as shown in Figure 6.10.

A.

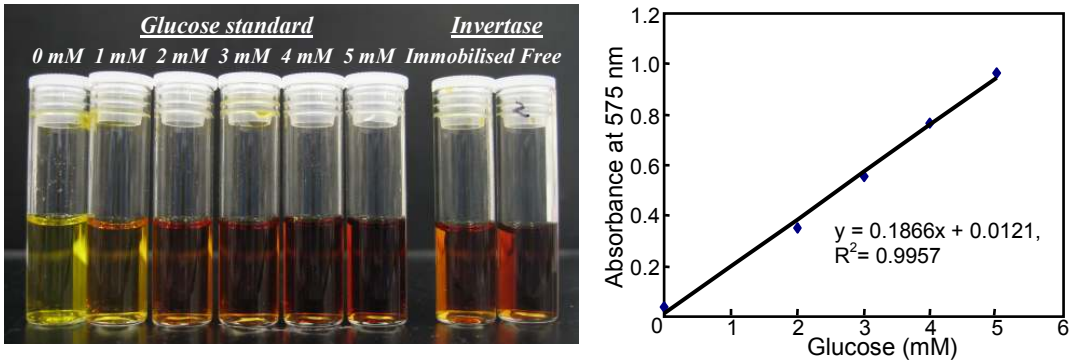

B.

Enzyme solution	Absorbance at 575 nm	Glucose concentration (mM)	Decomposition rate* (%)
Invertase immobilised Au-coated Janus particle (diameter 3 μm)	0.4702	1.7 mM	5.7 %
0.23 %w/v Invertase (10 U/mL)	0.8083	4.2 mM	14 %

** Decomposition rate = (no. mole of produced glucose/no. mole of initial sucrose) ×100*

Figure 6.10: Enzyme activity of invertase immobilised at the Au coated Janus particles using the modified DNS method (A) Invertase samples: Immobilised and free invertase as a control (B) Calculated invertase activity by the calibration curve in (A).

It can be seen that both immobilised invertase on the Au surface of the Janus particles and free invertase in the solution have a catalytic activity. The result qualitatively proves the immobilisation of invertase on the Au-coated Janus polystyrene latex particles indirectly.

6.2.1.4 The motility of invertase immobilised Janus particles

The temperature and the pH are very important factors for the enzyme activity. In a previous study,[22] the maximum residual activity for both free and cellulose membrane immobilised invertase has been observed at pH 5.0. Moreover, the optimum temperature of both free and immobilised enzyme is around 45 °C. Therefore we examined the motility of invertase immobilised Janus particles at pH 4.5 in an aqueous solution containing 1–5 wt% sucrose. A suspension of invertase immobilised Janus particles in 10 mM acetate buffer (pH 4.7) containing 1 to 5 wt% sucrose was prepared and was injected into a perfusion chamber mounted on a clean glass slide. We prevented the sedimentation of the particles to the bottom surface using a mixture of pure water and deuterium oxide (density: 1.107 g/cm^3 at 25 °C) to 1:1 volume ratio which can balance the density between aqueous phase and the particles with at 25 °C. The motility of the particles was monitored at various temperatures ranging from 25 to 40 °C for 1 h as shown in Figure 6.11. At 40 °C the convection during the observation is negligible compared to that at room temperature.

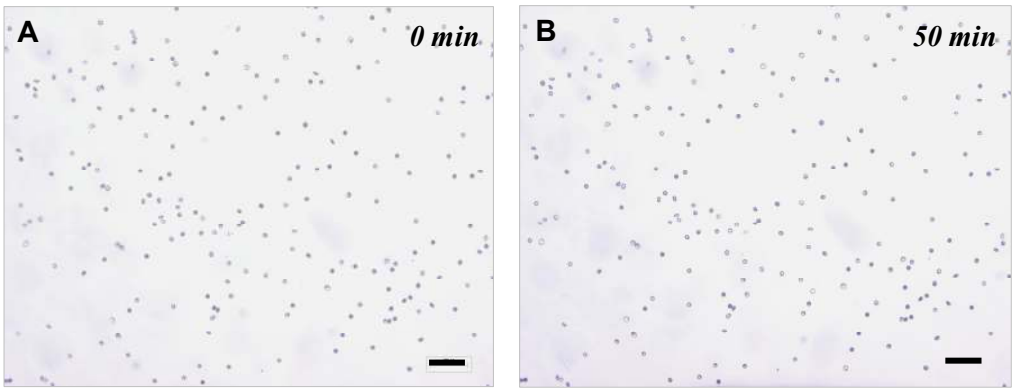

Figure 6.11: Observation of the motility of invertase immobilised Janus particles (15.47 μm diameter carboxylated modified latex particles) in 2 wt% sucrose in 10 mM acetate buffer (pH 4.7) which is composed of 1:1 (v/v) pure water and deuterium oxide at 30 °C. All scale bars are 200 μm.

In most cases a few particles showed very slow self-propulsion and self-rotation in an aqueous phase whereas almost particles moved randomly by Brownian motion or

convection. The velocity of the particles showing the directional movement was less than 0.2 μm/s. The variation of the invertase concentration in the conjugation reaction, the sucrose concentration and the pH in an aqueous solution for motility observation did not produce the propulsion of the particles significantly.

These results lead us to the conclusion that the invertase immobilised Janus particle cannot generate the sufficient osmotic pressure gradient to propel the particle possibly due to insufficient activity of invertase or the low coverage of immobilised invertase on the Au surface of the Janus particle. In our strategies the immobilisation of invertase is based on the spontaneous cysteine-Au interaction via a thiolate linkage as shown in Figure 6.5 therefore the content of cysteine in invertase is important to the immobilisation of invertase onto the Au surface. Native yeast invertase has two cysteine residues (Cys-108 and Cys-205) which are located in the catalytic site and they are important in enzyme activity.[23] These two cysteine residues might be hindered or not enough to form a strong covalent linkage between invertase and the Au surface of the Janus particle. Thus, we have investigated another method to immobilise invertase to the Au surface of the Janus particle such as a well-known coupling reaction using *N*-ethyl-*N*′-(3-dimethlyaminopropyl) carbodiimide hydrochloride (EDAC) and *N*-hydroxysuccinimide (NHS).[24]

6.2.2 Preparation of catalase reaction driven Janus particles

6.2.2.1 Immobilisation of catalase on Au-coated Janus particles

As discussed above, for the insufficient propulsion activity of invertase immobilised Au-coated Janus particle we have investigated relatively highly active enzyme catalase as a substitute for invertase for immobilisation on the surface of the Au-coated Janus particles as shown in Table 6.1.

Table 6.1: Comparison of the catalytic properties of catalase and invertase

Enzyme	k_{cat} / min^{-1}	K_m /M	(k_{cat}/K_m) /$M^{-1}min^{-1}$	*Active unit/mg of solid* [e]
Catalase [a]	2.28×10^9	1.1	2.07×10^9	13,500 units [c]
Invertase [b]	5.66×10^5	2.61×10^{-2}	2.16×10^7	401 units [d]

a. Data from Ref. 25 (at pH 7.0, 30 °C), *b*. Data from Ref. 23 (at pH 5.0, 37 °C)

c. One unit will decompose 1.0 μmole of H_2O_2 per min at pH 7.0 at 25 °C.

d. One unit will hydrolyse 1.0 μmole of sucrose per min at pH 4.5 at 55 °C.

e. Bovine liver catalase and yeast baker's invertase activity from Sigma-Aldrich.

Catalase is reported to have a superior catalytic activity to decompose hydrogen peroxide into water and oxygen[26] as following reaction:

$$2\ H_2O_2\ (aq) \rightarrow O_2\ (g) + 2\ H_2O\ (l) \qquad [9]$$

The activation energy of the reaction is about 75 kJ/mol in the absence of catalyst and platinum metal catalysts can lower the activation energy to about 49 kJ/mol. The catalase enzyme, which is found in blood, lowers the activation energy to below 8 kJ/mol, which corresponds to an increase in the rate of reaction at physiological temperature by a factor of 2×10^{11} or more. Table 6.2 shows the catalytic activities of various catalysts which are calculated for 1 M of H_2O_2 and 1 M catalyst (or catalytic active sites) so fair comparison can be made. Catalase can also react with alkyl hydrogen peroxides instead of H_2O_2, such as methylperoxide and ethylperoxide. Catalase has been immobilised on numerous carrier materials such as controlled pore glass,[12] magnesium silicate,[27] chitosan,[14] and kappa-caragenan by covalently linking with glutaraldehyde, ultrafine silica particles, and calcium hydroxyapatite by adsorption, and polyacrylamide gels by entrapment.

Table 6.2: Comparison of the catalytic activities of various catalysts on the decomposition of hydrogen peroxide

Catalyst	Rate/ - $d[H_2O_2]/dt$ ($M^{-1}s^{-1}$)	E_a (kJ/mol)	
		Ref.28	Ref.29
None	10^{-8}	71	75
HBr	10^{-4}	50	-
Pt	-	-	49
Fe^{2+}/Fe^{3+}	10^{-3}	42	-
Hemoglobin or hematin	10^{-1}	-	-
$Fe(OH)_2$ triethylenetetramine	10^{3}	29	-
Catalase	10^{7}	8	8

We immobilised bovine liver catalase (Sigma-Aldrich) on the surface of the uncoated side of the Au coated carboxylate modified latex (CML) Janus particle using *N*-ethyl-*N'*-(3-dimethylaminopropyl) carbodiimide hydrochloride (EDAC). This is one of the universal methods for connecting biomolecules such as proteins to other materials. However, this process leads to undesirable side reactions of intermolecular conjugation of proteins, because most proteins are rich in both amine groups and carboxylic groups on their surface. This intermolecular connection can be avoided by using a two-step process[30]: carboxylic acid groups are first converted to active esters via diimide-

activation, and then the active esters are reacted with the amine groups on proteins without the presence of diimide. Thus, the process can guarantee homogeneous attachment of proteins onto carboxylate modified latex particles. Figure 6.12 shows the overview of the covalent attachment process. The carboxylic acid groups were activated by EDAC, forming a highly reactive O-acylisourea active intermediate.

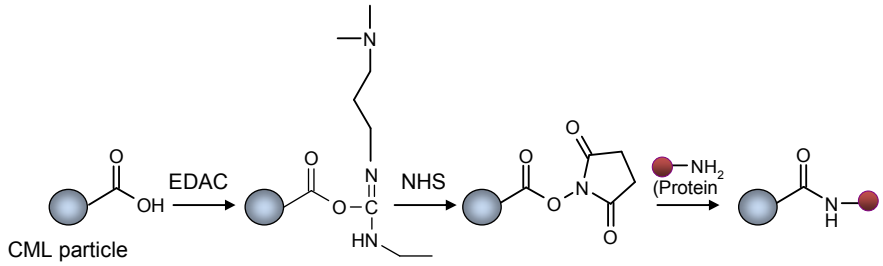

Figure 6.12: Schematic view of the attachment of proteins to carboxylate modified polystyrene latex (CML) particle via a two-step process of diimide-activated amidation.

The intermediate is unstable in an aqueous solution, and does not have a sufficient lifetime for the two-step conjugation procedure. However, in the presence of *N*-hydroxysuccinimide (NHS), a more stable active ester (succinimidyl intermediate) can be formed. The active ester undergoes nucleophilic substitution reaction with the amine groups on proteins, resulting in the formation of an amide bond between the CML particles and proteins.

The catalase was immobilised according to the procedure supplied by Interfacial Dynamics Corporation (IDC).[31] 0.25 mL of CML particles (40 mg/mL) were washed with 1 mL of 0.025 M 2-(*N*-morpholino)ethanesulfonic acid (MES) buffer solution (pH 6.0) three times and re-suspended in 0.5 mL of MES buffer at ~20 mg/mL. Then 0.08 mL of fresh EDAC aqueous solution (50 mg/mL) and 0.12 mL of catalase in MES buffer solution (1.7 mg/mL) were added to 0.2 mL of above suspension. After incubating the mixture at 20 °C with frequent shaking for 4 h, the particle suspension was centrifuged and washed with 0.1 M phosphate buffer saline (PBS) (pH 7.0) three times to remove unbound catalase. The washed catalase-CML particle conjugates were dispersed in 0.1 M PBS (pH 7.0) and stored at 4 °C until used.

We also prepared the platinum (Pt) coated Janus particles using the same procedure mentioned in section 2.2.5 except for Pt instead of Au as a coating material. Saccoccia *et al.* examined the catalytic activities of four different metallic wires (gold,

platinum, palladium and silver) to decompose hydrogen peroxide solution.[32] From their results silver seems to be the most active catalyst followed by platinum, palladium and gold (Ag > Pt > Pd > Au) at room temperature. However, in some of the tests, silver wire dissolved with time, indicating that its life as a catalyst could be limited. Therefore, we choose the platinum as a catalyst to generate the osmotic pressure gradient on the surface of metal coated Janus particles.

6.2.2.2 Motility of catalase immobilised and Pt-coated Janus particles in hydrogen peroxide solutions

For an observation of the motility of catalase immobilised Au-coated and Pt-coated Janus particles in H_2O_2 solution, a perfusion chamber (9 mm in diameter and 35 μL chamber volume, Sigma-Aldrich) was mounted onto a glass slide. Then 10 μL of 1 wt% H_2O_2 in pure water was mixed with 10 μL of a suspension of one of the tracers in pure water, dispended into the perfusion chamber, and placed under a microscope to observe particle motility at 20 °C. In aqueous solutions of hydrogen peroxide, the motion of Pt-coated Janus particles was visibly non-Brownian as they moved in the opposite direction of Pt-coated surface forming gaseous O_2 (Figure 6.13 and 6.14). The formation of oxygen bubbles and the speed of moving particles were seen to be very differently between the particles and not all the Pt-coated Janus particles formed O_2 bubbles.

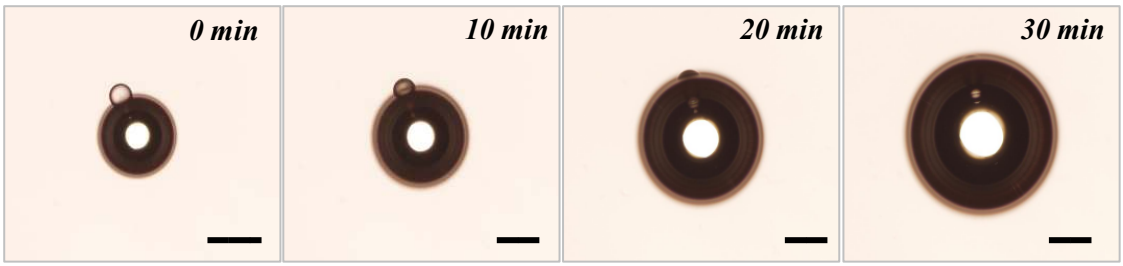

Figure 6.13: Formation of gaseous O_2 on Pt-coated Janus PMMA particles (87.5 μm in diameter) in 0.5 wt% H_2O_2 aqueous solution at room temperature. All scale bars represent 200 μm.

Batch 1:

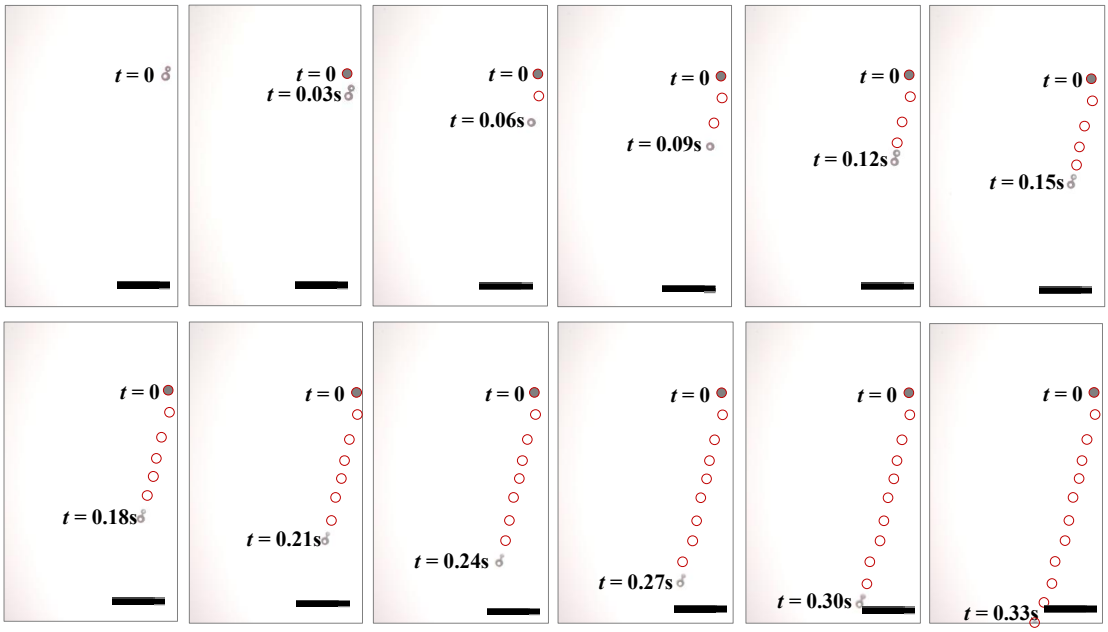

Batch 2:

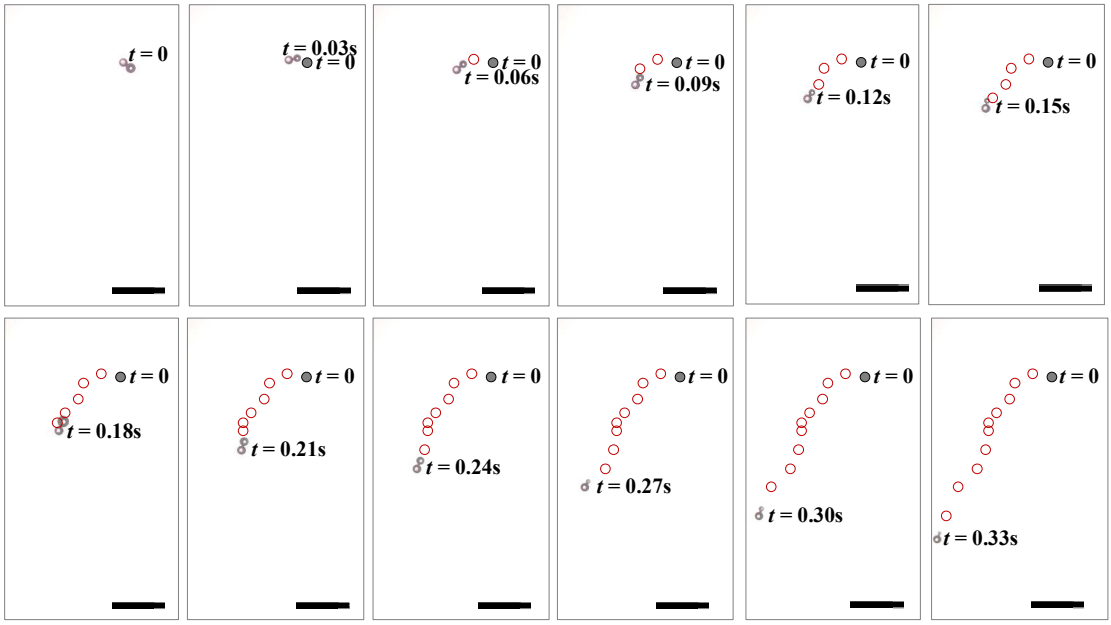

Figure 6.14: Self-propulsion of the Pt-coated spherical polystyrene latex Janus particle (15.47 μm in diameter) in 4.5 wt% H_2O_2 solution at room temperature. The red circles were added onto the images to indicate the direction of the movement and the grey circle represents the initial position at time zero. All scale bars represent 100 μm.

Table 6.3 shows that the frequency of bubble formation and speed of moving particles increase with increasing hydrogen peroxide concentration in aqueous solutions.

Table 6.3: Effect of H_2O_2 concentration in an aqueous solution on the bubble formation and the movement of Pt-coated Janus PMMA particles (87.5 μm diameter) at room temperature

Concentration of H_2O_2 /wt%	bubble formation	lifetime of bubbles	Movement
4.5	very fast	< 1 min	fast motion
3.7	very fast	< 1 min	slowly motion
1.0	fast	< 1 min	no motion
0.5	very slow	> 1 h	-
0.05	no formation	-	-
pure water	no formation	-	-

In the observation of the catalytic activity of immobilised catalase on chitosan film and free catalase the optimum reaction condition is known to 25 °C and pH is 7.0.[14] Catalase immobilised Au-coated Janus particles (CML particle in diameter 10 μm) were placed in a 1–3 wt% H_2O_2 aqueous solution, pH 7.0 at room temperature. When the particle was loaded in 3 wt% H_2O_2 aqueous solution the evolution of gaseous O_2 began immediately from the catalase immobilised surface of the particle which is opposite the dark Au-deposited side but slowly increased until blowing-up as shown in Figure 6.15.

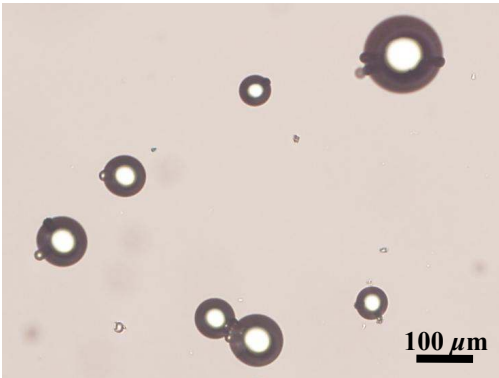

Figure 6.15: Formation of gaseous O_2 on catalase-immobilised Au-coated Janus particles (CML particle in diameter 10 μm) in 3 wt% H_2O_2 aqueous solution at room temperature.

A few particles moved significantly driven by the fast formation and burst cycles of small bubbles from the catalase immobilised side of the particle. However, the propulsion of the particles was too slow and the period of the propulsion was too short compared to Pt-coated Janus particles at the same condition. This bubble formation was not detected in most particles. Therefore, these catalase immobilisation conditions are

not effective to produce sufficient catalase-conjugates with CML particles. In all cases the motility of catalase immobilised and Pt coated Janus particles in hydrogen peroxide solutions were mainly driven by the oxygen bubble formation at the catalytic surface than the osmotic gradient which we expected as a driving force of propulsion. Therefore, we need to increase the solubility of oxygen gas in an aqueous solution in order to generate osmotic gradient without the bubble formation. In addition, the spherical enzyme immobilised Janus particle showed its slow self-rotating motion rather than a rapid axial movement in an aqueous solution. Movement in the axial direction is preferred for rod-shaped objects rather than a spherical shape because the drag force is minimized in this direction.[33]

6.3 Diffusion driven porous Janus particles

In section 6.2 we attempted to prepare the enzyme immobilised Janus particle driven by osmotic pressure gradient generated by the catalytic activity of the immobilised enzyme. For this purpose we had to choose a highly active pure enzyme and to immobilise enough enzyme on the surface of the particle. The simple diffusion (i.e. concentration gradient) driven colloidal particles seems to be simpler than enzymatic reaction driven ones (e.g., less chemical modification steps). Many attempts to prepare the particles moving on the liquid surface have been investigated such as the solvent-driven gel motor.[7,8] It may be more difficult to prepare a self-propelling particle in an aqueous solution instead of on the aqueous surface by the friction force caused by viscous liquids. In this section, we describe our method where Au-coated porous silica Janus particle is used as a carrier for a soluble load (e.g., glucose) which dissolution is used as a generator of an osmotic pressure gradient. As shown in Figure 6.2B the driving force of the present case is the osmotic pressure gradient generated by the release of glucose molecules from the opposite side of the Au-coated surface of a Janus particle. There should be an advantage in utilizing an asymmetric dissolution order to convert it directly into a mechanical work.

6.3.1 Preparation of Au-coated porous silica Janus particles

For a carrier particle of organic fuels we have used a porous hydrophilic silica particle Aeroperl® 300/30 which is polydisperse with the size ranging from 2 to 70 μm. The particles were separated using a series of test metal sieves (Endecotts, UK) from polydisperse particles as received to collect bigger particles (diameter > ~ 50 μm) and

dried in a dry oven at 60 °C before use. Before the preparation of Au-coated Janus particle we observed the absorption of glucose into the cavity of the silica particles as shown in Figure 6.16. After incubation in 10 wt% glucose solution for 1–2 h at room temperature and dried at 60 °C for 1 h, the glucose absorbed silica particles showed a dark brown colour. However, the amount of glucose absorbed into the particles was different among the particles by comparison of the colour of the particles as shown in Figure 6.16B.

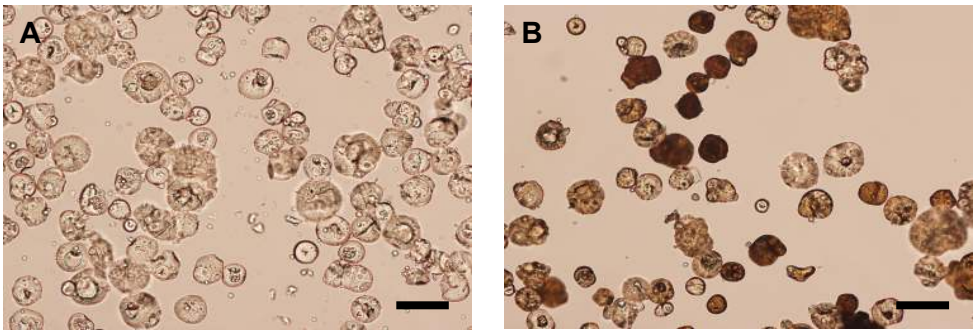

Figure 6.16: Optical images of dried fumed silica particles Aeroperl® 300/30 before (A) and after (B) incubation with 10 wt% glucose solution for 2 h at room temperature. The dark brown colour of the particles comes from the adsorbed glucose into the cavity of the particles. All scale bars represent 100 μm.

For Au evaporation onto the particles using the glass sliding technique (GST) 20 wt% glucose aqueous solution was used as a spreading solution to produce a monolayer of silica particles and to protect the bottom side of the silica particles from Au coating instead of 2-propanol because the absorbed glucose in the particle was released into 2-propanol during the spreading process on a glass slide. As in our previous studies (section 6.2.1), 100 μL of 10–20 wt% glucose solutions were used to make a glucose film to protect the bottom side of polystyrene latex and PMMA particles which were spread on a glass slide from being coated with Au. When 100 μL of 20 wt% glucose solution was used to produce a monolayer of the glucose absorbed silica particles, almost all the glucose spreading solution was absorbed into the silica particles rather forming the glucose film on a glass slide during a dry period as shown in Figure 6.17. After adding more 20 wt% glucose solution onto the monolayer of the silica particles on the glass slide until the monolayer of the silica particles was partially embedded in glucose solution the particles were coated with 10–20 nm Au film as described in section 2.2.5.

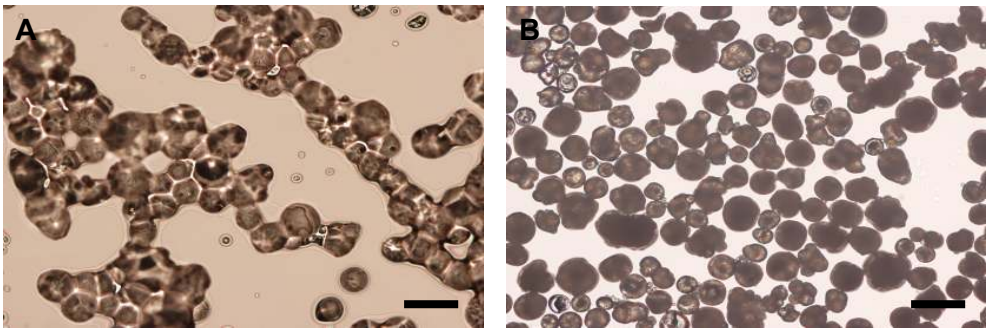

Figure 6.17: Glucose absorbed silica particles (A) after spreading on a glass slide with 20 wt% glucose solution at room temperature and (B) after drying in air for 2 h. The glucose solution was quickly absorbed into the silica particles and could not form the glucose layer between the particles. All scale bars represent 100 μm.

However, the Au layer on the particles was separated from the particle after flushing with pure water using a micropipette for a collection as shown in Figure 6.18A. To minimise the physical force acting on to the Au layer during the isolation the glucose film on a glass slide was dissolved through incubation with a drop of pure water on the glass slide. Figure 6.18B shows the separated Au layer from the silica monolayer after incubation with pure water and this separated Au layer settled down to the bottom of a glass slide.

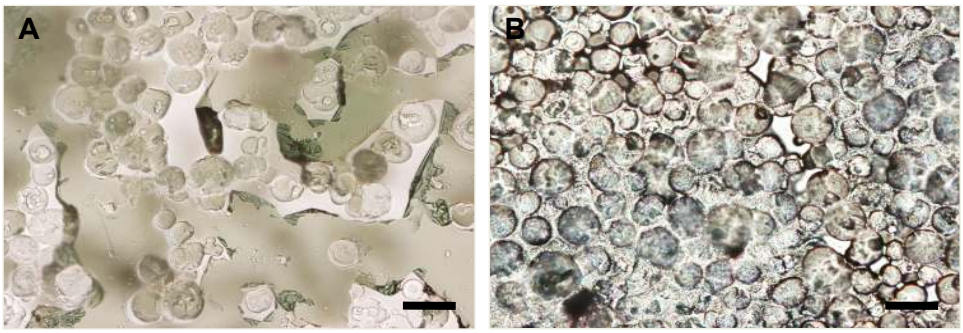

Figure 6.18: Separation of coated Au layer from glucose absorbed porous silica Janus particles during the isolation from a glass slide. (A) Thin separated Au layers after flushing with pure water and (B) thick separated Au layers after incubation with pure water. All scale bars represent 100 μm.

We hypothesized the reason why the coated Au layer was separated from the surface of silica particles. Firstly, the glucose solution was too much doped on the surface of the silica particles during the spreading step. This glucose film might form a barrier between the surface of silica and the Au layer and it was easily dissolved in pure water and caused the coated Au layer to peel off from the surface of silica particles. Secondly,

the direct deposition of Au by a thermal evaporation on the surface of the silica particle did not form a strong adhesion of the Au layer onto the surface of the particle. In our previous results to prepare a stable Au-coated Janus particle, the particle was coated with chromium (Cr) first and then coated with Au. Therefore, we decided to prepare Au-coated porous silica Janus particles using another method which does not involve using of any spreading solution.

We have developed a new simple method to prepare metal coated Janus particles using an adhesive sticky tape as a support of the particles instead of PDMS (GTT) and glucose (GST). This method is convenient to prepare Janus particles using porous materials without any spreading solution (e.g., glucose solution), and therefore prevents the separation of a coated Au layer from the particles.

The dried porous silica particles Aeroperl® 300/30 were spread on an adhesive sticky tape (Invisible tape No. 184.835, IMPEGA) which was attached on a glass slide, and then blew the excess silica particles on the tape with air in Figure 6.19. The prepared monolayer of dried silica particle was coated with Cr and then Au with a thickness about 15–20 nm each layer according to the same metal coating procedure used before.

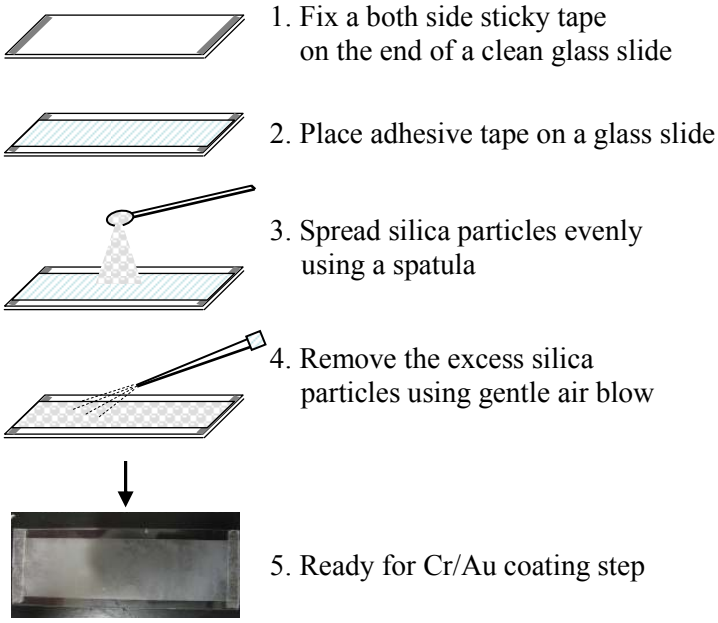

Figure 6.19: Schematic representation of the preparation procedure of the monolayer of Au-coated porous silica Janus particles on an adhesive sticky tape.

Figure 6.20 shows the prepared well spread monolayer of silica particle on the surface of the tape (Figure 6.20A and B) and well maintained particle shapes (Figure 6.20C and D) before and after Cr and Au coating onto the samples.

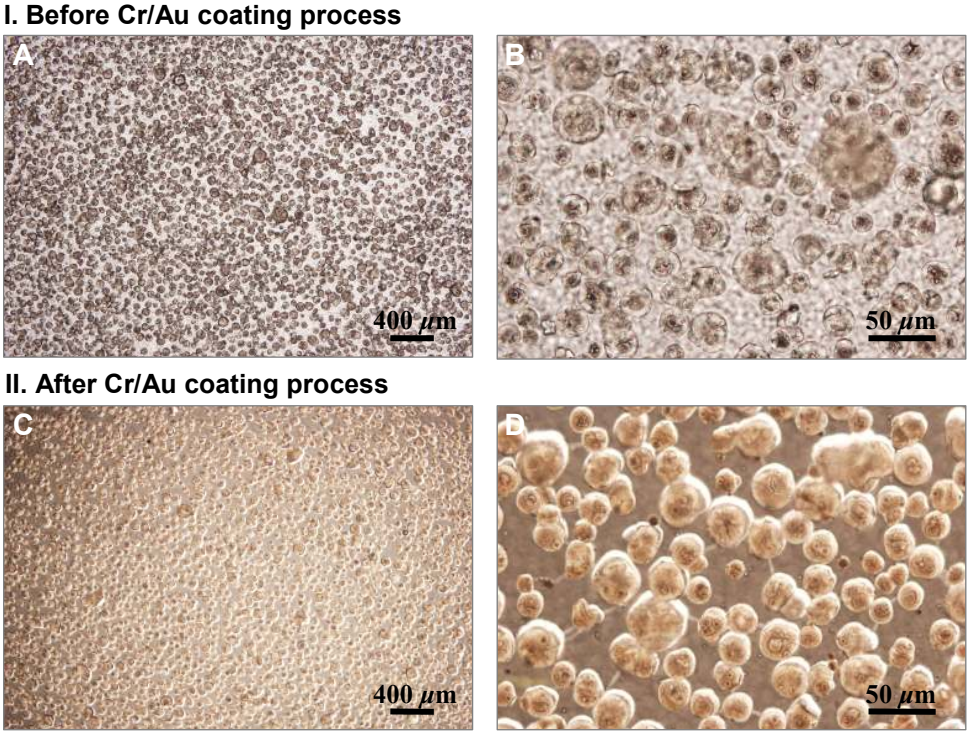

Figure 6.20: Optical images of the monolayer of porous silica particles Aeroperl® 300/30 on an adhesive sticky tape (IMPEGA invisible tape) (A-B) before and (C-D) after the coating step with chromium (Cr) and gold (Au).

The prepared monolayer of the porous silica particles was coated by two different methods to form the different Au coverage onto the particles. The evaporated metal was deposited onto the monolayer of particles: (1) from the top of the particles on a tape (flat coating) and (2) from different angles with respect to the particle monolayer three times (inclined coating). Using the inclined coating method, the deposited Au covers a larger surface area of the particles than the flat coating method, which decreases the diffusion rate of glucose from the Janus particle into a liquid phase as shown in Figure 6.21. This would allow us to control the speed of the Janus particle propulsion induced by the diffusion of stored glucose in the particle according to the coverage of Au of the particle using this strategy.

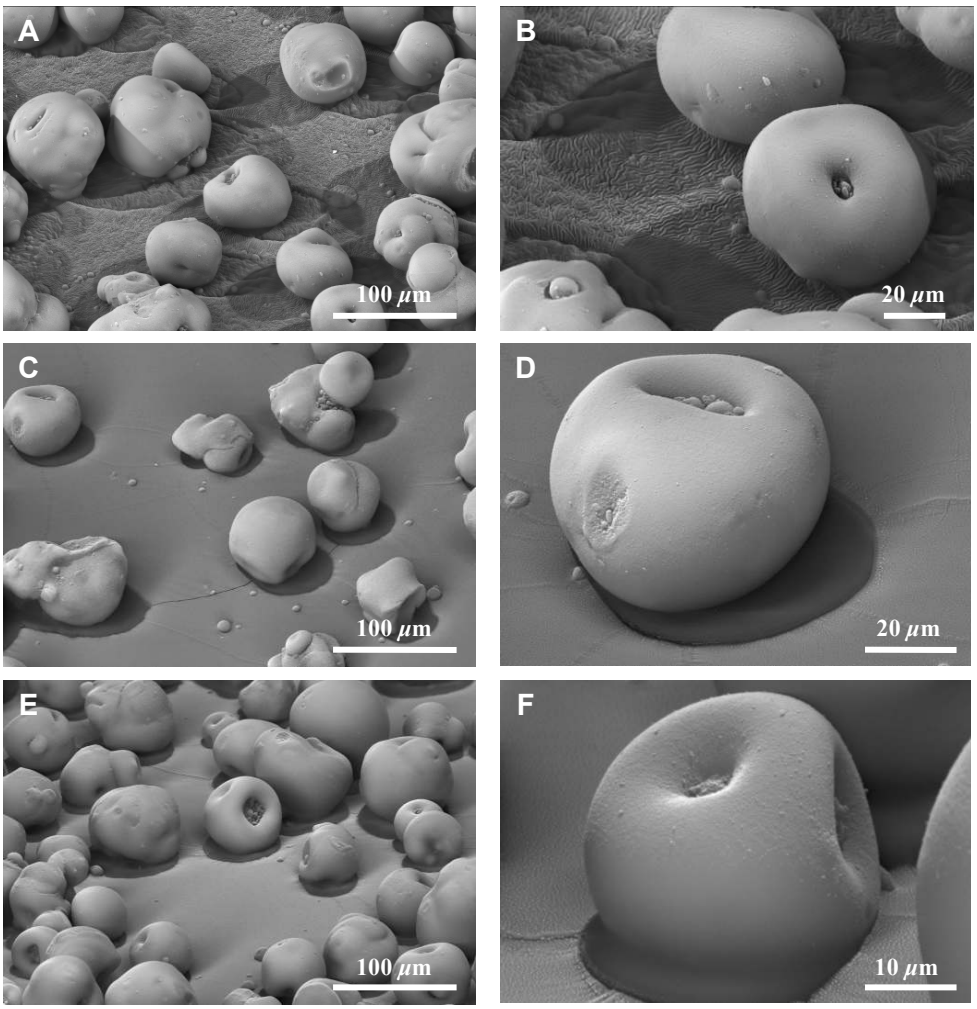

Figure 6.21: Scanning electron microscope (SEM) photographs of Au-coated porous silica Janus particles on an adhesive tape using two different metal coating procedures: (A-B) flat coating and (C-F) inclined coating at three different angles. The metal coating can be shown on the top surface of the particle and the shadow of the particle relates with the metal coating at the opposite side.

6.3.2 Preparation of Au-coated porous Janus particles carrying glucose

After Cr and Au deposition to the monolayer of the particles we examined the recovery of Au-coated porous silica Janus particles from the adhesive tape by flushing with various organic solvents (e.g., ethanol, methanol, acetone) and then washing with pure water several times for the absorption of glucose. Among examined solvents, ethanol was the best solvent for our purpose (e.g., ease of particle detachment, less damage) than others. However, some particles were partially broken and isolated together with an adhesive material of the adhesive tape (Figure 6.22).

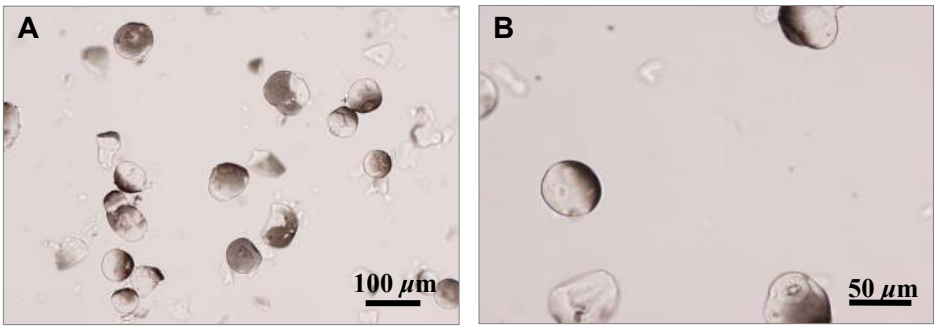

Figure 6.22: Optical images of Au-coated porous silica Janus particles in pure water after isolation from an adhesive tape on a glass slide using ethanol. For image B the dark area is the Cr/Au-deposited area of the Janus particle.

For absorption of glucose into the particle the isolated Au-coated silica Janus particles were incubated with 20 wt% glucose aqueous solution with gentle mixing for 3 h at room temperature. The glucose absorbed Au-coated Janus particles were recovered by centrifugation at 14,500 rpm for 1 min using MiniSpin centrifuge (Eppendorf, Hamburg, Germany) and then dried in a dry oven at 60 °C before use (Figure 6.23).

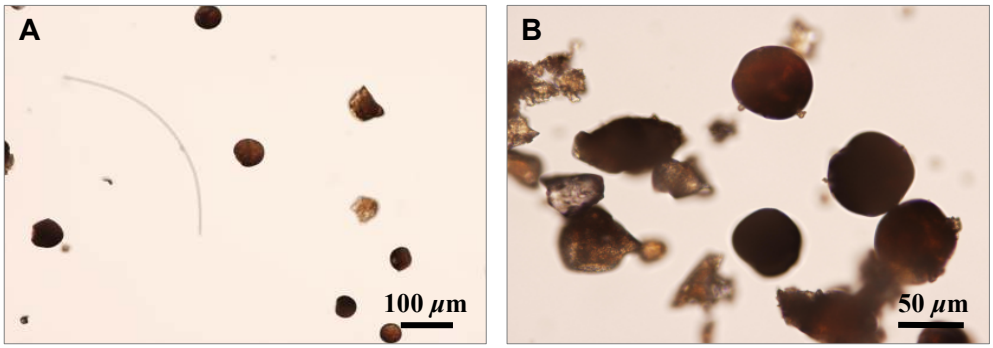

Figure 6.23: Optical images of dried Au-coated porous silica Janus particles in air after incubation with 20 wt% glucose solution for 3 h at room temperature and dried in a dry oven. The dark brown colour of the particles comes from the absorbed glucose into the cavities of the particles.

6.3.3 Motility of glucose absorbed Au-coated porous Janus particles

We observed the motility of the prepared glucose absorbed Au-coated porous silica Janus particles in pure water at room temperature. The dried glucose absorbed Janus particles were spread on a clean glass slide and covered with a perfusion chamber. Just after the perfusion chamber was filled with pure water the motility of the particles was monitored under a microscope at room temperature for 40 min. The particles did not show significant motility at this condition as shown in Figure 6.24.

In some particles bubbles came from the surface of the particles and they slightly expanded according to the incubation time.

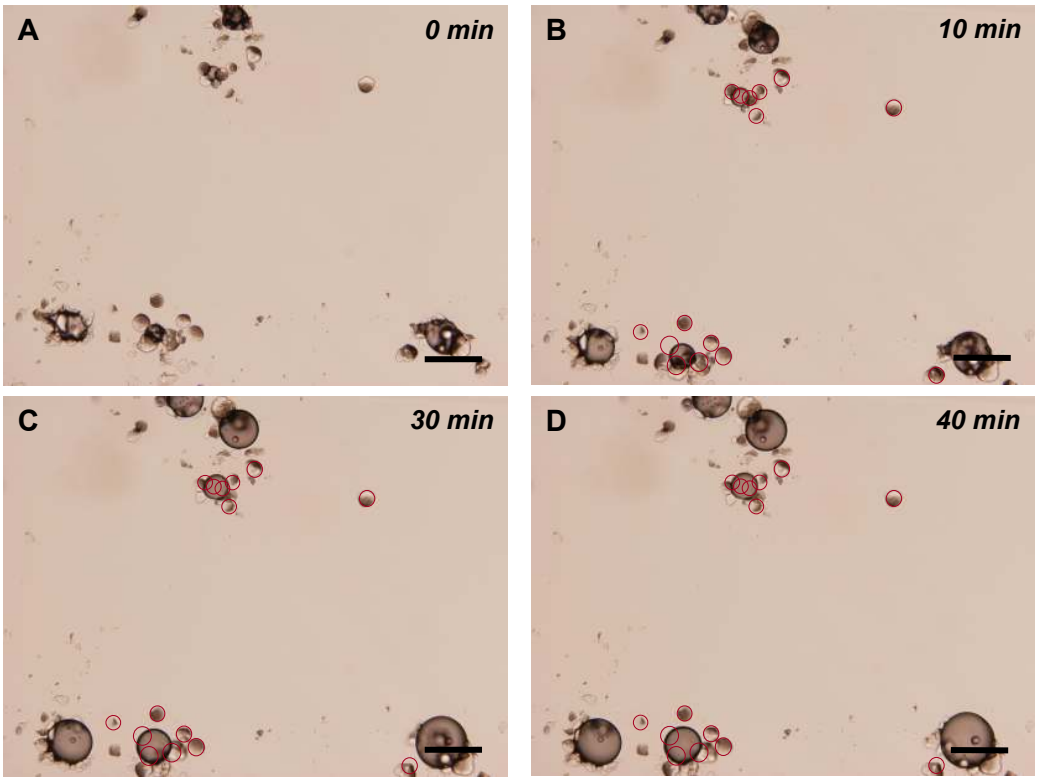

Figure 6.24: Optical images of motility of glucose absorbed Au-coated porous silica Janus particles in pure water at room temperature for 40 min. Red circles in image B, C, and D are the original positions of the Janus particles at 0 min. All scale bars represent 200 μm.

The results obtained above suggest that the diffusion of glucose in pure water might be too fast to observe the propulsion of the particles after injecting with pure water into a perfusion chamber under a microscope. To confirm this proposition we investigated the effect of other organic solvents to slow down the diffusion of glucose into the liquid instead of pure water.

Total glucose solubility in various alcohols 40 and 60 °C are presented in Table 6.4.[34] It is shown that a small temperature increase leads to a significant increase of both the total glucose solubility whereas the total solubility of glucose decreases with increase in the number of carbon atoms in the solvent when comparing separately normal alcohols (1-butanol < 1-propanol < ethanol < methanol) or branched alcohols (*tert*-butyl alcohol < 2-propanol). Additionally, when comparing alcohols with the same

number of carbon atoms, it is noticed that glucose presents higher solubility in branched alcohols (1-butanol < *tert*-butyl alcohol and 1-propanol < 2-propanol).

Table 6.4: Experimental equilibrium concentrations of glucose in different alcohols[34]

solvent	solubility/g·L^{-1} at 40 °C		solubility/g·L^{-1} at 60 °C	
	α-D-glucose	β-D-glucose	α-D-glucose	β-D-glucose
tert-butyl alcohol	0.58 ± 0.03	0.66 ± 0.03	1.65 ± 0.07	1.86 ± 0.08
1-butanol	0.27 ± 0.00	0.32 ± 0.01	0.69 ± 0.03	0.78 ± 0.04
2-propanol	-	-	1.82 ± 0.08	1.96 ± 0.09
1-propanol	-	-	1.77 ± 0.11	1.95 ± 0.09
ethanol	1.82 ± 0.09	1.99 ± 0.11	4.51 ± 0.06	4.51 ± 0.06
methanol	14.52 ± 0.29	14.24 ± 0.34	-	-
10 wt% water in ethanol	10.72 ± 0.22	10.51 ± 0.17	20.83 ± 0.71	21.26 ± 0.55

We measured the dissolution rate of glucose in a water-alcohol mixture under a microscope at room temperature as shown in Table 6.5. Addition of alcohol into pure water is likely to decrease significantly the dissolution rate of glucose at room temperature.

Table 6.5: Effect of the addition of alcohols into pure water on the dissolution rate of glucose crystal at room temperature

solvent	dissolution rate /sec
water	~5
water: methanol = 50:50% (v/v)	~190
water: ethanol = 50: 50% (v/v)	~301

From the result, we expected that the water-alcohol mixture could delay the diffusion of the glucose stored in the Janus particle into an aqueous solution and we could observe the motility of the particles. We examined the motility of glucose absorbed Au-coated porous silica Janus particles in various water-alcohol mixtures such as 50 vol% ethanol in pure water at room temperature. However, the particles did not show any rapid axial movement meanwhile they showed only a self-rotation and a simple Brownian motion similar to the results observed in the invertase immobilised Janus particles in sucrose solutions (section 6.1.2.4).

6.4 Conclusions

In this chapter, we systematically investigated the possibility to induce propulsion using various kinds of Janus particles driven by osmotic pressure gradient. The motion is originated from asymmetric diffusion of water-soluble substrates (e.g., glucose, oxygen) from the core, or the surface of metal coated Janus particles to the exterior aqueous solution to produce the imbalance of the concentration of solutes in the aqueous phase, whereupon the osmotic pressure generated in the particles would keep pumping the solute for a prolonged period of time.

The main conclusions from this chapter are:

- We developed two modified methods, the glass sliding technique (GST) and the adhesive tape spread technique to easily prepare the metal coated Janus particles.
- Using these methods we designed the enzymatic reaction and diffusion driven self-propulsion particles using spherical polystyrene latex and PMMA particles size ranging from 0.97 to 87.5 μm.
- The enzyme immobilised and glucose absorbed Janus particles did not show a rapid axial movement in an aqueous solution as we expected. In the glucose absorbed Au-coated porous silica Janus particle, we assume that the particles might release glucose into a liquid too fast to observe their motility under a microscope although we even failed to observe a propulsion using highly Au covered Janus particles.
- We created the self-propelling Pt-coated Janus particle in H_2O_2 solution by a bubble formation (i.e. a bubble engine) not by osmotic pressure gradient. The average instantaneous speed of the catalytically powered Pt-coated Janus particle (15.47 μm in diameter) in 4.5 wt% H_2O_2 solution is on the order of ~1 mm/s. The results are consistent to a previous study[1] in which the H_2O_2/Pt system is the most reproducible of the combinations of energy and catalyst that generate motion rather than other systems such as a catalase embedded hydrogel. We need to increase the solubility of the formed oxygen gas in a liquid to generate the osmotic gradient without a bubble formation.
- These all results imply that we need more active enzyme that can create enough imbalance of a solute in a liquid. The increase of the amount of immobilised enzyme on the surface of Janus particles would produce stronger osmotic pressure gradient which would propel the particles in a liquid.

6.5 References

1. R. F. Ismagilov, A. Schwartz, N. Bowden and G. M. Whitesides, "Autonomous movement and self-assembly", *Angew. Chem., Int. Ed.* **2002**, *41*, 652-654.
2. W. F. Paxton, K. C. Kistler, C. C. Olmeda, A. Sen, S. K. St. Angelo, Y. Cao, T. E. Mallouk, P. E. Lammert and V. H. Cresp, "Catalytic nanomotors: Autonomous movement of striped nanorods", *J. Am. Chem. Soc.* **2004**, *126*, 13424-13431.
3. S. Nakata, Y. Doi and Y. Hayashima, "Intermittent motion of a camphene disk at the center of a cell", *J. Phys. Chem. B* **2002**, *106*, 11681-11684.
4. S. T. Chang, V. N. Paunov, D. N. Pestev and O. D. Velev, "Remotely powered self-propelling particles and micropumps based on miniature diodes", *Nature Mater.* **2007**, *6*, 235-240.
5. Y. Wang, R. M. Hernandez, D. J. Bartlett Jr., J. M. Bingham, T. R. Kline, A. Sen and T. E. Mallouk, "Bipolar electrochemical mechanism for the propulsion of catalytic nanomotors in hydrogen peroxide solutions", *Langmuir* **2006**, *22*, 10451-10456.
6. W. F. Paxton, P. T. Baker, T. R. Kline, Y. Wang, T. E. Mallouk and A. Sen, "Catalytically induced electrokinetics for motors and micropumps", *J. Am. Chem. Soc.* **2006**, 128, 14881-14888.
7. J. P. Gong, S. Matsumoto, M. Uchida, N. Isogai and Y. Osada, "Motion of polymer gels by spreading organic fluid on water", *J. Phys. Chem.* **1996**, *100*, 11092-11097.
8. T. Mitsumata, K. Ikeda, J. P. Gong and Y. Osada, "Controlled motion of solvent-driven gel motor and its application as a generator", *Langmuir* **2000**, *16*, 307-312.
9. R. C. Weast and M. J. Astle, *CRC Handbook of Chemistry and Physics 62 ed.*, CRC Press: Boca Raton, Florida, 1981, F-40.
10. S. Zhang, N. Wang, H. Yu, Y. Niu and C. Sun, "Covalent attachment of glucose oxidase to an Au electrode modified with gold nanoparticles for use as glucose biosensor", *Biochemistry* **2005**, *67*, 15-22.
11. M. Rebroš, M. Rosenberg, Z. Mlichová and Ĺ. Krištofíková, "Hydrolysis of sucrose by invertase entrapped in polyvinyl alcohol hydrogel capsules", *Food chemistry* **2007**, *102*, 784-787.
12. S. Sasaki and Y. Arai, "Oscillatory reaction using immobilised catalase", *Anal. Sci.* **2004**, *20*, 895-898.

13. E. Kokufuta and Y. Aman, "A biochemo-mechanical system consisting of polymer gels with immobilised glucose dehydrogenase", *Polym. Gels & Networks* **1997**, *5*, 439-454.
14. Ş. A. Çetinus and N. Öztop, "Immobilisation of catalase on chitosan film", *Enzy. Micro.Tech.* **2000**, *26*, 497-501.
15. E. Toru, E**. 2007** *Self-propelling microparticles* (Report) University of Hull.
16. X. Hu, W. Cheng, T. Wang, E. Wang and S. Dong, "Well-ordered end-to-end linkage of gold nanorods", *Nanotech.* **2005**, *16*, 2164-2169.
17. K. Naka, H. Itoh, Y. Tampo and Y. Chujo, "Effect of gold nanoparticles as a support for the oligomerization of L-cysteine in an aqueous solution", *Langmuir* **2003**, *19*, 5546-5549.
18. W. A. Staines, B. Meister, T. Melander, J. I. Nagy and T. Hökfelt, "Three-colour immunofluorescence histochemistry allowing triple labelling within a single section", *J. Histochem. Cytochem.* **1988**, *36*, 145-151.
19. J. B. Summer and E. B. Sisler, "A simple method for blood sugar", *Arch. Biochem.* **1944**, *4*, 333-336.
20. G. L. Miller, "Use of dinitrosalicylic acid reagent for the determination of reducing sugar", *Anal. Chem.* **1959**, *31*, 426-428.
21. G. Wang, T. J. Michailides and R. M. Bostock, "Improved detection of polygalacturonase activity due to Mucor piriformis with a modified dinitrosalicylic acid reagent", *Phytopathology* **1997**, *87*, 161-163.
22. U. Bora, K. Kannan and P. J. Nahar, "A simple method for functionalization of cellulose membrane for covalent immobilisation of biomolecules", *J. Memb. Sci.* **2005**, *250*, 215-222.
23. A. Reddy and F. Maley, "Studies on identifying the catalytic role of Glu-204 in the active site of yeast invertase", *J. Biol. Chem.* **1996**, *271*(24), 13953-13958.
24. D. Li, Q. He, Y. Cui, L. Duan and J. Li, "Immobilisation of glucose oxidase onto gold nanoparticles with enhanced thermostability", *Biochem. Biophys. Res. Commun.* **2007**, *355*, 488-493.
25. J. Harber and P. Walde, "Activity and spectroscopic properties of bovine liver catalase in sodium bis(2-ethylhexyl)sulfosuccinate/isooctane reverse micelles", *Eur. J. Biochem.* **1993**, *217*, 567-573.
26. L. Stryer, *Biochemistry,* 4th ed., **1995**, W. H. Freeman and Company, New York, p553.

27. S. S. Tukel and O. Alptekin, “Immobilisation and kinetics of catalase onto magnesium silicate”, *Process. Biochem.* **2004**, *39*, 2149-2155.
28. I. Tinoco, K. Sauer, J. C. Wang and J. D. Puglisi, *Physical Chemistry; Principles and Applications in Biological Sciences*, 4 Ed. Prentice Hall, 2001.
29. *The Catalytic Decomposition of Hydrogen Peroxide*: http://chemed.chem.purdue.edu/demos/moviesheets/10.8.html, [Accessed 12 July 2007]
30. K. Jiang, L. S. Schadler, R. W. Sigel, X. Zhang, H. Zhang and M. Terrones, “Protein immobilisation on carbon nanotubes via a two-step process of diimide-activated amidation”*, J. Mater. Chem.* **2004**, *14*, 37-39.
31. *Covalent coupling of proteins to IDC Ultraclean carboxylate modified Latex (CML):*www.idclatex.com/body_bgrounder-superactive-protocol-2.asp, [Accessed 12 July 2007].
32. C. Bramanti, A. J. Musker and G. Saccoccia, “Experimental Characterization of Advanced Materials for the Catalytic Decomposition of Hydrogen Peroxide”, *American Institute of Aeronautics and Astronautics (AIAA) paper*: http://www.esa.int/gsp/ACT/doc/PRO/ACT-RPR-PRO-JPC2006-HP%20catalysts%202006-5238.pdf, [Accessed 5 November 2008]
33. R. F. Probstein, *Physicochemical Hydrodynamics: An Introduction, 2nd Ed.* John Wiley & Sons, Inc., New York 1994, pp 109-112.
34. G. Leontarakis, P. Tsavas, E. Voutsas, K. Magoulas and D. Tassios, “Experimental and predicted results of anomeric equilibrium of glucose in alcohols”*, J. Chem. Eng. Data* **2005**, *50*, 1924-1927.

Chapter 7

Summary of the Main Conclusions and Future Work

Chapter 7

Summary of the Main Conclusions and Future Work

7.1 Summary of the main conclusions

The main conclusions from this work are:

Chapter 3:

- We have investigated a DNA sensor based on adsorption of DNA species and their hybridisation with complementary DNA sequences at the interface between a nematic liquid crystal (LC) and water.
- The adsorption of cholesteryl and saturated dodecyl modified DNA-surfactants from water phase to the LC-water interface did not trigger an optical transition of 5CB from planar to homeotropic anchoring above their cmc regardless of ionic strength. The most likely reason for this is that their highly charged bulky headgroups and their looped configuration at the interface prevent the formation of a dense surfactant monolayer at the interface to trigger the anchoring transition.
- The adsorption of DNA-cationic surfactant complex from water phase to the LC-water interface triggers an optical change from planar to homeotropic anchoring of 5CB. However, after washing with a salt solution, the induced homeotropic anchoring of 5CB is reverted to planar due to desorption of cationic surfactant from the complex leaving DNA alone at the interface.
- Using these systems we were able to understand better the interfacial behaviour of DNA-cationic surfactant complex at the LC-water interface depending on various conditions (e.g., ionic strength, the length and structure of DNA).

Chapter 4:

- We have designed a UV senor device based on adsorption of polymerisable surfactants at the LC-water interface.
- The adsorption of polymerisable surfactants of sufficient hydrophobic chain length from either the water or LC phase to the 5CB-water interface triggers a change from planar to homeotropic anchoring of 5CB.

- The UV polymerisation within the adsorbed polymerisable surfactant monolayer triggers the transition of anchoring of 5CB from homeotropic to planar anchoring and the UV induced planar anchoring is reversible.
- These systems form the basis of UV sensor devices whose response is visible to the naked eye and which have potential applications in the signalling and avoidance of over exposure to harmful UV radiation.

Chapter 5:

- We have attempted to design a self-propelling micro-device based on self-oscillating gel particles driven by either the BZ reaction or an electric field.
- The periodical conformational oscillation of ruthenium catalyst immobilised poly(*N*-isopropylacrylamide) based hydrogels did not generate enough fast volume changes to propel the gel particle in an aqueous solution.
- In order to design a self-actuating anisotropic gel particle we developed a novel simple method to synthesise a modulated bigel structure with a strong adhesion between two gel components by UV polymerisation. The prepared bigels show transitions of their shapes depending on the temperature, pH, and composition of solvents. The gel functions obtained from this modulation method are based on the fact that the volumes of different gels are sensitive to different aspects of the external environment.
- We observed different anisotropic swelling behaviour of polyelectrolyte gels in a surfactant and salt solution depending on the gel size and electric fields as follows:
  (1) Under *dc* electric field a small cylindrical gel (< 2 mm length) shows propulsion whereas bending-straightening motion for a larger cylindrical gel (> 1 cm length).
  (2) Under *ac* electric field, a cylindrical gel (~ 2 cm length) shows vibration at high frequency whereas bending-straightening motion at low frequency.
- Applications of the modulation method could be extensive and the modulated gels may find applications in the fields of robotics and automobiles (e.g., gel display devices, switches or valves).

Chapter 6:

- We have attempted to design a new type of self-propulsion Janus particles based on an osmotic pressure gradient produced on the surface of the particles.
- We showed that it is possible to power the motion of microscale objects by using platinum-coated Janus particles into hydrogen peroxide solution. However, the catalase and invertase immobilised Janus particles could not lead to unidirectional but only rotational motion in a liquid mainly by an insufficient osmotic gradient generation from the particles.
- In this study, we have developed a novel methods for preparation of Janus particles based on direct thermal evaporation of metal onto monolayers of particles deposited on a glass slide (the glass sliding technique) and a sticky tape. They provide a quick simple way to produce metal-coated Janus particles which are easily functionalised without any special equipment (e.g., immobilisation with enzymes onto a particle).

7.2 Future work

We can summarise our future objectives as follows:

- Examination of LCs instead of 5CB to screen more sensitive materials to detect adsorption of surfactants at the LC-water interface.
- Improvement of the sensitivity of UV sensors at high temperature by investigating new components of LC optical cells (e.g. polymerisable surfactants, photo-initiators and LC with a high T_{NI}).
- Investigation of the methods to hydrophobise UV transferable flexible film to prepare a supporting material of LC, which can produce a homeotropic anchoring of LC at the LC-water interface.
- Preparation of a highly purified ruthenium catalyst monomer and examination the self-oscillation reactions in the BZ substrates before synthesising of modulated polymer gels.
- Enhancement of immobilisation of enzyme on Janus particles using a chemical modification and preparation of a highly purified enzyme for immobilisation.
- Establishment of a new fabrication method to prepare anisotropic particles (e.g., cone-shaped particle) in a micrometer scale to reduce the relatively large transition times known from our bulk objects.